Universitas Muhammadiyah Sumatera Utara

Indonesian Engineer Society of Wind and Earthquake Resistant Structures
HASTAG

USM Universiti Sains Malaysia

Proceedings

The 3rd International Conference on the Geohazard Information Zonation and 5th Seminar & Short Course of HASTAG

(GIZ2014 - HASTAG5)

Sustainable Development under Unpredicted Geohazard

Editors

Ade Faisal
Fauziah Ahmad

Medan, Indonesia
October 20-22, 2014

USU press

Proceedings

The 3rd International Conference on the Geohazard Information Zonation and

5th Seminar & Short Course of HASTAG

(GIZ2014 - HASTAG5)

Sustainable Development under Unpredicted Geohazard

Edited by

Ade Faisal, Ph.D
Head of Civil Engineering Program,
Universitas Muhammadiyah Sumatera Utara.
Co-Chairman of HASTAG.

Prof. Dr. Fauziah Ahmad
School of Civil Engineering,
Universiti Sains Malaysia

Medan, Indonesia
October 20-22, 2014

USU press
2014

USU Press
Art Design, Publishing & Printing
Gedung F, Pusat Sistem Informasi (PSI) Kampus USU
Jl. Universitas No. 9
Medan 20155, Indonesia

Telp. 061-8213737; Fax 061-8213737

usupress.usu.ac.id

ISBN 979 458 758 3

Perpustakaan Nasional: Katalog Dalam Terbitan (KDT)

The 3rd International Conference on the Geohazard Information Zonation and 5th Seminar & Short Course of HASTAG / Ade Faisal, Fauziah Ahmad – Medan: USU Press, 2014.

viii, 238 p. ; ilus.: 29 cm
Bibliografi

ISBN: 979-458-758-3

Dicetak di Medan, Indonesia

FOREWORD

The geological hazards are natural phenomenom that we have frequently faced in this earth. Over the years, many geohazards have left many lessons to be learned by people, scientist, and engineering comunities. It is essential for us in putting forward policy to mitigate similar natural hazard in future. There are so many factors to be considered that it is practically difficult to forecast the geohazard and its level of the damage to the built system. Sharing idea, insight, and knowledge in such an event is very critical to promote the mitigation of geohazard.

The Civil Engineering Program, Universitas Muhammadiyah Sumatera Utara (UMSU); Indonesian Engineers Society of Wind and Earthquake Resitant Structures (HASTAG); and School of Civil Engineering, Universiti Sains Malaysia, have collaboratively conducted the 3rd International Conference on the Geohazard Information Zonation and 5th Seminar & Short Course of HASTAG (GIZ2014-HASTAG5) in Medan, Indonesia, from October 20-22, 2014. The program was consisted of conference, seminar, and exhibition of construction and material technology in two days. A short course of Structural Modeling for Earthquake Engineering with OpenSees was proceeded in the final day. Therefore we pleased to present this collection of papers submitted to GIZ2014-HASTAG5.

The program committee would like to thank all those who submitted papers for review. Papers were evaluated regarding their relevance to GIZ2014-HASTAG5, originality, significance, information content, clarity, and soundness on an international level. Each aspect was objectively evaluated, with alternative aspects finding consideration for application papers. Therefore, we would like to thank the members of the GIZ2014-HASTAG5 technical committee from School of Civil Engineering, Universiti Sains Malaysia, namely Associate Professor Ahmad Shukri Yahaya, Associate Professor Dr. Taksiah A. Majid, Dr. Lau Tze Liang, Dr. Mohd Ashraf Mohamad Ismail, and Dr. Fadzli Mohammed Nadzli. Their continuing support has been essential to further improve the quality of accepted submissions the resulting success of the conference.

We are very grateful to the many colleagues who helped in organizing the conference. In particular, we would like to thank the members of the GIZ2014-HASTAG5 committee. The GIZ2014-HASTAG5 committee members from HASTAG are Herri Suryadi Samosir (Chairman of HASTAG), Martono Anggusti, Daniel Rumbi Teruna, Sunarlim Satio, Sherly Meyklya Sembiring, Fuad Halimoen, Antony Tanoto, Limantoba, Wadi Huang, Mahadianto Ong, Susanto Limurti, Nurjulisman, Besman Surbakti, Sanci Barus, Semangat Surbakti, Partogi Simanjuntak, and Marudut Simanjuntak. The GIZ2014-HASTAG5 committee members from UMSU are Dr. Agussani, Dr. Muhyarsyah, Ahmad Sinaga, M. Arifin Gultom, Rahmatullah, Munawar Alfansury Siregar, Khairul Umurani, Irma Dewi, Zurkiyah, M. Husin Gultom, Andre, Wirdatunnafiah, Tondi Amirsyah Putera, and Muhammad Irwan Syahputra.

We are also grateful for support by PT. Arsidi Bumi Pondasi, PT. Powerblock Indonesia, PT. Dexton, PT. Growth Sumatera, PT. Doshin Rubber, Bank OCBC NISP, PT. Adiwarna Anugerah Abadi, CV. Kokoh Bersama Sukses, PT. Jaya Beton, PT. Asia Sinar Inti Abadi, PT. Bilah Baja Makmur Abadi, PT. Greenland Garden Reality (Manhattan), PT. Cemindo Gemilang (Semen Merah Putih), PT. Putra Baja Deli, PT. Rekayasa Geoteknik Utama, PT. Provi Sinar Concrete, PT. NS Bluescope Lysaght Indonesia, Pt Hari Rezeki Kita Semua, PT. Datascrpit, PT. Multiplast Prima Jaya, PT. Kimia Konstruksindo, PT. Bata Pressindo, PT. Mulindo Raya Sejati, PT. Dutaraya Sejati, Royal Sumatra, Bank Mestika Dharma, PT. Perintis Pondasi Teknotama, PT. Catur Hagen Sentosa, CV. Indo Makmur Sentosa, Bank CIMB Niaga, PT. Tirta Kimia Engineering, PT. Kogelahar Indonusa, PT. Bina Baja Sejati, PT. Alvalaval Indonesia, PT. BASF Indonesia, Ramset, PT. Kreasi Beton Nusapersada.

Most importantly, we wish to express again our sincere gratitude and respect towards Professor Mamoru Mimura from Kyoto University, Japan; Dr. Netra Prakash Bhandary from Ehime University, Japan; Associate Professor Dr. Michael H. Scott from Oregon State University, US; Professor Shuyang Cao from Tongji University, Republic of China; and Professor Lap-Loi Chung from National Taiwan University, Republic of China.

Thank you all for your contribution to GIZ2014-HASTAG5.

Editor

Dr. Ade Faisal (UMSU, HASTAG)
Prof. Dr. Fauziah Ahmad (USM)

RUNDOWN OF PROGRAM

DAY 1 Monday (October 20, 2014)

Time	Activity	Presenter/Paper No.	Room	Time	Activity	Presenter/Paper No.	Room
08.00 - 09.00	Registration		Voyeur	08.00 - 09.00	None		Jupiter
09.00 - 09.45	Opening Ceremony		Ball room	09.00 - 09.45	None		Jupiter
09.45 - 10.15	Coffee Break		Ball room	09.45 - 10.15	None		Jupiter
10.15 - 11.10	**Keynote Speech 1**	*Prof. Mamoru Mimura*	Ball room	10.15 - 11.00	None		Jupiter
11.10 - 12.05	**Keynote Speech 2**	*Prof. Michael H. Scott*	Ball room	11.10 - 11.55	None		Jupiter
12.05 - 13.05	Lunch break		Ball room	12.05 - 13.05	None		Jupiter
13.05 - 15.20	*Construction & Material Exhibition 1*		Ball room	13.05 - 15.20	***Parallel Session 1***	GH01, GH02, GH03, GH04, GH05, GH07, GH11	Jupiter
15.30 - 16.00	Coffee Break		Ball room	15.30 - 16.00	Coffee Break		Jupiter
16.00 - 18.00	*Construction & Material Exhibition 2*		Ball room	16.00 - 18.00	***Parallel Session 2***	GH12, GH33, GH34, GH35, GH36, GH37	Jupiter
18.00 - 20.00	Break						
20.00 - 21.30	Welcoming Dinner		The Edge				

DAY 2 Tuesday (October 21, 2014)

Time	Activity	Presenter/Paper No.	Room	Time	Activity	Presenter/Paper No.	Room
08.30 - 10.00	*Construction & Material Exhibition 3*		Ball room	08.30 - 10.00	***Parallel Session 3***	GH19, GH20, GH21, GH22, GH27	Jupiter
10.00 - 10.15	Coffee Break		Ball room	10.00 - 10.15	Coffee Break		Jupiter
10.15 - 11.10	*Construction & Material Exhibition 4*		Ball room	10.15 - 11.10	***Parallel Session 4***	GH30, GH31, GH28	Jupiter
11.10 - 12.05	**Keynote Speech 3**	*Prof. Shuyang Cao*	Ball room	11.10 - 12.05	***Parallel Session 5***	GH29, GH32, GH38	Jupiter
12.05 - 13.00	Lunch Break		Ball room	12.05 - 13.00	Lunch Break		Ball room
13.00 - 15.00	*Construction & Material Exhibition 4*		Ball room	13.00 - 13.55	**Keynote Speech 4**	*Dr. Netra Prakash B.*	Jupiter
15.00 - 16.30	**Parallel Session 7**	GH08, GH09, GH16, GH17, GH18	Ball room	13.55 - 16.30	***Parallel Session 6***	GH14, GH15, GH13, GH23, GH26, GH24, GH06	Jupiter
16.30 - 16.45	Coffee Break		Ball room	16.30 - 16.45	Coffee Break		Jupiter
16.45 - 17.40	***Keynote Speech 5***	*Prof. Lap-Loi Chung*	Ball room				
17.40 - 18.10	Clossing Ceremony		Ball room				

DAY 3 **Wednesday (October 22, 2014) Short Course:** ***Structural Modeling for Earthquake Engineering with OpenSees***

TABLE OF CONTENT

GEOTECHNICAL ENGINEERING

GEOLOGY AND SEISMOLOGY ENGINEERING

HIDROLOGY AND CLIMATE CHANGE

KEYNOTE PAPERS

ISBN 979-458-758-3
Proceedings of the 3rd International Conference on the Geohazard Information
Zonation and 5th Seminar & Short Course of HASTAG (GIZ2014-HASTAG5)
Organized by UMSU, HASTAG, USM
Medan, Indonesia, October 20-22, 2014

Development of Geoinformatic Database and Its Utilization to Engineering Practice

Mamoru Mimura [1], Koji Yamamoto [2]

[1] Dept. Urban Management, Graduate School of Engineering, Kyoto University, Kyoto, Japan
[2] Geo-Informatics Engineering Group, Geo-Research Institute, Osaka, Japan

Abstract. Various databases for underground information have been developed in Japan. They have been independently developed and used for regional geotechnical research, construction management, evaluation for geo-hazard and geo-environmental assessment. The present status of geoinformatic databases in Japan is briefly explained followed by the several examples for application of them. Kansai geoinformatic database is selected to explain the utilization for description of subsoil structures. Discussion is extended to assessment for liquefaction potential that become the fundamental information for the regional action planning of disaster mitigation. The sophisticated procedure for integration and interconnection of the individual databases is also discussed by proposing the concept of "Representative Soil Profile Model" that is the mesh subsoil model for 250m square block. This mesh modeling is now conducted in the main large cities in Japan to establish the seamless national subsoil model to be utilized for the nationwide disaster mitigation planning.

Keywords: *Geotechnical Database, Boring Data, Geo-informatics, Liquefaction Potential, Geo-hazard*

1. Introduction

In the past several decades, huge amount of subsurface information has been accumulated in urban, suburban and rural areas in many countries for various purposes such as disaster mitigation, infrastructure development, urban development, and construction of high-rise buildings. Tremendous cost, energy and time have been spent for collecting the subsurface information. They are presented in various forms such as, for example, borehole logs, soil cross sections, soil test data sheets, geotechnical investigation reports, topographic maps, geological maps, and underground structure details. Presently they are scattered at various organizations (public and private) and stored in various ways (organized and disorganized). Some of the information may be buried under accumulated soil reports, or may be discarded periodically or at whatever time.

Being aware of huge amount of accumulated geotechnical information and the scatter and loss of valuable information that our predecessor collected in the past several decades, we, geotechnical engineers, as one would expect, think that such geotechnical information should be systematically collected, stored, and maintained and should be utilized effectively. Our world still has lots of problems to tackle as listed below for example, and money should not be wasted for repeating the same work.

- Disaster mitigation: Earthquakes, volcano eruptions, local down pours
- Problems particular to urban areas: Ground subsidence, flooding of underground space, slope collapses, heat island phenomena, contamination of soil and groundwater
- Infrastructure development and maintenance

Difficulties to handle past and old subsurface data actually existed because of;

- Data stored in analog form (paper)
- Insufficient computer processing ability to handle huge volume of data
- Lack of data storage technology
- Lack of application technology

The above difficulties, however, have gradually been removed due to advance of information technology, including computer hardware, digitizing technology, communication technology, data storage technology, and graphic technology.

Figure 1 shows the present status of geoinformatic databases regionally developed in Japan [1]. The individual databases have independently been developed with different procedures. It is true some of them are systematically constructed and operated, but many of them still remain as private and personal ones without opening to public. As is already stated above, geoinformatic databases have well been utilized for various purposes. However difference in the procedure of development and the structure of databases prevent the individual databases from linking, integrating one after another. Furthermore, the difference in the quality of these databases causes the uneven analyzed outputs based on them.

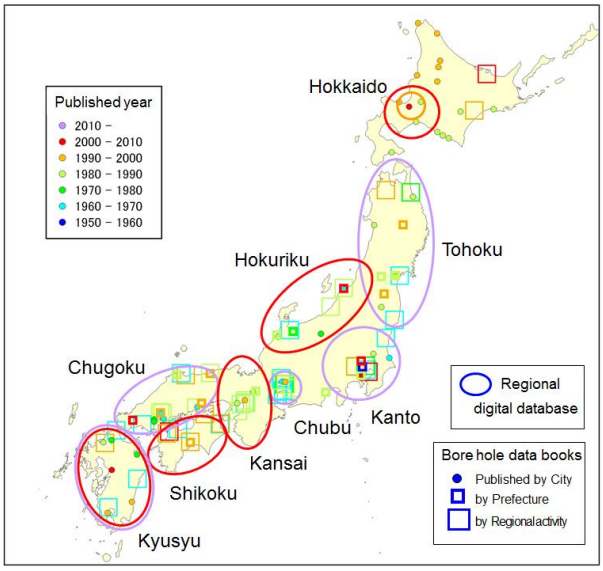

Figure 1 Location of the developed Geoinformatic Databases in Japan [1]

In the present paper, importance and significance of the development of geoinformatics databases are discussed particularly for the assessment of earthquake induced geo-hazard. It should be recognized that the modelling of subsoil structure seriously influences the evaluating ground motion. Liquefaction is also one of the most serious geotechnical problems of public concern. Geoinformatic database play a significant role to evaluate the possible occurrence of liquefaction. Examples of the latest achievement of liquefaction assessment in Japan are explained.

2. Development of Geoinformatic Database

Procedures to develop geoinformatics databases are not unique but full of variety [2]. They are strongly prescribed by local characteristics of geology as well as the status of development of the basic boring data. It means that the common procedures adopted without exception do not exist. The procedure to develop a geoinformatics database is hence explained by exemplifying the pioneer action in the Kansai area, Japan.

2.1. General description of Geo-informatics Database in Kansai

The Kansai Geo-informatics Database (GIbase) is comprised of more than 38,000 borehole data of geotechnical investigation and has been developed by cooperation among industrial-government-academic organizations in Kansai region over the past two decades [3]. Figure 2 shows the historical developments of GIbase. As already stated above, many large cities such as Osaka and Kobe have been developed on the Osaka Plains and adjacent coastal area along Osaka Bay where soft grounds are widely spread. Then, the development of these coastal areas required careful site investigations with a large number of borehole data. Extensive investigations of the Osaka Bay seabed were necessary for the waterfront development, such as Kansai International Airport and Phoenix Project of landfill for waste disposals. The Research Committee on Seabed Deposit of Osaka Bay (1984 – 1991) was established by the Kansai Branch of Japanese Geotechnical Society. Then, it was succeeded to the Research Council of Geotechnical Information on Osaka Bay. Based on the research activities under this council "Geotechnical Information Databases in Osaka Bay area" was constructed as the marine database. On the other hand, the Research Committee on Utilizing of Underground Space was established in 1989, mainly for dealing with development of public infrastructures by utilizing deep underground spaces in Osaka, Kobe and Kyoto. It was succeeded to the Geo-Database Information Committee on Kansai. The research activities under this

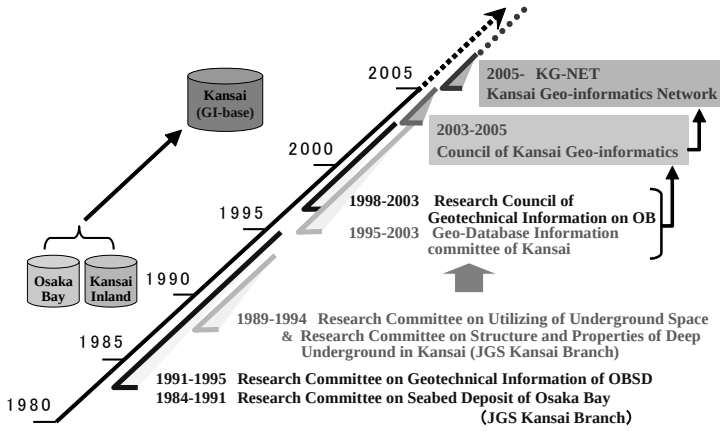

Figure 2 History of development of GIbase

committee have produced “Geotechnical Information Database in Kansai Inland”. These two databases were integrated into a single system in 2003, controlled by the Council of Kansai Geo-informatics and then the council has reorganized to form the Kansai Geo-informatics Network (KG-NET).

2.2. System and Input Data for Database

Kansai Geo-informatics Database (GIbase) was constructed by using Database for Information of Ground (DIG) system that was originally developed by Geo-Research Institute [4], [5]. The system used for DIG was constructed with a core management system assembling the boring data with its inherent format by extending the concept of relational database. It is composed of the following four functions:

(1) Function of total control (Host DB)

(2) Function of data input control (local DB)

(3) Function of data extraction and processing (AP)

(4) Function of data addition (Layer DB)

The main operation system is controlled by UNIX whereas the local DB is controlled by WINDOWS. For personal use, the WINDOWS version is provided for data extraction and processing (AP). By utilizing these functions, GDS stores the borehole investigation data of strata identification, SPT N-value, gradation test result etc. These data are utilized for prediction of liquefaction in sandy deposits during earthquake. Table 1 shows the input data and data structure of DIG. In addition to GDS, the information related to active faults and micro-topography is also stored by Geographical Information System (GIS).

The necessary handling functions to control the Geo-informatics database, DIG consists of five components, such as reference, extraction, processing, analysis and display. The fundamental functions of DIG are as follows:

(1) Indicating the location of each boring on the map and selecting the optional ones using mouse operation

(2) Referring the boring on optional condition

(3) Creating cross-sectional view of the ground by processing the selected borings

(4) Creating a summary table for soil properties and experimental results

(5) Processing experimental data and display the distribution chart, correlation chart etc.

Table 1 Input data and data structure of DIG

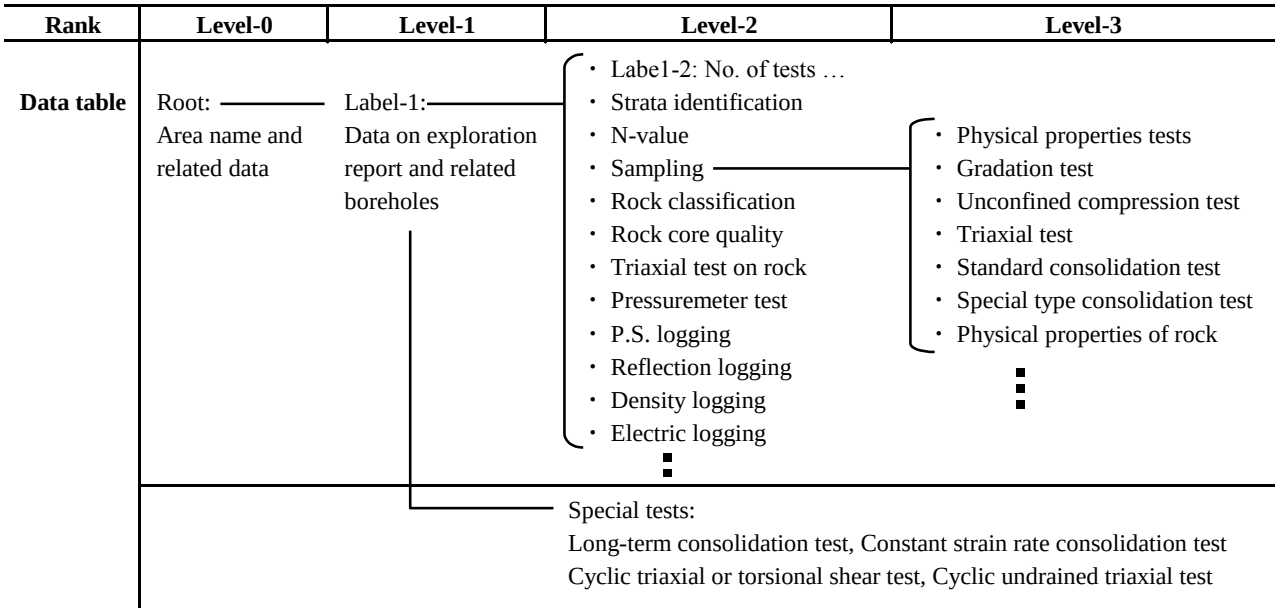

In addition to such basic functions, DIG also interfaces with application program for the extraction of regional ground characteristics or the examination results of earthquake disaster such as liquefaction

potential. The assessment of liquefaction introduced in the present paper, is effectively conducted by using the function of AP. DIG also has a special function that examines the quality of data by checking the treated data and getting rid of unsuitable ones for the purpose of forming data group. It is of importance for Geo-informatics database to be in high quality with reliability.

3. Investigation of Subsoil Condition Based on GIbase

Assessment for earthquake-induced geo-disasters strongly requires the subsoil condition together with the physical and mechanical properties. In the sense, the sophisticated database is indispensable to provide enough information on demand. In the following section, the relevant examples of the performance by GIbase for Osaka Plain and Kyoto Basin are introduced.

3.1 Osaka Plain

A representative cross-sectional view of subsurface ground for Osaka Plain is shown in Figure 3 based on the Kansai Geoinformatic Database [6]. The selected line is the east-west one including the center of Osaka City along the north of Osaka Castle. Uemachi Upland is located in the heart of Osaka where all strata are tilting by the prevalence of folded structure developed by the tectonic movement of the Uemachi Fault. Geological interpretation provides the identification of the individual subsoil layers, such as Ma and Dg as shown in Figure 3. Here, Ma and Dg denote "marine clay" and "Pleistocene sand gravel" respectively. On the west side of Osaka, the thick Holocene marine clay (Ma 13) layer exists underlain by the Pleistocene gravel layer (Dg 1) and the alternating Pleistocene deposits. The strata are rather stable and horizontally even. On the eastern part of Osaka, the basin structure can be seen between the Uemachi Upland and the Ikoma Mountains. The Holocene clay in this region is well-known as sensitive clay. At the Uemachi Upland, the old layers heaved by the tectonic movement and appear near the surface of the ground.

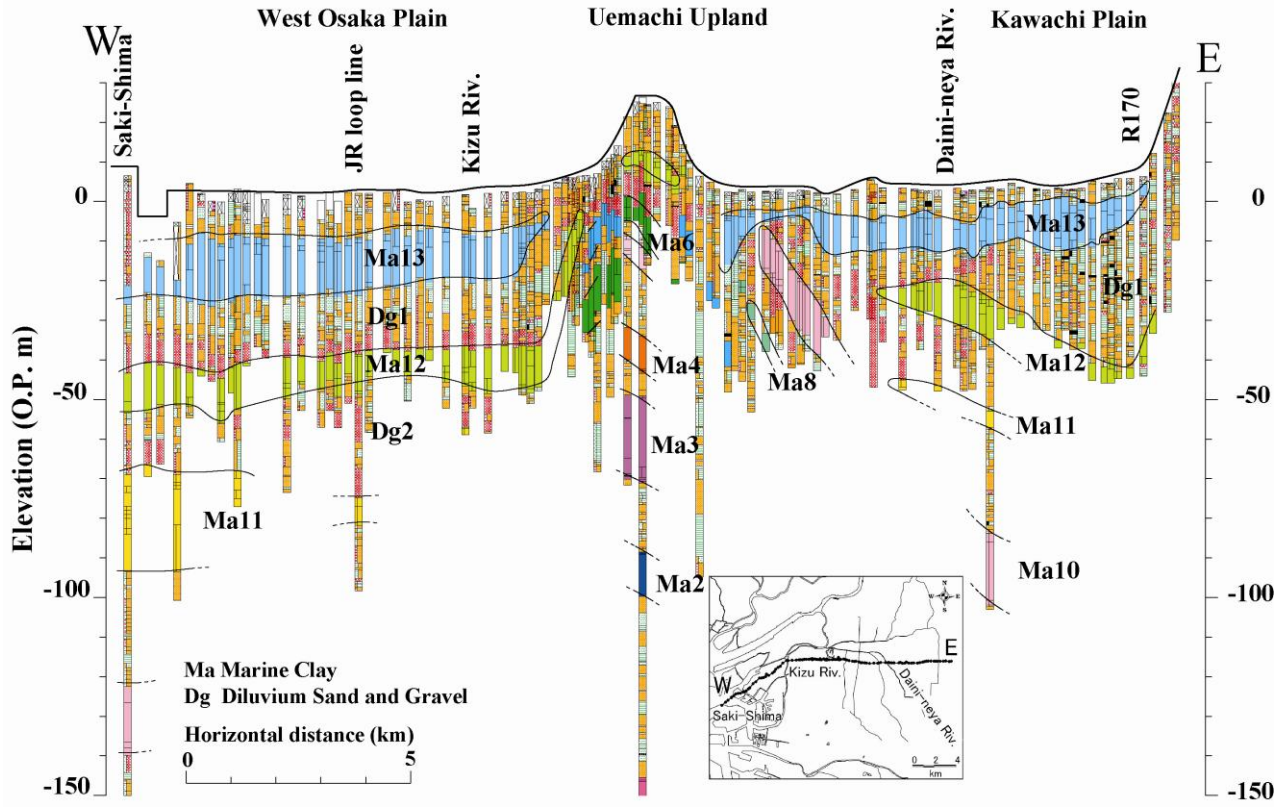

Figure 3 Example of the cross-sectional east-west view of subsurface ground in Osaka Plain

3.2 Kyoto Basin

A representative cross-sectional view of subsurface ground for Kyoto Basin is shown in Figure 4 drawn by the Geo-database [7]. The selected line crosses the center of Kyoto Basin from north to south. On the basis of the geological characteristics, the area can be divided into 4 regions. The elevation of the ground at the north end (north of Kyoto City) of this line exceeds 100m and continuously declines to the south. The

ground surface becomes almost flat at the Keihan Railway in region C. The difference in elevation is almost 90m between the north of Kyoto City and the Keihan Railway in a distance of about 17km. Compared to region I, the surface of region III and IV is flat with an elevation O.P. +10m to +20m. As is easily known, the subsoil of Kyoto Basin consists mainly of gravels in the northern part (region A and B) while soft fine soils such as silt and sand can be seen at the shallow part in the southern part (region C and D). Pleistocene marine clay (Ma 9) appears at the elevation of –40m to –50m. This clay was found from the deep borings, KD-1 and KD-2 and confirmed as marine clay by pollen analysis.

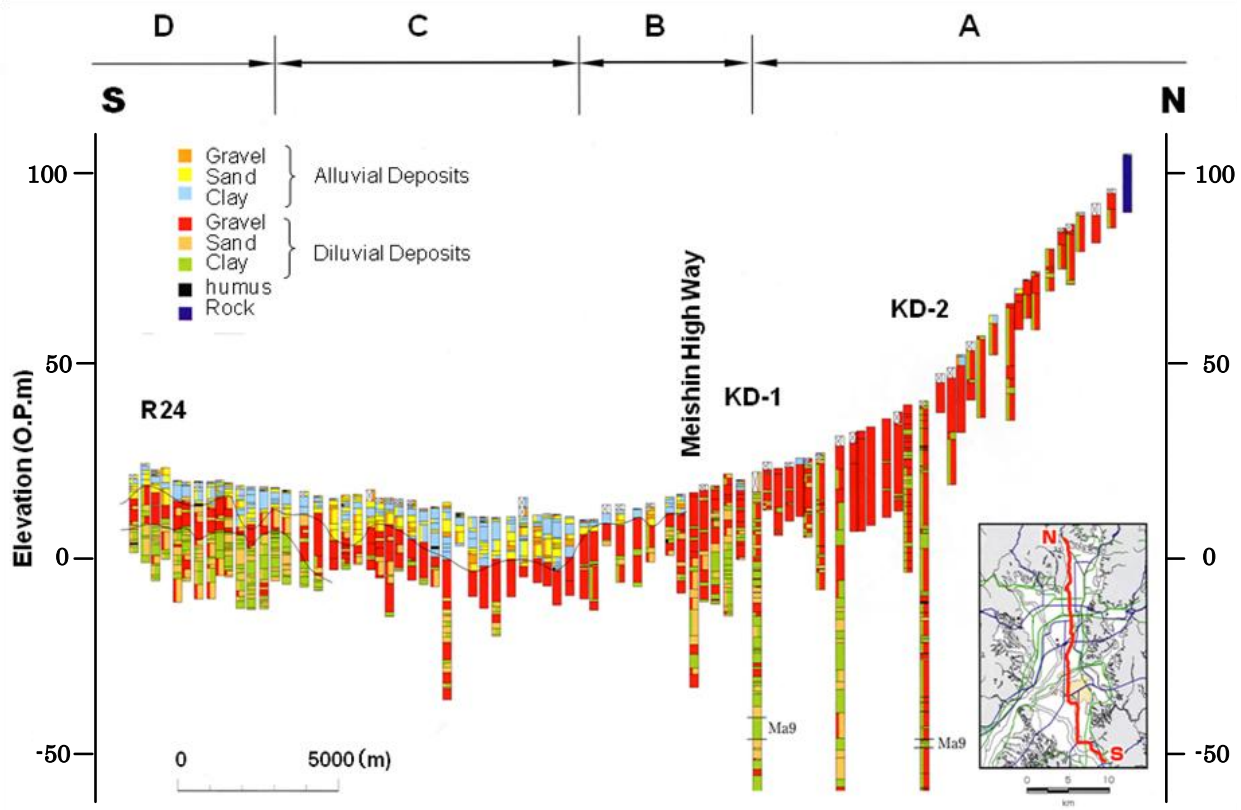

Figure 4 Example of the cross-sectional east-west view of subsurface ground in Kyoto Basin

4. Application to Geotechnical Problems ~Liquefaction Assessment~

Liquefaction has been highlighted since serious disaster induced by liquefaction occurred at Niigata Earthquake and Alaska Earthquake in 1964. A number of procedures for assessing liquefaction have been proposed and updated on the basis of the records of liquefaction by earthquakes taking place one after another. Laboratory tests such as undrained cyclic triaxial tests on reconstituted sand specimen have played significant roles for those studies on liquefaction. It is true that the experimental approach is important to know the mechanism of liquefaction, but the results from laboratory tests often have not provided a reasonable solution for the actual liquefaction disaster because liquefaction in the field is definitely the boundary value problem far from the laboratory conditions. In the practical sense, the regional distribution of hazardous area against liquefaction due to earthquake can provide very important and useful information for disaster mitigation. For this purpose, geo-database can function efficiently. In this chapter, simplified procedure assessing liquefaction potential is introduced and applied to evaluate the regional liquefaction potential based on the geoinformatic database.

4.1 Simplified procedure based on the geoinformatics database

The simplified procedure assessing liquefaction potential used in the present paper is a so-called F_L method specified in the "Specifications for highway bridges" by Japan Road Association [8]. This method has commonly used in Japan for designing the foundations. First, the safety factor against liquefaction, F_L is defined as follows:

$$F_L = R/L \tag{1}$$

Here, R denotes a liquefaction resistance and calculated by $R = c_w \cdot R_L$. The parameter, c_w is a correction factor depending on the type of earthquake. R_L is a cyclic stress ratio defining liquefaction in the laboratory. This parameter is usually derived from N_{SPT} values from standard penetration test (SPT) because it is not so common to carry out the undrained triaxial cyclic test on good quality sand samples. SPT is a simple and economical method to know the resistance of the foundation ground in the field, and commonly carried out for subsoil investigation. Naturally the Geo-database has the data of N_{SPT} profiles for almost all boring logs. Therefore, it is advantageous to introduce the present procedure for liquefaction assessment based on the N_{SPT} values. R_L can be calculated by the following equations:

$$R_L = \begin{cases} 0.0082 \cdot \sqrt{N_a / 1.7} \ \Lambda \ \Lambda \ \Lambda \ \Lambda \ \Lambda \ \Lambda \ \Lambda \ \Lambda \ \Lambda \ \Lambda \ \Lambda \ \Lambda \ (N_a < 14) \\ 0.0082 \cdot \sqrt{N_a / 1.7} + 1.6 \times 10^{-6} \cdot (N_a - 14)^{4.5} \ \Lambda \ \Lambda \ (N_a \geq 14) \end{cases} \quad (2)$$

Here, N_a is a corrected N_{SPT} value in terms of the effect of fine components and expressed as follows:

$$N_a = c_1 \cdot N_1 + c_2 \quad \text{(for sand)} \quad (3)$$

$$N_a = \left[1 - 0.36 \log_{10}(D_{50}/2)\right] \cdot N_1 \quad \text{(for gravel)} \quad (4)$$

Here, N_1 is a corrected N_{SPT} value in terms of confining stress. As is easily known, N_a can be calculated with mean particle size, D_{50} (in mm) and N_1 whereas more effect of fine components should be taken into account for sand with the correction coefficients c_1 and c_2. The coefficients c_1 and c_2 are assumed as follows:

$$c_1 = \begin{cases} 1 \Lambda \ \Lambda \ \Lambda \ \Lambda \ \Lambda \ \Lambda \ (0\% \leq FC \leq 10\%) \\ (FC + 40)/50 \Lambda \ (10\% \leq FC \leq 60\%) \\ FC/20 - 1 \Lambda \ \Lambda \ \Lambda \ \Lambda \ \Lambda \ (60\% \leq FC) \end{cases} \quad (5)$$

$$c_2 = \begin{cases} 0 \Lambda \ \Lambda \ \Lambda \ (0\% \leq FC \leq 10\%) \\ (FC - 10)/18 \Lambda \ (10\% \leq FC) \end{cases} \quad (6)$$

Here FC denotes fine components less than 74μm of diameter included in sand. As stated here, the liquefaction resistance, R_L can be derived from N_{SPT} values. The parameter, L denotes shear stress ratio mobilized in the ground during an earthquake and is expressed in the following form:

$$L = r_d \cdot c_z \cdot k_{hG} \cdot \frac{\sigma_v}{\sigma_v'} \quad (7)$$

Here, σ_v and σ'_v are total and effective overburden stresses in kgf/cm^2, c_z is a regional correction factor (c_z = 1.0 for Osaka, Kobe and Kyoto) that is determined on the basis of the probability of earthquake occurrence, k_{hG} is a horizontal seismic coefficient at the ground surface. The parameter, r_d is a reduction factor of the shear stress ratio during an earthquake in the vertical direction to consider the non-rigid response of the ground and expressed as follows:

$$r_d = 1.0 - 0.015 \cdot z \quad (8)$$

Here, z denotes a depth from the ground surface. Soil layers with F_L value larger than 1.0 are considered to be non-liquefiable while liquefaction potentially takes place in the case of $F_L \leq 1.0$. It is true

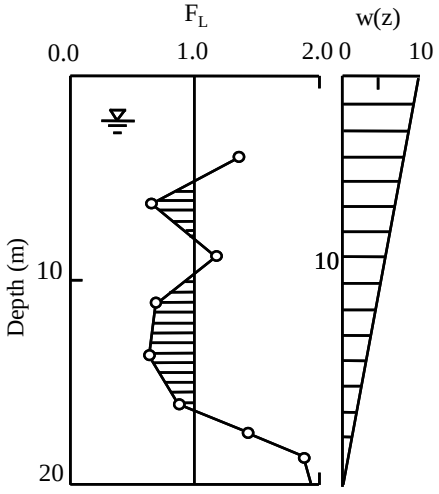

Figure 5 Derivation of liquefaction potential, P_L

that F_L denotes the safety factor at a certain depth but the integrated safety factor, P_L (Figure 5) is considered to represent the liquefaction of mass foundation, which directly induces serious geotechnical disaster. In the sense, P_L has been selected as the index for assessing liquefaction potential of regional ground in this paper. The integrated safety factor, P_L against liquefaction is defined as follows [9]:

$$P_L = \int_0^{20} F_L \cdot w(z)dz \qquad (9)$$

Here, w is a weighting function in terms of depth. Values of F_L are determined to be zero for $F_L \geq 1.0$ whereas 1- F_L for F_L <1.0.

4.2 Calculated performance for the Osaka Plain

On the basis of the development of evaluation procedure for liquefaction potential after 1995 Hyogoken-Nambu Earthquake, the assessment of liquefaction potential of Osaka Plain has been updated. In the present section, the latest outcome for the liquefaction potential of Osaka Plain [10] is explained following the prescribed scenarios of the earthquake occurrence. The flowchart of the assessment procedure is shown in Figure 6. The simplified procedure in terms of P_L method was also introduced, as is the case of Kobe and the adjacent area.

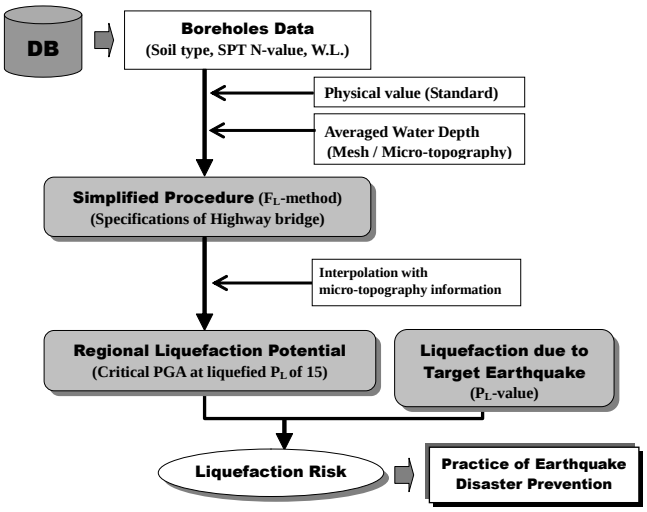

Figure 6 Flowchart of liquefaction assessment with simplified method

Each municipal office of local governments has earnestly begun to establish an action plan for earthquake disasters. The realistic action plan has to be associated with the possible earthquake disaster. For that purpose, the scenario earthquakes should be set on the basis of the knowledge by seismology and earthquake engineering. In the present section, the earthquakes induced by the Uemachi Fault, the typical and influential near fault earthquake, and by Tonankai/Nankai Earthquake, typical subduction zone earthquake, which hit Japan with 100 to 140 years interval are introduced for assessment. The hybrid method has been introduced to derive the realistic ground motion. The seismic ground motion on the engineering basement with S-wave velocity of more than 500m/s is calculated by the hybrid method with the Stochastic Green's Function Method and the 3-Dimensional Finite Differential Method. At the same time, the free surface response is considered based on the equivalent linearization technique and/or nonlinear analysis. Calculated distribution of P_L values of Osaka Plain is shown in Figure 7 (a) for Uemachi Earthquake and (b) for Tonankai/Nankai Earthquake based on the prescribed scenarios. As shown in Figure 7 (a), the expected liquefied area (P_L is larger than 15) is concentrated along the fault where the severe earthquake-induced acceleration is predicted because the Uemachi Fault is a reverse one situated in the central Osaka Plain. On the contrary, little liquefaction is expected to occur on the Uemachi Plateau where they have no soft soils in the ground. Liquefaction is also expected along the coast of Osaka bay as well as the areas along rivers where soft soils are normally situated with relatively high underground water table. It is found that serious liquefaction-induced disaster takes place all over Osaka Plain when the Uemachi Fault breaks. Figure 7 (b) shows the distribution of P_L values due to Tonankai/Nankai Earthquake. It is true P_L values are high for the coastal area as well as the areas along rivers but compared to the case of the Uemachi Earthquake, we have smaller P_L for this subduction zone earthquake because the maximum acceleration expected by this earthquake is not so large. Liquefaction disasters by this subduction zone earthquake seems to be more mild for the present scenario by the estimated P_L values while the easily liquefied area is widely expected to distribute. However, it does not mean that the possible liquefaction-induced disasters by Tonankai/Nankai Earthquake because the effect of long-term duration of tremor by the subduction zone earthquake on the liquefaction is still unknown. The assessment of the important facilities against liquefaction has to be conducted with more sophisticated manner such as the finite element analysis based on the effective stress.

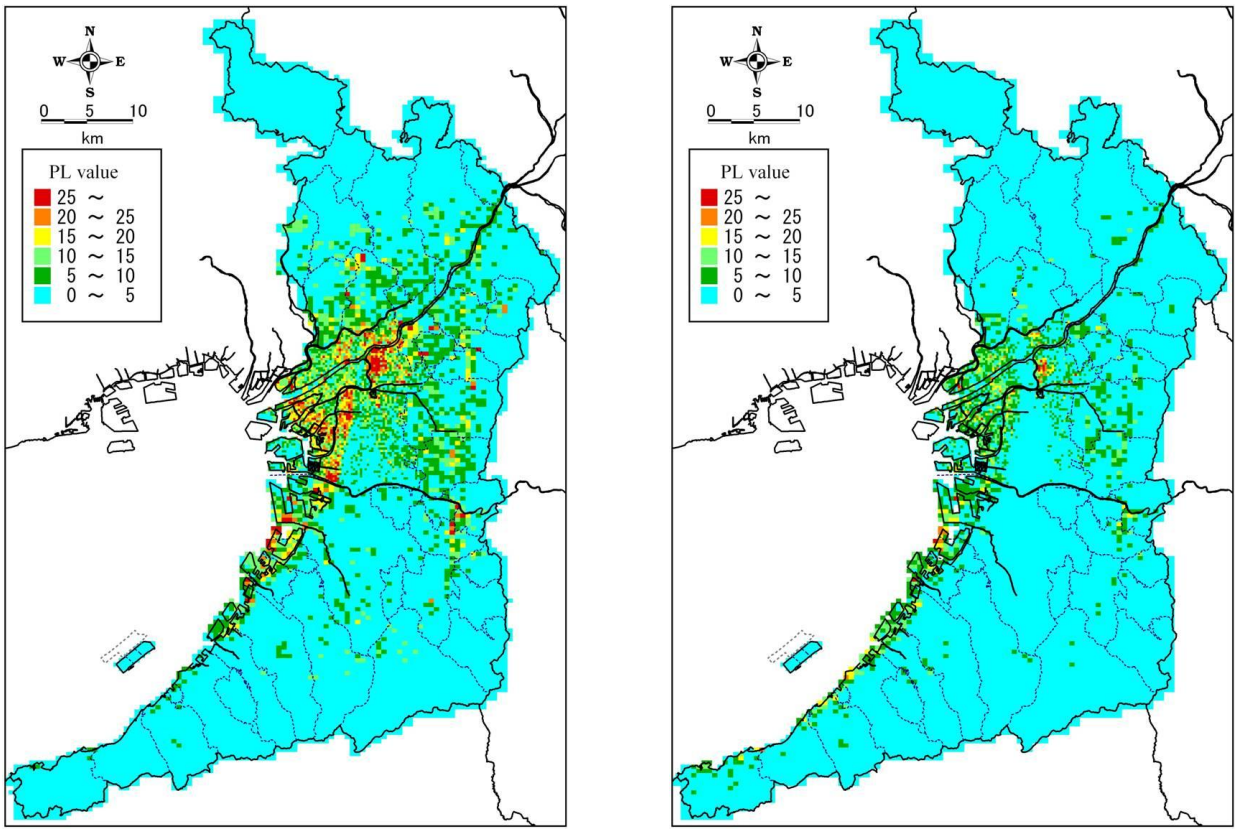

Figure 7 Liquefaction assessments in terms of the calculated distribution of P_L for (a) near fault earthquake (Uemachi Fault) and (b) subduction zone earthquake (Tonankai/Nankai Earthquake)

As is the case for Kobe area, the critical acceleration that is defined as the acceleration by which the estimated P_L value becomes 15 is calculated as a threshold for the occurrence of liquefaction-induced disasters [11] also for Osaka Plain. The distribution of the critical accelerations for Osaka Plain is shown in Figure 8 (a) by the near fault earthquake and (b) for the subduction zone earthquake respectively. In both figures, seriously fragile area coincides with the heart of Osaka metropolitan zone. The lowlands along Yodo River as well as the reclaimed coastal area also cannot resist against liquefaction. The main reasons for those results consist in the facts that they have thick weak sandy deposits on the very thick sediments together with high groundwater tables. As the impact of the earthquake intensity by the near fault earthquake is stronger, the induced hazard by the liquefaction is more serious compared to the subduction zone earthquake with much more huge magnitude. However, another factor of duration of tremor should be considered for the subduction zone earthquake. The seismic wave with a long period is expected to propagate and keep on hitting the Osaka Plain in the case of the subduction zone earthquake, such as Tonankai/Nankai Earthquake. In summary, the level of acceleration expected on the Osaka Plain by the subduction zone earthquake is not so severe, but the tremor continues for a long time. Here, the question arises; “Does the present evaluation with the simplified procedure based on the acceleration function well?” The contribution of the long duration of tremor with relatively low acceleration to the occurrence of liquefaction could be an issue.

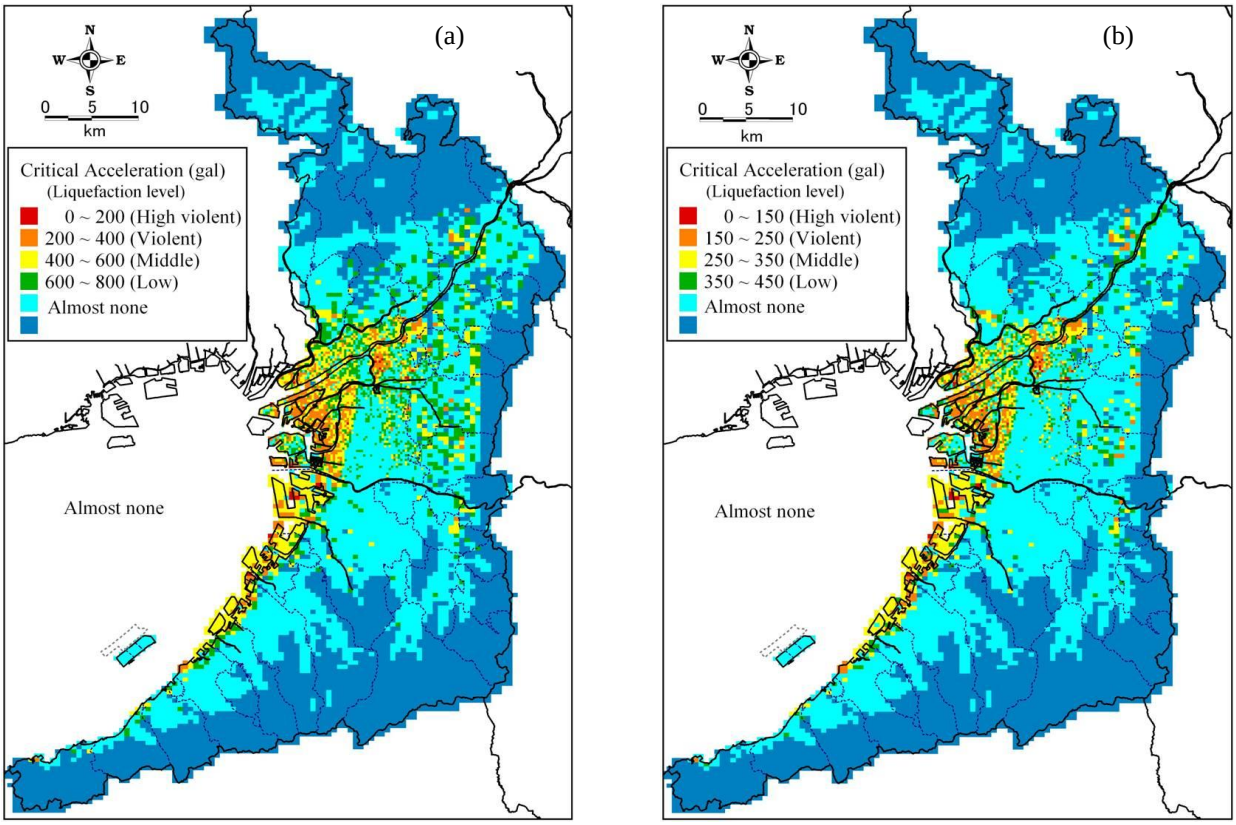

Figure 8 Fragility for liquefaction in terms of critical acceleration that induces liquefaction for (a) near fault earthquake (Uemachi Fault) and (b) subduction zone earthquake (Tonankai/Nankai Earthquake)

5. Representative Soil Profile Model

Representative soil profile model is defined as a set of soil models of the Holocene layers that are developed for 250m square mesh with the nation-wide prescribed standard code. It is true the present existing geoinformatic databases have been utilized mainly for disaster mitigation analysis but we still have serious problems shown as follows:

(1) It is not easy to unite individual geoinformatic databases that have been locally developed independently because the procedure to develop databases is not always the same and the data contained in the individual database are manifold.

(2) Not all existing databases are freely accessible because various regulations are imposed for opening to the public based on the ownership for boring data included in databases.

In order to overcome the above shortcomings, the idea of RSPM has been contrived [12]. RSPM is developed by collecting individual boring data in the geoinformatic database in the target mesh with 250m square, and the representative soil types and properties are rationally determined with depth based on the professional knowledge of topography, geology and geotechnology. The modeling with professional interpretation guarantees RSPM to be reliable and user friendly. Additionally, RSPM can be open to the public without any difficulties because the completed RSPM no longer contains individual information of each boring that is often regulated by the ownership. RSPM should be utilized for disaster mitigation planning by municipal sectors, evaluation of nation-wide geotechnical condition and basic information to purchase a residential lot.

5.1 Procedure to develop RPSM

A procedure to develop RSPM is shown in Figure 9 [13]. Individual local geoinformatic databases and RSPM are sound foundations for the nation-wide RSPM. It should be emphasized that even local RSPM has to be developed by the nation-wide prescribed standard code to keep common structures among them. The basic concept to develop RSPM advances as follows:

(1) The base data are prepared based on the local geoinformatic database supported by the accumulated topographical, geological and geotechnical research.
(2) Representative soil information for 250m square mesh is extracted.
(3) Design soil layers are set and sorting the data within the target mesh.
(4) Representative soil profile models are completed.

Here, note that the irreducible minimum information should be installed to keep an equivalent quality among the individual RSPM considering the networking and unification. The names of soil classification are designated as gravelly soils (G), Sandy soil (S), Clayey soil (Cs), Organic soil (O), Volcanic fine soil (V), Peaty soil (Pt) and Artificial soil (Am) by obeying the JGS standard.

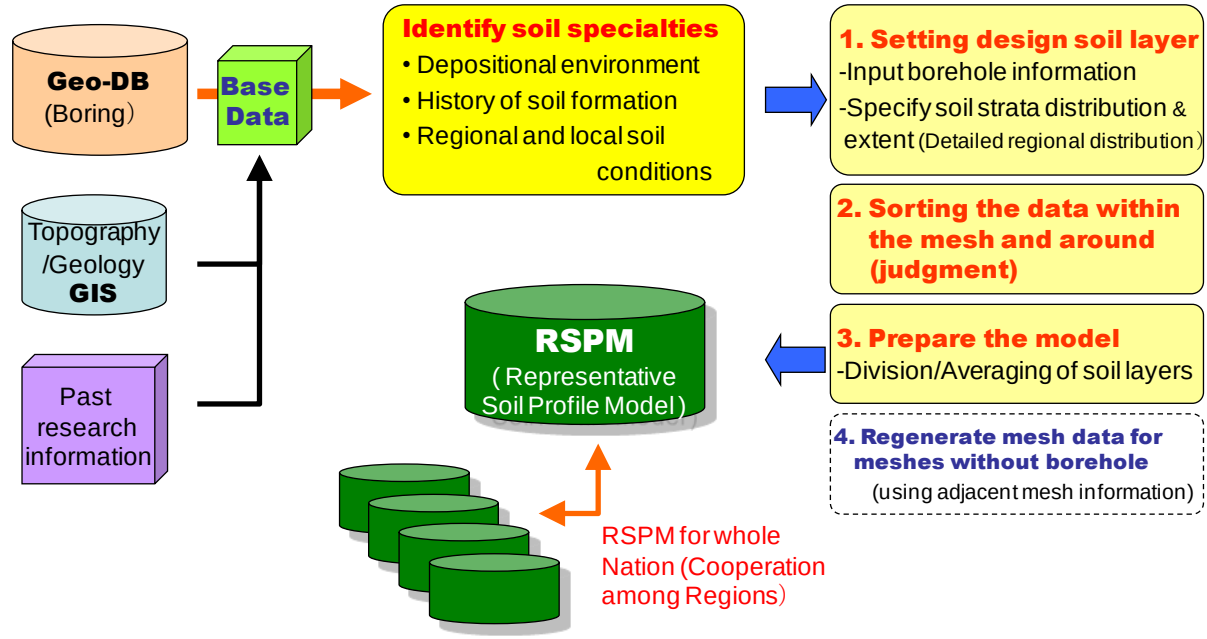

Figure 9 Procedure to develop Representative Soil Profile Model (RSPM)

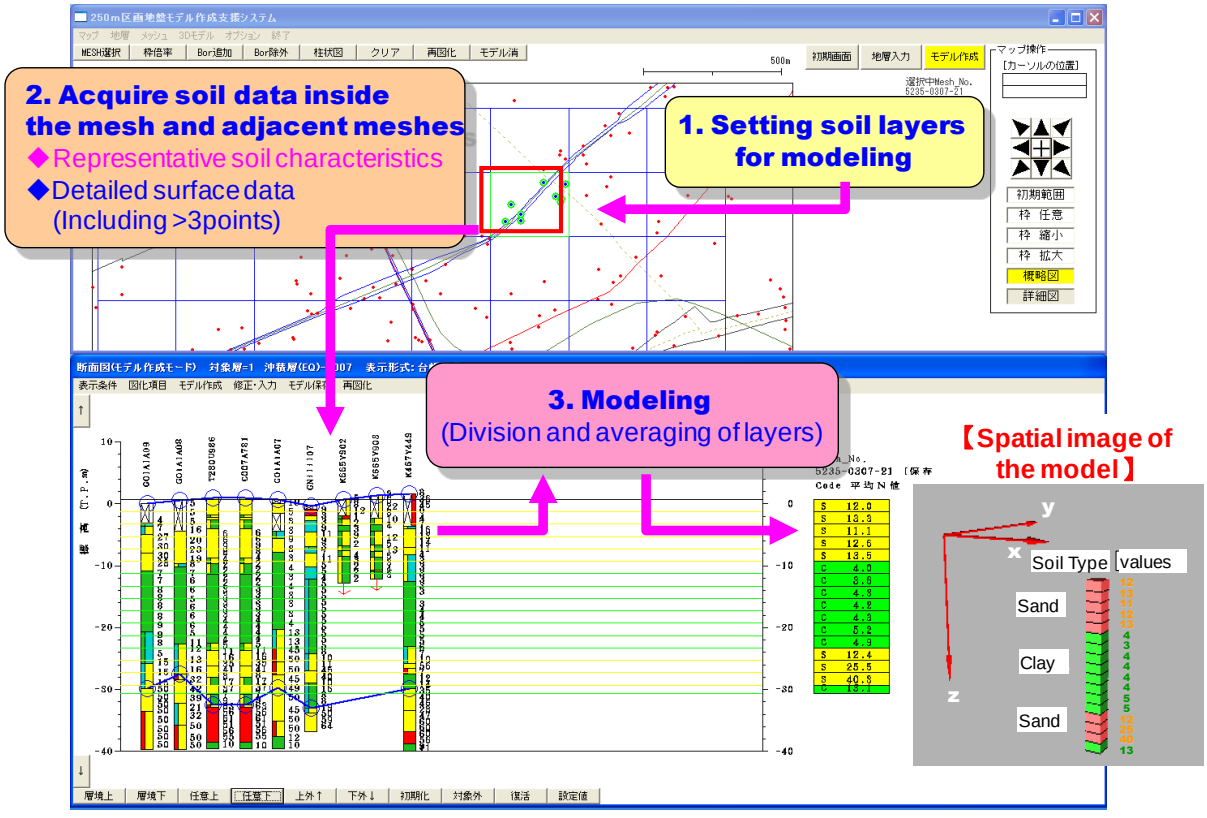

Figure 10 Operating window of the supporting system to develop Representative Soil Profile Model (RSPM)

Figure 10 shows the operating windows of the supporting system for RSPM development. First, the target soil layers are set for individual borings in the target mesh. At present, the target soil layer is designated as the Holocene one. Secondly, the necessary soil data inside the mesh and the adjacent mesh are acquired considering the representative soil characteristics. At the time, the selected borings are shown as a columnar chart with the Holocene borders. Thirdly, the appropriate soil columnar model for the target mesh is developed from the selected boring data. During this process, the boring data that do not represent the geotechnical characteristics of the target mesh are eliminated. In the present procedure, the soil layers are divided into every 2m thickness. The predominant soil type is selected as a representative with the average N_{SPT} and soil properties. The derived soil model and the spatial image of the model are also shown in Figure 10. Finally RSPM for a certain area is developed by unifying the individual soil model.

5.2 Example of RSPM for Osaka Basin

The area of 10km square in the heart of Osaka is selected as a pilot area for developing RSPM. This area is characterized by the existence of the Uemachi Upland of the Pleistocene origin that divides Osaka Plain into western lowland with coastal reclaimed area and eastern Osaka Plain. Various subsoil conditions can be encountered in this target area, namely, almost flat thick Holocene clay is widely situated in western Osaka Plain whereas very sensitive Holocene clays locally exist on the buried valley in eastern Osaka Plain. Those characteristic subsoil conditions have been reported in detail [6]. Figure 11 shows the distribution of the number of borings in individual mesh with 250m square. Proportion of the number of borings in 250m mesh in Osaka Plain is shown in Figure 12. As is shown clearly, 40% of all meshes contain more than 4 borings because the big metropolis such as Osaka city has a large number of borings due to sufficient number of construction projects. On the other hand, 40% of all meshes contain less than 2 borings and 12% of all have no boring in the 250 square area. We have to adopt the rational scheme for interpolation for such vacant meshes.

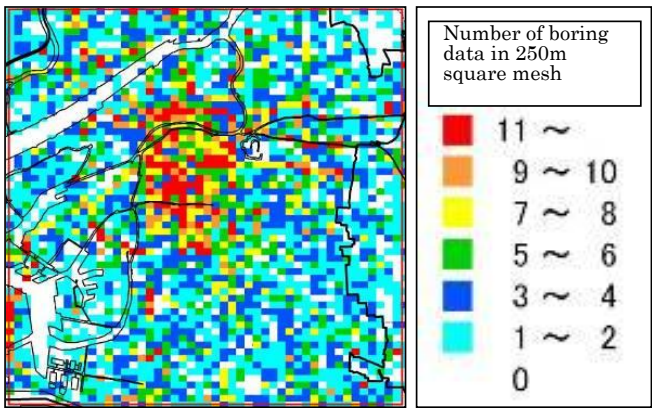

Figure 11 Distribution of the number of borings in 250m square mesh in the Osaka Plain

Here, when appropriate boring data are selected to develop the representative soil profile model, we have to attach importance to the following points. (1) The selected borings should exhibit the topographical, geological and geotechnical characteristics. (2) The scheme should be free from a personal arbitrariness. (3) The scheme should hold enough efficiency and be plain. Considering the above-mentioned demands, three different methods have been introduced to develop RSPM as follows:

Method A: All boring information in the target mesh is implicitly averaged.

Method B: Boring data are added from the surrounding areas with the 1.5 times of the target mesh. Then, all boring information including the subjoined one is implicitly averaged.

Method C: Appropriate borings are selected to reflect the topographical, geological and geotechnical characteristics of the target mesh. All boring information selected is averaged.

For the present pilot study, when the number of borings in the mesh is more than three and the borings distribute uniformly (see Figure 12), Method A is adopted because this method is the easiest and completely free from personal arbitrariness. When the number of borings is less than 2 and/or the distribution of boring location seems unbalanced even if we have sufficient borings, Method B is adopted to increase the number of borings and reflect the representative geotechnical characteristics of the target mesh. Both Method A and B are adopted for the meshes whose subsoil condition is rather

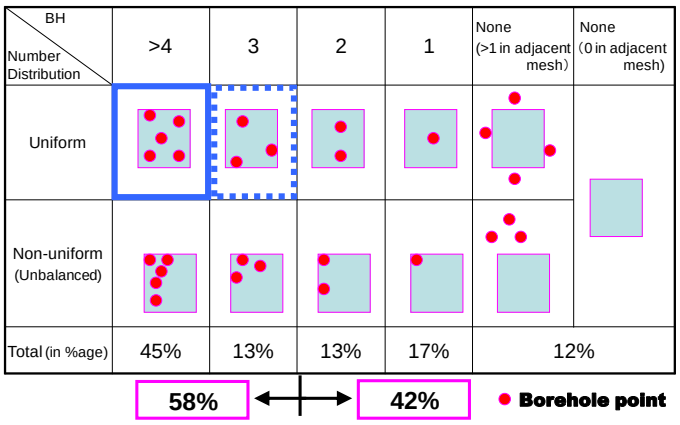

Figure 12 Proportion of the number and pattern of location of borings in 250m square

uniform and stable. However, in the case that the subsoil condition is non-uniform or changes drastically, those methods cannot be adopted even if we have sufficient number of borings in the target mesh. When the complicated subsoil condition is expected such as fault effect and existence of buried valleys and so on, Method C has to be adopted. It is not automatically determined which methods should be used for a certain mesh. Topographical, geological and geotechnical experts can judge which ones to be adopted on the basis of their scientific knowledge. In the present pilot study, Kansai Geoinformatic Database has functioned well to evaluate the subsoil conditions of Osaka Plain. Produced example of RSPM is shown in Figure 13. The target mesh has only 2 borings and they are also non-uniformly located at the north of the mesh. Under this circumstance Method A provides the model of sandy layers underlain by gravel stratum. To overcome non-uniform distribution of the borings Method B is also applied by subjoining another 2 borings from the adjacent mesh obeying the rule to enlarge the target area by 1.5 times. Then, the derived model consists of clayey soils having sandwiched gravelly layer due to too much effect of the existence of clayey deposit in the southern mesh. According to Kansai Geoinformatic Database, clayey stratum becomes poorer towards west and sandy layer holds mode gravels in this area. Based on this scientific knowledge, the authors selected 2 borings from the adjacent southern mesh by eliminating 2borings selected for Method B. Then Method C provides the model of alternating clayey and sandy layers underlain by gravel stratum. Because geographical and geological interpretation has support the subsoil model by Method C, the model by Method C has become RSPM for this mesh.

A representative cross-sectional view of subsurface ground for Osaka Plain is shown in Figure 13. The selected line is the one through the downtown Osaka on the north of the Osaka Castle. Uemachi Upland is located in the heart of Osaka where all strata are tilting by the prevalence of folded structure developed by the tectonic movement of the Uemachi Fault. On the west side of Osaka, the thick Holocene marine clay (Ma 13) layer exists underlain by the Pleistocene gravel layer and the alternating Pleistocene deposits. The strata are rather stable and horizontally sedimented. On the eastern part of Osaka, the basin structure can be seen between the Uemachi Upland and the Ikoma Mountains. The Holocene clay in this region is well-known as sensitive clay. The characteristic subsoil structure of the Osaka Plain is found to be well represented by the RPSM.

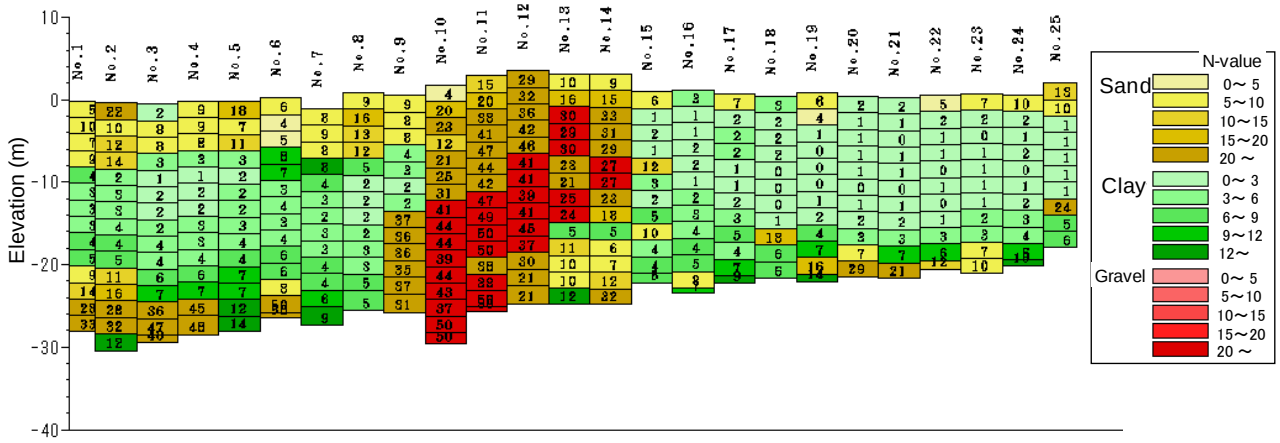

Figure 13 Example of cross-sectional view for subsoil stratification of Osaka Plain by "Representative Soil Profile Model" (Each column is a representative in 250m square mesh)

6. CONCLUSIONS

The present status of geoinformatic databases is Japan was briefly introduced. Various geoinformatic databases have recently been developed under the auspices of associations, national or local government and private sectors and utilized for geotechnical research, construction planning and assessment of disaster mitigation etc. The example of subsoil structures for Osaka Plain and Kyoto Basin were exhibited on the basis of Kansai Geoinformatic Database. The subsoil structure of Osaka Plain as a deltaic plain with the fault is completely different from that of Kyoto Basin as an alluvial fan. It should be noted that geological interpretation is indispensable to make the quality of the individual geoinformatic databases higher because the environment of sedimentation and the tectonic movement remarkably reflect the subsoil stratigraphy.

The Kansai Geoinformatic Database is utilized for the research of local foundations in Kansai, the primary information to construction projects and political assessment of disaster mitigation etc. As a typical

example, the application to the assessment of liquefaction is explained in the present paper. Huge number of boring data is required to assess the liquefaction potential for metropolitan area like Osaka to cover the whole widely spread area. In the case, the geoinformatic database can easily provide the necessary geological and geotechnical information which are directly connected to the various procedures to evaluate liquefaction and the induced geo-disasters. The expected earthquakes are assumed to occur and the scenario earthquake induced forces are calculated based on the knowledge of seismology and earthquake engineering. The simplified method provided the local fragility for liquefaction in terms of "critical acceleration" to derive P_L values of 15 that coincides with the occurrence of serious liquefaction induced disasters. On the other hand, the distribution of P_L values calculated using the scenario earthquakes (near fault and subduction zone earthquakes) exhibited the same mode of liquefaction occurrence qualitatively. Long-term tremor is another point of discussion to evaluate the liquefaction potential when the subduction zone earthquake, such as Tonankai/Nankai Earthquake hit Kansai area because the present procedures have never been validated for such type earthquake yet.

Representative Soil Profile Model (RSPM) has been developed by collecting individual boring data in the target mesh with 250m square, and the representative soil types and properties are rationally determined with depth based on the professional knowledge of topography, geology and geotechnology. RSPM is constructed with the nation-wide standard code to have a common structure among the individual RSPM considering the networking and unification. The fundamental concepts for RSPM are as follows: (1) Selected borings should exhibit the topographical, geological and geotechnical characteristics. (2) The scheme should be free from a personal arbitrariness. (3) The scheme should hold enough efficiency and be plain. 10km square of Osaka Plain has been selected as a pilot site for RSPM. Considering the subsoil conditions, we have to use different procedures to develop the representative soil profile models for the target meshes. A due attention should be paid to the case in which the complicated subsoil condition is expected such as fault effect and existence of buried valleys and so on. It is noted that non-automatic procedure with topographical, geological and geotechnical interpretation should be introduced to develop RSPM for the area with the complicated subsoil condition. The nationwide project to link the individual databases by introducing the concept of RSPM is being advanced in Japan to make the seamless subsoil model in the equivalent quality.

7. REFERENCES

[1] H. Todo, K. Yamamoto. Geological Models and Geotechnical Models -Lessons from Development of Japan-wide Geotechnical Ground Models -. *Proc. of Conference on the 3rd Geohazard Information Zone and the 5th Seminar and Short Course of HASTAG*: 2014, (in printing)

[2] ATC10 UrbanGeo-informatics. Case Histories of Urban Geo-informatics –the first draft-.: 2003, 104p

[3] Y. Tanaka, and Y. Tsukada. Geotechnical Database of Kansai - History and Developments- *Proc. of the International Symposium on Geo-informatics and Zoning for Hazard Mapping*: 2009, pp.85-92

[4] K. Yamamoto, Y. Iwasaki, and S. Suwa, S. Concept and Development for Database System of Geotechnical Engineering Information", *Proc. 34th soil engineering symposium, JGS*, 1989, pp.195-202 (in Japanese).

[5] Y. Iwasaki, S. Suwa and K.Yamamoto. Concept and Development of Geotechnical Database System for Regional Geotechnical and Geological Iinformation. *Geoinformatics*, Vol.1, No.1, 1990, pp.103-113 (in Japanese).

[6] Geo-Database Information Committee of Kansai. Shin Kansai Jiban -Osaka Plain-, 2007, 450p., (in Japanese).

[7] Geo-Database Information Committee of Kansai. Shin Kansai Jiban -Kyoto Basin-, 2002, 196p., (in Japanese).

[8] Japan Road Association. Earthquake resistant design, specifications for highway bridges. 2012, 318p., (in Japanese).

[9] T. Iwasaki, F. Tatsuoka, K. Tokita and S. Yasuda. Estimation of Degree of Soil Liquefaction During Earthquake, *TSUCHI-TO-KISO*, Vol. 28, No. 4, 1980, pp.23-29, (in Japanese).

[10] M. Mimura and K. Yamamoto, Development of Geo-database and Its Utilization for Assessment of Liquefaction. *Proc. International Geotechnical Symposium "GEOTECHNICAL ENGINEERING FOR DISASTER PREVENTION & REDUCTION"*, 2007, pp. 91-102.

[11] F. Oka, F, M. Mimura and K. Yamamoto. Liquefaction Due to Hyogoken-Nambu Earthquake and Prediction Methods. *Proc. Symp. on mechanism of liquefaction and prediction & design methods for liquefaction*, JGS, 1999, pp.511-516, (in Japanese).

[12] M. Mimura and K. Yamamoto. Representative Soil Profile Model Based on Geoinformatic Database. *Proc. International Symposium on Geoinformatics and Zoning for Hazard Mapping*, 2009, pp. 71-78.

[13] M. Mimura and K. Yamamoto. Development of Representative Soil Profile Model Based on Geoinformatic Database. *Proc. International Symposium and Exhibition on Geoinformation 2008*, Keynote Session 1, CD-R, 2008.

ISBN 979-458-758-3
Proceedings of the 3rd International Conference on the Geohazard Information
Zonation and 5th Seminar & Short Course of HASTAG (GIZ2014-HASTAG5)
Organized by UMSU, HASTAG, USM
Medan, Indonesia, October 20-22, 2014

The Evolution of OpenSees: Is the Open Source Model a Success?

Michael H. Scott[1]

[1]Associate Professor, School of Civil and Construction Engineering, Oregon State University, Corvallis, USA
Email: michael.scott@oregonstate.edu

Abstract. OpenSees, the Open System for Earthquake Engineering Simulation, was created in 1997 as an object-oriented framework for structural finite element analysis. At that time, many similar frameworks were developed with implementation details archived in peer-reviewed journal articles, but they rapidly disappeared. OpenSees on the other hand, has endured in the structural and geotechnical engineering communities for both research and practical use. A history of the evolution of OpenSees from a Ph.D. dissertation on parallel computing to its current broad international user base is provided along with a trace of its initial functionality to the wide array of applications for which it is deployed today. The reasons for OpenSees' longevity are explored in addition to the advantages and disadvantages of its open source development model weighed in conjunction with its flexible software design.

Keywords*:* *Computer simulation, structural engineering, geotechnical engineering*

ISBN 979-458-758-3
Proceedings of the 3rd International Conference on the Geohazard Information
Zonation and 5th Seminar & Short Course of HASTAG (GIZ2014-HASTAG5)
Organized by UMSU, HASTAG, USM
Medan, Indonesia, October 20-22, 2014

Advanced Physical and Numerical Modeling of Atmospheric Boundary Layer

Shuyang Cao
[1]*Professor State Key Lab for Disaster Reduction in Civil Engineering, Tongji University, Shanghai, China, shuyang@tongji.edu.cn*

Abstract. Appropriate modeling of an Atmospheric Boundary Layer is necessary in order to estimate the wind load on structures. Modeling of an ABL usually involves the modeling of statistical features of the flow such as mean velocity, turbulence intensity, power spectrum and so on, but sometimes also requires the reproduction of the time series of wind speed when transient features of the wind are of concern. This paper introduces the improvements of mathematical, physical and CFD approaches utilized to model the Atmospheric Boundary Layer flow for structural wind engineering applications. The necessity of considering the organized turbulence structure of an ABL is emphasized. In addition, CFD simulations of the ABL over hilly terrain and sea surface are introduced.

Keywords: ABL, CFD, Wind tunnel, Random process, hilly terrain, sea surface

Introduction

Wind load and wind-resistance performance of wind-sensitive structures such as high-rise buildings, long-span bridges and large-roof structures are the great concerns of structural engineers. Because the structures are immersed in an Atmospheric Boundary Layer (ABL), appropriate modeling of an ABL is a premise of the procedure in estimating the dynamic interaction between the wind and structure. Modeling of an ABL usually involves the modeling of statistical features of the flow such as mean velocity, turbulence intensity, power spectrum and so on, but sometimes also requires the reproduction of the time series of wind speed when transient features of the wind are the study subject. This paper introduces the mathematical, wind tunnel and CFD approaches adopted to model the ABL flow in the structural wind engineering filed. The necessity of considering the organized turbulence structure of the ABL is emphasized. In addition, CFD simulations of the ABL over hilly terrain and sea surface are introduced as examples of the CFD approach.

Mathematical methods

A fast Fourier transform (FFT) based mathematical method is often employed to transform signals between time (or spatial) domain and frequency domain, which has many applications in physics and engineering [Bracewell R.N. (1986), Brigham E.O. (1988)]. One of the most important parts of the mathematical simulation methodology is the generation of the stochastic processes, fields and waves involved in the problem. The generated sample functions must accurately describe the probabilistic characteristics of the corresponding stochastic processes, fields or waves that may be either stationary or non-stationary, homogeneous or non-homogeneous, one-dimensional or multi-dimensional, univariate or multi-variate, Gaussian or non-Gaussian [Shinozuka and Deodatis (1996)]. Initially, the mathematical simulation techniques focused on the generation of one-dimensional and univariate processes. The simulation of processes with more than a single

dimension or a single component was first addressed by Borgman [1969] and Shinozuka [1970, 1972], and Shinozuka and Jan [1972]. Traditionally, the method based on the summation of trigonometric series with random phase angles has been the most popular, perhaps due to its simplicity. The multivariate processes are generated by implementing a stochastic decomposition scheme that exploits the concept of decomposing a set of correlated processes into a number of component processes. When the cross-spectral density matrix of an *n*-variate process is specified, its component processes can be simulated as the sum of cosine functions with random frequencies and random phase angles. Meanwhile, simulation of multivariate processes based on digital filtering was accomplished by first simulating a family of uncorrelated processes and subsequently imposing the appropriate correlation structure by a transformation [Li and Kareem 1993]. More developments in digital filtering techniques include state space modeling, autoregressive (AR), moving average (MA), and the combination autoregressive and moving averages (ARMA) models [Kareem 1987, Reed and Scanlan 1984, Li and Kareem 1993]. In addition, the wavelet transform, Hilbert transform and POD analysis have been incorporated into the mathematical approaches, which make the simulation of evolutionary characteristics of transient winds possible [Kitagawa and Nomura 2003, Wang 2006].

Although the above techniques vary in their applicability, complexity, computer storage requirement, and computing time, many simulated data show excellent agreement with the specified wind features, including the target spectral characteristics of the wind that makes the mathematical method very suitable to wind engineering application. The mathematical technique has immediate applications to the simulation of real-time processes, e.g., simulate the evolutionary characteristics of transient winds in order to explore the non-stationary thunderstorm wind loading on structures [Wang et al. 2013]. Meanwhile, the time-dependent velocity fluctuations modeled by mathematical approach are often utilized as the inlet flow boundary condition for the CFD approach. On the other hand, the movement of wind flow in the ABL is determined by the governing equations of the fluids, so the atmospheric turbulence is not a pure random process. It contains organized turbulence structures as other turbulent boundary layers. However, with more wind speed features considered in the process of mathematical simulation, we may expect that the simulated flow field approaches to the real one and is suitable to wind engineering application.

Wind tunnel modeling

The model test in a wind tunnel is considered the most reliable approach to study the wind effects on structures. The current wind load codes/standards are formulated under the premise that wind loads on structures are simulated in wind tunnels. The pioneer researchers in the wind engineering field such as Danvenport, Cermark, Cook and others had established the experimental technique related to the boundary layer wind tunnel test while creating the framework of wind resistant design of structures [Daveport and Isyumov 1967, Cermak and Cochran 1992]. In short, wind tunnel simulation of ABL is a well established practice, and the boundary layer wind tunnel has become a necessary tool for wind resistance design. In order to investigate the wind effects on structures realistically, the model tests should be conducted in wind tunnel flows with characteristics similar to those of natural wind. The natural atmospheric boundary layer over a variety of ground conditions are categorized into a limited number of terrain categories, which can be modeled in the boundary layer wind tunnels by different combinations of passive devices including spires, barriers and roughness blocks. Based on the assumption that velocity fluctuations can be adequately modeled by stationary mean and turbulent flow properties, attempts to simulate an atmospheric flow in a wind tunnel have so far been confined to the reproduction of the statistical characteristics, including power spectrum, vertical profiles of mean velocity and turbulence intensity and sometimes coherence.

Special devices are sometimes added into the wind tunnel to achieve a better modeling of a particular feature of the atmospheric turbulence, such as turbulence intensity [Teunissen 1975]. Makita developed a turbulence generator to model homogeneous flow field with high turbulence

Reynolds number. Kobayashi [1994] and Nishi and Miyagi [1993] considered that the simulation of wind velocity history was of equal importance with the reproduction of the statistics. If the "raw" wind velocity history can be reproduced and the wind effects on structures are investigated in it, the obtained results would be more convincible. Fig.1 compares the time histories of the target and reproduced wind speeds in a multiple-fan wind tunnel [Nishi et al. 1999]. Recently a huge wind storm facility was built at the Insurance Center for Building Safety Research with a capacity to generate Category 3 winds (>130 mph) on a 220 sq m two-story building [Smith 2009].

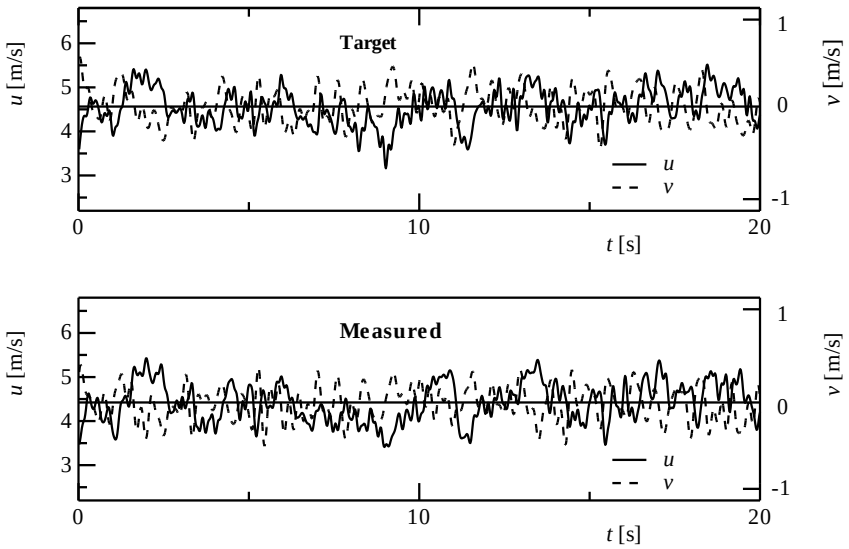

Fig.1 Comparison of the target and modeled wind speeds

CFD approach

Computational Fluid Dynamics (CFD) is basically a numerical approach to simulating or predicting phenomena and quantities of a flow by solving the equations of motion of the fluid at a discrete set of points. It has wide applications in flow-related engineering fields including aeronautical, mechanical and civil/architectural fields, although the difficulties in applying it to particular problems in these fields are different. The structural CWE usually involves the combination of problems of bluff body aerodynamics, inflow turbulence, wake turbulence, grid generation and high Reynolds number (up to the order of 10^7 to 10^8). All these problems require special attention in numerical simulation.

Many fundamental CFD studies have been conducted to simulate the turbulent channel or half-channel flow, in order to check the performance of numerical method or turbulence model as well as in order to investigate the characteristics of the boundary layer over smooth or rough plates. CFD has been shown to be very powerful in predicting wind field over kinds of terrain categories. In this paper, two examples of CFD simulation of turbulent boundary layers over hilly terrain and sea surface are provided.

ABL over hilly terrain

Turbulent flow over hilly terrain involves complicated flow phenomena such as spatial development, stable or unstable, i.e., intermittent, separation and reattachment according to the hill slope, and downstream recovery of the turbulent boundary layer. Thus, any disturbance that may influence the behavior of the separated shear layer and its interaction with the ground would change the global and local turbulent structure and thus influence the wind characteristics around hilly terrain. The slope of hilly terrain and the surroundings, especially upstream roughness conditions, are two important factors in determining the dynamic behavior of the turbulent boundary layer over a hilly terrain. With the increased concern about wind energy and wind loading problems in hilly terrains, many investigations have studied the turbulent boundary layer flow over an isolated hill,

which is usually a start point in research on flow over complex terrain. In this study two representative hill shapes were considered, i.e., a steep one with stable separation and a low one without stable separation, as well as two representative upstream roughness conditions, i.e., a smooth one and a rough one corresponding to two kinds of velocity profile of the incoming flow.

Generation of inflow turbulence and modeling the effects of roughness blocks play important roles in simulating the turbulent boundary layer over hills. Spatially developing turbulent boundary layers over smooth and rough plates were simulated to generate the inflow turbulence. The methods of Lund et al. (1998) and Nozawa and Tamura (2002) were applied for the smooth and rough surface conditions, respectively. The point of Lund's method of generating inflow turbulence was to rescale the velocity field at a downstream station, and re-introduce it as a boundary condition at the inlet, to allow for the calculation of spatially developing boundary layer in conjunction with pseudoperiodic boundary conditions applied in the streamwise direction. The method of Nozawa and Tamura (2002) is an extension of Lund's method for rough wall conditions. Meanwhile, rectangular blocks were arranged on the ground/hill surface to simulate the rough condition. An immersed boundary method (IBM) proposed by Goldstein et al. (1993) was used to model the no-slip boundary condition at all surfaces of roughness elements by adding an external force term in the governing equations of fluids. Note that the no-slip boundary condition was not imposed directly at the surfaces of the roughness elements. The coupling of the external force and the time derivative acceleration term corresponded to a kind of oscillation system. Fig. 2 and Fig.3 illustrate the instantaneous flow field over a smooth steep hill and a rough low hill respectively.

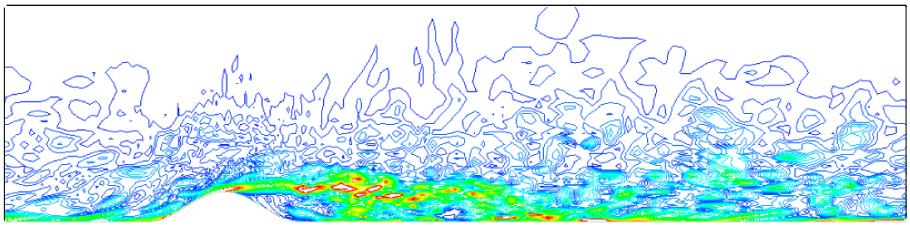

Fig.2 Contours of the instantaneous vorticity magnitude over smooth steep hill

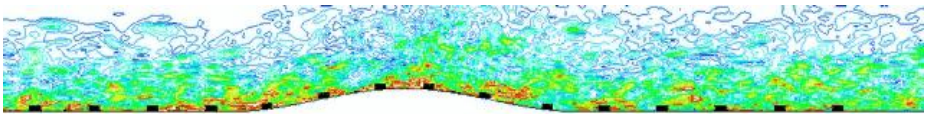

Fig.3 Contours of the instantaneous vorticity magnitude over a rough low hill.

ABL over sea surface

Wind load codes/specifications usually consider sea exposure as the smoothest condition of ground roughness, and specify a smallest power law index for the mean velocity profile at the coast. However, many field measurements have shown that sea surface wind stress, drag coefficient and aerodynamic roughness length are depended on the coupling effect of wind-wave interaction (e.g. Charnock 1955). Waves may perform as surface roughness in determining the boundary layers. Powell et al (2003) analyzed the wind velocity profiles over oceans measured by GPS sonde during tropical cyclones and reported reduced drag coefficient for high wind speeds in tropical cyclones. It means that the roughness length does not increase with the increase in wind speed at high wind speed. The sophisticated air flow field over waves is in great need of investigation as a guarantee of human offshore activities and facilities involved with oceans, such as oil and natural gas exploitation, long span sea bridges and offshore wind turbine farms that are sensitive to wind loads. Thus, study of the mean velocity profile and turbulence structure of atmospheric boundary layers over waves is an important and urgent issue to solve for wind engineers.

The air-sea interface is a complex system of interacting waves and atmospheric turbulence over a wide variety of spatial and temporal scales. The exchange of momentum and energy across the sea surface, for the most part, occurs on a molecular scale, involving both turbulent and laminar processes modified by wave breaking, surface tension, the structure of the wind boundary layer, and

the ocean mixed layer, among other effects. Although the oceanographers and meteorologists have conducted many studies concentrating on sea surface wind stress, drag coefficient or its counterpart aerodynamic roughness length, the parameterizations of wind stress and wind profile still remain controversial, especially in high wind and very young sea conditions (Jones and Toba, 2001). Recently, Sullivan (2000, 2008) conducted a series of study on the flow over waves based on Couette-flow approximation. In the present study, Large-eddy simulation (LES) is performed to study the mean velocity profile and turbulence structure of fully developed Atmospheric Boundary Layers (ABL) over waves. The Reynolds number that is based on wavelength λ and bulk velocity of the air U_b is 10^4. The water waves are idealized to be two-dimensional, periodic, non-evolving waves. Different wave steepness defined by a/λ(a: wave amplitude) and wave age defined by c/U_b (c: phase velocity of the wave) are considered. Furthermore, wave ages are categorized into three groups, i.e., wave moves upstream against wind, downstream with a speed lower or higher than wind, for which different characteristics of the mean velocity profiles and velocity fluctuation profiles are elaborated. This study is aimed to provide the information about wind characteristics off the coast during typhoons for wind engineering applications.

The dependence of the characteristics of atmospheric boundary layer over waves on both wave age and wave steepness is investigated systematically in this study. Three kinds of wave steepness are considered to study the effects of wave steepness, i.e., a =0.025, 0.05 and 0.075, corresponding to small, medium and large wave amplitude. Another important parameter concerned in this study is the wave age c/U_b that describes the evolution state of wave. Wave ages are categorized into three groups, i.e., wave moves upstream against wind, downstream with a speed slower or faster than wind. Concretely, c/U_b =-0.5 (wave opposing wind), 0.5 (wave following wind) and 1.5 (wind following wave) are considered for $a/\lambda = 0.025$ and 0.075, while more velocity combinations, i.e., c/U_b =-1.5, -1.0, -0.5, 0, 0.5, 0.75, 1.0, 1.5 and 2.0 are considered for $a/\lambda = 0.5$ to elaborate the different characteristics of the mean velocity profiles and velocity fluctuation profiles over waves.

Fig.4 illustrates the mean velocity profiles at different wave ages at a/λ=0.05. β denotes wave age in Fig.4. The mean velocity profiles of the flow over a flat plate and a stationary wave are shown together as references. The mean velocity is averaged both in span-wise direction and in phase. The change of gradient height and power law index, and the change of roughness length and friction velocity with wave age are illustrated in Fig.5a and Fig.5b respectively.

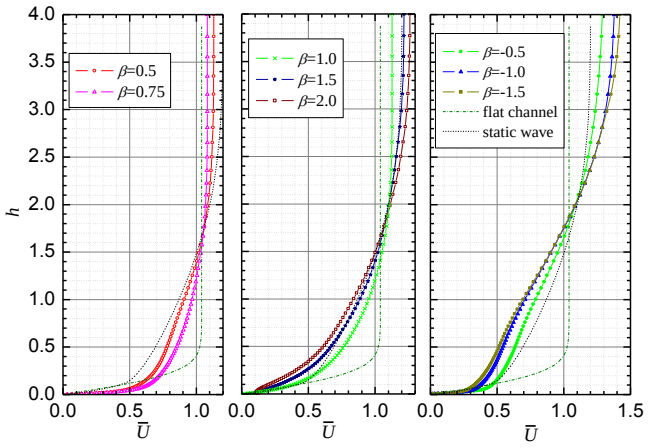

Fig.4 Mean velocity profiles over waves at different wave ages

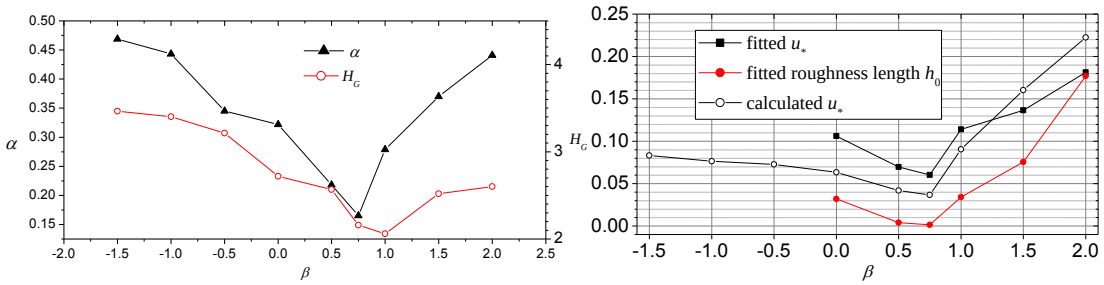

(a) Gradient height and power law index (b) Roughness length and friction velocity

Fig.5 Change of aerodynamic parameters associated to velocity profile

Conclusion

This paper introduces the improvements of mathematical, physical and CFD approaches utilized to model the Atmospheric Boundary Layer flow for structural wind engineering applications. CFD simulations of the ABL over hilly terrain and sea surface are introduced as examples of CFD approach. More detailed description and comparison of these methods will be presented at the conference.

Acknowledgement

This research was funded in part by Natural Science Foundation of China (NSFC) Grant number 51278366, and the 973 project of Ministry of Science and Technology.

References

[1] Borgman, L. E. (1969), "Ocean wave simulation for engineering design," J. Wtrwy. Harbor Div., ASCE, 6(3), 557-583.

[2] Bracewell R.N. (1986), Fourier Transform and its application, McGraw Hill.

[3] Brigham E.O. (1988), Fast Fourier Transform and its application, Prentice Hall.

[4] Cermak, J.E., Cochran, L.S. (1992), "Physical Modeling of the Atmospheric Surface Layer," J. of Wind Eng. Ind. Aerodyn., 41-44, 935-946.

[5] Charnock H. 1955. Wind Stress on a Water Surface. Qtly. J. Royal Met. Soc., 81, 639-640.

[6] Daveport, A.G., Isyumov, N. (1967), "The application of the boundary layer wind tunnel to the prediction of wind loading," Proc. of Intl. Research Seminar on Wind Effects on Buildings and Structures, 1, 201-230.

[7] Goldstein, D., Handler, R., Sirovich, L., (1993), "Modeling a no-slip flow boundary with an external force field," Journal of Computational Physics 105, 354–366.

[8] Jones I.S.F., Toba Y. (2001), Wind Stress over the Ocean. Cambridge University Press.

[9] Kareem, A. (1987), "Wind effects on structures: a probabilistic viewpoint," Probabilistic Engrg. Mech., 2(4), 166-200.

[10] Kitagawa T., Nomura T. (2003), "A wavelet-based method to generate artificial wind fluctuation data," Journal of Wind Engineering and Industrial Aerodynamics, 91, 943-964.

[11] Kobayashi, H., Hatanaka, A., Ueda, T. (1994), "Active simulation of time histories of strong wind gust in a wind tunnel," J. of Wind Eng. Ind. Aerodyn., 53, 315-330.

[12] Li Y., Ahsan K. (1993), "Simulation of multivariate random processes: Hybrid DFT and digital filtering approach," J. Eng. Mech., 119, 1078-1098.

[13] Lund, T.S., Wu, X., Squires, K.D., (1998), "Generation of turbulent inflow data for spatially-developing boundary layer simulations," Journal of Computational Physics 140, 233–258.

[14] Nishi, A. , Miyagi, H.(1993), "Computer controlled wind tunnel," J. Wind Eng. Ind. Aerodyn., 46-47, 837-846.

[15] Nishi, A., Kikugawa, H., Matsuda, Y. and Tashiro, D. (1999), "Active control of turbulence for an atmospheric boundary layer model in a wind tunnel," J. Wind Eng. Ind. Aerodyn., 83, 409-419.

[16] Nozawa, K., Tamura, T., (2002), "Large-eddy simulation of the flow around a low-rise building immersed in a rough-wall turbulent boundary layer," Journal of Wind Engineering and Industrial Aerodynamics 90, 1151-1162.

[17] Powell M.D., Vickery, P.J., Reinhold T.A. (2003), "Reduced drag coefficient for high wind speeds in tropical cyclones," Nature, 422, 279-283.

[18] Reed, D. A., Scanlan, R. H. (1984), "Autoregressive representation of longitudinal, lateral, and vertical turbulence spectra," J. Wind Engineering and Industrial Aerodynamics, 17, 199-214.

[19] Sullivan, P. P., McWilliams J. C., Moeng C.-H. (2000), "Simulation of turbulent flow over idealized water waves," J. Fluid Mech., 404, 47-85.

[20] Sullivan, P. P., Edson J. B., Hristov T., McWilliams J. C. (2008), "Large-eddy simulation and observations of atmospheric marine boundary layers above non-equilibrium surface waves," J. Atmos. Sci., 65, 1225-1245.

[21] Shinozuka, M. (1970), "Simulation of multivariate and multidimensional random processes (Part 2). J. Acoustical Soe. of Am., 49(1), 357-367.

[22] Shinozuka, M. (1972), "Monte Carlo solution of structural dynamics," Comp. and Struct., 2, 855-874.

[23] Shinozuka, M and Deodatis, G. (1996), "Simulation of multi-dimensional Gaussian stochastic field by spectral representation," Appl Mech Rev 49(1), 29-54

[24] Shinozuka, M. and Jan, C.-M. (1972), "Digital simulation of random processes and its applications," J. Sound and Vibration, 25(1), 111-128.

[25] Smith, J. et. (2009), "Validation of Facility Configuration and Investigation of Control Systems for the IBHS Windstorm Simulator," 11th Americas Conference on Wind Engineering, June, 2009

[26] Teunissen, H.W. (1975), "Simulation of the Planetary Boundary Layer in a Multiple-Jet Wind Tunnel," Atmospheric Environment, 9, 145

[27] Wang, L. (2007). Stochastic Modeling and Simulation of Transient Events, Civil Engineering and Geological Sciences. University of Notre Dame, Notre Dame.

[28] Wang L., McCullough M., Kareem A. (2013), "A data-driven approach for simulation of full-scale downburst wind speeds," Journal of Wind Engineering and Industrial Aerodynamics, 123, 171-190.

ISBN 979-458-758-3
Proceedings of the 3rd International Conference on the Geohazard Information
Zonation and 5th Seminar & Short Course of HASTAG (GIZ2014-HASTAG5)
Organized by UMSU, HASTAG, USM
Medan, Indonesia, October 20-22, 2014

Use of a Sparse Geo-info Database and Ambient Ground Vibration Survey in Earthquake Disaster Risk Study −A Case of Kathmandu Valley−

Netra Prakash Bhandary [1+], Ryuichi Yatabe [1], Koji Yamamoto [2], and Youb Raj Paudyal [3]

[1] Graduate School of Science and Engineering, Ehime University, Japan
[2] Geo-Research Institute, Japan
[3] Department of Education, Government of Nepal

Abstract. Building a reliable geo-info database and using it in various civil engineering projects as well as geo-disaster risk reduction study largely depends on the accuracy of available borehole information as well as borehole distribution density. In a developing country like Nepal, the available borehole information even in the most developed urban areas is highly sparse, which does not really help achieve the purpose of generating a geo-info database out of the available borehole information. Kathmandu Valley, the capital city area of Nepal accommodates about 3 million people in densely populated urban settlements of many poorly built and over-aged houses and buildings. It consists of thick lake deposits measuring more than 500 meters at some locations. This particular study is aimed at building a geo-info database system out of sparsely distributed borehole information, using the geo-info database in reliability check of ambient ground vibration survey results, and preparing a ground shaking map for earthquake disaster risk reduction in the Kathmandu Valley. The sparsely distributed borehole locations and different purposes of boring obviously lead to a less reliable geo-info database system. So, an extensive ambient ground vibration survey, which consists of a total of 176 survey points in about 1-km grid spacing, was conducted in Kathmandu Valley to predict the ground behavior in case of seismic shaking. The results of the geo-info database system and the ambient ground vibration survey were compared for reliability check of the latter. Finally, a ground shaking map was proposed for earthquake disaster risk mitigation in the Kathmandu Valley. The main understandings are: 1) specific use of the geo-info database system built out of the available borehole information may still be in question, but a broader implication, especially in terms of predicting the nature of soil deposit in the Kathmandu Valley can be adequately made; 2) the ground structure can be broadly predicted out of the ambient ground vibration data analysis, which in case of the Kathmandu Valley has been well confirmed by comparing the previously reported ground profiles and the results of the ambient ground vibration survey; and 3) the densely populated urban areas in the Kathmandu Valley are mostly situated over the soft and thick deposits with longer period of shaking, so longer period (i.e., 1.0-2.0 s.) structures here are prone to seismic damage.

Keywords: ambient ground vibration, geo-info database, ground shaking map, Kathmandu Valley

1. Introduction

Building and maintaining geo-info databases out of existing borehole information, particularly in medium- to large-scale urban areas in Japan gained significant momentum in the past one decade. There are basically two main purposes for building such a database. The first is reusing available borehole information for any further geotechnical projects, while the second is making an optimum use of ground information and material properties in geo-disaster risk mitigation efforts, such as understanding earthquake damage risk. In a developed nation like Japan, most big cities in most occasions have a dense distribution of borehole locations, but when it comes to developing or underdeveloped nations, obtaining borehole information may not be easy. As such, building of geo-info database system in Japan started in 1970s, but it was only in 2006, the Japanese Geotechnical Society formed a group of experts from academia, government agencies, and private firms for the purpose of gathering borehole information in major urban areas, such as Tokyo, Osaka, Kobe, etc. to build a geo-info database system for each big urban area in Japan leading to developing a digital subsurface model of the major urban areas in Japan, which is now on the web for public use. As of October

+ Corresponding author. Tel.: + 81-89-927 8566; fax: +81-89-927 8566.
E-mail address: netra@ehime-u.ac.jp; netrapb@gmail.com.

2014, this digital subsurface model map created in 250-m mesh size includes 31 medium- to large-scale urban areas of Japan.

Unlike Japan, however, the status of borehole information availability in most developing nations in Asia is still poor. There may be two reasons for this: poorly maintained borehole exploration documentation and sparse or extremely low-density distribution of existing borehole information. For example, the Kathmandu Valley in Nepal (Fig. 1), which lies in one of the most earthquake disaster prone areas on the Himalayan thrusts, greatly lacks a well explored ground information system and enough number of existing boreholes that could help build a reliable geo-info database system and study the earthquake disaster risk level in the valley. There is a big number of urban areas in Asia as well as in the world that have a similar situation as that of Kathmandu when we talk about exiting borehole information and geo-disaster risk mitigation efforts. Most ground exploration techniques involve a massive amount of cost, which has led to little geophysical exploration study in Kathmandu-like urban areas. So, because of the cost involvement, neither it is feasible to go for increased number of planned borehole explorations, nor is it possible to adopt heavily expensive geophysical exploration techniques in a country like Nepal. Making use of existing borehole information is one solution, but the reliability involved in the maintained data and extremely sparse distribution of the available borehole information make it difficult to use a geo-info database system in earthquake disaster risk study.

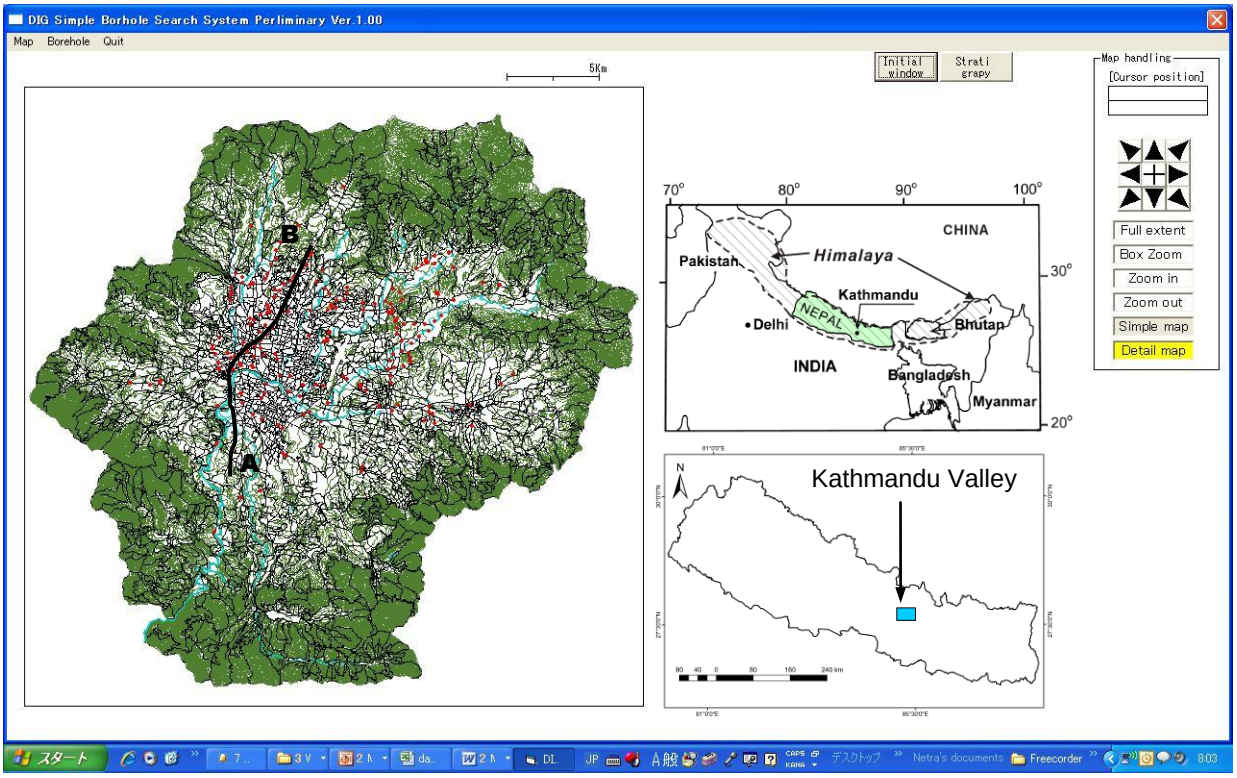

Fig. 1: The windows look of the geo-info database system and Kathmandu.

Situated over the subduction zone of Indian plate underneath the Eurasian continent, Nepal awaits a big earthquake in the next 10-20 years. Earthquake history in the region indicates that a big earthquake, equal to or greater than M8.0 takes place every 80-100 years, and from the latest big earthquake of 1934 measuring M8.0, it is soon going to be 80 years. Moreover, the locations of epicenters of the earthquakes in the past 300-400 years indicate that the area from west to mid Nepal lies in a zone of seismic gap [1], which has increased the risk of next big earthquake in this zone. While the predicted earthquake disaster risk in the valley is one of the highest in the world, the risk mitigation efforts have mostly focused at non-geological and non-geotechnical issues. One of the most prominent issues to be addressed when talking of earthquake disaster risk mitigation in the Kathmandu Valley is soft-layer deposit and its role in water-bowl effect during an earthquake. Similar studies have been conducted in various parts of the world, and most researchers have identified the Kathmandu Valley to be somewhat similar to Mexico City that suffered a tremendous loss during the 1985, M8.0 earthquake. Based on the earthquake occurrence frequency in Nepal and the Himalayan Region and the damage caused by 1934 Earthquake, it has been predicted that the capital area of

Kathmandu Valley (Fig. 1) will sustain severe damage in case of a big earthquake, mainly because of its ground structure, which is made of soft lake deposits. The 2002 JICA study on earthquake disaster risk in Kathmandu Valley estimates that more than 40,000 people will be killed, tens of thousands of people will be injured, and more than 200,000 houses and buildings will be damaged [2]. Moreover, lifelines including roads, bridges, electricity, water supply, and communication will remain dysfunctional for several days.

In this study, we first build a simple geo-info database system for the Kathmandu Valley out of the existing borehole information. Next, we try a comparatively cheaper method based on ground frequency measurement, commonly known as microtremor observation technique [3] to interpret the ground structure in terms of soft and hard deposits or shallow and deep deposits in the valley. Then, the ground structure interpretation is used in predicting the earthquake disaster risk level in terms of predominant period-based ground shaking map. The interpretation is also used in estimating the basement topography of the valley. Finally, to crosscheck and validate the frequency measurement-based method of ground structure prediction, we compare the ground profiles interpreted from this method with the ground profiles obtained from the geo-info database.

2. Material and Method

2.1. Geo-info database preparation

Kathmandu Valley measures about 25 km east-west and about 20 km north-south. There have been various attempts of borehole exploration in the valley for different purposes, and the collected borehole data consist of borehole logs of about 500 locations. However, due to lack of enough information, particularly in relation with the ground strata and geotechnical data, only the data from about 300 boreholes were used in preparing preliminary geo-info database for the Kathmandu Valley (Fig. 1). The information entered into the database system mainly includes: 1) soil types in six categories consisting of sandy, silty, clayey, organic clay, gravel-rich, and bedrock, 2) groundwater level, and 3) SPT N-value. A typical ground profile extracted from the database system is shown in Fig. 2.

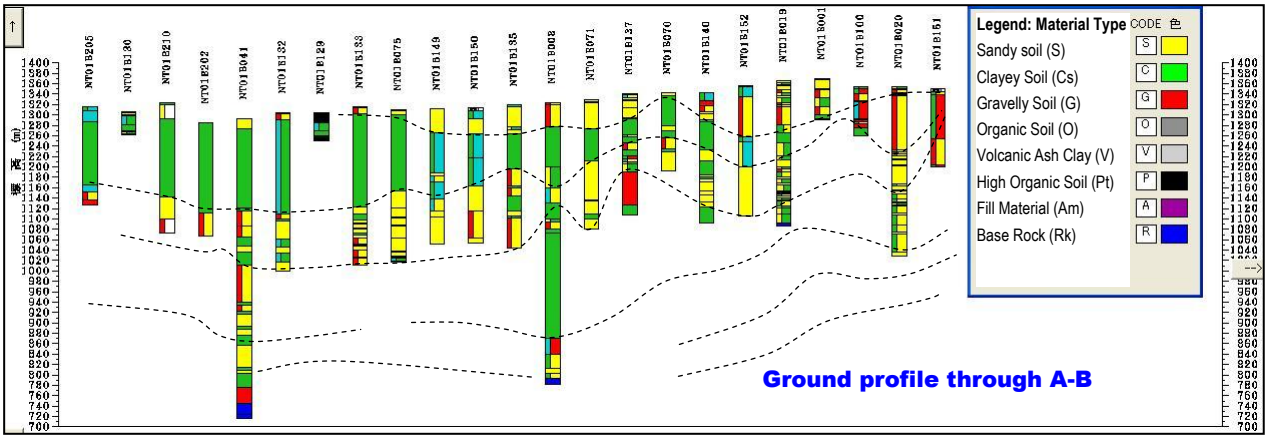

Fig. 2: Ground profile through line A-B (Fig.1)

2.2. Ambient ground vibration survey

Ambient ground vibration survey (also often referred to as microtremor survey) was conducted in the valley core in an area covering 18km east-west and 11km north-south with a grid spacing of one kilometer (Fig. 3) using a portable microtremor measurement device (NewPIC: by System and Data Research (SDR) Co. Ltd., Japan). Sampling frequency was set at 100 Hz. At each survey point, the data were recorded for 300 seconds (i.e. 30,000 samples at a sampling rate of 100 Hz), and velocity time histories of three components of all recorded data were drawn. Each component of signal was corrected by the base line and divided into 15 windows; each window consisting of 2048 samples (i.e., 20.48 s). For each point, 8-12 windows were picked up for analysis, omitting the windows that are influenced by nearby noise sources. Fourier analysis of the each window was carried out using Fast Fourier Transform (FFT) computer program, and the obtained spectra were smoothed using Parzen window of bandwidth 0.5 Hz. The average spectral ratio of horizontal-to-vertical components was obtained from Eq. (1) [4].

$$H/V = \sqrt{(F_{NS}^2 + F_{EW}^2)/(2F_{UD}^2)} \quad (1)$$

Where, F_{NS}, F_{EW} and F_{UD} are the Fourier amplitude spectra in the north-south (NS), east-west (EW) and up-down (UD) directions, respectively.

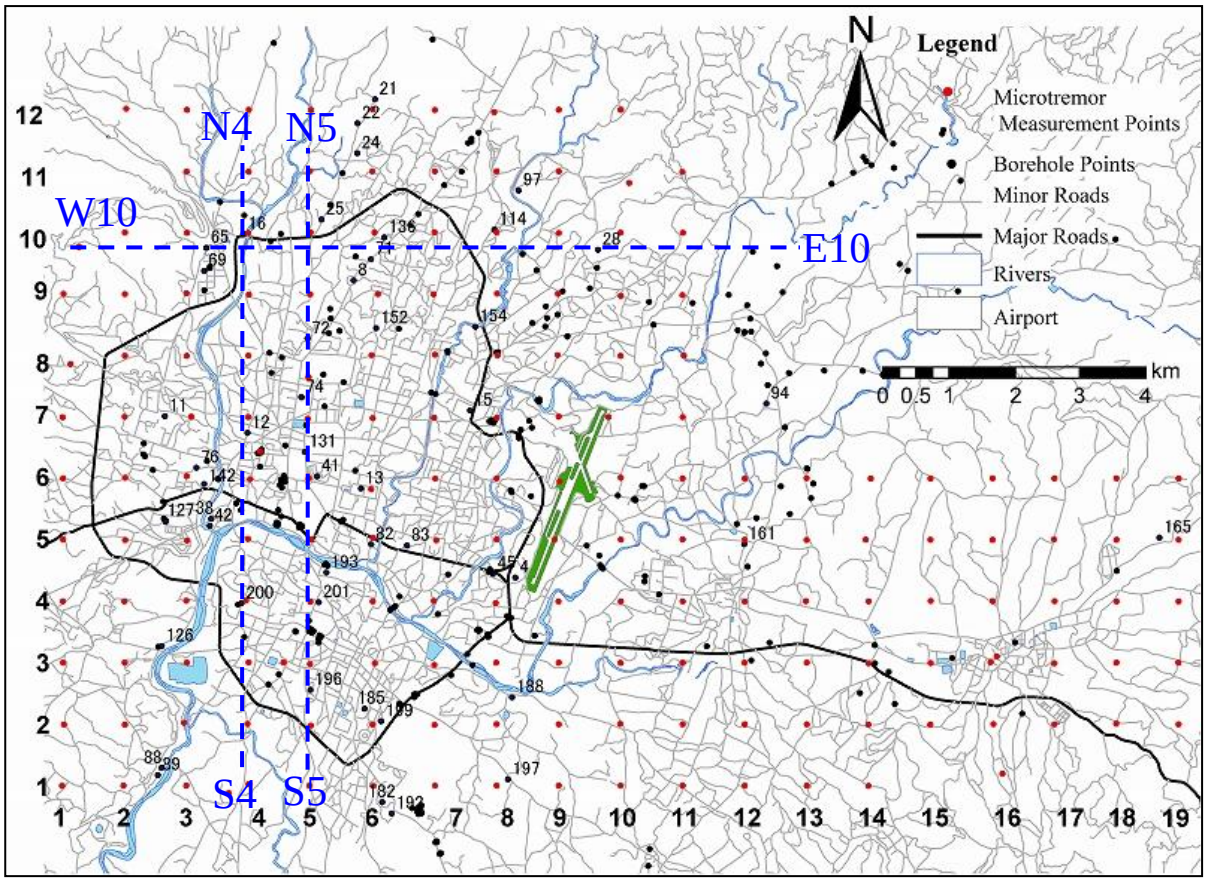

Fig. 3: Distribution of borehole points and ambient ground vibration (microtremor) survey points.

The ambient ground vibration or microtremor analysis has been widely applied in the last two decades for different purposes, such as site effects evaluation, wave amplification estimation, liquefaction vulnerability assessment, sediment depth estimation and microzonation studies in different geographical and geological regions of the world. In this study, the fundamental resonant frequency of the soil layer is used to estimate thickness of the soft sediments in the Kathmandu Basin. At the same time, the predominant period values obtained for each survey points were used to prepare a GIS-based ground shaking map for the study area.

3. Results and Discussion

3.1. Ambient vibration survey results

The results of the ambient ground vibration survey are expressed in terms of predominant frequency of each ground point, as typically shown in Fig. 4. This figure shows the H/V spectral ratio versus predominant frequency for four typical points in the study area. Variations in the shape of H/V curves can be noticed in this figure. These curves are representative to a particular site condition and they describe the overall seismic site response at that location. Based on the observed peaks in the H/V curves, the predominant period (i.e., inverse of the predominant frequency) is obtained, as shown for each South-North and West-East straight line in Fig. 5. These analysis results indicate that the predominant period in the surveyed area is found to vary from 0.11 sec to 2.05 sec. As in Fig.5, the predominant period is maximum approximately in the middle of the South-North lines, while it is maximum towards west for the West-East lines.

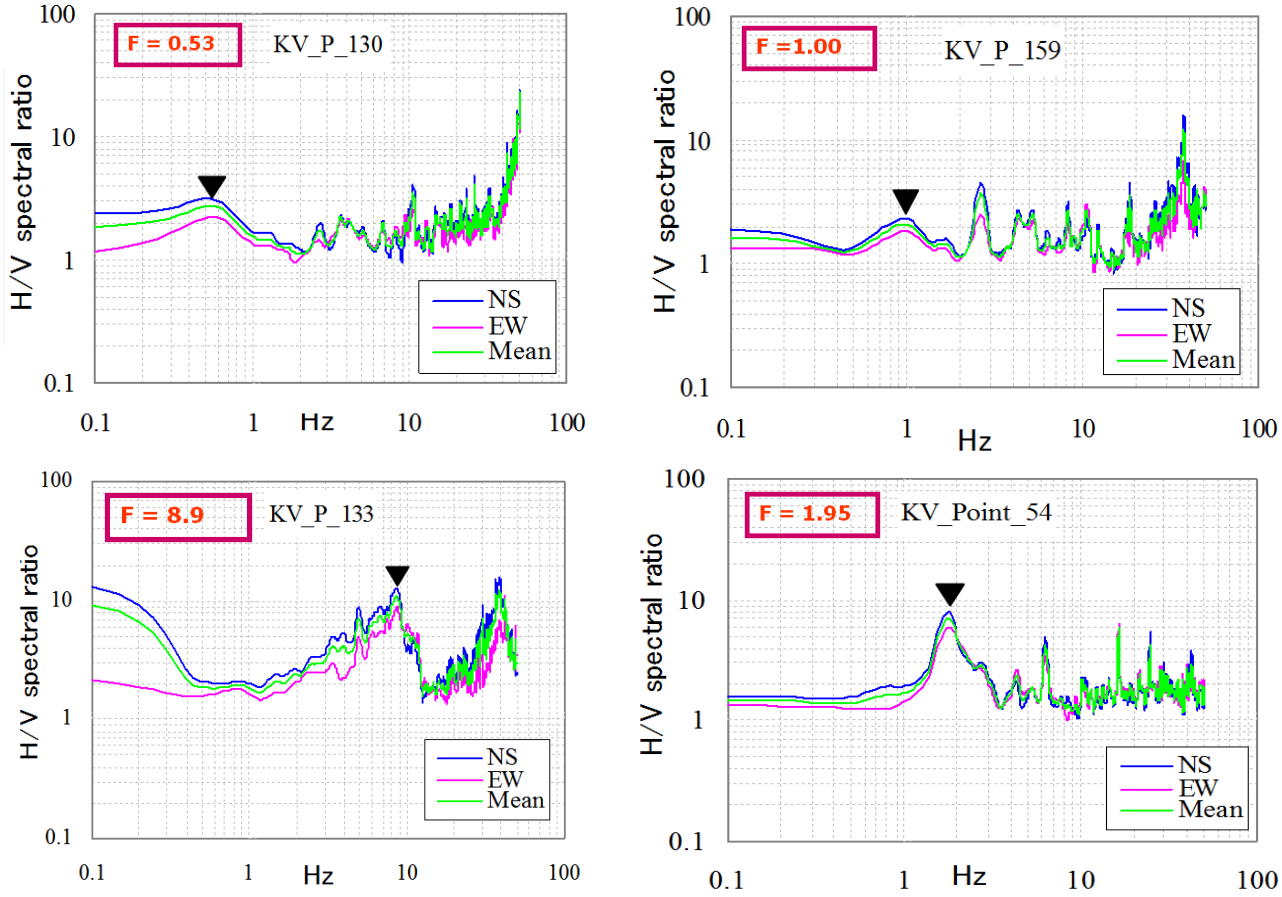

Fig. 4: Estimation of predominant frequency from the H/V spectra at four typical locations.

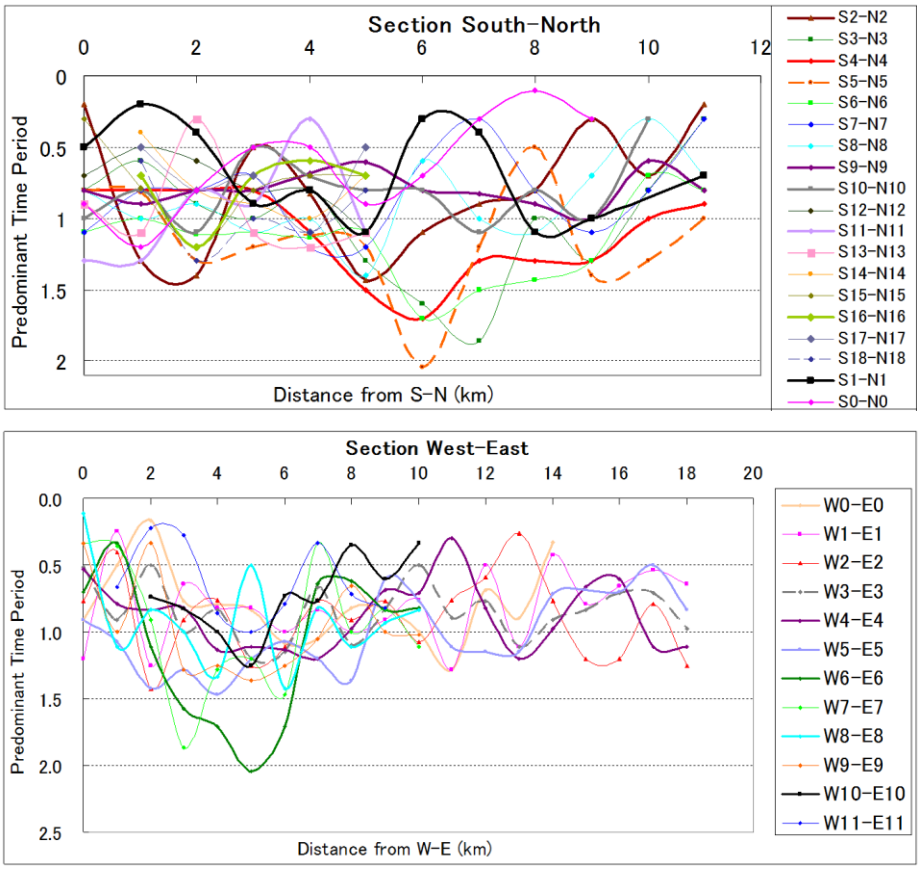

Fig. 5: Predominant period profiles of survey points in South-North and West-East straight lines.

3.2. Ground profiles interpreted from borehole logs and ambient vibration analysis

The ambient ground vibration survey results were interpreted in terms of predominant periods of the ground points. Based on the predominant periods, ground profiles through various lines were plotted and compared with the borehole log-based ground profiles. Fig. 6 shows typical profiles of the ground through line S5-N5 and W10-E10 (as in Fig. 3). This comparison indicates that there is some degree of reliability. This interpretation is based on the fact that the softer ground, i.e., the soil layers made of deeper clayey, silty materials has a longer natural period, while harder ground, particularly the bedrock mass at shallower depth has a shorter natural period.

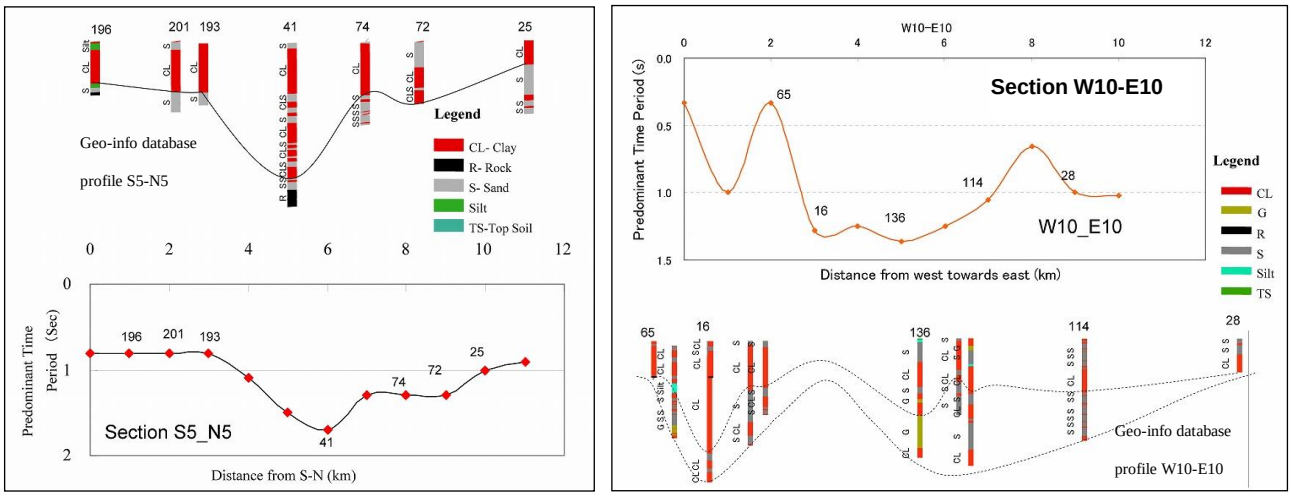

Fig. 6: Comparison of ground profiles interpreted from geo-info database and predominant period (S5-N5).

3.3. Predominant period and ground shaking map

Using GIS environment (ArcGIS9.0), the predominant period information, as estimated in Fig. 5, was attributed to each survey point, and then applying the method of krigging, a predominant period distribution map was prepared, as shown in Fig. 7. The whole area was divided into five zones of predominant period, as indicated in the figure, using natural breaks technique. The predominant period distribution map indicates that the core area has a predominant period of around 2.0 s, while it decreases to below 1.0 s towards the outskirts.

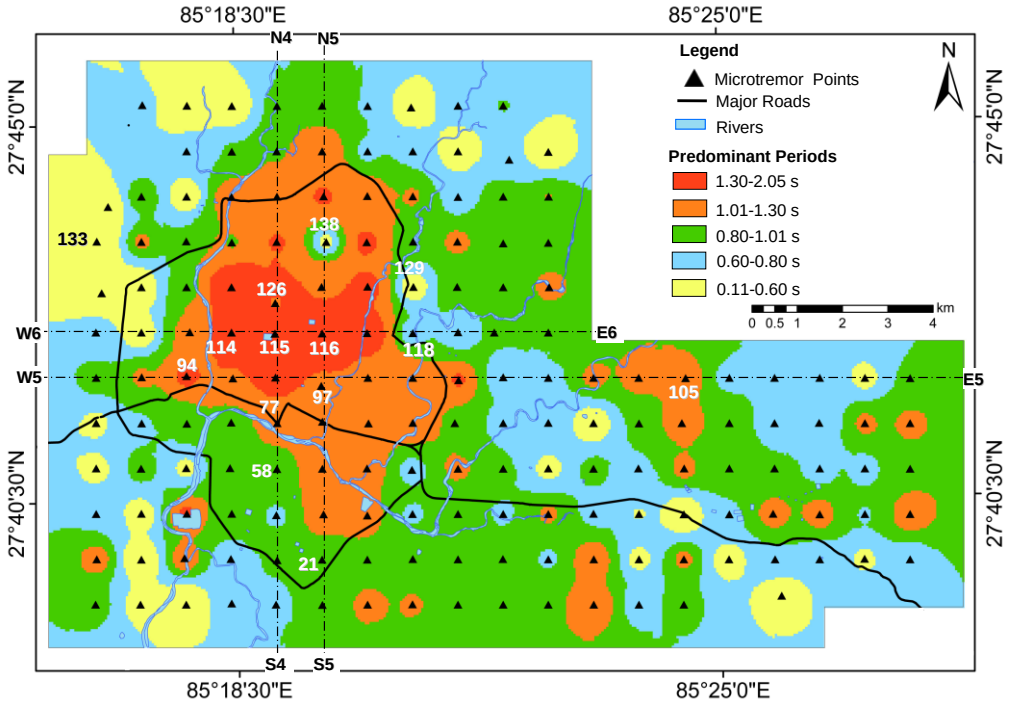

Fig. 7: Predominant period-based ground shaking map obtained from ambient ground vibration survey.

3.4. Sediment depth and predominant frequency

According to Ibs-von Seht and Wohlenberg [5], the fundamental resonant frequency (f_r) of a soil layer is closely related with its thickness (h) as:

$$h = af_r^b \tag{2}$$

where, a and b are standard errors of the correlation coefficients. They demonstrated that it was possible to establish a direct functional relationship between h and f_r even without the information of shear wave velocity (V_s). They also estimated a and b values, and proposed an empirical relationship (as in Eq. 3) between h and f_r based on the information of 34 boreholes of depth from 15 m to 1,257 m and 102 seismic stations data in western Lower Rhine Embayment in Germany. Likewise, Parolai et al. [6] have developed another empirical relationship (Eq. 4) between h and f_r for Cologne area in Germany based on the information of 32 boreholes of depth range from 20 m to 402 m and 337 seismic station data. More recently, Birgöen et al. [7] have derived another empirical relationship (Eq. 5) between h and f_r for Istanbul region (Turkey) based on the H/V ratios from 15 measurements at the borehole locations and velocity profile of two microtremor array measurement sites. They have shown a very strong relationship (R^2 value: 0.995) between the resonant frequency and the thickness of the sediment which varies from 20 m to 449 m. Özalaybey et al. [8] have also derived an equation (as in Eq. 6) for the sediment cover in Izmit Basin in Turkey which has as thick as 1200 m of sedimentary cover at the deepest point.

$$h = 96\, f_r^{-1.388} \tag{3}$$

$$h = 108\, f_r^{-1.551} \tag{4}$$

$$h = 150.99\, f_r^{-1.1531} \tag{5}$$

$$h = 141\, f_r^{-1.27} \tag{6}$$

To estimate the soft sediment thickness in the Kathmandu Valley, we adopt terrain specific equations given by above researchers. Using the above equations, theoretical thickness values of the sediments are first calculated considering the fundamental frequency (f_r) obtained from the ambient vibration or microtremor analysis at each measurement station. As shown in Fig. 8, the estimated depths, based on the above four equations, exhibit remarkable variation with an average standard deviation of 41.88 m.

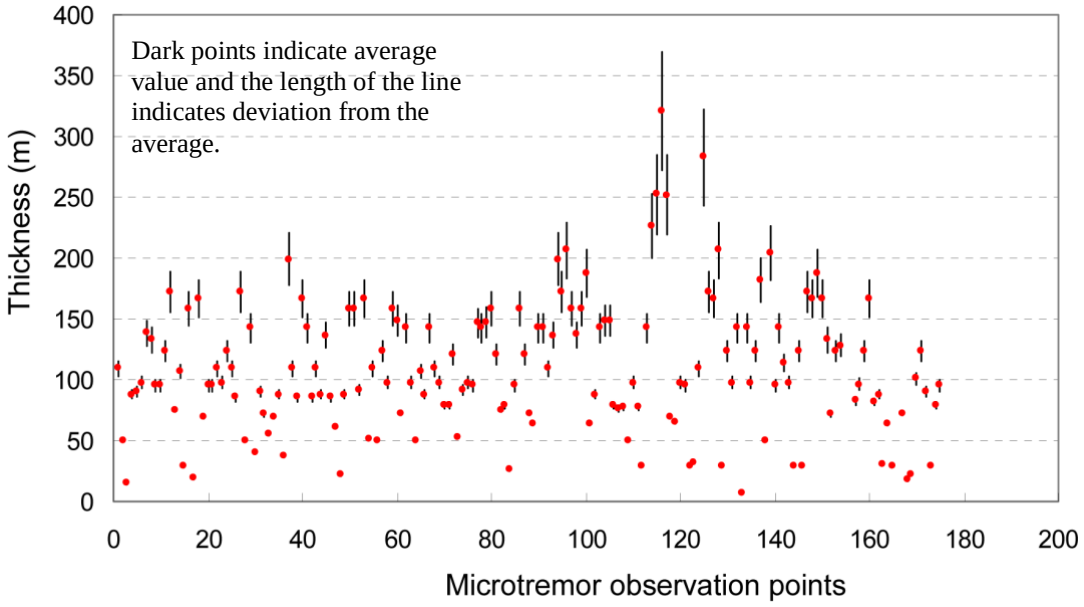

Fig. 8: Comparison between depths calculated by using Eq. 3 [5], Eq. 4 [6], Eq. 5 [7], and Eq. 6 [8]

In order to minimize the value of standard deviation and to obtain more reliable results, the depths estimated by the above equations are divided into two groups, emphasizing less variation of estimated depths in each group. In first group, the depth of the Kathmandu Basin sediments is estimated using Eq. 3 [5] and Eq. 4 [6], since these equations show more comparable results with each other. In second group, the depth is estimated using Eq. 5 [7] and Eq. 6 [8]. The standard deviation of each group is obtained as in Fig. 9 and Fig.

10, which show that the standard deviation of the first group (i.e., 48.55 m) is significantly higher than that of the second group (i.e., 7.44 m). It is also understood that thickness values obtained by Eq. 5 [7] and Eq. 6 [8] are more compatible with each other than the first two. In other words, sediment depths calculated by Birgöen et al. [7] and Özalaybey et al. [8] show negligible variation due to comparable geotechnical characteristics of the geological formations. Furthermore, we averaged the values obtained from Eq. 5 and Eq. 6 to obtain a best-fit equation for the Kathmandu Basin, which we have proposed as:

$$h = 146.01 f_r^{-1.2079} \tag{7}$$

This equation is used for obtaining primary information on relative variation in depth of the interface between two physically contrasting layers of lacustrine sediment and the underlain hard strata (or bedrock) in the Kathmandu Basin, which is validated by comparing with the results of the gravity contour map proposed by Moribayashi and Mauro [9] and also with the depth of the bedrock based on the borehole drilled for academic purposes in the Kathmandu Basin.

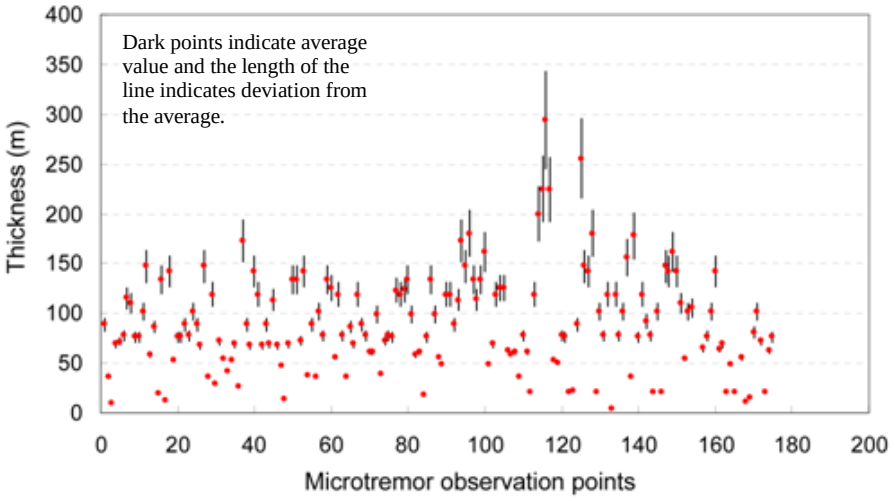

Fig. 9: Comparison of depths calculated by Eq. 3 [5] and Eq. 4 [6]

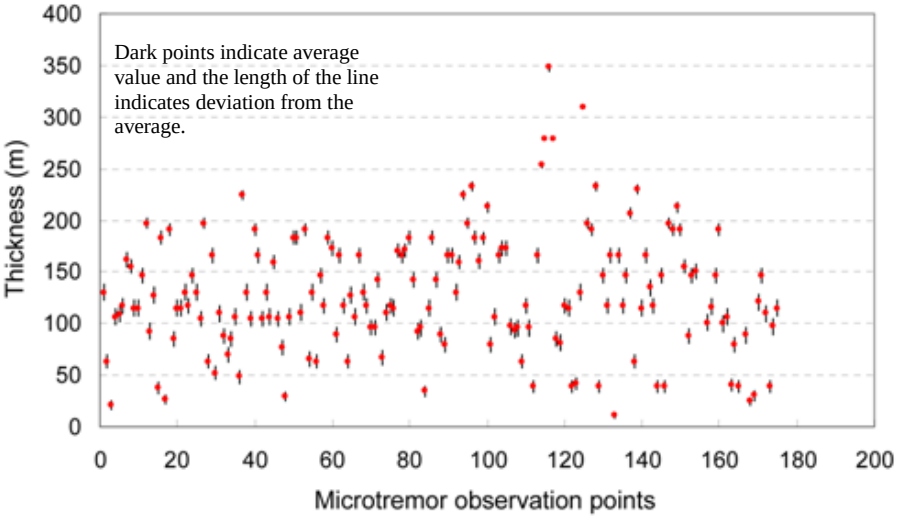

Fig. 10: Comparison of depths calculated by Eq. 5 [7] and Eq. 6 [8]

3.5. Basement topography

A bedrock contour map and a 3D view of basement topography of the Kathmandu Basin prepared out of the estimated soft sediment thickness are respectively shown in Fig. 11 and Fig. 12. As seen in the figures, the basin center consists of a deep interface of soft sediment (unconsolidated) and basement, while the basin outskirts consist of shallower interfaces. In Fig. 11, abrupt changes in the thickness can be seen at point A

(sediment thickness about 48 m, about 2 km north of central part) and point B (sediment thickness about 30 m, about 3 km north of central part), which indicate that the basement rock is close to ground surface.

The sediment depth elevation model suggests that the sediment distribution in the basin is far from uniform and have an undulating topography with steep relief in many locations in the basin. A closer analysis of the 3D view of the basement topography (Fig. 12) reveals two possibilities: first, the calculated depth of the sediment directly represents the total depth of lake deposit over the basement rock; second, it may not necessarily indicate the depth of hard basement rock, it rather represents the depth of basement layer beyond which the sediment does/may not contribute to amplification of the ground motion. From geotechnical point of view, however, this contrast corresponds to presence of bedrock.

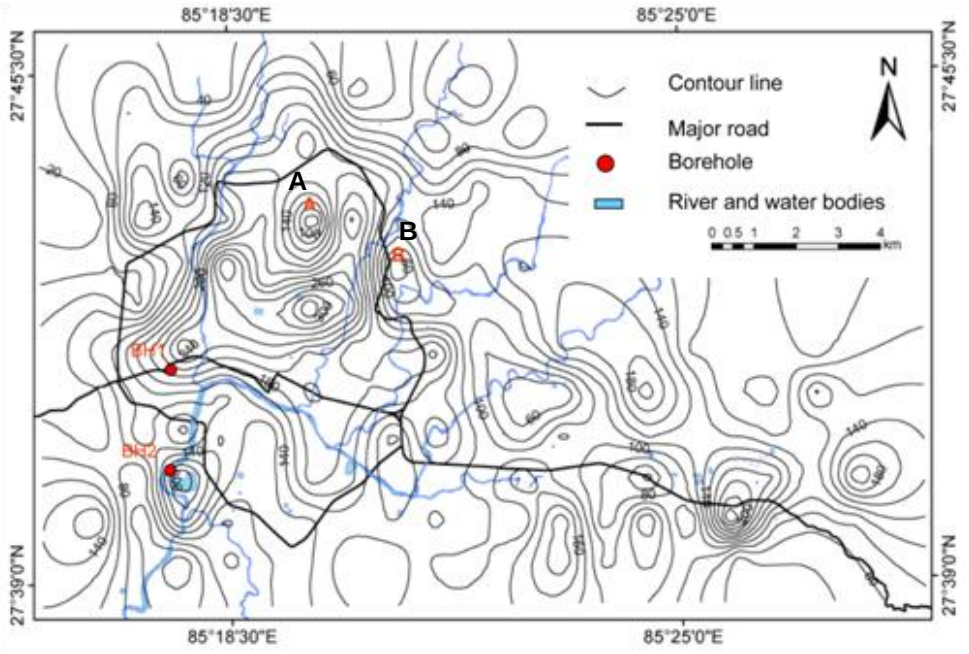

Fig. 11: Contour map of basement topography of the Kathmandu Basin.

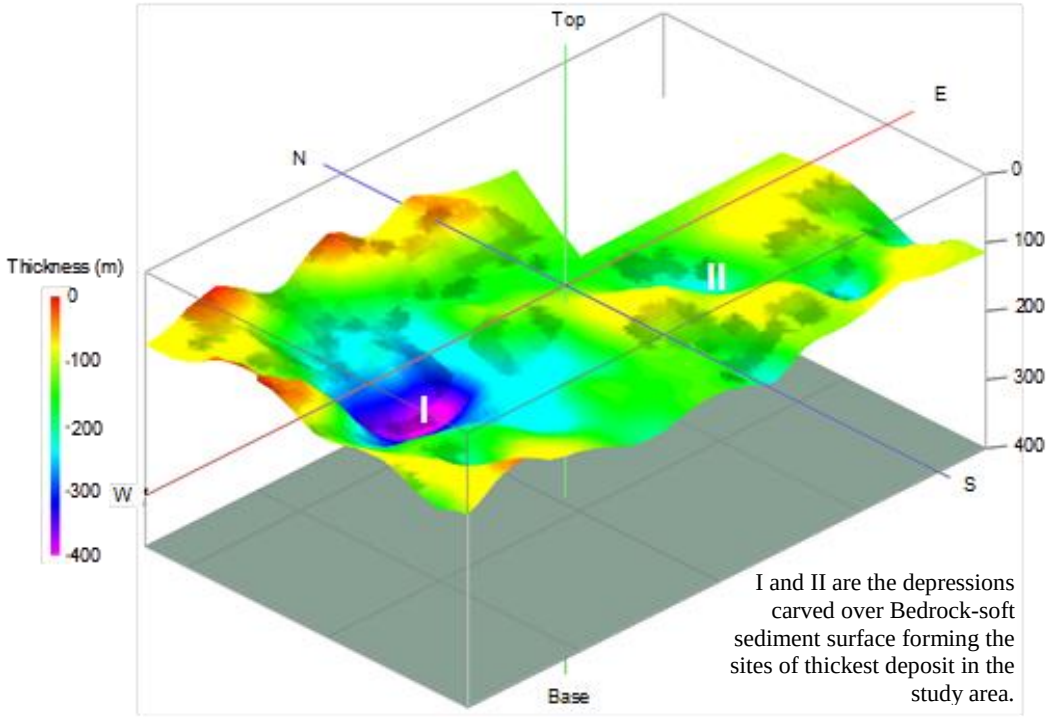

Fig. 12: Bedrock-soft sediment palaeo-topography of the Kathmandu Valley Basin (vertically exaggerated by 15 times).

4. Crosscheck and Validation

At first, we compared the basement topography results with the estimation of Moribayashi and Maruo [9] using gravitational method. Although owing to space restrictions we have not included their results here, our basement prediction was found to be quite similar to theirs. In their work, they have found that the gravity in the central part of the valley, where the thickness of the lacustrine sediments is high is lower, but it gradually increases towards the marginal area where the sediment thickness is low. They have also estimated that the maximum sediment thickness is about 650 m at the central part, but in reality, the density of lacustrine sediments is lower [2] than the value assumed by Moribayashi and Maruo [9] while calculating the gravity values. In addition, the actual density distribution of the bedrock and the overlain sediment should be based on the sediment types and depths, bedrock type, and degree of sediment consolidation. According to JICA [2], the average density of the Kathmandu sediment layer up to 30 m depth is about 1.52 g/cm3 and it varies from 1.43 g/cm^3 to 1.68 g/cm^3 according to the sediment types and depth, which is quite lower than the value (i.e., 1.87 g/cm^3) assumed by Moribayashi and Maruo [9]. This overestimated material density as well as assumption of the same value throughout the area might have resulted in greater depth of sediment in the Kathmandu basin.

Then, in order to verify the estimated sediment thickness, the sediment depth profiles through the center of the basin extracted from Fig. 10 were compared with the schematic cross section of the sediment proposed by Sakai et al. [10] and based on borehole exploration (Note: owing to space restriction, the diagrammatical comparison has been skipped in this paper), which revealed that the depth profiles are in good agreement with the profile proposed by Sakai et al [10].

Finally, the soft sediment depth estimated in this study was also compared with the borehole information-based ground profiles. Again for the space limitation, two typical comparative diagrams are shown in Fig. 11 and Fig. 12. Although, not very perfect, the comparison indicates that there is some degree of reliability in the ambient vibration analysis-based profile prediction.

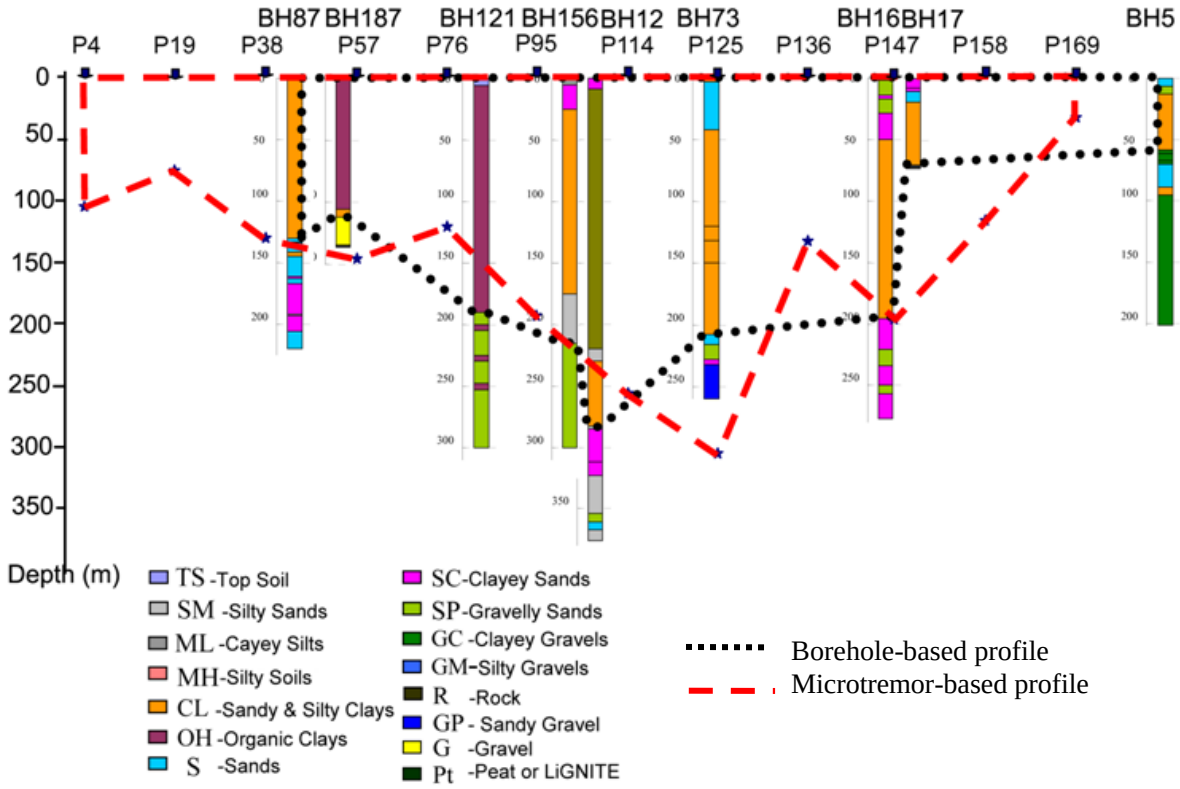

Fig. 11: Soft sediment depths based on geo-information database system and ambient ground vibration survey (Section S4-N4, Fig. 3).

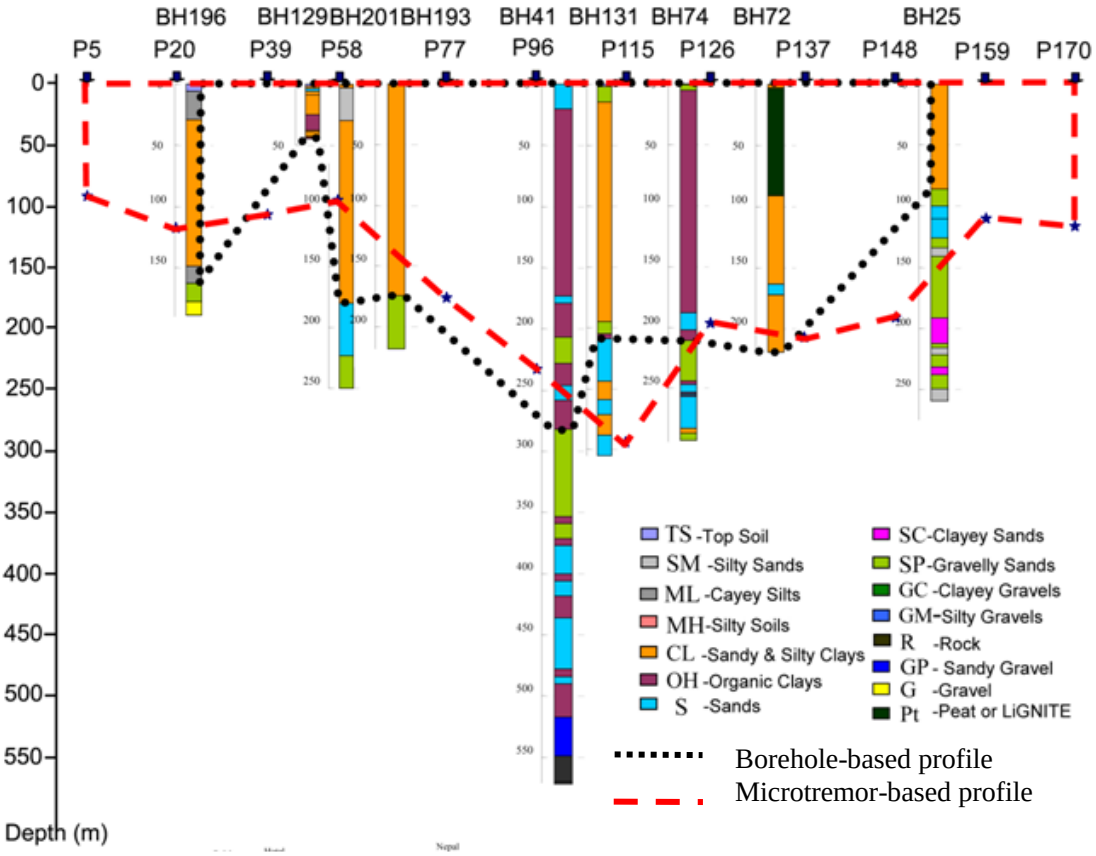

Fig. 12: Soft sediment depths based on geo-information database system and ambient ground vibration survey (Section S5-N5, Fig. 3).

5. Concluding Remarks

The reliability of the ground profile in the Kathmandu Valley drawn out of the available borehole logs is heavily reduced by the sparse distribution of the borehole points. In an attempt to prepare geo-info database towards earthquake disaster reduction efforts, about 300 borehole logs were entered in a windows-based database system. Sparse distribution of boreholes makes it largely difficult to accurately predict the ground profile of the valley, mainly because the borehole explorations were made for different purposes, which have led to dissimilar evaluation of the ground stratification. However, the interpretations of the ground profile from microtremor or ambient ground vibration analyses results in terms of predominant period have to some extent confirmed that the ground profiles drawn out of the borehole information are acceptable. Nevertheless, predicting the details of the ground stratification was still difficult because the present evaluation has been limited to estimating the sediment mass above the bedrock mass regardless of the soil layer types. It is expected that further analysis of the microtremor survey results may yield the presence of sandy, silty, or clayey layers underneath the points of measurement.

In this study, a predominant period-based shaking map for the Kathmandu Valley was also prepared out of the ambient ground vibration survey at 172 points. It was understood that in the urban cores and peripheral settlements of the valley, the predominant period varies from about 0.1 s to 2.0 s, and that it gradually decreases from a longer value in the central part to a shorter value in the outskirts. This trend is found to follow the distribution of sediment depth in the valley. This trend of predominant period distribution in the valley indicates that the possibilities of long-period ground vibration are higher in and around the valley center, which mostly consist of 5- to 7-story old masonry and reinforced concrete-framed buildings. Additionally, because of increasing population and development into a greater commercial hub, the central part has seen a sharp rise in the number of mid-height to tall buildings, which have been constructed under inadequate geotechnical investigations. In order to reduce the disaster risk, therefore, special considerations must be made in the seismic design of tall or long structures in the valley center. At the same time, it may also be necessary to consider enhanced seismic design criteria for medium- and short-period structures in the remaining part of the valley.

References

[1] Bilham, R., Larson, K., Freymueller, J. and Project Idylhim Members. GPS measurements of present-day convergence across the Nepal Himalaya. *Nature (Lond)*. 1997, Vol. 386, pp. 61-64.

[2] JICA. The Study on earthquake disaster mitigation in the Kathmandu Valley Kingdom of Nepal. Main Report. 2002 (Unpublished).

[3] Nakamura, Y. A method for dynamic characteristics estimation of subsurface using microtremor on the ground surface. *Quarterly Report of the Railway Technical Research Institute*. 1989, **30** (1): 25-33.

[4] Delgado, J., Casado, C. L., Lopez, Giner, J., Estevez, A., Cuenca, A., Molina, S. Microtremors as a geophysical exploration tool: applications and limitations. *Pure and Applied Geophysics*. 2000, **157:** 1445-1462.

[5] Ibs-von Seht, M.,Wohlenberg, J. Microtremor measurements used to map thickness of soft sediments. *Bulletin of the Seismological Society of America*. 1999, **89**: 250–259.

[6] Parolai, S., Bormann, P., and Milkereit, C. New relationship between Vs thickness of sediments and resonance frequency calculated by the H/V ratio of seismic noise for the Cologne area (Germany). *Bulletin of the Seismological Society of America*. 2002, **92** (6): 2521-2527.

[7] Birgören, G., Özel, O., Siyahi, B. Bedrock depth mapping of the coast south of Istanbul: comparison of analytical and experimental analyses. *Turkish Journal of Earth Science*. 2009, **18**: 315–329.

[8] Özalaybey, S., Zor, E., Ergintav, S. and Tapırdamaz, M. C. Investigation of 3-D basin structures in the İzmit Bay area (Turkey) by single-station microtremor and gravimetric methods. *Geophysical Journal International*. 1980, **186**: 883–894.

[9] Moribayashi, S. and Maruo, Y. Basement topography of the Kathmandu Valley Nepal- An application of the gravitational method to the survey of a tectonic basin in the Himalaya. *Journal of Japan Society of Engineering Geology*. 1980, **21**: 30-37.

[10] Sakai, H., Fujii, R., Kuwahara, Y., Upreti, B. N. and Shrestha, S. D. Core drilling of the basin-fill sediments in the Kathmandu Valley for paleoclimatic study: preliminary results. *Journal of Nepal Geological Society*. 2001, **25** (Special Issue): 9-18.

ISBN 979-458-758-3
Proceedings of the 3rd International Conference on the Geohazard Information
Zonation and 5th Seminar & Short Course of HASTAG (GIZ2014-HASTAG5)
Organized by UMSU, HASTAG, USM
Medan, Indonesia, October 20-22, 2014

Development and Application of Seismic Isolation and Energy Dissipation for Buildings in Taiwan

Lap-Loi Chung[1, 2]

[1] Research Fellow, National Center for Research on Earthquake Engineering
[2] Professor, Department of Civil Engineering, National Taiwan University

Abstract. Taiwan is located on the Circum-Pacific seismic belt, at the junction of the Eurasian plate and Philippines Sea plate. Hundreds of earthquakes, ranged from small to medium, occur every year. Thus, people in Taiwan have to live with earthquakes. According to reconnaissance report after earthquakes, more than 90% of casualty is attributed to damage and collapse of buildings. Therefore, retrofit of existing buildings and protection of new buildings become a stringent issue in Taiwan. Seismic isolation and energy dissipation is one of the alternatives to upgrade performance of existing and new buildings. Isolators are mounted in the interface between substructure and superstructure. The isolator layer is so soft that transmission of energy from the substructure to the superstructure is limited. Supplemental damping devices are also implemented to prevent the isolation layer from excessive displacement. There are two types of isolators: spring type and sliding type. Restoring forces are provided so that permanent displacement is minimized. Energy dissipators are mounted between stories. Their movements keep track of the relative displacement of mounting points at two different stories. With energy dissipators, vibration energy is allowed to transmit from the substructure to the superstructure but dissipated by the supplemental devices. There are two types of energy dissipators: displacement dependent and velocity dependent. The displacement-dependent dissipators provide stiffness in addition to damping. After 1999 Chi-Chi earthquake, passive control devices for seismic isolation and energy dissipation become more and more popular. Hundreds of buildings (new and existing) have adopted these devices. In this paper, the development and application of seismic isolation and energy dissipation in Taiwan is introduced.

.

STRUCTURAL ENGINEERING

ISBN 979-458-758-3
Proceedings of the 3rd International Conference on the Geohazard Information
Zonation and 5th Seminar & Short Course of HASTAG (GIZ2014-HASTAG5)
Organized by UMSU, HASTAG, USM
Medan, Indonesia, October 20-22, 2014

Nonlinear response of low rise hospital RC building in Malaysia due to far and near field earthquake

Taksiah A. Majid [1], Mohd Irwan Adiyanto [2] and Fadzli Mohamed Nazri [1+]

[1] Disaster Research Nexus, School of Civil Engineering, Universiti Sains Malaysia, Penang, Malaysia

[2] Postgraduate Student, School of Civil Engineering, Penang, Malaysia

Abstract. Geographically, Malaysia is situated in relatively far away from active seismic fault zones. Therefore, the earthquake hazard is not exist in Malaysian dictionary of life before the new century. Therefore, seismic consideration is not required in public buildings design. However, since a shock from a gigantic Mw 9.0 earthquake in Aceh, Indonesia on 26 December 2004, Malaysian authority and public citizen become aware of that hazard. The possibility to implement the seismic design start to be discussed at least for important structures such as bridge and dam. Hospital also cannot be ignored in discussion since the buildings is very important and must secure during disaster such as earthquake. This paper presents the study on the nonlinear response of three storey hospital reinforced concrete moment resisting frame designed for medium seismic region in Sabah, Malaysia. The typical frame had been designed according to Eurocode 8 for ductility class medium. The nonlinear response history analysis had been conducted on all five frames with far field and near field earthquake ground motion records as input. The result shows that the magnitude of interstorey drift ratio is strongly influenced by the value of behavior factor, q used in the design. The former is increases around 23% - 52% and 44% - 65% when subjected to the far field and near field earthquakes, respectively as the value of behavior factor, q is increases.

Keywords: Hospital, reinforced concrete, Eurocode 8, behaviour factor, interstorey drift ratio

1. Introduction

Since the gigantic Mw 9.0 earthquake in Aceh, Indonesia on 26 December 2004 which also triggered tsunami in the Indian Ocean, Malaysian authority and public citizen start to rethink about the earthquake hazard toward the nation. After 10 years, the number of tremors which can be felt in Malaysian soil due to Sumatra Andaman and Philippines earthquakes is rising. A lot of researches had been conducted related the that field including the possibility of considering seismic design. According to Mosti report [1], it is worth to consider seismic design for construction of new structures located in medium to high seismic region. Experience from the past earthquakes gave a very useful lesson that hospitals and health care facilities are considered as the most important facilities which must remain safe and operable after the disaster [2]. Damages on the non-structural elements and equipment also can make the building inoperable. As an example, in the 1999 ChiChi Taiwan earthquake, the whole Shiu-Tuwan hospital was closed due to damages of non-structural elements even the damages on structure was not severe. After a significant earthquake, the victims turn to hospitals where they expect to receive treatment for any injuries during the event. Therefore, in every community's post disaster plan, hospitals require special attention and should be the safest place because people's lives depend on its functionality [3,4].

To implement the seismic design in a developing country like Malaysia, the increment of cost also has to be taken into account. Due to economical reason, it is not practical to design structures that can behave elastically during earthquake [5]. This mean that the use of lateral force which had been derived based on elastic response spectrum for design purpose will result in very high cost of construction. Therefore, the concept of behaviour factor, q is proposed to reduce the force obtained from a linear analysis, in order to take into account the nonlinear response of a structure [6]. In American code [7], the concept of behaviour factor, q also proposed namely as force or strength reduction factor, R. The behaviour factor, q strongly influencing

+ Corresponding author. Tel.: +6045996206; fax: +6045941009
E-mail address: takziah@usm.my

the class of ductility, namely as low, medium and high. According to Borzi and Elnashai [8], both European and American codes are too conservative where the ductility demand which corresponds to the behaviour factor, q is higher than the ductility supply. The forward directivity ground motions require smaller value of strength reduction factor, R compared to the non-forward directivity ground motions [9]. Therefore, Jalali and Trifunac [10] suggested that the simple and effective modification is needed to replace the current value of behaviour factor, q.

This paper presents the nonlinear response of low rise hospital reinforced concrete (RC) building when subjected to the near and far field earthquakes. The typical three storey moment resisting frame (MRF) had been designed repeatedly based on different value of behaviour factor, q for ductility class medium (DCM). The seismic response is evaluated based on the value of interstorey drift ratio (IDR).

2. Material and method

2.1. 2 Dimensional MRF model

In this study, the nonlinear response history analysis had been conducted on the three storey RC MRF. A total of five typical model had been designed based on five different value of behaviour factor, q. According to Eurocode 8 [6], the value of behaviour factor, q for ductility class low (DCL) is equal to 1.5. for DCM structure, the value of behaviour factor, q lies in range of $1.5 < q < 5.85$ depend on the type of structure and material. The behaviour factor, $q \geq 5.85$ is used for the ductility class high (DCH). Therefore, the typical frame had been designed repeatedly based on five value of behaviour factor, q equal to 2.3, 3.1, 3.9, 4.7, and 5.5 for DCM. The typical frame is regular in plan and elevation where the floor to floor height is equal to 3.3 m for each stories. The frame is completed by three equal bays of 5.0 m. since this study focus on hospital building, the typical frame is classified into important class IV where the importance factor, γ_I used for design is equal to 1.4. All frames had been designed based on reference peak ground acceleration, a_{gR} equal to 0.12g to represent to the medium seismic region in Sabah, Malaysia [1,11].

The size of beam located at top storey is equal to 250 mm x 550 mm while at the first and second storey is equal to 300 mm x 600 mm. The size for all columns is equal to 375 mm x 375 mm regardless its position either interior or exterior column. All five frames had been designed based on the aforementioned size of sections so that the dynamic characteristic of all frames is similar with fundamental period of vibration, T_1 equal to 0.5 sec. All frames had been designed with seismic provision based on Eurocode 8 [6] with concrete compressive strength, f_{cu} and steel yield strength, f_y is equal to 30 N/mm^2 and 500 N/mm^2, respectively. The detail of steel reinforcement for all frames can be found elsewhere [12].

2.2. Nonlinear Response History Analysis

In order to study the nonlinear response of low rise hospital RC MRF in Malaysia, the nonlinear response time history analysis had been conducted on all frames using Ruaumoko program [13]. The nonlinear response history analysis simulates the response of the frames when subjected to the real earthquake represented by dynamic load which varies against time. For that purpose, the program requires input in form of ground acceleration against time known as ground motion records. A total of 25 ground motion records which had been downloaded from PEER database [14] is shown in Table 1. The list of near field ground motion records can be found elsewhere [15].

Table 1: List of Selected Far Field Ground Motion Records

No	Event	Comp	Station	PGA [g]	PGV [cm/s]	Mw
1	Duzce	ATS 030	Ambarli	0.038	7.4	7.1
2	Duzce	ATS 030	Ambarli	0.025	7.1	7.1
3	Morgan Hill	A01040	58375 Apeel 1	0.046	3.4	6.2
4	Morgan Hill	A01310	58375 Apeel 1	0.068	3.9	6.2
5	Chi Chi	CHY069 N	CHY 069	0.039	10.3	7.6
6	Chi Chi	CHY069 W	CHY 069	0.047	10.9	7.6
7	Chi Chi	TAP026 N	TAP 026	0.073	14.3	7.6
8	Chi Chi	TAP026 E	TAP 026	0.077	11.7	7.6
9	Chi Chi	KAU074 N	KAU 074	0.028	10.0	7.6
10	Chi Chi	KAU074 W	KAU 074	0.032	6.7	7.6
11	Chi Chi	CHY054 N	CHY 054	0.097	19.3	7.6
12	Chi Chi	CHY054 W	CHY 054	0.094	17.9	7.6
13	Chi Chi	KAU010 N	KAU 010	0.034	16.6	7.6

14	Chi Chi	KAU010 W	KAU 010	0.034	11.3	7.6
15	Chi Chi	TAP006 N	TAP 006	0.071	14.1	7.6
16	Chi Chi	TAP008 N	TAP 008	0.061	14.2	7.6
17	Chi Chi	ILA042 W	ILA 042	0.085	21.6	7.6
18	Chi Chi	TAP014 N	TAP 014	0.073	19.4	7.6
19	Chi Chi	TAP095 W	TAP 095	0.098	18.8	7.6
20	Chi Chi	CHY090 W	CHY 090	0.079	14.5	7.6
21	Chi Chi	KAU063 W	KAU 063	0.039	12.5	7.6
22	Chi Chi	TAP013 E	TAP 013	0.094	19.7	7.6
23	Loma Prieta	MEN360	Foster City Menhaden Court	0.098	17.2	6.9
24	Loma Prieta	LKS360	Larkspur Ferry Terminal	0.12	18.6	6.9
25	Loma Prieta	TRI090	Treasure Island	0.13	20.1	6.9

All ground motion records were recorded on soft soil with shear wave velocity, Vs < 180 m/s. Before being assembled as input in Ruaumoko program, all ground motion records had been scaled based on the spectral acceleration with damping ratio of 5% at the fundamental period of vibration, $Sa(T_1,5\%)$. The scaling process was referred to the Type 1 response spectrum of Eurocode 8 [6] for Soil Type D developed based on the reference peak ground acceleration, a_{gR} as mentioned in previous subsection.

3. Result and Discussion

The action of earthquake induces lateral displacement on the structures. Large lateral displacement will cause damage to the non-structural and structural elements and then lead to collapse. Performance-Based Earthquake Engineering (PBEE) concept proposed four different performance level which might be experienced by structures due to action of earthquake load. The performance level is namely as Operational (OP), Immediate Occupancy (IO), Life Safety (LS), and Near Collapse (NC) [16]. All performance levels can be evaluated through the magnitude of IDR, which can be expressed as the relative lateral displacement between two adjacent stories normalized to its storey height. The magnitude of IDR equal to 0.5%, 1.0%, 2.0%, and 4.0% indicates the OP, IO, LS, and NC performance level, respectively. Hospitals and health care facilities are considered as the most important facilities which must remain safe and operable after the disaster [2]. Hence, such buildings should be categorized as IO performance level. According Eurocode 8 [6], the IDR for structures in important class IV, such as hospital in this study is limited to 1.25%.

Fig. 1(a) shows the distribution of IDR over the height of all three storey RC MRF used in this study when subjected to the far field earthquakes. Since a total of 25 ground motion records had been used in the nonlinear response history analysis, the magnitude of IDR presented here is the mean value. The frames designed based on lower behaviour factor, q experienced lower magnitude of IDR compared to the same frame designed with higher behaviour factor, q. For example, at the bottom storey, the IDR of frames designed with behaviour factor, q = 2.3 and q = 3.9 is equal to 0.56% and 0.72%, respectively. When designed based on behaviour factor, q = 5.5, the magnitude of IDR at same storey is rising to 0.85%. This trend is clear and indicates that frames designed with higher value of behaviour factor, q experienced larger lateral displacement compared to the frames designed with lower behaviour factor, q. This result is in good agreement with previous study which stated that the increase of force reduction factor, R always leads to an increase of the inelastic displacement ratio [17].

The distribution of IDR over the height for all five frames due to action of near field earthquakes in shown in Fig. 1(b). It is also observed that the magnitude of IDR is higher for frames designed with higher behaviour factor, q. This proves that the latter is weaker which result in larger lateral displacement. At the bottom storey, the magnitude of IDR for frames designed with behaviour factor, q equal to 2.3, 3.1, and 3.9 is equal to 0.66%, 0.95%, and 1.0%, respectively. When designed based on behaviour factor, q equal to 4.7, and 5.5, the magnitude of IDR is increasing around 61% and 65% higher from the IDR of frame with the lowest behaviour factor, q. From Fig. 1(a) and Fig. 1 (b), it can be clearly observed that the distribution of IDR over the height is in typical form regardless the value of behaviour factor, q used in design. The type of ground motion record, neither far field nor near field earthquake also did not influencing the form of IDR distribution over the height. For all frames, the maximum IDR is concentrated at the bottom storey.

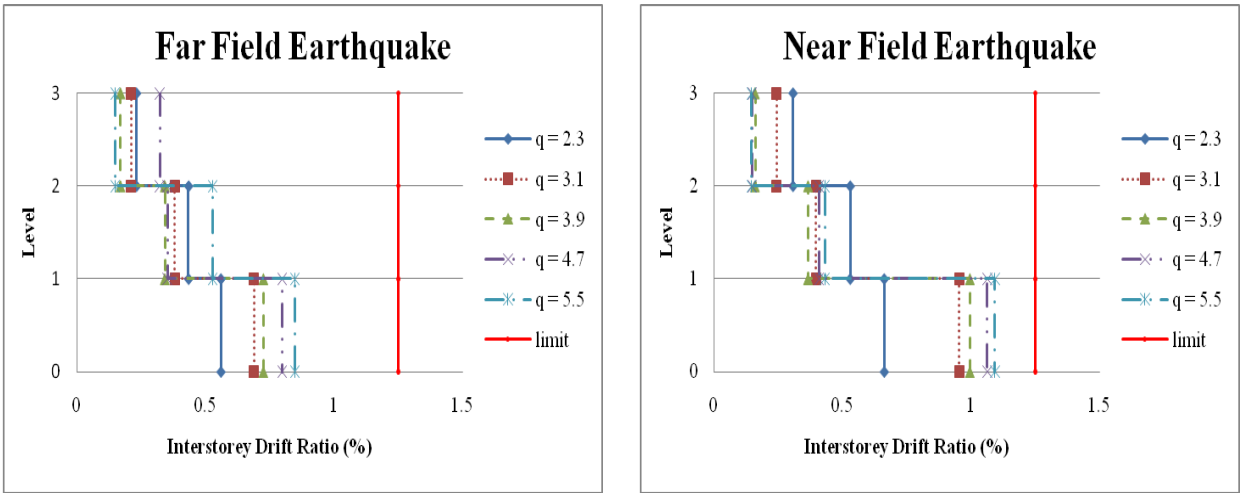

(a) (b)

Fig. 1: Interstorey drift ratio of 3 storey frame (a) Far Field Earthquake (b) Near Field Earthquake

Fig. 2 depicts the maximum IDR obtained from action of both far field and near field earthquakes on all five frames. As discussed in previous paragraph, the maximum IDR is concentrated at the bottom storey. It can be clearly observed that the action of near field earthquake induced higher magnitude of IDR for all frames. This result mean that even designed based on similar behaviour factor, q the IDR due to near field earthquake is higher compared to the one resulted from far field earthquake. As an example, for frame designed with behaviour factor, q equal to 3.9, the magnitude of IDR correspond to the far field and near field earthquakes is equal to 0.72% and 1.0%, respectively. However, in this study, it is found that the magnitude of IDR caused by both far field and near field earthquakes is lower than the limit of 1.25% regardless the value of behaviour factor, q used in design. Therefore, in term of seismic performance, the design of all frames are acceptable. However, the design also has to consider the total cost of material which is discussed elsewhere [12].

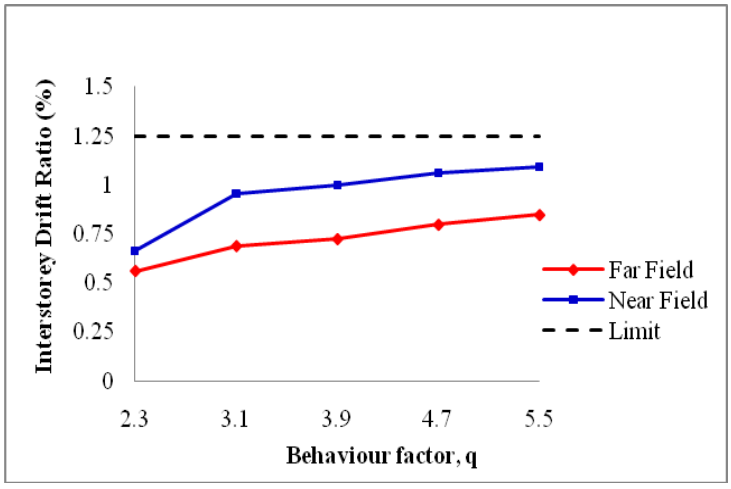

Fig. 2: Maximum interstorey drift ratio of 3 storey frame

4. Conclusion

This paper presents the study on the nonlinear response of three storey hospital RC MRF designed for medium seismic region in Sabah, Malaysia. The typical frame had been designed according to Eurocode 8 [6] for DCM. Five different value of behaviour factor, q had been used for designed which is equal to 2.3, 3.1, 3.9, 4.7, and 5.5. Then, the nonlinear response history analysis had been conducted on all five frames with far field and near field ground motion records as input. The following conclusions can be drawn from this study:

- The value of behaviour factor, q used in design strongly influencing the magnitude of IDR where the latter is increases as the former is increases and concentrated at the bottom storey.
- Due to far field earthquake, the magnitude of IDR is increases in range of 23% to 52% as the value of behaviour factor, q used in design is increases.
- Due to near field earthquake, the magnitude of IDR is increases in range of 44% to 65% as the value of behaviour factor, q used in design is increases.
- For all frames, it is observed that the action of near field earthquake caused greater IDR compared to the far field earthquake.
- In this study, the magnitude IDR for all frames is below than the limit regardless the type of earthquake ground motion records, either far field or near field. Therefore, the design of all frames is acceptable in term of seismic performance. The cost evaluation is needed to find the most economic design.

5. Acknowledgement

The authors gratefully acknowledge the facilities provided by Universiti Sains Malaysia and financial support from MyBrain15, a scholarship provided by Ministry of Education Malaysia to accomplish this study.

6. References

[1] MOSTI. Seismic and tsunami hazards and risks study in Malaysia. Final Report, 2009.
[2] M. Hossain Nazer, and F. Nateghi Elahi. Seismic vulnerability of nonstructural components of hospitals. *Proc. of 13th World Conference on Earthquake Engineering*. Canada. 2004, paper no. 1250.
[3] J. Lewis, and M. Wang. Seismic risk mitigation of operational and functional components in hospitals – the British Columbia experience. *Proc. of 13th World Conference on Earthquake Engineering*. Canada. 2004, paper no. 1636.
[4] E.A. Tingatinga, and R.W. Arriesgado. Earthquake response analysis and simulation of sensitive hospital equipment in the Philippines. *Proc. of 15th World Conference on Earthquake Engineering*. Lisbon. 2012.
[5]FEMA NEHRP. Recommended provisions design examples, Topic 7: Concepts of Seismic-Resistant Design, FEMA 451B, *Building Seismic Safety Council for the Federal Emergency Management Agency*. 2006.
[6] CEN Eurocode 8. Design of structures for earthquake resistance, *Part 1: General rules, seismic actions and rules for buildings*, Brussels. 2003.
[7] ICC. International Building Code, United States of America. 2006.
[8] B. Borzi, and A. S. Elnashai. Refined force reduction factors for seismic design. *Engineering Structures*. 2000, **22**: 1244 – 1260.
[9] J. L. Gillie, A. R. Marek, M. D. Cole. Strength reduction factors for near-fault forward-directivity ground motions. *Engineering Structures*. 2010, **32**: 273 - 285
[10] R.S. Jalali, and M.D. Trifunac. A note on strength-reduction factors for design of structures near earthquake faults. *Soil Dynamics and Earthquake Engineering*. 2008, **28**: 212-222.
[11] A. Adnan, Hendriyawan, A. Marto, P.N.N. Selvanayagam. Development of seismic hazard maps of east Malaysia. *Advances in Earthquake Engineering Applications*. 2008: 1-17.
[12] M.I. Adiyanto, T.A. Majid, F.M. Nazri. Cost optimization of seismic design of low rise hospital RC frame in Malaysia. *Submitted to the15th Asia Conference on Earthquake Engineering*. Taiwan. 2014.
[13] A.J. Carr. RUAUMOKO 2D-user manual for the 2-dimensional version. *Department of Civil Engineering, University of Canterbury*, Christchurch. 2007.
[14]Pacific Earthquake Engineering Research Center. *PEER strong motion database*, [accessed 08.12.13] http://peer.berkeley.edu/smcat.
[15] M.I. Adiyanto, and T.A. Majid. Seismic performance of three storey hospital RC frame subjected to multiple earthquake in moderate seismic region. *Proc. of International Congress on Natural Sciences and Engineering*. Kyoto. 2014.
[16] M.N. Fardis. *Seismic design, assessment, and retrofitting of concrete buildings*. Springer. New York. 2009.
[17]G.D. Hatzigeorgiou. and D.E. Beskos. Inelastic displacement ratios for SDOF structures subjected to repeated earthquakes. *Engineering Structures*. 2009, **31**: 2744-2755.

ISBN 979-458-758-3
Proceedings of the 3rd International Conference on the Geohazard Information
Zonation and 5th Seminar & Short Course of HASTAG (GIZ2014-HASTAG5)
Organized by UMSU, HASTAG, USM
Medan, Indonesia, October 20-22, 2014

Assessment of Pull-through Failure of Nail Connection for Rural Roofing system Under Wind Load in Malaysia

Noram I. Ramli [1+], T. A. Majid [2], F.A. Wan Chik[1], M.K.A Muhammad [1], S. A. Che Deraman[1]

[1] Phd Candidates, School of Civil Engineering, Universiti Sains Malaysia, Nibong Tebal,Pulau Pinang, Malaysia
[2]Coordinator Disaster Research Nexus, School of Civil Engineering, Universiti Sains Malaysia, Nibong Tebal,Pulau Pinang, Malaysia

Abstract. Roof collapse due to wind load impact on roof sheeting during thunderstorm was reported. In most cases, failure of roof sheeting based on two points, either on material roof sheeting or at connection of roof sheeting. It was observed that the most failure of roof sheeting is likely occurred for non-engineered building. Base on MS 1553:2002 wind load for building structure, structural elements should be able to resist wind speed up to 32.5 m/s. Therefore this study is conducted to identify the possibility of the pull-through failure of nail connection with Corrugated Galvanized Iron (CGI) roof sheeting for non-engineered buildings. This study is focus on the connection between roof sheet metal and nail connection with various spacing between the connections. Finite Element Method was used in this study to analyze and identify the load distribution. From the result it shows that the maximum spacing of nail connection is 480 mm to resist the wind load recommended by MS 1553:2002. From the result it can be concluded that as the spacing of connection increases the failure of CGI metal roof also increases.

Keywords: Corrugated Galvanised Iron, Wind Storm, Rural Roofing,

1. Introduction

The rapidly increase in numbers of damage due to wind-related disaster events over the last few years in Malaysia has created the awareness among the Malaysian society. In order to enhance the resistance of the building structure to withstand wind storms, further understanding on characteristic of wind - structure interaction is needed. Malaysia is located near the equator. In general, the wind climate is dominated by the two monsoon seasons and the inter-monsoon thunderstorms. The north-eastern monsoon blows from December to March, usually accompanied by heavy rains. Around June to September, wind blows in the south-western monsoon which is slightly tranquil. Thunderstorms frequently occur during the inter-monsoon periods. Although thunderstorms are localized phenomena, they often produce significant strong and gusty surface winds. These winds from thunderstorms are relatively stronger and more turbulent than those of monsoon winds. [1] Unlike in cyclone prone region, the thunderstorms in Malaysia occurs in micro scale [11]. Despite their small size and short duration of thunderstorm which is about 15 to 30 minutes, many damages has been reported in Newspapers. From the previous study, roof was the most damaging components due to wind storm [5]

2. Failure in rural roofing system

2.1 Malaysia Climate

Malaysia is a country located near the equator. It is equally important to know the flow pattern of wind across Malaysia is dominated by two major monsoons. The characteristic features of the climate of Malaysia are uniform temperature, high humidity and copious rainfall and they arise mainly from the maritime exposure of the country. The climate in this country is almost the same through out the year. Though the wind over the country is generally light and variable, however there are some uniform periodic changes in

[+] Corresponding author. Tel.: + (60199300803); fax: +(6045941009**).**
E-mail address: (mrnoram@gmail.com).

the wind flow patterns across Malaysia. Flow pattern of wind system across Malaysia is dominated by two major monsoons.

I. Southeast monsoon flow from mid April until September.
II. Northwest monsoon flow from early November until March.

During the transition of two major monsoons, there are two shorter inter monsoon seasons. These two monsoons are transition between two major monsoons. In this transition monsoon, many thunderstorm events occur.

2.2 Rural Roofing Failure

Numbers study or research on the wind load effect on the roof structure has been conducted overseas but very few towards Malaysian environment in Malaysia [6][7][8], (Tamura, et al., 2001, 2009, 2010; Uematsu and Isyumov, 1999). Most of the rural houses are considered as non-engineered structures. Corrugated Galvanized Iron (CGI) sheet metal is commonly used in rural house roofing system. However there are no specific guidance on how the sheet zinc metal are assemble. CGI sheet metal frequently experienced a pull-through failure during the thunderstorm due to uplift forces. According to Mahaarachchi & Mahendran [4] from the field and laboratory investigations have shown that damage of steel roofs has often occurred due to the failures of their connections. From the previous study,a single nail connection can be withstand up to 0.71 kN [2]. In this study, CGI sheet metal was examined under wind load of 13 m/s to 32.5 m/s. SAP 2000 software was used to analyse the wind load effect of CGI sheet metal. This study focus on the effect of nail connection spacings on CGI sheet metal until failure. The usual CGI sheet metal and nail that widely used in Malaysia is shown in **Figure 1a** and **Figure 1b**. In this study the CGI sheet metal model are examined with various wind speed and spacing of nail connections.

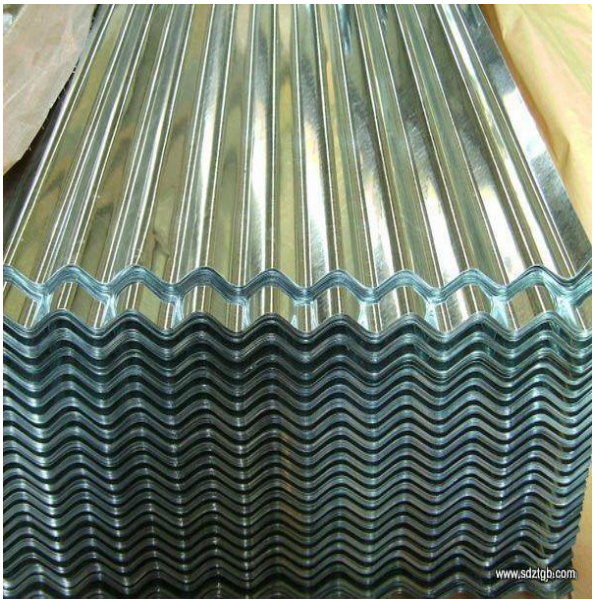

Figure 1a : CGI Sheet Metal

Figure 1b : Nail

.

2.3 Equivalent Static Wind Load

In this study Equivalent Static Wind Load (ESWL) are been considered. Newton first law says that force, F can be calculated from mass and acceleration as follows.

$$F = ma \quad (1)$$

Where, m (mass) is equal to volume x density (ρ) and a, acceleration is equal to changing wind speed over an interval of time. From **equation 1** force can be calculated, **equation 2** also relates between wind speed and force. Winds have its own density and the acceleration can be calculated by measuring the wind speed changes within a specified interval of time. Another equation introduced by Bernoulli give more accurate assumption in calculation of static wind load.

$$p + 0.5\rho V_s^2 = 0 \quad (2)$$

Where p is sum of static pressure, ρ is air density and V is velocity. This equation is called *hyrodynamica,* which specifies that the sum of static pressure, p and the velocity pressure, $0.5\rho V_s^2$ is constant along streamline. From equation 2 design wind speed pressure can be measured by:

$$q = 0.613V_s^2 \quad (3)$$

Equation 3 has been used until now as a guideline to calculate static pressure from basic wind speed for all major codes. It been also adopted in ISO 4354 as a guideline for drafting national codes of practice.

2.4 Result and Discussion

Table 1: Pull Through Force per Connection

Spacing between nail connection		0.3 m	0.45 m	0.6 m	0.9 m
Wind Speed (m/s)	**ESWL (kN/m^2)**	**Force (kN)**			
32.5	0.65	0.4	0.49	1.18	1.46
28	0.48	0.39	0.43	1.15	1.33
23	0.32	0.39	0.39	1.12	1.21
18	0.20	0.39	0.35	1.09	1.11
13	0.10	0.38	0.32	1.08	1.04

Table 1 shows, the value of force of each single point of nail connection for various spacingbetween nail connections. It clearly shows that as the distance between the connection increases,the force acting on each nail connection increases. From previous study [2] the maximum load before the pull through failure is identify at 0.7 kN. By using interpolation the 0.7 kN force will be estimated occur at the spacing between the nail connection of 480 mm. Consequently, the risk of pull through failure will occur if the spacing is greater than a 480 mm.

2.5 Conclusion

From this study,it can be concluded that the spacing of the connection are very important in order to resist wind load. By increasing the distance between the nail connections will affect the performance of the CGI sheet metal roofing. Base on MS 1553:2002 the minimum wind load design is $0.65kN/m^2$. Hence, the nail connection should not be allowed greater than 480 mm in distance to complying the minimum wind load recommended by MS1553:2002.

3. Acknowledgements

The research team thanks Universiti Sains Malaysia for the financial support from the Delivering Excellence Grant.

4. References

[1] Choi, E.C.C, Extreme wind characteristics over Singapore - An area in the equatorial belt, *Journal of Wind Engineering and Industrial Aerodynamics* Volume 83, November 1999, Pages 61-69

[2] Lee Sid Hwa , Failure of roof structrure due to wind load. Master Project, *Faculty of Civil Engineering, Universiti Teknologi Malaysia*, 2008

[3] Mahaarachi Dhammika & Mahendran A strain criterion for pull-through failures in crest-fixed steel claddings. *Engineering Structures*, *31*(2), 2009 pp. 498-506.

[4] MS 1553:2002 "Malaysia Standard Code of Practise on Wind Loading for Building", Department of Standards Malaysia, 2002

[5] T.A.Majid, Noram I.Ramli, M.I.Ali, M,Syamsyul H. Saad, M. Hashim, I. Zakaria Malaysia Country Report 2010 *APEC Wind Engineering Workshop, Gangneung Korea,* 2010

[6] Tamura, Y., Kikuchi, H. and Hibi K., (2001), Extreme wind pressure distributions on low-rise building models, Journal of Wind Engineering and Industrial Aerodynamics, pp 1 – 2, 1365 – 1366.

[7] Tamura, Y. Wind induced damage to buildings and disaster risk reduction, *Proceedings of the APCWE-VII*, 2009 Taipei, Taiwan.

[8] Tamura, Y. and S. Cao. Climate change wind-related disaster risk reduction. *Proceedings of the 2010 APEC-WW and IG-WRDRR joint workshop wind-related disaster risk reduction (WRDRR) activities in Asia-Pacific region and cooperative actions*. 2010 Korea

[9] Uematsu, Y. and Isyumov, N., (1999), Wind pressures acting on the roof and wall edges of a low-rise building Part 4 Review of previous papers, Journal of Wind Engineering, JAWE,(78),(1999),13-27.

[10] Wan Chik, F.A, Ramli, N.I, Muhammad M.K.A, Majid, T.A, Amirul Hafiz, A Study on rural roofing system due to strong wind in Northern Peninsular Malaysia, The Eighth Asia-Pacific Conference on Wind Engineering, December 10-14, 2013, Chennai, India

[11] Yusoff A , "A study on the characteristics of thunderstorm at Telekom Malaysia communication center, Seberang Jaya, Penang"., *MSc Dissertation, School of Civil Engineering, Universiti Sains Malaysia*, 2005

ISBN 979-458-758-3
Proceedings of the 3rd International Conference on the Geohazard Information
Zonation and 5th Seminar & Short Course of HASTAG (GIZ2014-HASTAG5)
Organized by UMSU, HASTAG, USM
Medan, Indonesia, October 20-22, 2014

Axial Load Variations of Irregular RC Frames with Setback under Vertical Earthquakes

Awang Taib[1], Mohd Zulham Affandi Mohd Zahid[1], Ade Faisal[2], Saffuan Wan Ahmad[3]

[1]Department of Civil Engineering Technology, Faculty of Engineering Technology, Universiti Malaysia Perlis, 02600, Arau, Perlis, Malaysia
[2]Program Studi Teknik Sipil, Universitas Muhammadiyah Sumatera Utara, Medan, Indonesia
[3]Faculty of Civil Engineering, Universiti Teknologi Malaysia, 81310, Skudai, Johor, Malaysia

Abstract. In past decades, most of the studies in earthquake engineering concentrated on the effect of horizontal ground motion on the civil engineering structures. With the increase of near field ground motion records and field evidence of significant effect of vertical ground motion on the damaged civil engineering structure, the vertical earthquake has attract the earthquake engineering community to assess the safety of existing structures under its excitation. Furthermore, the analytical assessment to support the field evidence is very limited. The aims of this study are to evaluate the effect of vertical ground motions to the irregular reinforced concrete frames with setback. The frame models are subjected to ten horizontal and vertical ground motions with various peak ground acceleration ratios between horizontal and vertical ground accelerations (V/H) ranging from 0.3 to 1.9. The structural response quantities are expressed in term of variation of axial load. It is found that the variations of axial load are significant in interior columns as well as exterior columns that may endanger the shear capacity of the reinforced concrete buildings.

Keywords: vertical earthquake, axial load, reinforced concrete buildings.

1. Introduction

In general, civil engineering structures are subjected to earthquake ground motion in three directions, i.e. two horizontal and one vertical. In the past few decades, most of the research focuses on the horizontal ground motion and very limited study dealt with vertical ground motions. This is due to the belief that the existing structures are already strong vertically. However, there were many field evidences reported the effect of vertical earthquake components cannot be taken for granted in seismic assessment and design of civil structures, for instance; [4], [5] and among others. However, there were a few numerical simulation carried out by researchers to underpin the above mentioned field evidence. Di Sarno et al [5] assess the performance of RC columns and a plane two storey-two bay RC frames subjected to only vertical ground motions recorded during the 2009 L'Aquila earthquake. The highest V/H ratio was 1.164 and PGAs were 0.659g and 0.522g in horizontal and vertical direction, respectively. Before that, Kim and Elnashai [6] who also evaluate the effect of vertical ground motion on the regular and irregular with transfer beam RC buildings considered 7 ground motions with the highest V/H is equal to 0.99 and the greatest PGAs were 1.13g and 0.84g for horizontal and vertical components, respectively. Therefore this study attempts to investigate the variation of axial load in the columns of irregular buildings with setback under vertical ground motion with a higher V/H ratio compare to previous study, which is from 0.3 up to near 2.0.

2. Ground motions and RC frame models

This study employs 10 natural earthquake records downloaded from NGA Database [3] and listed in Table 1. The ratio of peak ground acceleration of vertical to horizontal earthquake (V/H) is frequently used by researchers in order to represent the consequence of vertical ground motions. Newmark et. al. [1] suggested scaling down the horizontal spectral shape by factor of 2/3 to obtain spectral shape for vertical components and this procedure is widely used, for instance, in UBC97. However, many previous studies

+ Corresponding Author: Mohd Zulham Affandi Mohd Zahid. Tel.: +6049798626; fax: +6049798636.
E-mail address: mohdzulham@unimap.edu.my.

([5]; [6] and among others)have proved that the 2/3 scaling down is not conservative for near field ground motions (d < 30 km) and over conservative for far field ground motions (d > 30 km). The use of this procedure may results in badly underestimate the actions on the buildings in near field area and absolutely the building is not safe for occupants. Meanwhile, in low seismicity area it will highly over estimate the actions on the building and eventually wasting the money. Furthermore, Eurocode 8 suggests using factor of 0.9 for high and moderate seismicity area (Ms > 5.5) and factor of 0.45 for low seismicity area (Ms < 5.5). However, Kim et. al. [6] observed that there were many cases where the V/H ratio for near field region are around 2 and there were also several cases where V/H ratio more than 2.5. Therefore, since V/H ratio as a main characteristic employed to evaluate the effect of vertical earthquake component, this study considers ground motions records with wide range of V/H ratio which is from 0.3 as the lowest ratio to 1.9 as the highest V/H ratio. According to EC8 if the peak ground acceleration of vertical earthquake component is exceeding 0.25g at any particular area the vertical component of ground motion should be take into account in the design process for five cases of structural systems, therefore, in this study all the selected ground motions are strong earthquake (M_w > 5) with minimum PGA of 0.4g and 0.32g in horizontal and vertical direction, respectively. The hypocentral distance of all earthquakes are less than 20 km in order to consider only near field ground motions as the effect of vertical earthquake components in far field regions (> 30 km) is not significant [4].

This study employed 8-storey RC frames with setback as shown in Figure 1. Frame IS1 was designed for gravity load only and Frame IS2 was also designed to resist horizontal earthquake with PGA equals to 0.2g and soil class B according to EC8. The detail information on the design of these frames can be found in Hartzigeogiou and Lilios's [7]. As we can see, the cross sectional area of structural members for both models is identical, i.e. 350mm x 350mm for columns and 300mm x 500mm for beams. In terms of steel reinforcements, frame IS2 has 65% and 27% more steel reinforcement area, A_s, compared to IS1 model for columns and beams, respectively. This shows that the IS2 model is more ductile than the IS1 model and makes it satisfactory to resist earthquake in near field area. Furthermore, modal analysis and nonlinear time history analysis have been carried to compare the dynamic characteristic and interstorey drift ratio (IDR) of these frame models. In Hartzigeogious and Lilios' study [7], the 8 storey irregular gravity and earthquake designed frames with setback were designated as B4 and A4, respectively. Table 2 shows the dynamic characteristic of the frame models and the one from Hartzigeogious and Lilios' study [7]. In terms of vibration periods, it shows that the vibration period of the frames used in this study are very close with the original one and the biggest different is in mode 2 for IS1 frame model which is about 0.05 s. Furthermore, the Mass Participation Factor of both models also very near with the original models. Therefore, it can be deduced that the model used in this study have similar dynamic properties with Hartzigeogious and Lilios's [7] models. The nonlinear response of both models also was examined and compared using nonlinear time history analysis. The Imperial Valley earthquake recorded at station 5055 Hotville P.O. was employed in this analysis and the resulting Intestorey Drift Ratio (IDR) for model B4 and IS1 was plotted as shown in Figure 4. It is found that the both models exhibit similar fashion of IDR along the height of models in which the IDR increase as the height increases and it shows a little drops at top storey. The greatest IDR occurred at storey 6 and 7 for both models. This proved that nonlinear response along the height of the models have a similar trend.

3. Axial loads in columns

In this study, the nonlinear time history analysis was carried out according to Newmark's method and the following dynamic equilibrium equation is used to determine the response of the frames:

$$M\ddot{u} + C\dot{u} + Ku = -Ma_g \quad (1)$$

Where M is Mass, C is Damping, K is stiffness, a_g is ground motion acceleration and the upper dots stand for time derivatives. The Ruaumoko [8] software was utilized to solve the above equation. Each of the RC frame models were excited by 20 ground motions; 10 horizontal earthquakes only (HGM) and 10 vertical plus horizontal ground motions (VHGM). In total, there were 40 nonlinear time history analyses were performed. The response of the frames due to vertical earthquake is quantified in terms of axial load variation or axial load ratio in the columns. The axial load ratio is determined as follows:

$$Axial\ Load\ Ratio = \frac{P_{v+h}}{P_h} \quad (2)$$

Where, P_{v+h} = axial load in column induced vertical and horizontal earthquake

P_h = axial load in column induced by horizontal earthquake only

Table 1: List of ground motions.

No	Date	Earthquake Name	Mag(M_w)	Hypo Dist.	Station	PGA (H)	PGA(H)	PGA (V)	V/H < 1
1	24/4/1984	Morgan Hill	6.2	0.1	57217 Coyote Lake Dam	0.71	1.30	0.39	0.30
2	15/10/1979	Imperial Valley	6.5	2.5	5054 Bonds Corner	0.59	0.78	0.43	0.55
3	21/7/1986	Chalfant Valley	6.2	18.7	54428 Zack Brothers Ranch	0.40	0.45	0.32	0.72
4	16/7/1978	Tabas,Iran	7.4	3	9101 Tabas	0.84	0.85	0.69	0.81
5	9/5/1983	Coalinga	5	12.6	1607 Anticline Ridge Pas	0.41	0.45	0.38	0.84
6	18/10/1989	Loma Prieta	6.9	14.5	47125 Capitola	0.44	0.53	0.54	1.02
7	15/10/1079	Imperial	6.5	0.6	cerro array	0.38	0.46	0.54	1.17
8	26/4/1981	Westmorland	5.8	13.3	5169 Westmorland Fire Sta	0.37	0.50	0.84	1.69
9	17/05/1976	Gazli, USSR	6.8	3	Karakyr	0.61	0.72	1.26	1.76
10	23/12/1985	Nahanni, Canada	6.8	6	6097 Site 1	0.98	1.10	2.09	1.90

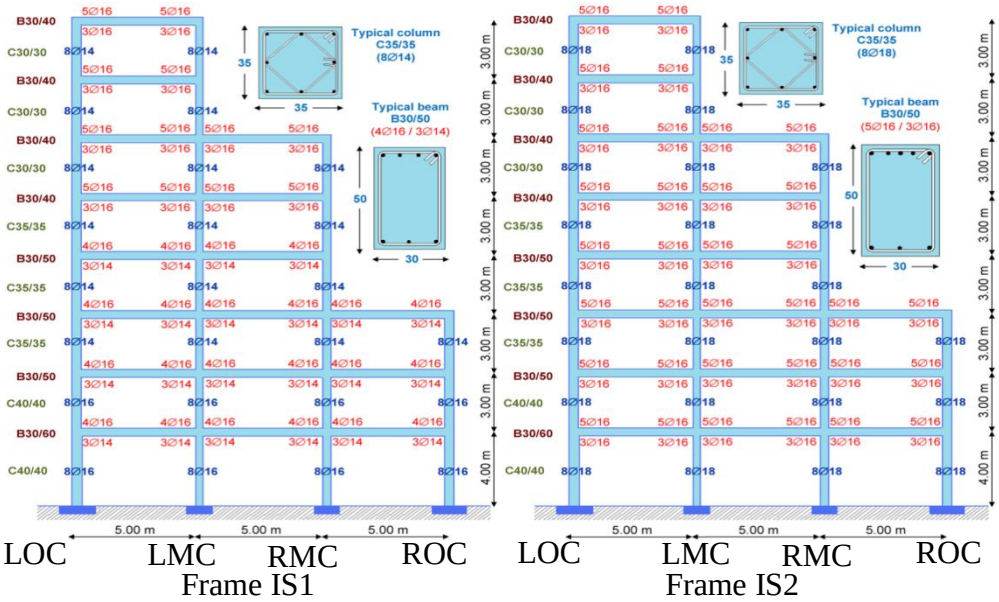

Figure 1: Irregular frames with setback [7]

Figure 5 shows the variations of axial load ratio along the height of the frame models. Positive sign indicates the tension forces and negative sign indicates the compression force. It is found that, the axial load ratio increases as the V/H ratio increases, especially in LMC columns. Under the excitation of Morgan Hill Earthquake (G1) which have V/H = 0.3, the axial load in the column induced by VHGM is almost identical with the one that induced by HGM. However, when the V/H ratio increase to 0.81 (G4 – Tabas Earthquake), the axial load in LMC column under VHGM increases up to 3 times. Then, the axial load in LMC column increases up to 5 times when the V/H ratio increases to 1.76 (G9 – Gazli Earthquake). Besides that, the LOC column also shows an increase of axial load ratio as the V/H ratio increases, especially in higher storey, i.e. 7^{th} and 8^{th} storey. This significant increase of axial load in LMC and LOC columns may reduces the column's ductility capacity and results in brittle failure mechanism. Furthermore, Figure 6 plotted the maximum axial load ratio for all columns (i.e.: LOC, LMC, RMC and ROC) of the IS1 model under ten ground motions with various V/H ratios, start from 0.3 until 1.9. The square and diamond shape of points indicate the compression and tension forces, respectively. It clearly show that the maximum axial load ratio increases as the V/H ratio increases except for ROC columns. The greatest increase of axial load is in LMC column, where, the VHGM of Nahanni earthquake (V/H = 1.9) induced 6 times greater compression forces compare to HGM. The most affected column for setback type of frames is the inner column (LMC). Furthermore, this study also found that the exterior columns (LOC) badly affected by the vertical ground motion. As illustrated in Figure 6, when VHGM is considered, the axial load in LOC column may amplified up to 3.5 times higher compared to the one without vertical components. This finding against the results obtained recently by Di Sarno et. al. [5], in which, they deduced that the variations of axial load in exterior columns when VHGMs are considered is negligible. This is because, the 6 April 2009 L'Aquila Earthquake

that they considered posses low PGA and V/H ratio compared to this study. Therefore, in the near field region, the vertical earthquake component should be taken into account to design earthquake resistant structures. It also worth to highlight that, the vertical ground motion affects significantly the axial load in columns when its PGA is about 2/3 (70%) of its horizontal counterpart. There is also not much different between IS1 and IS2 buildings in term of the variation of axial load in the columns.

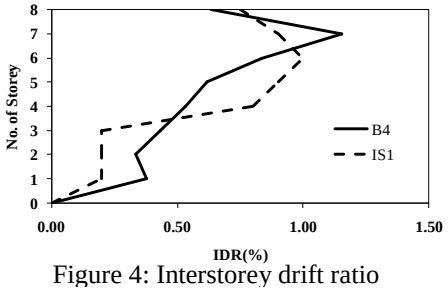

Figure 4: Interstorey drift ratio

Table 2: Dynamic Characteristic of Frames

	Vibration period, T (s)				Mass Participation Factor, MPF (%)			
	IS1	B4	IS2	A4	IS1	B4	IS2	A4
MODE 1	0.9645	0.9673	0.9665	0.9673	71	73	75	73
MODE 2	0.3908	0.4469	0.4289	0.4469	90	93	92	93
MODE 3	0.2431	0.2746	0.2616	0.2746	96	98	97	98

4. Conclusion

Numerous field evidents showed the devastating effect of vertical earthquake on the RC structures and a numbers of analytical study have been carried out to prove the field evident but not for setback type of buildings under various V/H ratio from 0.3 until near 2.0. This work investigated the effect of vertical ground motion on the irregular buildings with setback. For that purpose, this study considered ten natural earthquake records with epicentral distance less than 20 km. This study cannot be considered exhaustive. However, this study found that the vertical earthquake components may increase the axial load in interior columns up to 6 times higher than when on horizontal ground motion is considered. The exterior columns also may affected by the vertical ground motion especially when V/H more than 1 and PGA of the vertical earthquake more than 1g. This may reduces the ductility capacity of the column and result in brittle failure in shear. Therefore, the vertical earthquake components should be considered when designing a new structure or strengthening the existing one for both type of columns (exterior and interior).

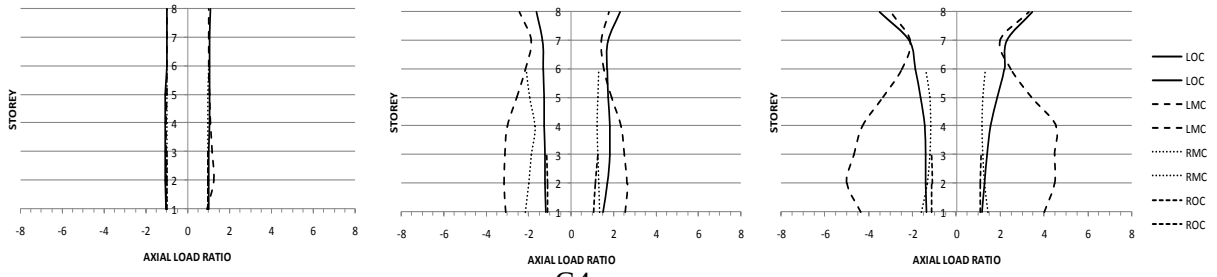

G1 G4 G9

Figure 5: Variation of axial load ratio along the height

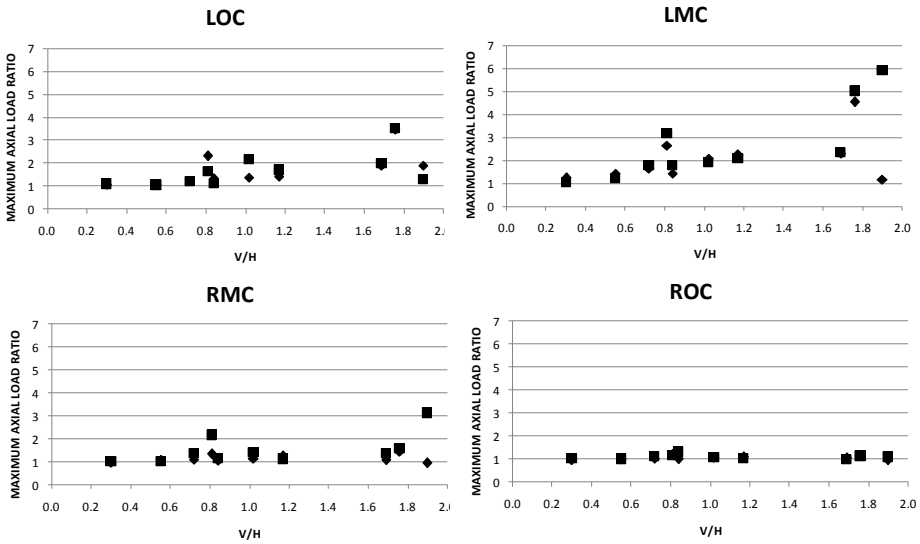

Figure 6: Maximum axial load ratio

5. Acknowledgement

The contribution of Ms Tan Mio Gin is gratefully acknowledged. Financial support for this research was provided by the Ministry of Education, Malaysia through a grant FRGS 9003-00407.

6. References

[1] Nathan N. Newmark. A Study of Vertical and Horizontal Earthquake Spectra. United State Atomic and Energy Commission. 1974

[2] CEN. Eurocode 8: Design of Structures for earthquake resistance. Part 1: General rules seismic actions and rules for buildings. Final Draft prEN 1998. European Committee for Standardization. Brussels. 2003

[3] PEER (2008). PEER NGA Database, available at *http://peer.berkeley.edu/nga/*.

[4] Papazoglou A.J. and Elnashai A.S. Analytical and field evidence of the damaging effect of vertical earthquake ground motion. *Earthquake Engineering and Structural Dynamic.*1997. 25:1109-1137

[5] Di Sarno, L., Elnashai, A.S. and Manfredi, G. Assessment of RC Columns Subjected to Horizontal and Vertical Ground Motions Recorded during 2009 L'Aquila (Italy) Earthquake. *Engineering Structures*. 2011. 33:1514-1535.

[6] Kim., S. J., & Elnasha., A. S. Seismic assessment of rc structures considering vertical ground motion. MAE Central Report No. 08-03. University of Illinois, Urbana, Illinois. 2008

[7] Hatzigeorgiou., G. D., & Liolios., A. A. Nonlinear behaviour of RC frames under repeated strong ground motions. *Soil Dynamics and Earthquake Engineering*. 2009. In press

[8] Carr, A.J. (2008). RUAUMOKO – inelastic dynamic analysis program. Department of Civil Engineering, University of Canterbury, Christchurch, New Zealand

ISBN 979-458-758-3
Proceedings of the 3rd International Conference on the Geohazard Information
Zonation and 5th Seminar & Short Course of HASTAG (GIZ2014-HASTAG5)
Organized by UMSU, HASTAG, USM
Medan, Indonesia, October 20-22, 2014

Case Study: Wind Speed Estimation of High-Rise Building Using Surface Interpolation Methods

Deraman, S. N. C[1], Wan Chik, F. A[1], Muhammad, M. K. A[1], Noram I. Ramli[1], Majid, T. A[2], M. S. S. Ahamad[2]

[1]Postgraduate Student, [2]Associate Professor
Disaster Research Nexus, School of Civil Engineering, Universiti Sains Malaysia,
Engineering Campus, 14300 Penang, Malaysia

Abstract. This paper is based on the event in Penang that caused fatality, injuries and damages. This study focuses on high-rise building near to the incident area using the wind speed during that event. The aim of this study is to compare the best interpolation methods from the results of estimated wind speed at that respective building. The interpolation process used IDW and TIN method using GIS IDRISI Selva software. IDW method covers for all the area but TIN method do not cover beyond the triangulation point. The value of wind speed is 17.46 m/s for both IDW and TIN method but the most preferable method is IDW. The value of wind speed can be higher or lower than the estimation value if the factors that can change the value of wind speed had been considered in the mapping.

Keywords: Surface interpolation, GIS, Wind Speed

1. Introduction

Windstorm is one of natural disaster happen in our country besides epidemics, floods, earthquakes, mass movement dry and mass movement wet. According to CRED [1], 21.19% of natural disaster in Malaysia related to storm. This number is not a small number but it is something to be aware and worry not only by the government but also individual itself. The common damages caused by windstorm are uprooted trees and blown off roofs. Penang state can be classified as a sub-urban area with a lot of high-rise buildings. There were too many incident related to windstorm and high-rise building. One of the incidence happened in Penang in 2013 that caused damages, injuries and fatal. This study focuses on the high-rise building near to the location of incident using the data during the incident provided by MET. Ramli et al. [2] reported that average of wind speed will increase as the height increase and force acting on structures depends on terrain category [3]. Liu [4] stated that, building or structures deflect winds, causing a change in wind speed and direction around the buildings or structures. Frictional effects show an important role for wind near the ground surface. Thus, the mean wind speed may change in direction slightly with height, as well as magnitude [5]. As stated in MET [6] report, the general features of the climate in Malaysia are uniform temperature, high humidity, copious rainfall and light wind. It also reported that the southwest monsoon season usually happened in the late half of May or early June and in September. Wind climate in Malaysia is conquered by two monsoon seasons and inter-monsoon thunderstorms Majid et al. [7].

The estimation value of the wind speed at that building was determined using surface interpolation method available in GIS software tools (IDRISI Selva). IDRISI Selva is one of the GIS software that commonly used in mapping the wind speed other than ArcGIS.

+ Corresponding author. Tel.: + 04-5995999 Ext. 6282; fax: +04-5941009
E-mail address: taksiah@usm.my

Spatial interpolation is the process of calculating an unknown at the specific point using a set of sample point with known values that are distributed across the area. The rules about the spatial variation and location of data collection points are important because they can significantly affect the results [9]. Apaydin et al. [8] stated that spatial interpolation has its own special which can be used to estimate meteorological variable at other location. The aim of this study is to compare the best result using two surface interpolation methods from the results of estimated wind speed at the respective building at the height of 10 m from ground surface.

2. Methods

2.1. Datasets

The map was interpolated by using the datasets that provided by Malaysian Meteorological Department (MET) on the same date and time as the incident happened. The minimum numbers of point to be interpolated are four points which are Alor Setar, Langkawi, Butterworth and Bayan Lepas. The selected points based on the closer distance from the location of incident. There are two methods that have been used in this study which are Inverse Distance Weighted (IDW) and Triangulated Irregular Network (TIN). Both methods are used for surface interpolation purposes. Spatial interpolation is often an important strategy for creating a continuous surface when taking irregular point data [10]. Apaydin et al. [8] stated that the interpolation techniques were group into two main categories which are deterministic and geostatistical and IDW are categorized as deterministic because this technique create surface from measured points, based on either extent of similarity.

2.2. Inverse Distance Weighted (IDW)

IDW interpolation is commonly used in GIS to create raster overlays from point data. Once the data are on a regular grid, contour lines can be threaded through the interpolated values and the map can be drawn as either a vector contour map or as a raster-shaded map [11]. Luo [12] and Chinta [13] has quoted the paper from Theissen [14] and stated that IDW interpolation combines the idea of proximity espoused. The IDW function is used when the set of points is dense enough to capture the extent of local surface variation needed for analysis; therefore, it was used in this study [15]. The principle of IDW methods is to assign more weight to nearby points than to distant points.

The usual expression is,

$$Z(s_0) = \sum_{i=1}^{n} \lambda_i . \hat{Z}(s_i) \qquad (1)$$

where,

$Z(s_0)$ = the value to be predicted for location s_o

n = the number of measured sample points surrounding the prediction location that will be used in the prediction

λ_i = the weights assigned to each measured point to be used

$\hat{Z}(s_i)$ = the observed value at location si

2.3. Triangulated Irregular Network (TIN)

TIN is another tool in GIS and it is a vector data structure. It creates a surface formed by triangles of nearest points. The sample data points become the vertices of a set of triangular facets that completely cover the study area. In IDRISI, the TIN is generated and then used to create a continuous raster surface model.TIN creates a constrained or non-constrained TIN from isoline or point data. In TIN method, there are two principal phases to be generated which are the selection of the point data and connection into triangular facets [16]. In this study, the IDRISI TIN module is created from the input of isoline data from fours stations in Northern region of Peninsular Malaysia. In doing so, the TIN can be constrained so no triangular facet edge crosses an isoline. This forces the triangulation to preserve the character of the surface as defined by the isolines [17].

3. Result and Discussion

The interpolated results of wind speed using GIS IDRISI Selva software is calculated from four sets of reading during the event and at the same time. The data attribute information contains wind speed and wind direction. The wind speed data is in the unit of meter per second while the wind direction data is in unit of degree. Table 1 shows the maximum wind speed during that event for each station.

Table 1: Summary of Wind Speed Data (MET)

Station	Wind Direction (^{o})	Maximum Surface Wind (m/s)
Butterworth	300	19.1
Bayan Lepas	320	15.9
Alor Setar	210	14.0
Langkawi	270	14.9

The data from Table 1shows that the highest wind speeds during the incident is 19.1 m/s at Butterworth station. Since the reading at respective high-rise building cannot be collected during the incident, the surface interpolation method has been applied by using GIS IDRISI Selva tools. For this study, only two techniques are applied to find the compatible and applicable methods. The red points in Figure 1and 2 describe the location of the station which is in Bayan Lepas, Butterworth, Alor Setar and Langkawi while the white triangle shape shows the location of the respective high-rise building (Building A). The interpolated value of wind speed of the building at 10 m height is approximately 17.46 m/s during the event as shown in Figure 1. Triangulated Irregular Network (TIN) method as shown in Figure 2 is the alternative method applied to determine interpolated wind speed. It verifies the value of wind speed to be approximately 17.46 m/s as well i.e. same results with IDW method. Based on Beaufort scale, the value of this wind speed for both methods can be categorized as fresh gale.

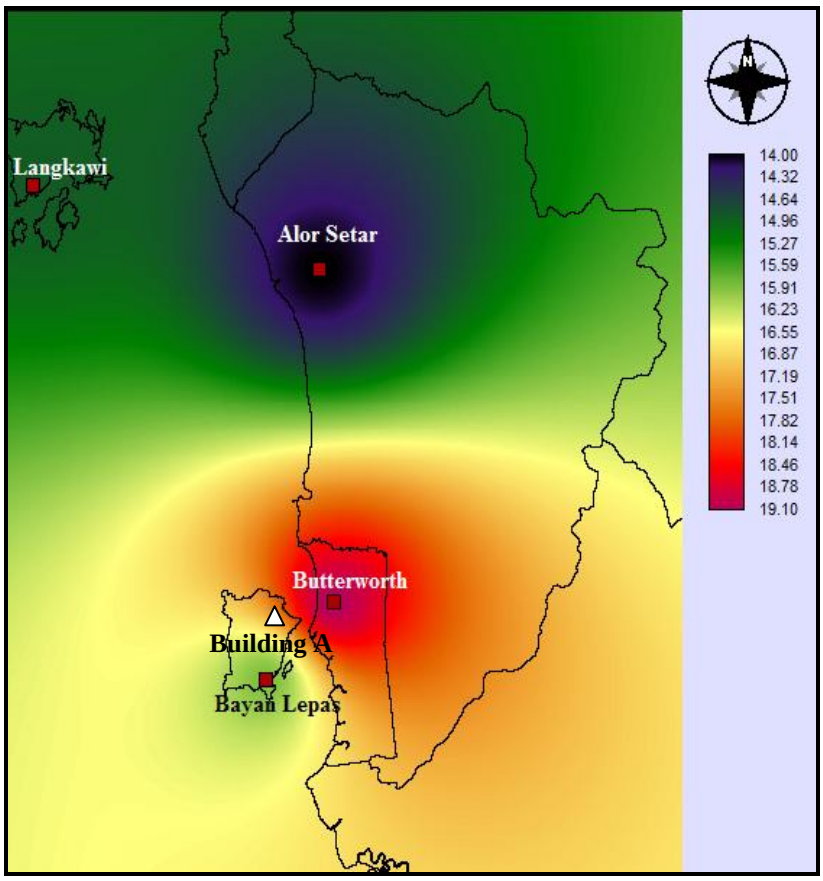

Figure 1: Wind Speed Map using IDW Method

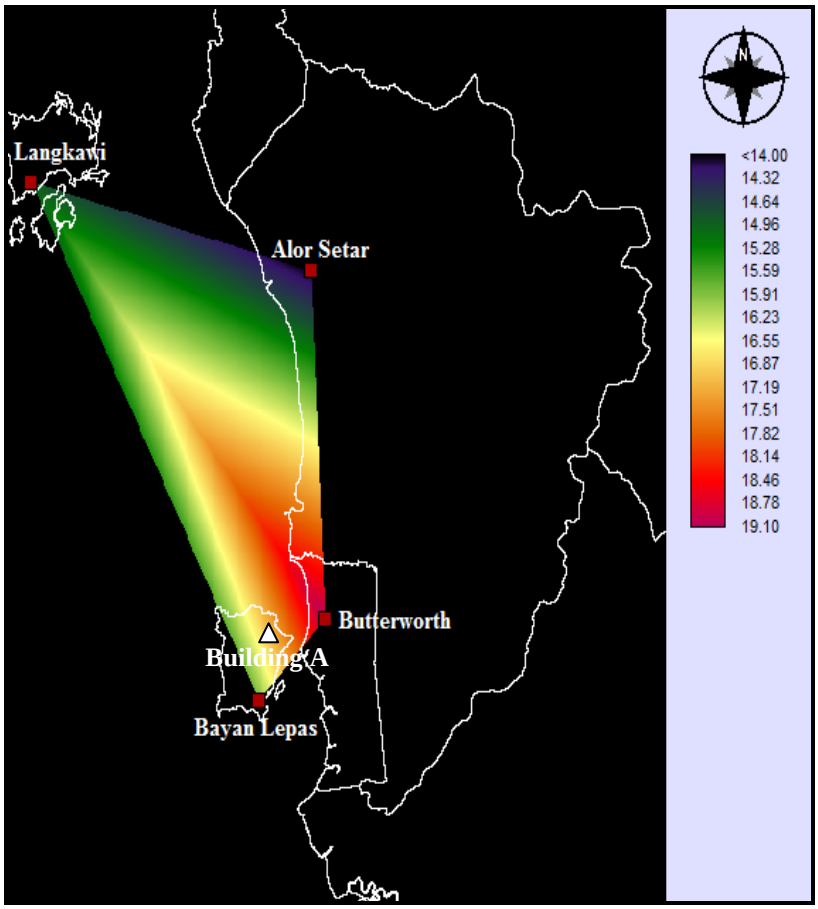

Figure 2: Wind Speed Map using TIN method

Liu [4] stated in his book that many factors may slow down the wind in certain regions, shielding or accelerate such as topography, woods, buildings and other structures and are be able to change the speed or direction of the wind. Besides that, when turbulent flows from a different surface layer to another surface layer, the wind flow may accelerates or decelerates depending to the change of surface roughness. The rougher the terrain is, the more it retards the wind speed.

This study interpolates the wind speed without considering other factors that may change the direction or speed of wind. The estimation value of wind speed at respective building can be higher or lower than the exact value. As stated in the book of Liu [4] that topography and structures are one of the factors that may change the wind speed and direction, this building absolutely affected by this factor since it is surrounded by the hills and highest building that are more than 10 m.

The interpolation using TIN method is not smooth as IDW method because of discontinuous slope at the triangle edges and it is not suitable for extrapolation beyond the area with the set of sample point. Fortunately, in this study, the respective location (Building A) falls within interpolation area using TIN method but the IDW method covers all the area.

4. Conclusion

The result from IDW and TIN method give the same value of wind speed which is 17.46 m/s at the height of 10 m from ground surface. This value is not the worst that can cause the structure collapsed. It may caused by the failure of the structure itself. The use of surface interpolation is to predict the value at specific location and the most preferable method to be applied is IDW because it can be used for interpolation and extrapolation. Morever, to get the accurate value of wind speed at that building, the factors that will affected the wind speed must be considered before doing interpolation process.

5. Acknowledgement

The authors would like to thank to Ministry of Education Malaysia under MyBrain15 for providing financial support during this study, Research Creativity Management Office (RCMO) for the APEX Delivering Excellence (DE) Grant 2012, Universiti Sains Malaysia and Institute Postgraduate Studies (IPS), Universiti Sains Malaysia for the IPS Graduate Fund.

6. References

[1] Centre of Research on the Epidemiology of Disaster (CRED) (2009). Malaysia Country Profile- Natural Disasters. Retrieved March 30, 2014 from http://www.emdat.be/result-country-profile

[2] Ramli, N. I. (2005). Determination and Validation of Terrain Height Multiplier for Type 3: Suburban Area for MS 1553: 2002

[3] Husain, N. M. (2007). Development of Terrain Height Multiplier for Seberang Jaya, Suburban Area. Master's Thesis, Universiti Sains Malaysia

[4] Liu, H. (1991). Wind Engineering: A Handbook for Structural Engineers. Prentice-Hall, Inc.: New Jersey, 1-44

[5] Holmes, J. D. (2001). Wind Loading of Structures. Second Edition. British Library Cataloguing in Publication Data: London and New York, 1-57

[6] Malaysia Meteorological Department (2014). General Climate of Malaysia. Retrieved,August 28, 2014, from
http://www.met.gov.my/index.php?option=com_content&task=view&id=75&Itemid=1089

[7] Majid, T. A., Ramli, N. I., Ali, M. I. and Saad, M. S. H. (2012). Wind Related Disaster Risk Reduction and Environmental Issues. Malaysia Country Report 2012

[8] Apaydin, H., Sonmez, F. K. and Yildirim, Y. E. (2004). Spatial interpolation techniques for climate data in the GAP region in Turkey. Climate Research, 28: 31-40

[9] Andrews, B. D., Gares, P.A., and Colby, J. D. (2002).Technique for GIS modeling of coastal dunes. Geomorphology, 48, 289-308

[10] Kane, R. W. (2009). Modeling Wind Resources for Harnessing Potential Energy.Wind Resources. University of Berkeley

[11] Burrough, P. A. and McDonnell, R. A. (1998).Principles of Geographical Information Systems.Clarendon Press, Oxford

[12] Luo, W., Taylor, M. C. and Parker, S. R. (2008). A comparison of spatial interpolation methods to estimate continuous wind speed surfaces using irregularly distributed data from England and Wales. International Journal of Climatology, 28, 947-959

[13] Chinta, S. (2014). A comparison of spatial interpolation methods in wind speed estimation across Anantapur district, Andhra Pradesh. Journal of Earth Science Research, 2, 48-54

[14] Thiessen, A. H. (1911). Precipitation averages for large areas. Monthly Weather Review, 39, 1082-1084

[15] Alamdari, P., Nematollahi, O. and Mirhosseini, M. (2012).Assessment of wind energy in Iran: A review. Renewable and Sustainable Energy Reviews, 16, 836-860

[16] Peucker, T. K., Fowler, R. J., Little, J. J. and Mark, D. M. (1978). The triangulated irregular network. Amer. Soc. Photogrammetry Proc. Digital Terrain Models Symposium

[17] Clark Labs (2012).IDRISI Selva. GIS and Image Processing Software. Retrieved February 7, 2013 from http://www.clarklabs.org/products/upload/IDRISI-Selva-GIS-Image-Processing-Specifications.pdf

ISBN 979-458-758-3
Proceedings of the 3rd International Conference on the Geohazard Information
Zonation and 5th Seminar & Short Course of HASTAG (GIZ2014-HASTAG5)
Organized by UMSU, HASTAG, USM
Medan, Indonesia, October 20-22, 2014

Behaviour of trapezoidal roof cladding under different location of point load

Majid, T.A [1], Muhammad, M.K.A [2+], Noram, I.Ramli[1], Che Deraman, S.N.A [1,] Wan Chik, F.A [1], and Marcus, N.G[1]

[1] Graduate student, School of Civil Engineering,Universiti Sains Malaysia,Penang, Malaysia
[2]Coordinator, Disaster Research Nexus, School of Civil Engineering,Universiti Sains Malaysia,Penang,Malaysia

Abstract. The failures of roof claddings are very often caused by the uplifting force from the wind. The uplifting force normally will cause damage the support of the roof cladding which are attached to the purlins. When the roof cladding is subjected to wind uplift/ suction force, local dimpling or pull- through failure occur prematurely at their screw connections because of large stress concentration in the cladding at the vicinity of the screw heads. Currently, the design of roof cladding is mainly based on time consuming and expensive laboratory testing. In this study, a finite element model of trapezoidal was developed and validated with the experimental result to study the effect of point load to the trapezoidal roof sheeting. This paper presents the details of the finite element analysis using LUSAS.

Keywords: Uplifting force, pull – through, steel cladding, LUSAS

1. Introduction

Thin roof claddings are commonly made of thin and high strength steels widely used as roofing system for rural area in Malaysia. During high wind events such as thunderstorm, these cladding suffer from local pull through failure at fastener connection due to wind uplift loading. Loss of claddings always leads to a progressive collapse of the entire buildings. From the past research and field damage investigation shown that light gauge steel cladding may fail locally in the vicinity of screw fastener. Under the high wind uplift loading, the light gauge steel cladding often pull through the fastener head, in the presence of large stress concentration around the screw holes [1].

Recently, there are many available commercial finite element analysis programs available in research. The used of finite element software can reduced time consuming and increasing the efficiency of the research. Finite element analysis (FEA) can be utilized to develop a numerical model of roof cladding subject to a variety of loads, proving the opportunity to study the response of roof cladding both efficiently and cost effectively.

Previous studies developed the numerical models of roof cladding using FEA, have been successful in simulating the behaviour of cladding subject to static uplift pressure. The behaviour of cladding under static load was necessary for understanding the mechanism of local and global deformation. In order to simplify the model, both numerical models corrugated and trapezoidal cladding subject to static uplift pressure was often used in past study. [2, 3, 4].

2. Development of Finite Element model

2.1. Structure model

The single span with single sheet model of trapezoidal roof cladding was analyzed using finite element program LUSAS Version 14. As a typical cases, a trapezoidal roof cladding system as shown in Figure 1 is

+ Corresponding author. Tel.: + 6045996201 fax: +6045941009
E-mail address: taksiah@usm.my

considered in this paper. The span (L), depth (d), pitch (p) and thickness (t) of the cladding are 750 mm, 23mm, 190 mm and 0.3mm respectively.

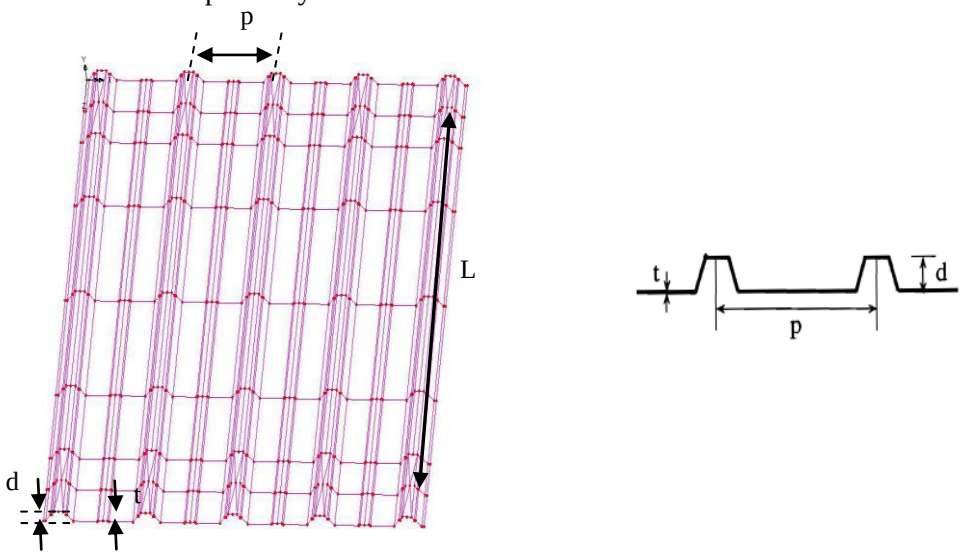

Fig. 1: Trapezoidal steel cladding

2.2. Element and Meshing

Two types of element were used. Four – node, quadrilateral thin shell elements (QSI4) with linear interpolation were used to model the trapezoidal steel cladding. Meanwhile, Three – node, triangle thin shell elements (TS3) with linear interpolation was used around the fastener hole. Selection of mesh size is a critical in the finite element modeling. As shown in Figure 2a, finer mesh was used around the fastener hole due to high local stress and deformation in the steel sheeting. To reduce the analysis time, course mesh was used to model pan and rip of the trapezoidal steel cladding. Figure 2b shows the course meshing used in the analysis.

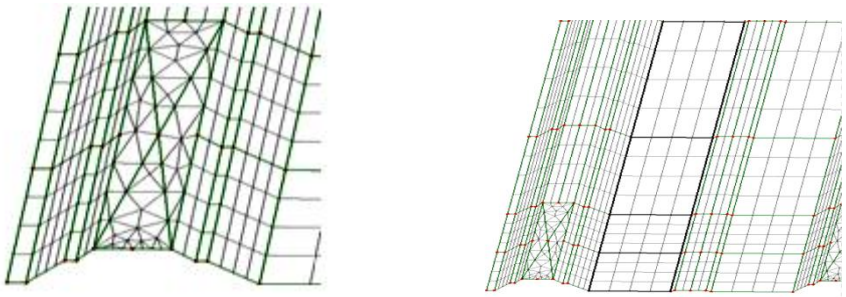

(a) (b)

Fig 2: Meshing used in the analysis a) fine mesh b) course mesh

2.3. Material Properties

The isotropic material properties of the trapezoidal roof cladding were included in the model. The material properties were obtained from the manufacturer. The following material properties of steel were used in the analysis: Modulus of elasticity E= 209 000 MPa and Poisson`s ratio assumed as 0.3.

2.4. Load and Boundary Condition

Due to the symmetrical of the model, only upper quadrant of the model was consider in this study. Nine different location of point load was applied to the model to study the effect of location of point load. The static load applied to the model until failure occurred. The fastener constituted the boundary conditions of the model. To simplify the model, a fastener was assigned as pinned support at alternating crest which is fixed translation and free rotation in all direction. Figure 3 shows the location of point load applied to the trapezoidal steel cladding.

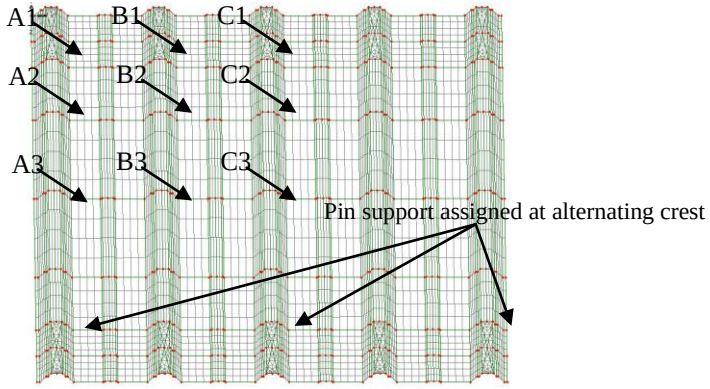

Fig 3: Location of point load

3. Validation of the Finite Element Model

The FEA model`s performance was evaluated by comparing the response of the trapezoidal steel cladding with the corresponding experimental result. An inspection of deformation and deflection of the trapezoidal steel cladding. Experimental work has done with five different span which is 750mm, 850mm, 950mm, 1150mm, 1250mm under the similir loading sequence. However, the FEA used the 750mm span as the percentage difference shows a good argument between finite element method and experimental method All experimental testing method and apparatus used can be found elsewhere [5]. Figure 4 shows the comparison of experimental and FEA model result.

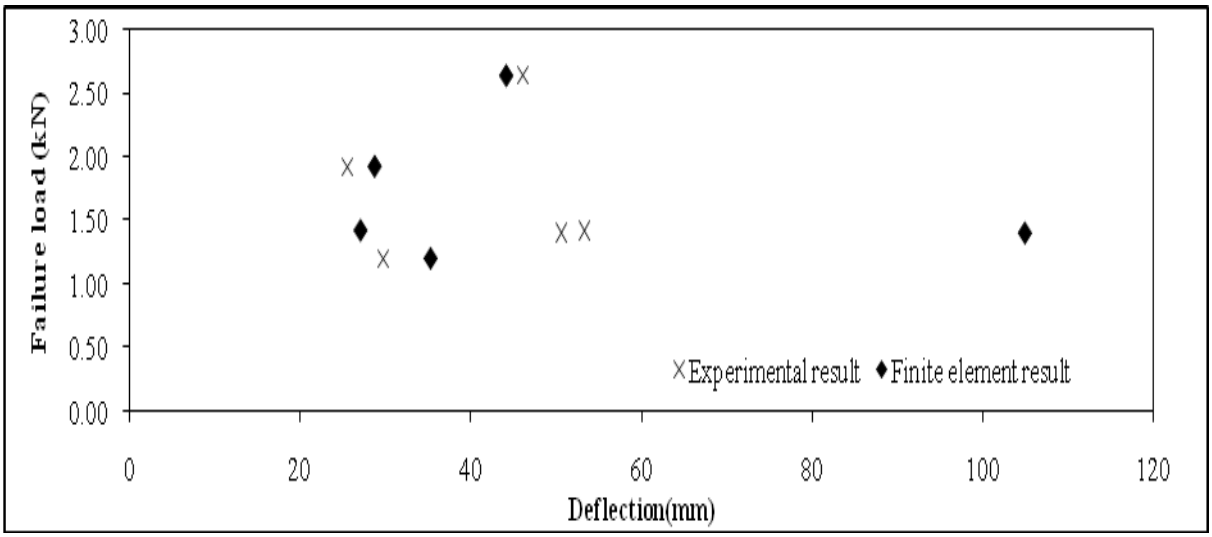

Fig 4: Comparison of experimental and FEA result

4. Result and Dissucsion

4.1. Point load on unsupported crest

Point load on unsupported crest shows almost similar behaviour in all point 1B, 2B and 3B. The failure loads of all 3 point are almost similar, which is more than 2.0 kN. Failure for point 1B is 2.3kN, point 2B is 2.5kN and point 3B is 2.4kN. These values shows that at any point of the unsupported crest the failure load will vary around 2.0kN. Although the failure loads are almost similar, the deformation of the roof sheet may show different patterns. The stress versus load graph with combined lines of point 1B, 2B and 3B are relatively close to each other as shown in Figure 5. This shows that the behaviour for all three points is similar to each other with gradient of only slight difference. The failure load for the unsupported crest is much higher compare to the supported crest near the edge. This shows that loads acting on the unsupported crest does not induced a lot of stress compared to the supported crest at the edge.

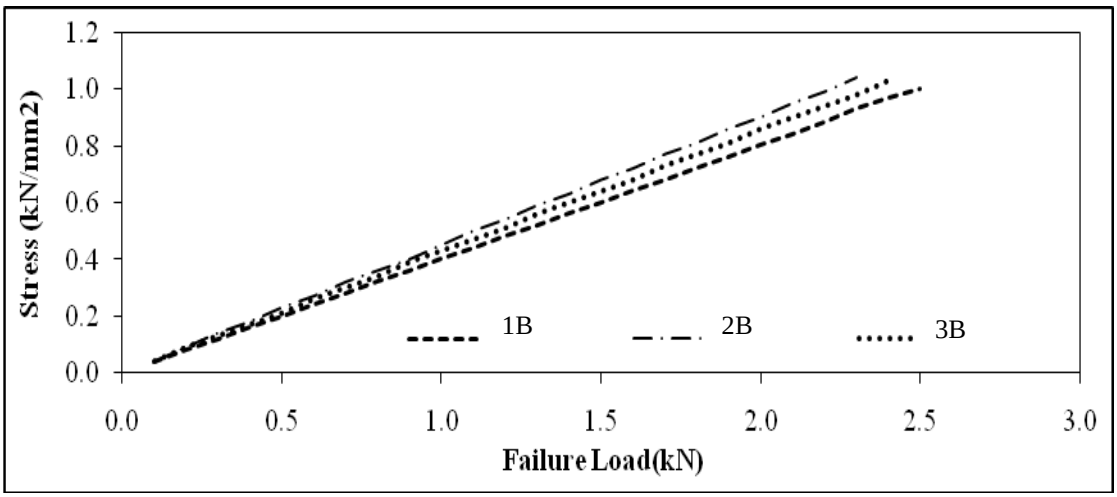

Fig 5: Stress Versus load for point load locate at 1B, 2B and 3B

4.2. Maximum Stress and deform mesh

The stress contour for all three locations shows almost similar patterns. The stress area for unsupported crest is very large compared to the supported crest at the edge. From the contour as well it can be seen that the maximum stress are located at the support. This time failure occurs near the pin support area. The deformation of the model is very large as well as compared to deformation on supported crest. The large deformation explains the large area of stress around the model. The large deformation does not yield large stress although the stress area is quite wide. The large deformation can be explained by flexibility of the material with very small thickness therefore the stress is small. Figure 6 shows the stress contour and deformed mesh for location 1B, 2B and 3B respectively.

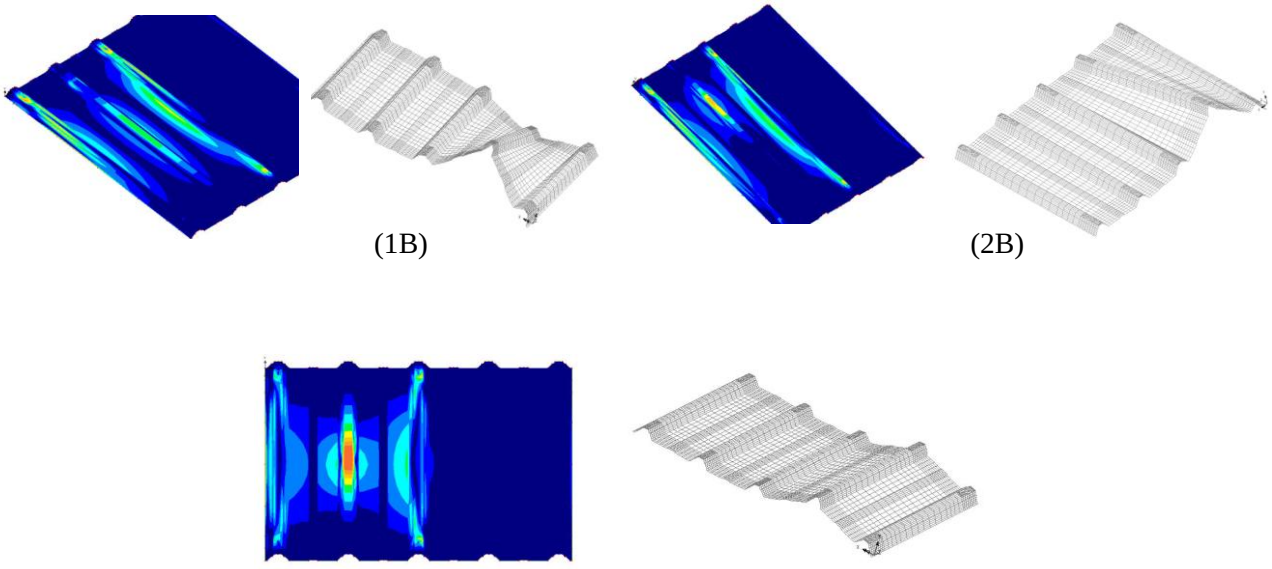

(1B) (2B)

(3B)

Fig 6: Maximum stress contour and deformed mesh for location 1B, 2B and 3B

4.3. Comparing all failure load

Figure 7 shows the combination of all the results for the failure load at different location. It can be seen that the failure load ranges from 3.0kN to 0.8kN. Failure load at the centre crest of the model shows the most severe failure which is surrounding the support of the model. However, failure load at the other crests does not show any failure surrounding the support. Therefore, at the events of high wind speed it is best to avoid loading acting at the centre of the model which is the weakest point of the roof sheet. The behavior of the roof sheet can be estimated by how the roof sheet fails at different location of point load.

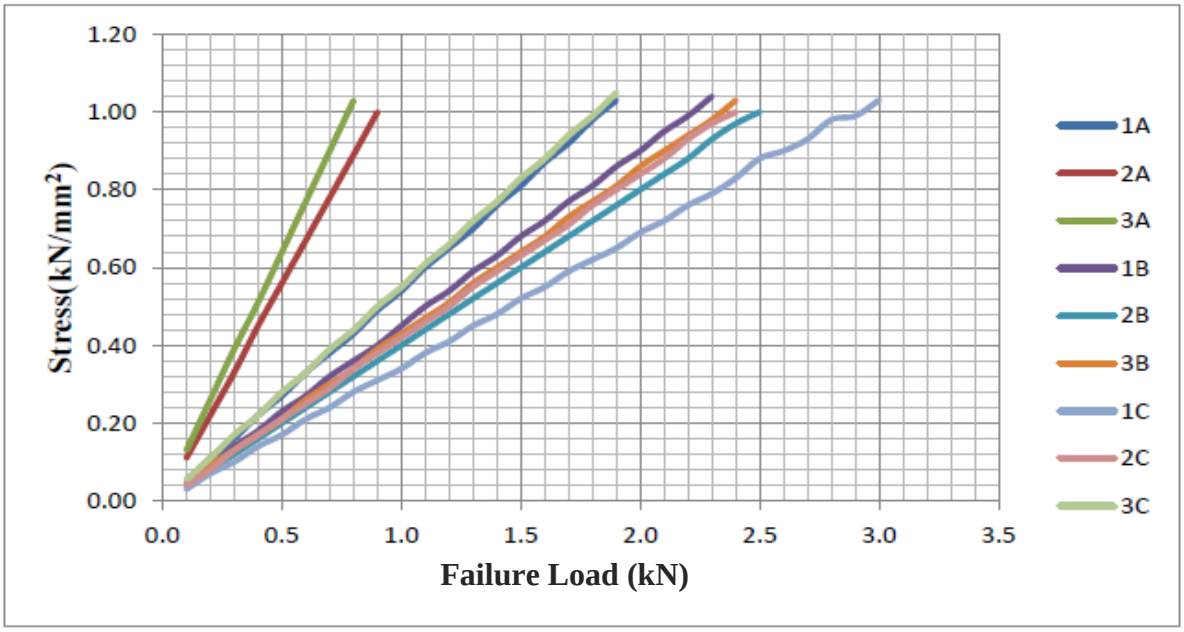

Fig 7: Combination of result for all different location of point load

5. Conclusion

Finite element analysis can be used to develop numerical model to simulate the behavior of trapezoidal roof sheeting subject to point loading. The captured characteristic of the deformed shape of the finite element model of trapezoidal roof cladding were successfully simulate the deformed shape observed during experimental work. The used of finite element analysis would ultimately enable a cost effective and efficient means of studying the behavior and response of steel cladding subject to a variety loads.

6. Acknowledgement

The author would like to express gratitude and thankful to Universiti Sains Malaysia for providing financial support from Delivering Excellence Grant for the research and Ministry of Education giving sponsorship under MyBrain15 throughout the studies.

7. References

[1] Mahaarachchi, D. 2003. Behaviour and Design of Steel Cladding Systems Subject to Pull through Failures, *PhD Thesis*, Queensland University of Technology, Brisbane, Australia

[2] Lovisa A.C., Wang,V.Z., Henderson, D. J. and Ginger, J.D.. 2012. A Finite element model for pierced- fixed, corrugated metal roof cladding subject to uplift wind loads. *Proc. Of Australasian Structural Engineering Conference 2012 (ASEC12*), 11-13 July 2012, Perth, WA, Australia.pp. 1-8.

[3] Xu, Y.L., and Teng, J.D. (1994). Local plastic failure of light gauge steel roofing sheets: Finite element versus experiment. *Journal of Constructional Steel Research*, 30(2), 125- 150.

[4] Mahaarachchi, M. and Mahendran, M. (2009). Wind uplift strength of trapezoidal steel cladding with closely spaced ribs. *Journal of Wind engineering and industrial Aerodynamics*. pp 140-150.

[5] Zahir, A.H., (2013), The Study of Rural Roofing System under Wind Load, *Final Year Dissertations*, School of Civil Engineering, Universiti Sains Malaysia

ISBN 979-458-758-3
Proceedings of the 3rd International Conference on the Geohazard Information
Zonation and 5th Seminar & Short Course of HASTAG (GIZ2014-HASTAG5)
Organized by UMSU, HASTAG, USM
Medan, Indonesia, October 20-22, 2014

The Effect of Site Classification on Incremental Dynamic Analysis for RC Buildings without Seismic Provision in Penang

Chee-Ghuan Tan [1+], Taksiah A. Majid [2], Kamar Shah Arriffin [2] and
Norazura Mohamad Bunnori [1]

[1] School of Civil Engineering, Universiti Sains Malaysia, Penang, Malaysia
[2] School of Material and Mineral Resources, Universiti Sains Malaysia, Penang, Malaysia

Abstract. Malaysia has been long term subjected to far field from neighboring country and local earthquake although it is not located in the active fault region. Local soil condition or site classification may play a major role in the soil dynamic characteristic correspond to the tremors. This study is to evaluate the effect of site classification on seismic response to the non-seismic design existing RC buildings in Penang. Five types of moment resistance RC building with 3, 8, 12, 16 and 20 storey are evaluated by using Incremental Dynamic Analysis (IDA). IDA result show that the non-seismic designed RC frames behaved low ductility and collapse at relatively lower IDR_{max} which between the performance level of Immediate Occupancy, IO (1%) and Life Safety, LS (2%). 20 storey buildings give the highest IDR_{max} followed by 8 storey buildings for every type of site classification. This phenomenon is more obvious in harder soil (Class B) and the effect reduces in softer soil condition by observing the slope reduction of the IDR_{max} vs T_1 curves.

Keywords: Site classification, incremental dynamic analysis, maximum interstorey drift ratio

1. Introduction

Dynamic soil properties provide important information on the dynamic response of the soil structure needed for the dynamic structural analysis of superstructures. Local site classification always plays a major role in the seismic soil amplification of a site, a critical factor affecting the level of ground shaking [1]. Although Malaysia is not located close to the seismic prone area with active fault, buildings erected on soft soils often exposed to the far-field earthquakes generated from along Sumatran fault and subduction zones, particularly in areas on the west coast of Peninsular Malaysia, such as in Penang, Johor Bharu, and Kuala Lumpur [2, 3].

In the past 30 years, over 40 earthquakes originating from the Sumatra fault and subduction zone have been recorded in Penang, two of which are among the greatest earthquakes in the world [4]. Table 1 summarises the most recent significant earthquake events (MMI ≥ IV) that have been felt in Penang and have caused panic to the local citizens. Malaysian Meteorological Department has recorded that a series of local earthquakes (intra-plate fault) in Peninsular Malaysia and Sabah in the past 5 years as shown in Table 2.

Malaysia has been long term subjected to far field and local earthquake, this have been raised questions on the structural stability and the integrity of the existing building which is not designed seismically in Malaysia in tackling of the far field earthquakes effect from Sumatra and local earthquakes. The vulnerability of these non-seismic BS designed buildings either a distance earthquake originated from at Sumatra or local source may also increase due the low performance of its joint ductility. This study is to evaluate the effect of site classification on seismic response to the existing reinforced concrete (RC) buildings in Penang.

Table 1: Recent earthquakes (MMI ≥ IV) from the Sumatran fault and subduction zone experienced by Penang (Malaysian Meteorological Department)

No.	Earthquake location	Date	Epicenter Coordinate (^{0})	Focal depth (km)	Magnitude	Distance to Penang (km)
1	Northern Sumatera	17 July 2013	5.4, 98.0	40	5.5 (M_w)	250
2	Southern Sumatera	30 Sept 2009	-0.9, 99.7	91	7.6 (M_s)	680
3	Mentawai Trough	12 Sept 2007	-4.4, 101.1	50	6.9 (m_b)	1075
4	Mentawai Strait	14 May 2005	0.8, 98.2	63	6.7 (m_b)	550
5	Nias	28 Mar 2005	2.0, 97.3	47	8.7 (M_w)	490
6	Aceh	26 Dec 2004	3.2, 95.9	30	9.3 (M_w)	540

+ Corresponding author. Tel.: + 60162918068
E-mail address: tuc_kheen@hotmail.com

Table 2: Recent local earthquakes in Malaysia (Mb ≥ 3.8) (Malaysian Meteorological Department)

No.	Location	Date	Epicenter Coordinate (°)	Magnitude (M_b)
1	Baling	20 Aug 2013	5.6, 100.9	3.8
2	Tasik Temenggor	20 Aug 2013	5.4, 101.4	4.1
3	Kudat	23 July 2013	6.8, 117.8	4.2
4	Kunak	29 May 2012	4.6, 118.3	4.4
5	Lahat Datu	21 Aug 2010	5.4, 118.4	4.2
6	Bukit Tinggi	07 Oct 2009	3.4, 101.8	4.2

2. Consideration of Site Classification in Structural Analysis

2.1. Models

Five types of RC building with storey height of 3, 8, 12, 16 and 20-storey were selected for the analysis in this study. The selections of these buildings are intended to consider the low, medium and the high-rise buildings in order to cover the wider range of building's fundamental period from 0.2 s to 1.4 s in the analysis. The selected frame which has 2 bays framing and 3.0 m storey height was structurally designed by using EsteemPlus software. British Standard 8110 [5] was adopted as the design code since the aim of the study is to evaluate the seismic resistance for the non-seismic designed RC buildings in Malaysia. The design parameters for the RC building are tabulated in Table 3.

Table 3: Design parameter of RC frames

Design Parameter	Description
Code of Practice for RC	BS8110
Concrete grade for slab, beam and column	30 N/mm^2
Concrete grade for foundation	35 N/mm^2
Characteristic strength for main reinforcement	460 N/mm^2
Characteristic strength for stirrup and link	250 N/mm^2
Statutory live load	2.0 kN/m^2
Superimposed dead load as floor finishes	1.0 kN/m

2.2. Soil-structure presentation

Pile foundations are considered since the buildings in this study consist of low, medium and high-rise buildings. According to Fema356 [6], the footing uncouple spring model shall be represented by a various spring stiffness in difference axes. The pile cap spring stiffness was expressed in the horizontal, vertical and rotational springs since the two dimensional frame were considered. The embedment of the pile caps are represented by the spring stiffness which is multiplied by the embedment factor according as shown in Table 4. The vertical axial spring stiffness, k_{sv} and rotational spring stiffness, k_{sr} of the pile group are shown in Table 5.

Table 4: Expression for spring stiffness and their corresponding embedment factor for pile cap [6]

Mode	Stiffness Coefficient	Embedment factor
Horizontal	$K_x = \frac{GB}{2-v}[1.2 + 3.4\left(\frac{L}{B}\right)^{0.65}]$	$\beta_x = \left(1 + 0.21\sqrt{\frac{D}{B}}\right).[1 + 0.16(\frac{hd(B+L)}{BL^2})^{0.4}]$
Vertical	$K_z = \frac{GB}{1-v}[0.8 + 1.55\left(\frac{L}{B}\right)^{0.75}]$	$\beta_z = \left(1 + \frac{D}{21B}\left(2 + 2.6\frac{B}{L}\right)\right).[1 + 0.32(\frac{d(B+L)}{BL})^{0.67}]$
Rotational	$K_\theta = \frac{GB^3}{1-v}[0. + 0.47\left(\frac{L}{B}\right)^{2.4}]$	$\beta_\theta = 1 + 1.4(\frac{d}{L})^{0.6}\ [1.5 + 3.7\left(\frac{d}{L}\right)^{1.9}\left(\frac{d}{D}\right)^{-0.6}]$

Note: G is the effective shear modulus; v is poisson's ratio; L is the length of the pile cap; B is the width of the pile cap; d is thickness of the pile cap; D is the embedment depth of the pile cap.

Table 5: Expression for spring stiffness of pile group [6]

Mode	Stiffness Coefficient
Axial spring stiffness	$K_{sv} = \sum_{n=1}^{N} \frac{AE}{L}$
Rocking spring stiffness	$K_{sr} = \sum_{n=1}^{N} k_{vn} {S_n}^2$

Note: A is cross-section area of a pile; E is modulus of elasticity of piles; L is length of piles; N is number of pile in group; k_{vn} is axial stiffness of *n*th pile; S_n is distance between *n*th pile and axis of rotation.

3. Incremental Dynamic Analysis

Incremental dynamic analysis (IDA) involves implementing a series of nonlinear time history analyses to a structure for multiple ground motion records by scaling every record to several levels of intensity to discover the full range of the structure's behaviour from elastic to yielding, nonlinear inelastic and eventually leading to global instability [7]. To comply with the minimum requirement of the codes, seven ground motions were used for the nonlinear time history analysis as tabulated in Table 6. Tan el al. [4] had concluded that the site classification of Penang consists of Soil Type B (V_s = 360 - 800 m/s), C (V_s = 180 - 360 m/s) and D (V_s < 180 m/s) as defined in Eurocode 8 [8], hence only ground motion records with these three soil types were selected. Moreover, far field ground motion records were selected due to the studied area only subjected to far field earthquakes. IDA carried out have covered (i) five types of fundamental period of moment resistance frame (MRF); (ii) four types of foundations (three flexible and one fixed); (iii) seven ground motions; (iv) fourteen types peak ground accelerations by using SAP2000. Total numbers of 1960 nonlinear time history analyses have been carried out in the IDA.

Table 6: Selected far-field ground motion records for nonlinear time history analysis (PEER)

No.	Earthquake	Year	Magnitude (M_w)	PGA (g)	Depth (km)	V_{s30} (m/s)	Time step size (s)	No. of time step
1	Morgan Hill	1984	6.2	0.067	8.5	158.80	0.005	5665
2	Hector Mine	1999	7.1	0.194	5.0	271.40	0.02	3000
3	Whittier Narrows	1987	6.0	0.038	14.6	332.80	0.02	1834
4	Landers	1992	7.3	0.119	7.0	370.80	0.02	2000
5	Northridge	1994	6.7	0.153	17.5	405.20	0.01	2999
6	Northridge Aftershock	1994	5.5	0.044	6.0	508.10	0.02	1000
7	N. Palm Springs	1986	6.1	0.099	11.0	684.90	0.005	4077

3.1. The Effect of the Site Classification on IDA

Figure 1 shows the IDA curves for 3, 8, 12, 16 and 20 storey buildings. Noted that the parameter of peak ground acceleration (PGA) was used as the intensity of seismic action in the IDA instead of the first mode spectral acceleration, Sa(T_1) because of PGA is more familiar and applicable to the academic and industry sectors in Malaysia. The results indicated that the increase of the building storey height and lower soil hardness had reduced the stiffness of the IDA curves. IDA curves show that buildings in Class D site have comparable much higher maximum interstorey drift ratios, IDR_{max} for the same PGA than other sites.

The typical performance levels and the associated damages state according to FEMA indicated that the concrete frame is expected to collapse at 3% to 4 % of the drift. However, all IDA curves found the non-seismic designed RC frames behaved low ductility and collapse at relatively lower IDR_{max} which between the performance level of Immediate Occupancy, IO (1%) and Life Safety, LS (2%). The discrepancy of this result can be explained by the finding of the Ghobarah [9]. He concluded that the drift limits in current available codes are found not suitable for the structures which designed without seismic detailing as in this study. The MRF of this structure behave in a non-ductile manner and often suffer in brittle failure modes due to poor confinement of lap splices, lack of shear reinforcement in the beam-column joint and inadequate embedment. More importantly, he had established the drift ratio limits associated with damage levels for various types of structures as shown in Table 7. His result concluded that the collapse of non-ductile MRF structures would happen at more than 1.0 % IDR which fully support the finding of the current study.

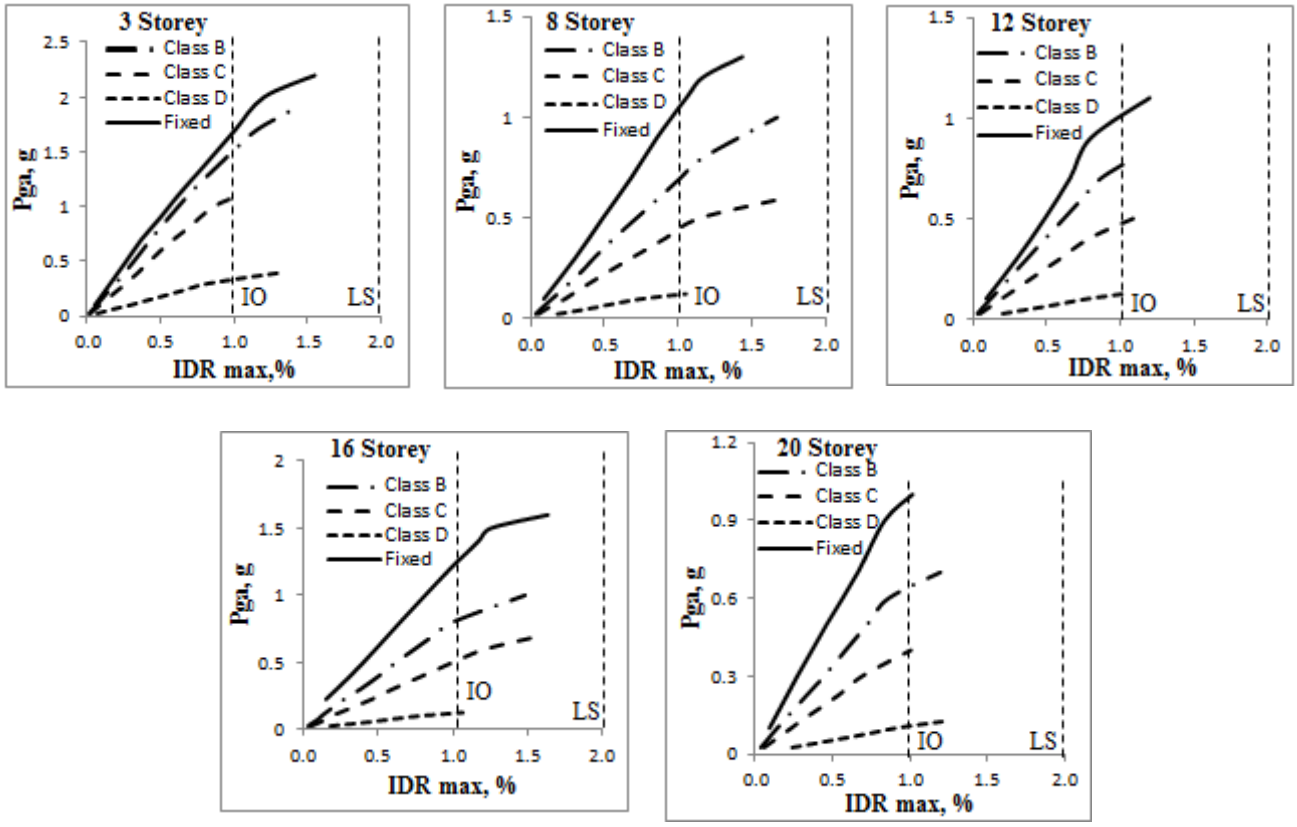

Figure 1: IDA curves for 3, 8, 12, 16 and 20 storey buildings

Table 7: IDR_{max} associated with various damage level [%] [9]

State of Damage	Ductile MRF	**Non-ductile MRF**	MRF with Infills	Ductile Walls	Squat Walls
No Damage	< 0.2	**< 0.1**	< 0.1	< 0.2	< 0.1
Repairable Damage	< 1.0	**< 0.5**	< 0.4	< 0.8	< 0.4
Irreparable Damage	> 1.0	**> 0.5**	> 0.4	> 0.8	> 0.4
Severe Damage	1.8	**0.8**	0.7	1.5	0.7
Collapse	> 3. 0	**> 1.0**	> 0.8	> 2.5	> 0.8

3.2. IDR_{max} with respective to Storey Height RC Buildings

IDR_{max} versus building fundamental period (T_1) with respect to various site classification and PGA are plotted as shown in Figure 2. The T_1 for 3, 8, 12, 16 and 20 storeys are 0.236 s, 0.567 s, 0.824 s, 1.071 s and 1.333 s, respectively. It noted that the maximum PGA plotted in these graphs are up to 0.7 g, 0.4 g and 0.125 g for Class B, Class C and Class D, respectively. The results show that the 20 storey buildings give the highest IDR_{max} followed by 8 storey buildings for every type of site classification. This phenomenon is more clearly observed in harder soil (Class B) and the effect reduces as the soil become soft by observing the slope reduction of the curves.

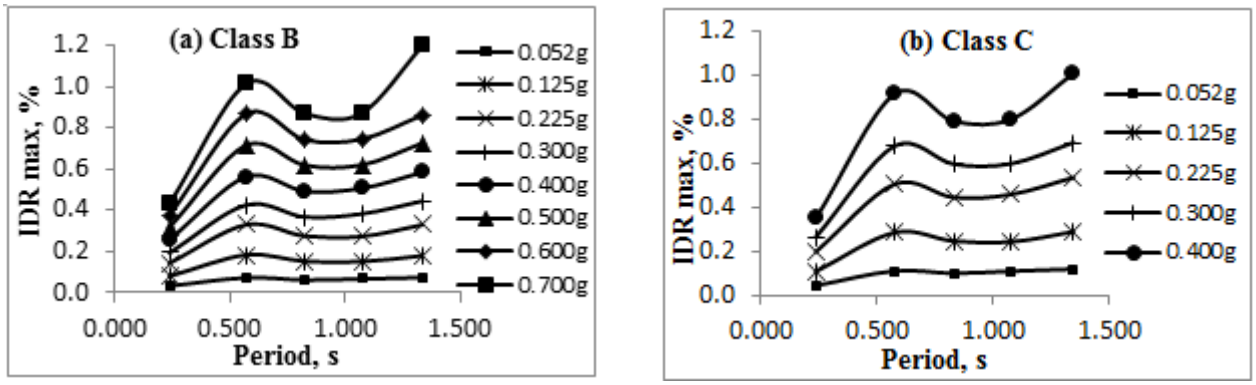

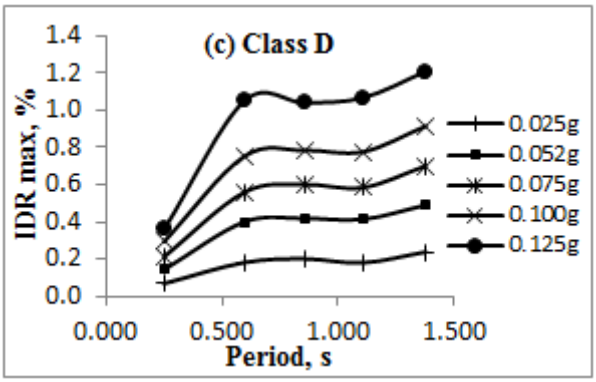

Figure 2: The IDR_{max} plot with respect to T_1 of the buildings for (a) Class B, (b) Class C and (c) Class D

4. Conclusion

Total numbers of 1960 nonlinear time history analyses have been carried out to produce the IDA curves for 3, 8, 12, 16 and 20 storey non-seismic designed RC buildings. IDA curves found the non-seismic designed RC frames behaved low ductility and collapse at relatively lower IDR_{max} which between the performance level of Immediate Occupancy (1%) and Life Safety, LS (2%). This may due to the non-seismic resistance RC structure behave in a non-ductile manner and often suffer in brittle failure modes due to poor confinement of lap splices, lack of shear reinforcement in the beam-column joint and inadequate embedment. IDA results shows that the 20 storey buildings (T_1 = 1.33 s) give the highest IDR_{max} followed by 8 storey buildings (T_1 = 0.57 s) for every type of site classification.

5. Acknowledgements

This study was sponsored by the Postgraduate Research Grant Scheme provided by Universiti Sains Malaysia. The authors would like to extend their gratitude to the Ministry of Education of Malaysia for the permission to collect MASW data from primary and secondary schools in the study area.

6. References

1. R.U. Maheswari, A. Boominathan, and G.R. Dodagoudar, Seismic site classification and site period mapping of Chennai City using geophysical and geotechnical data. *J. Appl. Geophys.*, 2010. **72**(3): pp. 152-168.DOI: 10.1016/j.jappgeo.2010.08.002.
2. A. Adnan, et al., Seismic hazard assessment for Peninsular Malaysia using Gumbel Distribution Method. *Jurnal Teknologi*, 2005. **42 (B)**: pp. 57-73.
3. H. Husen, et al. Development of design response spectra based on various attenuation relationships at specific location. *International Conference on Construction and Building Technology*. Kuala Lumpur, Malaysia 2008 pp. 511-518.
4. C.G. Tan, et al., Seismic microzonation for Penang using geospatial contour mapping. *Natural Hazards*, 2014.DOI: 10.1007/s11069-014-1093-8.
5. British Standard 8110, *Part 1. Structural use of concrete: Code of Practice for Design and Construction*, 1997: Milton Keynes.
6. FEMA356, *Prestandard and Commentary for the Seismic Rehabilitation of Buildings*, in *Federal Emergency Management Agency*2000: Washington, D. C.
7. D. Vamvatsikos and C.A. Cornell, Direct estimation of seismic demand and capacity of multidegree-of-freedom systems through incremental dynamic analysis of single degree of freedom approximation. *Journal of Structural Engineering*, 2005. **131**(4): pp. 589-599.
8. CEN., *Eurocode 8: Design of structures for earthquake resistance. Part 1: General rules, seismic actions and rules for buildings*, 2004, European Committee for Standardization: Brussels.
9. A. Ghobarah. On Drift Limits Associated with Different Damage Levels. *International Workshop on Performance-Based Seismic Design*. McMaster University 2004.

ISBN 979-458-758-3
Proceedings of the 3rd International Conference on the Geohazard Information
Zonation and 5th Seminar & Short Course of HASTAG (GIZ2014-HASTAG5)
Organized by UMSU, HASTAG, USM
Medan, Indonesia, October 20-22, 2014

Experimental Earthquake Excitation to Control Tower with Tuned Liquid Damper

Azlan Adnan[1+],Ong Peng Pheng[1] and Kenny Kwok[2]

[1]University of Teknologi Malaysia, Department of Civil and Structural Engineering
Skudai 81310, Malaysia
[2]University of Western Sydney, Institute for Infrastructure Engineering
NSW 2751, Australia

Abstract. The obscured investigation of airport control tower is the main purpose of this study. In this contribution, we present a testing method on a coupling effect of structure with variation of liquid height in the Tuned Liquid Damper (TLD). In the structural performance of reliable damper reported, halve of the findings mainly concentrated on Tuned Mass Damper, lesser have given attention to TLD application. This investigation was limited to the downsized structural application, concept of the TLD, physical background, and setting-up. Properties of such consideration show its ability to accommodate horizontal acceleration from ground excitation and the stabilizing effects. The experimental results indicated the peak excitation with TLD and model concurred to each other in limited situation of lower and higher bounds, set at 0.5-2% and 4-5% of mass ratio. Correspondingly, by employing probability density function, it enabled the interpreted data of getting not enough resistance action or too high sloshing to be analysed. This paper found that reduction of responses could be identified in 3 bounds: lower, middle, and upper, that coincided with mass ratio of liquid height. The efficiency significantly increased at the middle bound characterised as effective governing mass ratio occurred at 3% or vaguely between 2-4%.

Keywords: Tuned Liquid Damper (TLD), earthquake excitation, air control tower

1. Introduction

For Tuned Liquid Damper (TLD) to be effective within the natural frequency, sufficient mass ratio is observed to be able to provide damping for structures. Practical applications (Tamura, Fujii et al. 1995), (Hitchcock, Kwok et al. 1999) with full-scale installation to tower proved to be effective methods of increasing the total structural damping of the tower by reducing resonant response of the tower.By means of most common damper as just a tank, tuned liquid dampers have wide variety of application as a passive or semi-active control vibration in structures, namely liquid column vibration absorbers (LCVA) that offers much wider transition effects which occur as the liquid moves between columns at different cross-sectional areas depending on the performance requirements (Hitchcock, Kwok et al. 1997), (Hitchcock, Kwok et al. 1997). The shape of dynamic characterization of U-type of tuned liquid damper comprise in (Wu and Hsieh 2000), in which it mainly discussed about Lagrange's equations of motion for a horizontal plate carrying damper by uncoupling the structural system. Liquid V-damper that is a tube with V-shape filled with liquid that has an initial vertical deflection which is mounted mainly on bridges (Fink and Kuss 2009) and (Kuss and Fink 2012). Apart from much famous Tuned Liquid Column Damper as such in (Shankar and Balendra 2002), (Sadek, Mohraz et al. 1998), and (Lee, Lee et al. 2012), they consist of fundamental frequency of water sloshing effect on the tuned natural frequency to the structure. Application consists of tubes-like containers filled with liquid where energy is dissipated by the movement of liquid through an orifice. While (Casciati, Stefano et al. 2003) applies conical tuned liquid damper with semi-active control protection system. Additional energy dissipation in vessel which was installed in Shin-Yokohama Prince Hotel in 1992 reported by (Tamura, Fujii et al. 1995) was another system with further development in TLD application, besides Tokyo International Airport Tower in 1993 that has been using TLD but with floating particles to damp the projections of sloshing from over spilling.

+Corresponding author. Tel.: +(+607-553 8701);
E-mail address:(azlanadnan@utm.my).

2. Model Configurations

Steel frame configuration shown by rigid based bolted to shake table as in Fig. 1 and 2. The study based on the significant building requirement where the overall building layout is symmetrical as control tower could offer. The orientation positions the model in symmetrical layout, imitating the symmetrical elements of the control tower layout in.Approximated condition identified for the experiment at lab to be able to incorporate the TLD effect for dynamic model is the natural frequency. Though both structures in real model are difference, the experimental model with symmetrical rectangular frame is assumed to be similar in behaviour. Numerical model is estimated with natural frequency, fn at 0.649 Hz, while experimental model is 0.639 Hz.

Water density, $\rho = 1000$ kg/m^3
TLD diameter, $\phi = 200$ mm
Structural weight, $w_s = 126$ kg
Numerical modeling natural frequency, $f_n = 0.649$ Hz
Test natural frequency, $f_n = 0.639$ Hz

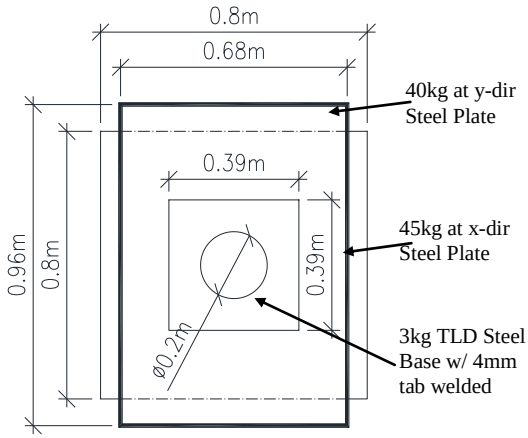

Fig. 1: Plan view schematic model

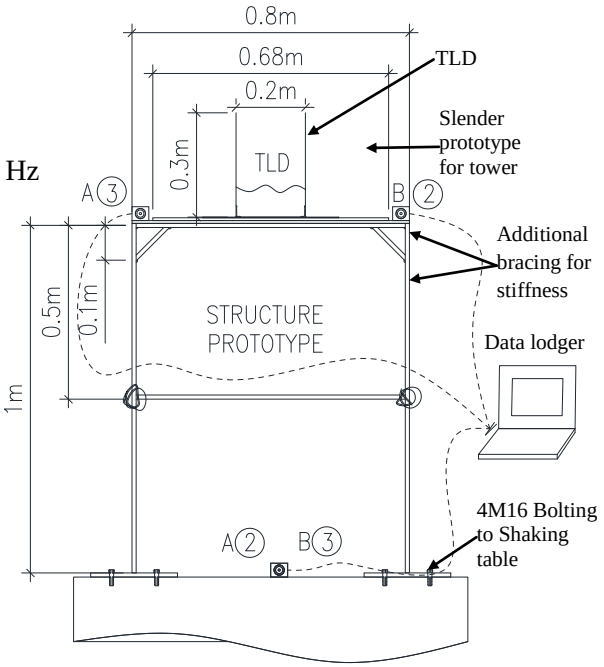

Fig. 2: Elevation view of schematic model

3. Tuned Liquid Damper to Control Tower

Air traffic control tower is crucial to airborne safe departure and arrival of passengers and cargoes. The tower comprises of 13-storey concrete circular frame lift-core with terminals, as well as shopping departments in addition to the ground level existing buildings. Overall height 124m and width of 8m diameter is fixed throughout external shear wall, but expanded at top floors from 23rd to 30th storeys. The top level tower consists of various purposes usage especially as an observation tower for air traffic.The report is discussing on the outcome of the turbulence modelling in laboratory with earthquake excitation to the liquid contained in the circular tank at different height. The molecules of water particles move in a chaotic fashion along complex irregular paths. The turbulence flow causes the various particles of water in different layer to mix thoroughly. The Newton Second's Laws of Motion imply that, in a collision of particles, there will be transferred of kinematic simulation as observed in two object developed into new system of moments, which depends on excitation impulses. The similarity observed is practically understudied as sloshing liquid. The chaotic motion causes momentum and energy exchange between the molecules and solid walls, turbulent flow leads to conceptualized theory of tuned liquid damper.

4. Experimental Model

Liquid containers is a general yet critical problem in many areas, i.e.: spacecraft, oil cargos, oil/chemical truck, storage tanks (Peng and Cai 2010) that could either generate excessive impact when the liquid sloshes, or mitigate the vibration of structures as in TLDs. Relationship between the above impact and damped condition is basically subjected to extreme and control environment. In this paper, the experimental model is subjected to earthquake time history. Tendency for impact excitaion is considered to be very high rather than damper as a function aim at this research.Imitation of the control tower to experimental model is considered

to be in Fig 5 and 6. Liquid sloshing container is a generally cylinder shaped practically to simulate the proposed shape of control tower. The scale effect has not been a consideration and concern, since the method of reporting with random excitation of probability density have greater contribution in these investigations.

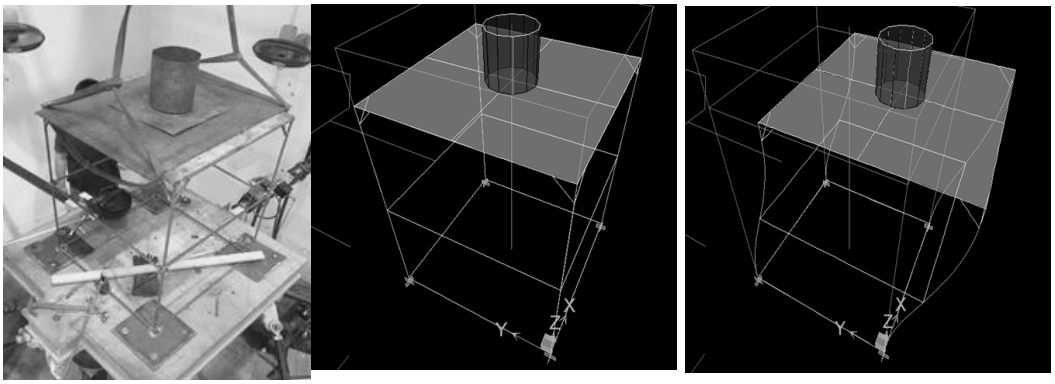

Fig.5: Laboratory setting on shake tableFig.6: Computational Simulation to model testing

The investigations of sloshing waves were carried out experimentally in a base excited square tank, by hydraulic pump actuator. Reference input is by signal impulse of the voltage feed. Similarly for the base excitation, the shake table used reference input from the time history reported in Fig. 7. Noise comes together with the hydraulic pump actuator that contaminated the residue vibration, caused by mechanical and the bubbles, same goes to small rotational shaper motor could induce the same noise (Hassan, Arafa et al. 2008). Control panel with errors input where the model sat on shake table too could contribute to the different set of data from time history, weight of the model and inertial forces could slow actuator down to lower excitation capacity. Setting up by mounting the model on the shaker slab top with 2 functional excitation at 2 axes, x and y direction. Acceleration records made by the accelerometers fixed on 2 locations interchangeably in order to repeat the process and obtaining the averaging results. Notation A2 and A3 is a first excitation, and B2 and B3 is a second excitation to ensure the consistency of records data. A2 is acceleration recorded on first run at the shake table as reference excitation output. A3 is the acceleration recorded on top of model. In second run, B2 and B3 vice-versa at top of first excitation as shown in Fig. 2, only different in notation numbering for shaker and model.The frame supporting the system used 12mm diameter steel bars. Supporting column for four slender legs braced with additional bracing as shown in Fig. 1 and 2. Initial test run to obtain natural frequency determined the vibration generalized mass to stiffness required additional horizontal steel bars, inserted which considered being pin connection.Fresh water has been used in the entire test series. The cylinder tank is made of mild thin steel plate and the fixed inner dimension of 200mm diameters, and 300mm height. The thickness is 2mm thin, so does the base plate which is fixed connection to the top centre part of model by welding.Metal has been chosen for the model as it has the slender effect of a tower and easy to assemble and repair or reshaped upon, bolting to shake table too is possible as well as to the base plate. The model framing system is welded to steel plate with four bolting able to position accurately to shaker, which is considered to be fixed connection. Therefore, numerical consideration of the structure can be considered in orthogonally isotropic nature.

4.1. Time History

Forecasts are based on data or observations on the variable of time series forms. The schemes used are data transformations and adjustments in forecasting methods for characterizing and monitoring the performance of forecasting model. A variation of parameter in TLD to structure model in some aspects is used to compete in performance measurements by statistical technique.The probability employed in describing response populations and in using sample information to make statistical inferences. The analysis begins with probability as defined in experiments to be any process of observation that has an uncertain outcome. The participating events are the experimental outcome that may or may not occur as in random excitation. Events of such responses measured by chances in probability methods or likelihood, in this particular case, focus mainly concentrated on acceleration output in comparison with various TLD depth and occurrences with events of RMS displacement as well as acceleration.Participating trend of interest is the

Rapid-KL Time History of Kuala Lumpur. The recorded excitation is non-dimensional in ug(t)/g by time step of 0.01 seconds. The vibration is non-stationary, where no distinctive pattern can be observed from the time to excitation parameter in Fig. 7.

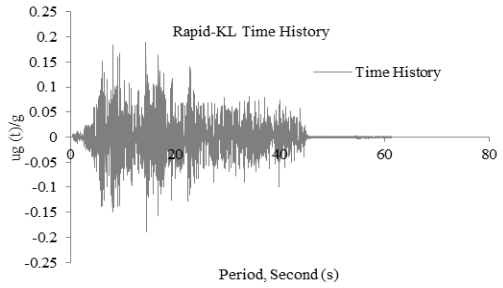

Fig. 7: Rapid-KL time history.

5. Results

Liquid containers is a general yet critical problem in many areas, i.e.: spacecraft, oil cargos, oil/chemical truck, storage tanks (Peng and Cai 2010) that could either generate excessive impact when the liquid sloshes, or mitigate the vibration of structures as in TLDs. Relationship between the above impact and damped condition is basically subjected to extreme and control environment. In this paper, the experimental model is The dynamic analysis and design is the first important step to determine the safe motion effects to tall buildings, bridges, dams, offshore drilling platforms and famous mechanical automobile, industrial machinery to vibration frequency. For acceleration recorded in a low earthquake risk areas, a rationale dynamic design must consider the inherent uncertainty of possible future earthquakes at a structural site. The ground acceleration where it is treated at definite time function can be built into random time functions, known as random processes. The dynamics characteristics are no longer definite, but are treated statistically by probability density function. The input dynamic excitations are treated as random vibrations to structures, provide random structural responses, and assessments are under such random excitations.The responses with different increases of mass ratio from 0 to 4.5% as in Table 1, differentiated into three conditions with identified trends of responses;

- Lower Bound
- Middle Bound
- Upper Bound

Fig 7 time history has a total of 14^{X} (2A+2B) sets of testing run on shake table. Two of the run of "A" setting, and another two of "B" setting. Each of the run carried with different TLD water levels. Test optimization determined in range between low bound < middle bound < upper bound. The samples interpreted in probability density with respect to quantity of random excitation that peaked in acceleration density. This shows that the samples records able to capture the condition of excited random acceleration rather than irregular situation which identified noise in most of the cases. The range of overall counts of spectral acceleration contained in the range of >0-0.06m/s^2. The test with peak acceleration response spectrum happened at 0.313 or 31.3% successful occurrences.

Table 2. Lower Bound

Depth in lower bound, h (mm)	***Peak density response, P(a)***
0	0.313
5	0.291
10	0.281
20	0.261

Table 3. Middle Bound

Depth in lower bound, h (mm)	***Peak density response, P(a)***
0	0.313
40	0.231
50	0.245
70	0.212

Table 4. Upper Bound

Depth in lower bound, h (mm)	***Peak density response, P(a)***
0	0.313
120	0.272
150	0.227
180	0.258

6. Conclusion

Higher tower buildings serviceability is increasingly affected by excessive acceleration experience at the top floors in earthquake and wind excitation.Successful Tuned Liquid Damper prototype setup in comparison with analytical model used to simulate the optimal performance of TLD effect to Structural performance is presented in this paper. It shows that the damper determined to be a possible configuration for structural

protection purposes.The performance of TLD by model experiments to a single directional configuration is studied by random excitation. Suggesting that responses of lower bound, middle bound has achieved the desired considerations in response reductions investigations. However, in upper bound situation, conditional sloshing motion by mistuned water with height consideration to test model has shown that the frequency is dependent to the excitation. Methods of analysing the experimental random excitations showed that by using statistical probability density function, it is possible to reflect the responses in clear and definite manner by having it categorised. Thus the finding of the outcome shows the initial model tests < (1^{st} highest) < (2^{nd} highest) < highest responses in comparison to initial model tests (value in respect to height of the water);

$$0 < 5 < 10 < 20$$
$$0 < 70 < 40 < 50$$
$$0 < 120 < 180 < 150$$

Investigation was limited to the downscale and simulation of real structure application. However, from the earthquake excitation with KL ground time history tested, the responses of TLD brought new discovery where behavioural of water in earthquake resistance is highly dependence of the nonlinearity of water sloshing. The summarised data in middle and high bound shows uneven trends but not so troubling for a TLD becomes a part of control tower damping system in overall. Further suggestion indicates for future endeavour, it should mainly to control and to mitigate the sloshing effect in balance and consistent manner.

7. Acknowledgements

The author would like to acknowledge the student financial contributions from the Ministry of Science, Technology and Innovation, apart from the University Teknologi Malaysia through the eSeergroupand technicians' assistance.

8. References

[1] Casciati, F., A. D. Stefano, et al. (2003). Simulating a conical tuned liquid damper.*Simulation Modelling Practice and Theory* 11(2003): 353-370.

[2] Fink, J. and S. Kuss (2009). Development and use of the liquid-v-damper against vertical bridge vibrations. part 1 - mechanical basics and mode of operation.*Stahlbau* 78(10): 698-705.

[3] Hassan, A. A., M. Arafa, et al. (2008). Design and optimization of input shapers for liquid slosh suppression.*Journal of Sound And Vibrations* 320(2009): 1-15.

[4] Hitchcock, P. A., K. C. S. Kwok, et al. (1999). Damping properties and wind-induced response of a steel frame tower fitted with liquid column vibration absorbers.*Journal of Wind Engineering and Industrial Aerodynamics* 83(1999): 183-196.

[5] Hitchcock, P. A., K. C. S. Kwok, et al. (1997). Characteristics of liquid column vibration absorbers (LCVA) - I.*Engineering Structures* 19(2): 126-134.

[6] Hitchcock, P. A., K. C. S. Kwok, et al. (1997). Characteristics of liquid column vibration absorbers (LCVA) - II.*Engineering Structures* 19(2): 134-144.

[7] Kuss, S. and J. Fink (2012). Development and use of the Liquid-V-Damper against vertical bridge vibrations. part 2 - Practical application and tests.*Stahlbau***81**(2): 123-132.

[8] Lamb, H. (1932). Hydrodynamics. London, *Cambride University Press*.

[9] Lee, S.-K., H.-R. Lee, et al. (2012). Experimental verification on nonlinear dynamic characteristic of a tuned liquid column damper subjected to various excitation amplitudes.*The Structural Design of Tall and Special Buildings* 21: 374-388.

[10] Peng, W. and C. S. Cai (2010). Prediction of tuned liquid damper damping force based on back propagation neural network.*Earth and Space*(2010): 3345-3354.

[11] Sadek, F., B. Mohraz, et al. (1998). Single- and multiple-tuned liquid column dampers for seismic applications.*Earthquake Engineering And Structural Dynamics* 27: 439-463.

[12] Shankar, K. and T. Balendra (2002). Application of the energy flow method to vibration control of buildings with multiple tuned liquid dampers.*Journal of Wind Engineering and Industrial Aerodynamics* 90(1893-1906).

[13] Tait, M. J., N. Isyumov, et al. (2008). Performance of tuned liquid damper.*Journal of Engineering Mechanics* 2008(134): 417-427.

[14] Tamura, Y., K. Fujii, et al. (1995). Effectiveness of tuned liquid dampers under wind excitation. Engineering Structures 17(9): 609-621.

[15] Wu, J. S. and M. Hsieh (2000). Study on the dynamic characteristic of a U-type tuned liquid damper.*Ocean Engineering* 29(2002): 689-709.

[16] J. Chin, Y. Chung, R. Yen. Recognition of Earthquake wave Based on Wavelet Analysis. In: L. Lin, et al (eds.). *Proc. of US-EuropeEarthquake Engineering Workshop*. Dallas: World Academic Press. 2010, pp. 1-8. (Use "References" Style)

ISBN 979-458-758-3
Proceedings of the 3rd International Conference on the Geohazard Information
Zonation and 5th Seminar & Short Course of HASTAG (GIZ2014-HASTAG5)
Organized by UMSU, HASTAG, USM
Medan, Indonesia, October 20-22, 2014

Fragility curves of a RC frame building subjected to seismic ground motions

Koktong Tan[1], Hashim Abdul Razak [1+], Meldi Suhatril[1] and Dagang Lu[2]

[1]Department of Civil Engineering, University of Malaya, 50603 Kuala Lumpur, Malaysia; [2]School of Civil Engineering, Harbin Institute of Technology, 202 Haihe Road, Nangang District, Harbin 150090, P.R. China

Abstract. This paper develops analytical fragility curves for a RC concrete frame building under ground shaking. A three story RC frame building was selected as a study case. The system was analyzed and compared for two different site soil conditions subject to a relatively small number of strong ground motion records. Nonlinear time history analyses were conducted using OpenSees [1] platform. The maximum inter story drift ratio for the building was compared to slight, moderate, extensive and complete limit states, as suggested by HAZUS [2]. The numerical result shows that the local soil conditions can significantly modify the fragility curves.

Keywords: fragility curves, site response analysis, RC frame buildings.

1. Introduction

Fragility curves are a useful tool for seismic risk analysis of structural systems. They relate the probability of reaching or exceeding a damage state to a given seismic hazard intensity. Different approaches can be used to develop the fragility curves, including empirical, judgmental, analytical and hybrid methods [3]. Analytical Fragility curves are based on damage distributions simulated from analyses of structural models under increasing earthquake loads as their statistical basis. The analytical approaches are the most popular since they are applicable to different structural types and geographical regions where damage records are insufficient. The objective of the current study is to develop analytical fragility curves for a RC frame building under peak horizontal ground acceleration (PHGA) at the 'seismic bedrock'. The effect of soil conditions underneath is investigated. Two different soil conditions are considered corresponding to soil profile type C and D of NEHRP with V_{s30} varying from 280m/s to 373m/s.

2. RC frame building

A three-story RC frame building is used for the fragility analysis. It is symmetrical and simple, ideally used for the purposes of the current study. The story height is 4m and the bay width is 26m. The total building height is 12m. The building was designed for gravity loads without seismically detailed. The compressive strength of concrete and the yield strength of steel are equal to 30MPa and 460MPa, respectively. The elevation of sample frame and alongside the details are shown in Fig. 1.

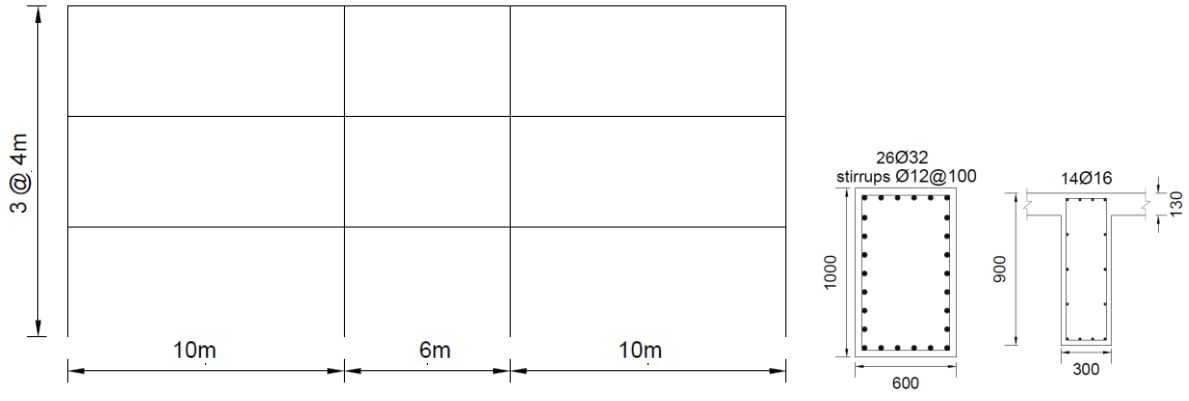

Fig. 1: Elevation of sample frame and reinforcement details.

+ Corresponding author. Tel. /fax: + 603-79675233.
E-mail address: hashim@um.edu.my.

3. Ground motion inputs

Equivalent linear ground response analyses are conducted to evaluate the soil surface ground motions. Two different soil conditions are considered, corresponding to soil profile type C and D of NEHRP with v_{s30} varying from 280m/s to 373ms (Fig. 2). In the first case, the soil profile consists of a surface 2.5m thick silt layer overlaying sand layers and the water table is located 2.5m below the ground surface. In the second case, the soil profile constitutes mainly of medium plasticity clay layers with a 4.5m thick sand layer at a depth of 13.5m below the ground surface. Water table is 6m below the surface. The fundamental elastic periods of the soil profiles are approximately 0.29 for soil profile type C and 0.36 for soil profile type D.

One-dimensional equivalent linear ground response analyses are performed using SHAKE91[4], assuming vertical propagation of seismic waves and horizontal soil layering. The variations of modulus reduction G/G_{max} and damping ratio D with shear strain γ are defined according to the typical results in the scientific literature. In particular, the confining-pressure dependent curves of Darendeli [5] are used in the current study (Fig. 3). For the seismic bedrock, the curves proposed by Schnabel, Lysmer [6] are employed. Each soil profile is discretized into a number of layers ranging from 0.5 to 1.5m thick. The ratio of effective and maximum shear strain is assumed equal to 0.65 and the critical damping is taken as 5%.

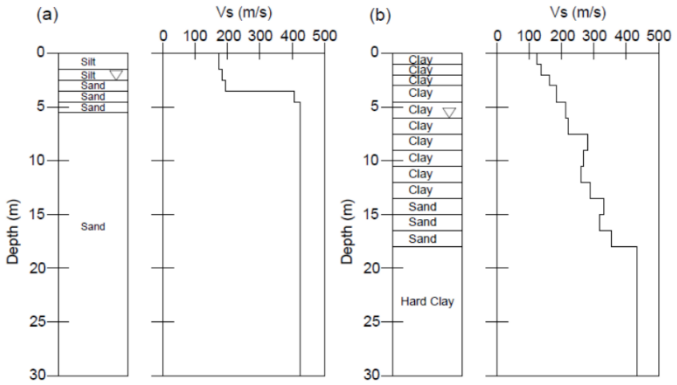

Fig. 2: Soil stratigraphy and shear wave velocity profile for soil profile type C (a) and D (b).

Five different earthquake records are selected as input motion in outcrop conditions for the one-dimensional ground response analyses: (1) Chi-chi, Taiwan, M_w=6.76 and R_{rup}=114.4km, 1999; (2) Off the coast of northern California, USA, M_w=7.10 and R_{rup}=132.9km, 2005; (3) Duzce, Turkey, M_w=7.10 and R_{rup}=183.5km, 1999; (4) Landers, California USA, M_w=7.30 and R_{rup}=121.1km, 1992; (5) India-Burma border, M_w=7.21 and R_{rup}=353.0km, 1988. No specific soil amplification factors are applied since this is explicitly taken into account through the numerical analysis. The records are selected to cover the inherent uncertainties related to the seismic motions, e.g. seismotectonic environment, amplitude, frequency content and significant duration. The hazard-consistent ground motions are generated using enhanced RspMatch [7] program. Enhanced RspMatch modifies a given record to render it compatible with a given spectrum while preserving the nonstationary character of the ground motion. An acceleration 'target' spectra representative of scenario corresponding to probability of 2% of being exceeded in 50 year equivalently, return period of 2475 year, is selected for the spectrum matching of the selected ground motions. The spectrum-matched time histories are scaled from PHGA of 0.05-3.5g at 0.05g interval in order to evaluate the soil surface ground motion for increasing levels of seismic intensity and to construct the corresponding fragility curves. The spectrum compatible acceleration time histories and alongside the target and matched spectra are shown in Fig. 4. A sample of the computed ground response in terms of maximum acceleration a_{max}, peak shear strain γ_{max}, normalized shear stiffness G/G_{max} and damping ratio D is shown in Fig. 5.

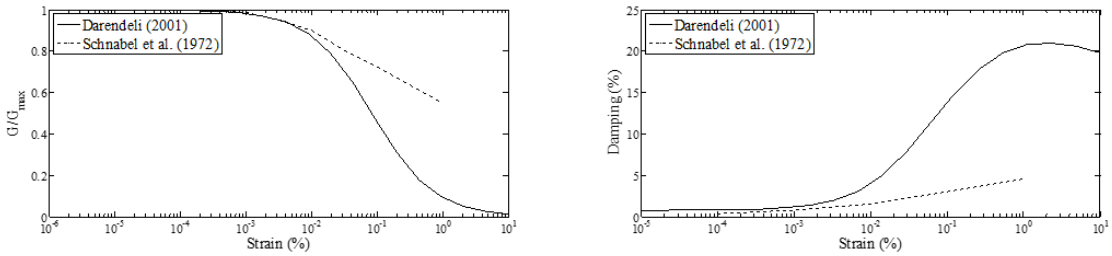

Fig. 3: Variations of shear modulus reduction (G/G_{max}) and damping ratio (D) with shear strain (γ) of the soil models.

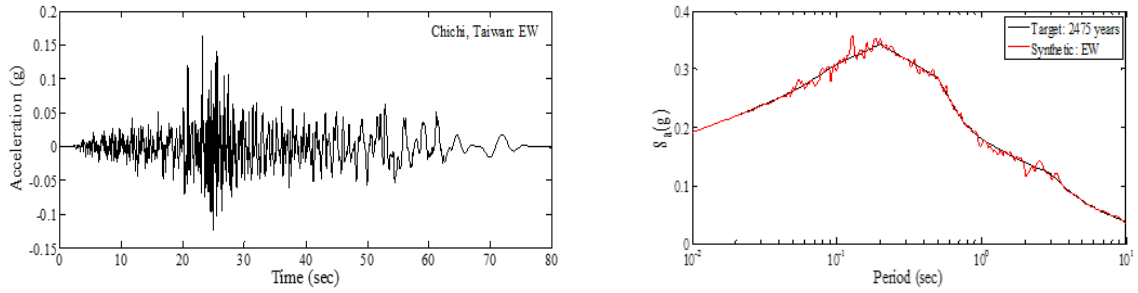

Fig. 4: Spectrum-matched ground motions.

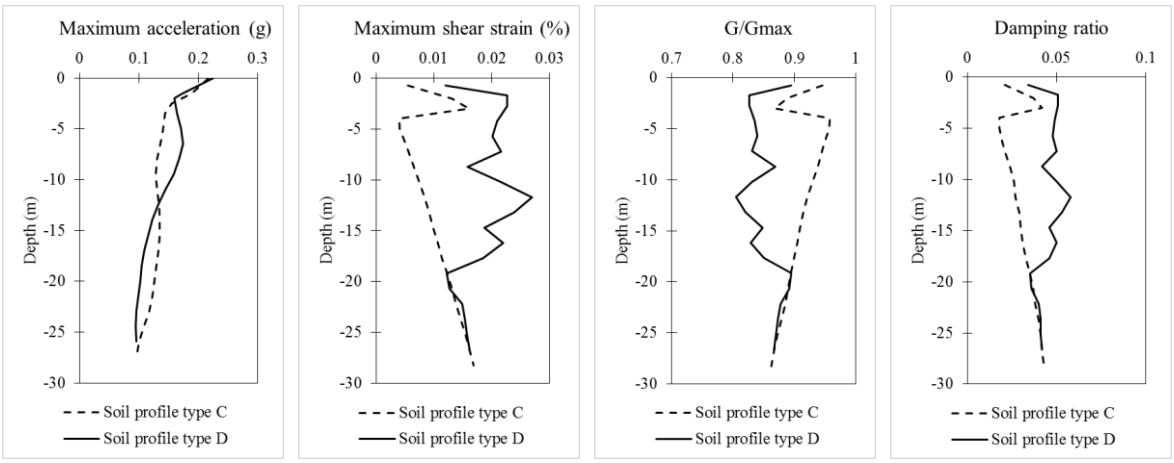

Fig. 5: Variation of maximum acceleration (a_{max}), normalized shear modulus (G/G_{max}), peak shear strain (γ_{max}) and damping ratio (D) with depth for the input motion Chichi scaled at 0.2g.

4. Damage state definition

Four different structural performance levels are considered in the current study, corresponding to slight damage, moderate damage, extensive damage and complete damage. They are described in terms of maximum inter-story drift ratio and cover the whole range of structural damage from serviceability to life safety, and finally to the onset of collapse. The threshold values of the maximum drift ratio corresponding to the damage states described in Table 1 are adopted and the fragility curves are developed accordingly.

Table 1. Definition of damage states for the three story RC frame building [2].

Damage state	Complete damage	Extensive damage	Moderated damage	Slight damage
Drift ratio (Pre code)	4%	1.6%	0.64%	0.4%

5. Finite element model

A 3D finite-element model of the structure was generated using the OpenSees [1]. Beam and columns were modeled with nonlinear beam-column elements characterized by fiber sections, which enforce the Bernoulli beam assumption. All elements are based on the non-iterative force formulation, considering the spread of plasticity along the elements. The concrete was modeled using a uniaxial Kent-Scott-Park model [8] with degrading, linear, unloading/reloading stiffness according to the work of [9] without tensile strength. This model allows an accurate estimation of the structural demand for flexure-dominated RC members despite of its relatively simple formulation [10, 11]. The reinforcement steel is modeled with a uniaxial Giuffre-Menegotto-Pinto [12] model. This model has a sufficient accuracy of satisfying the experimental tests, and taking into account the Bauschinger effect [13]. The rigid floor diaphragm is defined using the DOF coupling feature of Opensees. The column bases are fixed while shear deformation and bond-slip of reinforcement were neglected in the current study. The effects of gravity loads and second-order effects are considered through the geometric nonlinearities. Nonlinear dynamic time history analyses were performed to evaluate the structural response of the building subject to the previously computed soil surface ground motions.

6. Fragility curves development

According to the previously defined limit states, the fragility curve for the damage state (d_i, i=slight, moderate, extensive and complete) is the conditional probability that the building has a state of damage exceeding the damage state d_i at a specific level of peak horizontal ground acceleration (PHGA) at the 'seismic bedrock', which is express as:

$$P\left[D \geq d_i \middle| PHGA\right] = P\left[X \geq x_i \middle| PHGA\right] = 1 - \Phi\left[\frac{\ln(x_i) - \alpha}{\beta}\right] \tag{1}$$

$$\alpha = \ln \mu - \frac{1}{2}\beta^2 \tag{2}$$

$$\beta = \sqrt{\ln\left[1 + \left(\frac{\sigma}{\mu}\right)^2\right]} \tag{3}$$

where $\Phi(\cdot)$ is the standard normal cumulative distribution function, x_i is the drift limit for each damage state, α and β as given in Eqs. (2) and (3) are dependent on the PHGA level, μ and σ are the mean and standard deviation of seismic demand values in each PHGA level, respectively.

By this way, the fragility curves can be generated by plotting the input ground motion level represented in terms of PHGA and the probability of exceeding the damage states. As common practice, the fragility curves are also fitted to the lognormal cumulative distribution functions:

$$F_A(a) = \Phi\left(\frac{\ln(a) - \ln(m_A)}{\xi_A}\right) \tag{4}$$

where A is the random variable of the PHGA, m_A is the median of A, and ξ_A is the logarithmic standard deviation of A. Linear regression analysis was used to estimate the lognormal parameters of the fragility relationships.

7. Effect of soil conditions on the fragility parameters

Fig. 6 compares the fragility curves between the soil profile type C and D for the three-story RC frame building. It is observed that the fragility curves of the building in soil type D are higher than those in soil type C. For example, for a PHGA level of 1.05g, the fragility curve in soil type D estimates approximately 97% chance of extensive damage, while the fragility curve in soil type C estimates around 9% probability of the extensive damage. The differences increase for higher damage limit states. Therefore, the local soil conditions should be appropriately considered in the fragility analysis of RC frame buildings.

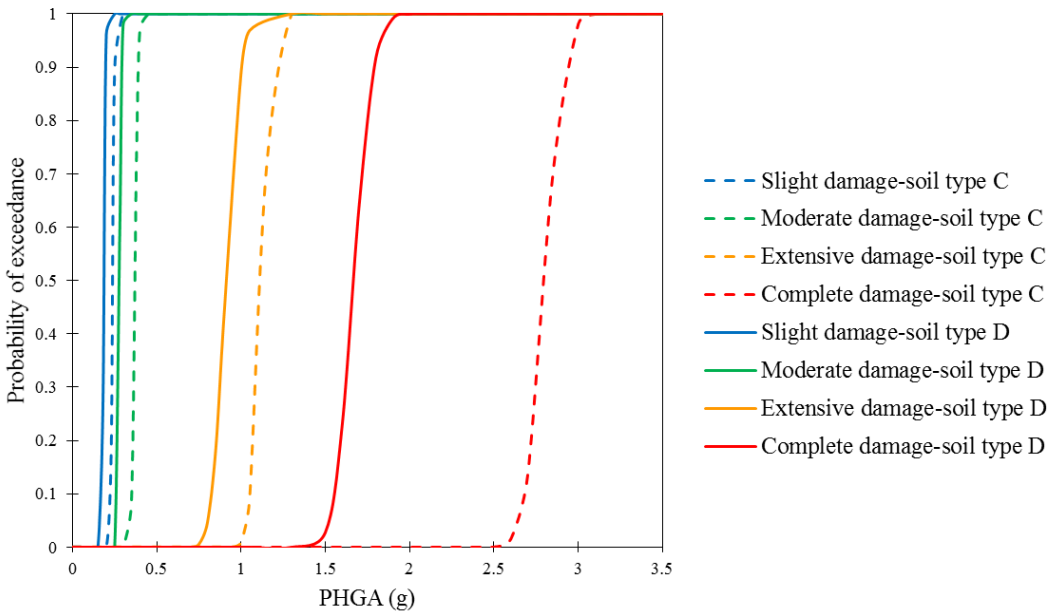

Fig. 6: Fragility curves for a three story RC frame building on soil profile type C and D.

8. Conclusions

In the current study, fragility curves of a three-story RC frame building are derived for two different soil conditions, classified as C and D of NEHRP. The effect of local soil conditions are the main focus of the study. The local soil conditions have a significant effect on fragility curves. Therefore, they should be considered in the fragility analysis for a building stock in a region.

Acknowledgments

The works developed in this paper were supported by University of Malaya and the Ministry of Higher Education (MOHE), Malaysia through research grants PV081/2011A and UM.C/625/1/HIR/MOHE/ENG/55. These supports are gratefully acknowledged.

References

1. Mazzoni, S., et al., *OpenSees command language manual – version 2.0*. 2007, University of California: Berkeley.
2. HAZUS, *Earthquake loss estimation methodology*, in *Technical Manual*. 1997, National Institute of Building for the Federal Emergency Management Agency: Washington, D.C.
3. Rossetto, T. and A. Elnashai, *Derivation of vulnerability functions for European-type RC structures based on observational data.* Engineering Structures, 2003. **25**: pp. 1241-1263.
4. Idriss, I.M. and J.I. Sun, *SHAKE91: a computer program for conducting equivalent linear seismic response analyses of horizontally layered soil deposits*. 1992, University of California: Davis, California.
5. Darendeli, M.B., *Development of a new family of normalized modulus reduction and material damping curves*. 2001, The University of Texas at Austing: Ann Arbor.
6. Schnabel, P.B., J. Lysmer, and H.B. Seed, *SHAKE: a computer program for earthquake response analysis of horizontally layered sites*, in *Report no. EERC72-12*. 1972, University of California: Berkeley.
7. Atik, L.A. and N. Abrahamson, *An Improved Method for Nonstationary Spectral Matching.* Earthquake Spectra, 2010. **26**(3): pp. 601-617.
8. Kent, D.C. and R. Park, *Flexural members with confined concrete.* Journal of the Structural Division, 1971. **97**: pp. 1969-1990.
9. Karsan, I.D. and J.O. Jirsa, *Behavior of concrete under compressive loading.* Journal of Structural Division ASCE, 1969. **95**(ST12).
10. Mitropoulou, C.C. and M. Papadrakakis, *Developing fragility curves based on neural network IDA predictions.* Engineering Structures, 2011. **33**(12): pp. 3409-3421.
11. Lagaros, N.D. and M. Papadrakakis, *Neural network based prediction schemes of the non-linear seismic response of 3D buildings.* Advances in Engineering Software, 2012. **44**(1): pp. 92-115.
12. Menegotto, M. and P.E. Pinto. *Method of analysis for cyclically loaded reinforced concrete plane frames including changes in geometry and non-elastic behavior of elements under combined normal force and bending*. in *IABSE symposium on resistance and ultimate deformability of structures acted on by well defined repeated loads*. 1973. Lisbon.
13. Li, Z. and G.D. Hatzigeorgiou, *Seismic damage analysis of RC structures using fiber beam-column elements.* Soil Dynamics and Earthquake Engineering, 2012. **32**(1): pp. 103-110.

ISBN 979-458-758-3
Proceedings of the 3rd International Conference on the Geohazard Information
Zonation and 5th Seminar & Short Course of HASTAG (GIZ2014-HASTAG5)
Organized by UMSU, HASTAG, USM
Medan, Indonesia, October 20-22, 2014

An Experimental Study on Wave Forces of Tsunami on Simplified Onshore Buildings at Penang Island, Malaysia

Wei Chek Moon[1], Kang Chin Tan[1], Tze Liang Lau[1]

[1] School of Civil Engineering, Universiti Sains Malaysia (USM)
14300 Nibong Tebal, Penang, Malaysia

Abstract. In this study, wave forces of tsunami on simplified onshore buildings at Penang Island were investigated. Single-storey and double-storey buildings were down scaled at a ratio of 1:100 and subjected to tsunami bores of various runup heights in a 1 m x 1 m with 40 m long wave flume. Tsunami wave height and velocity at the location of building model were obtained. The experimental results revealed that the nature of the wave attack on building model depends on the relationship between model height and nominal height of the wave. The time histories of forces in the horizontal and vertical direction and pressures on buildings due to simulated tsunami-like waves were measured. The relationships among the forces and pressures for the incident wave with nominal wave height around 40 mm were discussed in detail. It is observed that the maximum horizontal force and front pressure were attained when nominal height of the wave was achieved by the flow. The experimental results provide useful information in the dynamic analysis in the later stage of the study.

Keywords: Tsunami, wave force, wave pressure, Penang Island

1. Introduction

With up to 52 out of 68 total deaths in Malaysia, Penang Island was the most severely affected state in Malaysia during the devastating event of 2004 Indian Ocean Tsunami [1]. As the coastal areas of the state have been developed rapidly over the years, it is foreseen that even more lives will be claimed and more properties will be damaged should the next tsunami hit us. According to Nordin and Charleson [2], Malaysian coastal dwellings may be under threat from tsunami in the future. To date, a comprehensive study of tsunami runup and proper design of tsunami-resistant structure in Penang Island is yet to be formulated due to the lack of knowledge on tsunami impact topics.

At the high hazard areas, tsunami runup mechanism which includes wave breaking action and high-velocity water scouring can result in high overturning moment onto the buildings and cause serious structural damage [3]. The tsunami behaviours and characteristics are quite distinct from other coastal hazards and cannot be inferred from common knowledge or intuition [4]. Therefore, the investigation of tsunami runup characteristic is extremely vital in the context of tsunami disaster management and mitigation plans. In many scenarios of tsunami incomings, evacuation which frees people to impact-resistant building or higher ground is executed. However, the option can only work if and only if the evacuation center itself can withstand probable tsunami impact from structural failure. Incorrect estimation on the tsunami-induced forces on buildings could result in structural failure and thus endanger the life of escapees and evacuees. Therefore, the understanding on tsunami forces is vital in the proper design of tsunami-resistant structure [5].

The main objective of the study is to study the modelling of tsunami wave and its impact onto the simplified onshore buildings (total building height of 3.6 m and 6.6 m) each subjected to wave heights of 4 m at Penang Island, Malaysia.

2. Methodology

2.1. Data collection

The experiment simulated tsunami with nominal height of 4 m represented the documented runup height of 2004 Indian Ocean Tsunami at Penang Island. Bathymetry of Greater Indian Ocean was evaluated from the Gridded Bathymetric Data Sets of General Bathymetric Chart of the Oceans (GEBCO). In order to evaluate the bathymetric plane slope profile, slice normal to the shoreline was made on the bathymetry contour (Fig. 1). The derived bathymetric profile which represented the slope of chosen shore was then used

for the establishment of flume's platform. Fig. 2 shows the slope profile of NW3' - NW3 made on Penang Island's bathymetry contour.

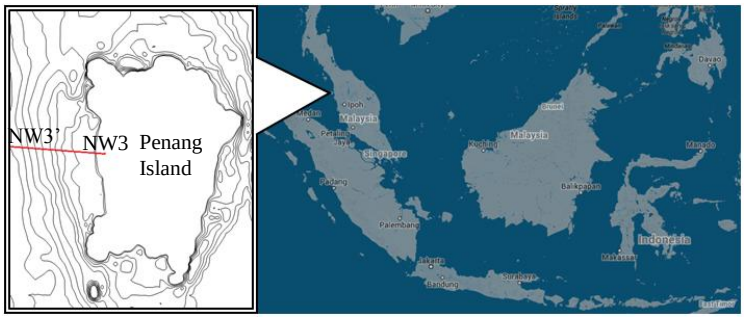

Fig. 1: Profile slice normal to the shore of Penang Island

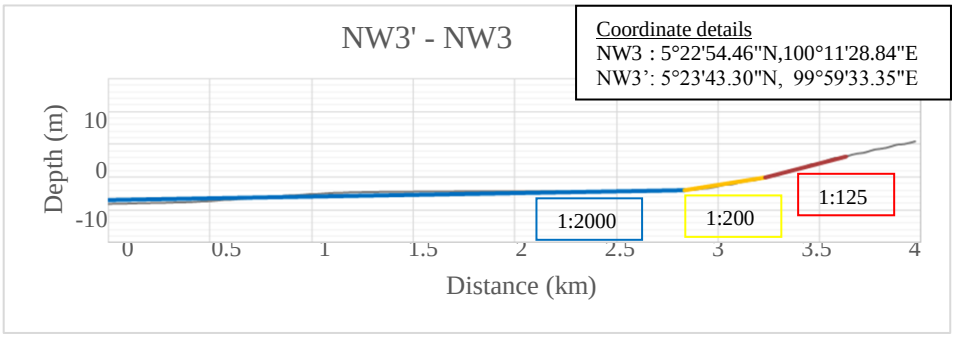

Fig. 2: Slope profile of NW3' – NW3

2.2. Laboratory setup of wave flume

The laboratory setup consisted of a 40 m long, 1 m wide and 1 m deep wave flume for experimental studies on tsunami topics. The flume's platform represented the bathymetric profile of Penang shore, and was comprised of a compound bed with continuous plane slope of 1:200 and 1:125. Physical modelling was down scaled to 1:100 based on Froude Number Similitude Law. Fig. 3 illustrates the schematic diagrams of the laboratory setup. The compound bed ended with a horizontal flat plane where the downscaled model subjected to tsunami loading was located. Onshore buildings were idealized and simulated as rigid rectangular block models which were constructed from acrylic plates. Long period solitary wave was generated by sudden releasing of mass water built up in a water tank located at the flume's furthest left. By varying the released volume from the tank, different wave forms and wave forces were produced. Upon released, water flowing through the wave baffle was regulated and eventually broke after travelled past the slope of 1:4. The broken wave then travelled and attacked the building model located at the flume's horizontal bed.

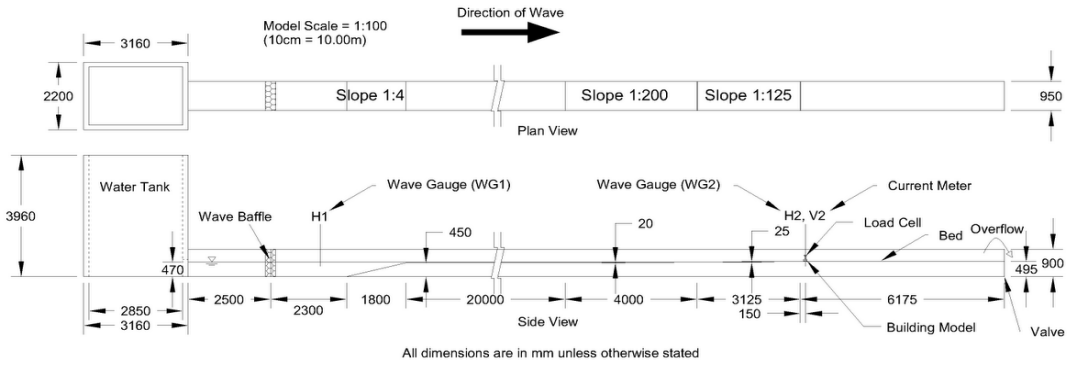

Fig. 3: Schematic diagrams of the laboratory setup

2.3. Physical modeling

The wave height, velocity, force and pressure are the physical quantities that were measured during the experiment. Fig. 4 shows the schematic diagram of the instrumentation and data acquisition system used in the experiment. Wave profiles at H1 and H2 as shown in Fig. 3 were obtained by using the capacitance type

wave gauge (KENEK CHT6-30E). Electromagnetic type current meter (KENEK VP1200) was used to record the velocity of wave in the flume for various wave heights. As for the wave forces (in the horizontal and vertical direction) and pressures, these physical quantities were measured by a calibrated high frequency three-axis load cell (Interface 3A120) and the diaphragm type pressure gauges (SKK P310-02). The wave gauge, load cell and pressure gauges were connected to the data logger (Kyowa EDX-10A) where the measured data were collected and stored. Besides, digital camera and video recorder were used to capture the motion of wave acting on the building model.

During the experiment, the free flow condition of the wave without any model was studied. Wave gauge and current meter were installed at same location of the model to measure the wave height and flow velocity respectively. After the completion of the free flow simulation, building model with the total height of 36 mm (H36) and 66 mm (H66) which had been mounted onto an I-section with a load cell was installed on the flume at a distance of 3.225 m from the shoreline and subjected to tsunami attacks (Fig. 5). The time histories of wave forces and pressure acted on the building model were obtained. The arrangement and positions of pressure gauges attached on the models are shown in Fig. 6. There are total eight pressure gauges used in the experiment. The front face of the model was defined as the face facing the incoming wave and hit directly by the wave.

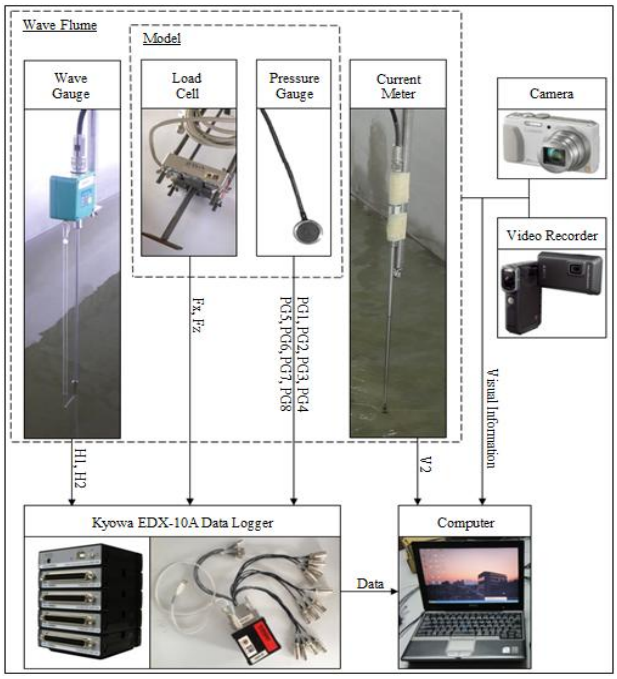

Fig. 4: Schematic diagram of the instrumentation and data acquisition system

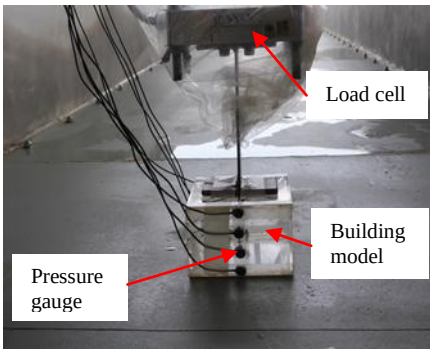

Fig. 5: H66 Building model

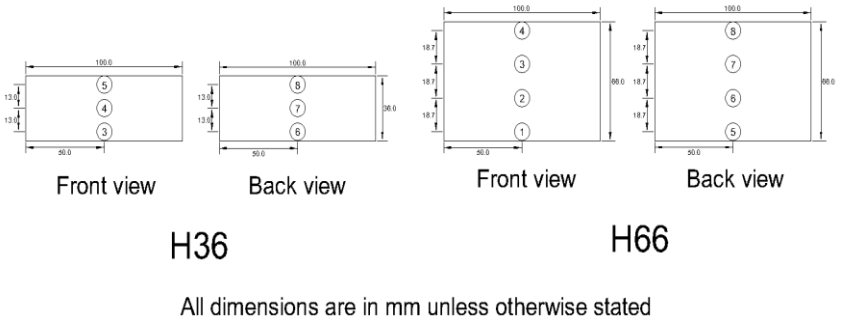

Fig. 6: Position of pressure gauges on building models

3. Results and Discussion

3.1. Wave height and wave velocity at building model

Time histories of wave height and wave velocity at the location of building model were recorded during free flow condition (without the presence of model) for incident wave with nominal height around 40 mm. The time t = 0 s denotes the time when the wave first hit the building model. Based on the experimental results, it is observed that the incident wave with nominal height (h) of 40 mm attain its maximum wave height at the time of around 2 s after the wave first reach the location of building model. The maximum wave height only occurs after some time when the wave has achieved its maximum peak velocity of approximately 1.30 m/s. As the wave height increases overtime, the velocity of the corresponding wave decreases gradually.

Video observation shows that the nature of the wave attack on building model depends largely on the relationship between model height and nominal wave height. The height of the H36 building model itself is smaller than the nominal wave height of 40 mm. As the leading edge of the wave strikes the H36 building model, part of the wave splashes up due to the obstruction of building model and falls freely on top of the building model which lead to massive wave impact (Fig. 7). The remaining wave splits and spreads to the sideway. The model was gushed over by the incoming flowing wave and submerged completely underwater until the wave passed after a considerable amount of time. The wave is said to overtop the building model. Such sequential wave attack was similarly observed for building model with height adequately greater than the wave nominal height, except where only minimal or no amount of water was found splashing down on the top surface of building model after the splashed up wave collapsed downward (Fig. 8).

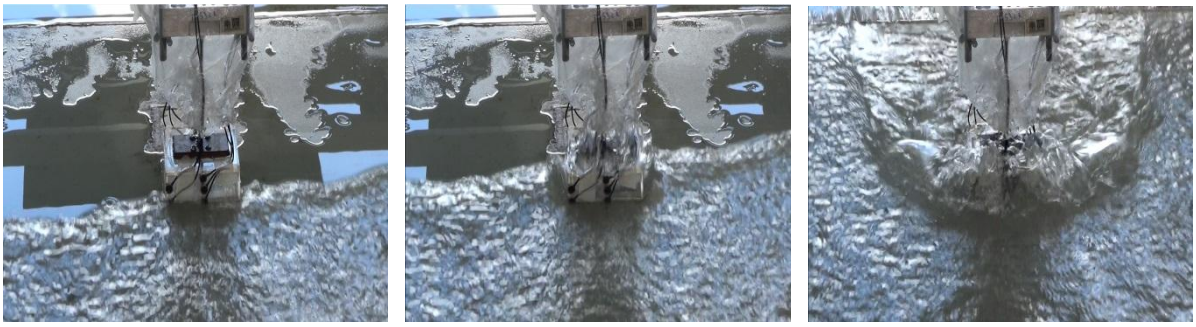

(a) t = 0.02 s (b) t = 0.14 s (c) t = 1 s

Fig. 7: Sequence of wave attack on the building model (Case No.: H36W40)

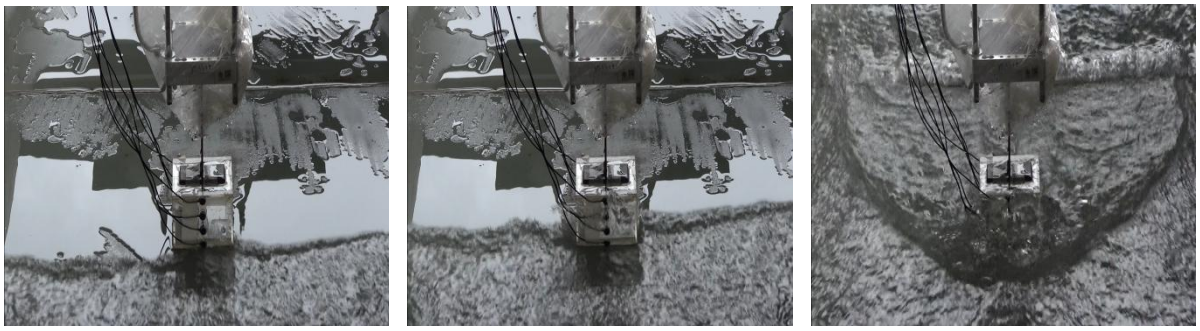

(a) t = 0.02 s (b) t = 0.14 s (c) t = 1.2 s

Fig. 8: Sequence of wave attack on the building model (Case No.: H66W40)

3.2. Wave force and pressure on building model

The recorded force time histories for the incident wave with nominal wave height around 40 mm were displayed in Fig. 9 (a) and Fig. 10 (a). The maximum horizontal force occurs during a time frame when nominal height of the wave is achieved by the flow. The force then decreases gradually until 0 when the both wave height at both front and back faces of building model are equal. As for the vertical force, it increases slightly with time in a positive manner. As comparing with H66 model, H36 model has slightly lower vertical resultant force. In fact, vertical forces experienced by the building model during tsunami event consist of both uplift and gravitational forces. This is evident for the case of H36 model, where the waves

overtop the building model, thus contributing a certain amount of gravitational force acting downward on the building model and eventually reducing the uplift force.

Fig. 9 (b) and Fig. 10 (b) show the recorded pressure time histories for the incident wave with nominal wave height around 40 mm. The front pressures exhibit almost a similar trend with horizontal force. After reaching the peak, the pressures then decrease gradually and remain at the hydrostatic pressure for a much longer period subsequently. Besides, it can be observed that the maximum horizontal force occurs almost at the same time instance with the occurrence of peak pressures recorded by the front pressure gauges. The front peak pressures on H36 and H66 building models are approximately 1.7 and 2 times the hydrostatic pressure respectively. It is noted that the pressure at the higher location of the models show lower or minimum reading. On the other hand, the wave pressure at back face of the building models pick up slightly later than the front pressure until it reaches to the hydrostatic pressure.

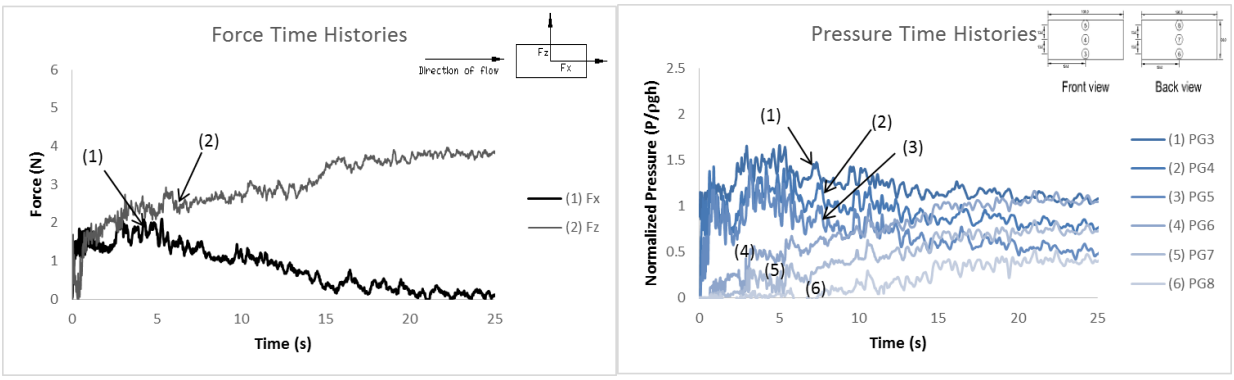

(a) (b)

Fig. 9: Time histories of (a) wave forces and (b) wave pressures on H36 building model

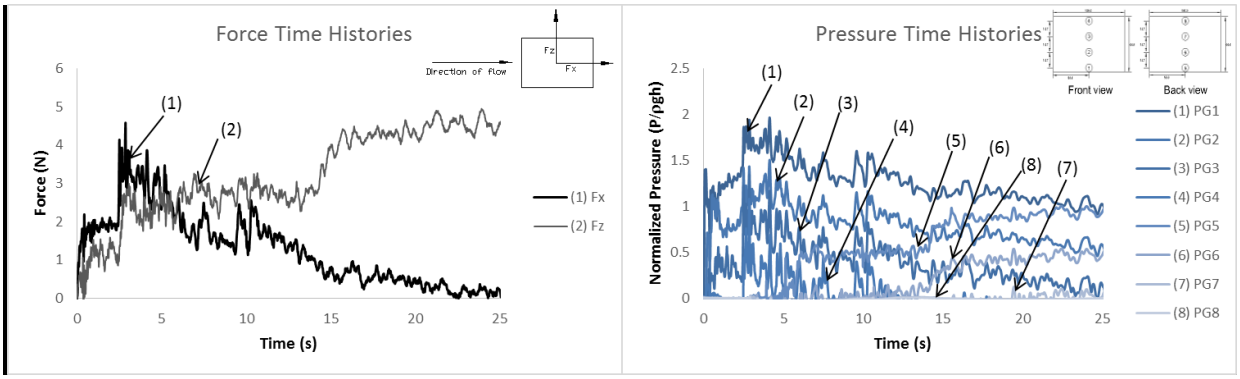

(a) (b)

Fig. 10: Time histories of (a) wave forces and (b) wave pressures on H66 building model

4. Conclusions

The experiment has significantly achieved the main objective of the study. Tsunami modeling and its impact onto the simplified onshore buildings (total building height of 3.6 m and 6.6 m) were successfully carried out. The forces and pressures acted on the building models are obtained. These results provide useful information for the dynamic analysis in the later stage of the study that will contribute towards the design of tsunami-resistant buildings in Penang Island.

5. Acknowledgements

The authors would like to express their gratitude to the Ministry of Science, Technology and Innovation (MOSTI), Malaysia for funding this study through ScienceFund Research Grant (Grant no. 305/PAWAM/6013411).

6. References

[1] Komoo, I. & Othman, M. 2006. The 26.12.04 tsunami disaster in Malaysia: an environmental, socio-economic and community well-being impact study. Institut Alam Sekitar dan Pembangunan (LESTARI), Malaysia.

[2] Nordin, J. & Charleson, A. W. 2009. Tsunami responsive architecture: reducing vulnerability of houses and other structures along the northwestern coast of Malaysia. *Proceeding of 4th Annual International Workshop & Expo on Sumatra Tsunami Disaster & Recovery*, Banda Aceh, pp. 20-24.

[3] Ramsden, J. D. 1996. Forces on a vertical wall due to long waves, bores, and dry-bed surges. *Journal of Waterway, Port, Coastal and Ocean Engineering*, Vol. 122, No. 3, pp. 134-141.

[4] FEMA P646 (2008), 'Guidelines for design of structures for vertical evacuation from tsunamis', FEMA P646, Federal Emergency Management Agency, Washington, D.C., 158 pp.

[5] Yeh, H. 2007. Design tsunami forces for onshore structures. *Journal of Disaster Research*, Vol. 2, No. 6, pp. 531-536.

ISBN 979-458-758-3
Proceedings of the 3rd International Conference on the Geohazard Information
Zonation and 5th Seminar & Short Course of HASTAG (GIZ2014-HASTAG5)
Organized by UMSU, HASTAG, USM
Medan, Indonesia, October 20-22, 2014

Effect of Repeated Earthquakes on the School Building in Northern Sumatra

Ade Faisal [1 +] and Tondi Amirsyah Putera [1]

[1] Program Studi Teknik Sipil, Universitas Muhammadiyah Sumatera Utara (UMSU), Medan, Indonesia

Abstract. The earthquakes struck a region near the active fault for many times. The yielded structures after an earthquake might become excessive damages after experiencing another earthquake. The concept of seismic design of building has not consider this type of hazard. Recent studies indicate that the effect of repeated earthquake is significantly occurred on the moment resisting bare frames, either made from steel or concrete material. This paper investigates the effect of repeated earthquake on the frames with infilled brick wall. The frames represent school building built on the regions near the Sumatran active fault, Indonesia. The result shows that the sequence of plastic hinges occur on the structures model after experiencing the repeated earthquake. It starts from the brick wall and then spreads to the columns and beams. For the single earthquakes, the brick wall of structures model tends to perform damage, but few of columns and beams experiences hinges. These conclude that the future repeated earthquake can not be underestimated.

Keywords: Nonlinear inelastic analysis, school building, repeated earthquakes, Sumatra.

1. Introduction

There are few studies have examined the effect of seismic repetitions on the buildings. Elnashai et al. [1] has predicted that the multiple earthquake ground motions can give ductility demand required significantly higher than that required by a single event. Continuous reduction in the lateral stiffness was also detected on a building built on soft soil having several low magnitude earthquake ground motions [2]. Amadio et al. [3] indicates that repeated earthquakes can imply a considerable accumulation of damage and a consequent reduction in the force reduction factor.

Hatzigeorgiou and Beskos [4] runs million nonlinear time history analyses on the elasto-plastic SDOF system with strain hardening and empirically introduced an expression to estimate the inelastic displacement ratio (defined as the ratio of maximum inelastic displacement and maximum elastic displacement) on the flexural-based RC and steel structures based on period of vibration, force reduction factor, site conditions, post-yield stiffness, and damping. It concludes that repeated earthquakes require increased displacement demands in comparison with single seismic events as in design earthquake. They find the inelastic displacement ratio for all SDOF systems built at all soil types generally appear to be increased 2 times or more with respect to that obtained for the corresponding single earthquakes.

Faisal et al. [5] have studied three-dimensional moment resisting frame under bi-directional seismic excitation. It explains that the story ductility demand of low-story reinforced concrete buildings are significantly affected by repeated earthquakes. It finds that as the force reduction factor decreases the effect of repeated earthquake is decreases. The effect could be neglected when the structures have force reduction factor of less than two. The upper level of the short structure tends to have the maximum demand when experiencing repeated earthquakes.

The aforementioned studies explore the bare moment resisting frame in two-dimensional and three-dimensional structural model under repeated earthquakes. Actually, most of reinforced concrete frame buildings have the infilled-wall in order to separating the space. Therefore this paper discusses the effect of repeated earthquakes on the single story buildings having infilled brick wall. The school buildings in the surrounding Sumatran fault are selected to be the model of single story buildings. This study observes the plastic hinge on the school building structures under the sequence of seismic motion.

+ Corresponding author. Tel.: + 62616622400; fax: +62616625474.
E-mail address: adefaisal@yahoo.com.

2.1. School Building Survey

The study surveys 8 school buildings situated in the cities near the Sumatran active fault. Table 1 shows the surveyed buildings, which are placed in 6 cities. All of the surveyed buildings are single story reinforced concrete (RC) buildings, which are consist of old and new buildings. Fig. 1 shows the example of surveyed building in Balige, which is the junior high school managed by the local government. Mostly, the old building is arranged in one block, whereas the other blocks are the new buildings. For the sake of simplicity in the modelling of structure, the term new in this case is represent the buildings that were built after the year of 2000. It is meant that the study assumed the surveyed buildings were designed in accordance with the building code released within this years.

Table 1: The school buildings considered in this study

No.	County	City	School name	Size of exterior column [cm]	Size of interior column [cm]	Size of tie beam [cm]	Rebar and ties
1	Toba Samosir	Balige	SMPN-1	20x20	15x15	15x20	4D10 (D6-20)
2	Tapanuli Utara	Tarutung	SMUN-2	15x20	15x15	17x20	4D10 (D6-20)
3	Humbang Hasudutan	Dolok Sanggul	SMPN-2	24x24	15x15	15x24	4D10 (D6-20)
4	Humbang Hasudutan	Dolok Sanggul	SMUN-1	20x20	15x15	15x20	4D10 (D6-20)
5	Pakpak Barat	Salak	SMPN-1	20x20	15x15	15x20	4D10 (D6-20)
6	Pakpak Barat	Salak	SMUN-1	20x20	15x15	15x20	4D10 (D6-20)
7	Dairi	Sidikalang	SMUN-1	20x20	15x15	15x20	4D10 (D6-20)
8	Tanah Karo	Kabanjahe	SMUN-2	20x20	15x15	15x20	4D10 (D6-20)

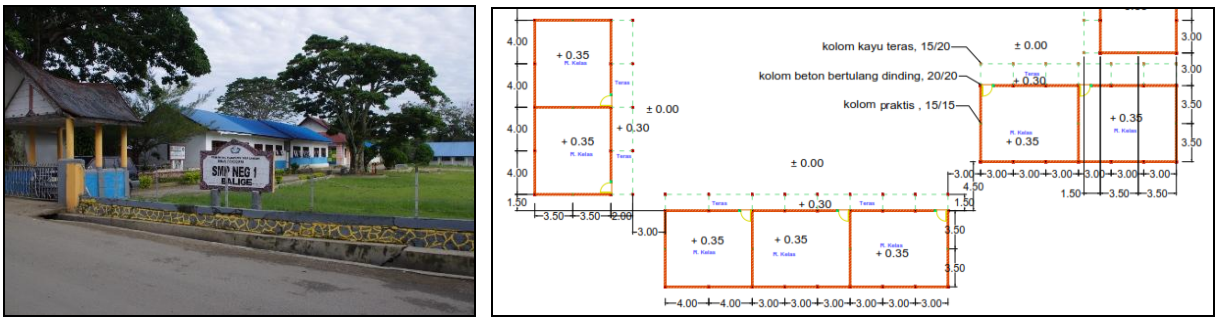

a) front view *b) partially plan view of the rear section*

Fig. 1: The junior high school in Balige.

During the field survey, the geometry of the school building is measured using laser meter and the strength of concrete material of the element is investigated using the rebound Hammer apparatus. The diameter and number of steel bar is identified visually. If this method is not possible to be done in the field, the number and diameter of rebar are assumed to be equal to the minimum requirement in the reinforced concrete design. It is done so because the as-built drawings are not available in the school office during the field survey.

2.2. Modeling of the School Building Structures

The junior high school building in Balige is used as an example in this study. The building has 2 class rooms with geometry dimension 8 x 7 m of each, as shown in Fig. 1a. This school building structures are modeled as the 3-dimensional moment resisting frames with infilled brick wall. The infilled brick wall is modeled as the strut-tie element or compressional member (Fig. 2a). The strength of infilled brick wall is assumed to be 3,54 MPa and its elastic moduli is 1000 MPa. The thickness of brick wall is assumed to be 10 cm. These values are based on the test done by Aryanto [6]. Therefore the equivalent depth and the ultimate

normal strength of brick wall are found to be 0,79 m and 470 kN, respectively. For the infilled brick wall with opening, this study uses the reduction factor to introduce to the ultimate strength of the brick wall.

The plastic hinge in the column and beam element is represented by moment-rotation relationship modelled using lumped plasticity model. To simulate the cyclic behavior of RC members in plastic hinge under load reversals, Modified-Takeda hysteresis rule is employed (Fig. 2b) with the unloading and reloading parameters (α = 0.3 and β = 0.6) for beam and column member are identical, as suggested by Fardis [7]. The backbone curve proposed by Zaerian and Krawinkler [8] is used, as demonstrated by thin line in Fig. 4. The yield rotation, θ_y, of a member is obtained by the ratio of M_y to elastic rotation stiffness (K_0=6EI/L). The cyclic strength degradation could increase the peak displacement demands significantly, particularly for short period of structures. The peak displacement demands are very sensitive to the changes of yield strength [9]. Therefore, this study considers the strength degradation of the member based on rotation ductility from Zareian and Krawinkler [8] backbone curve, which is developed based on hysteresis rule of Ibarra et al [10].

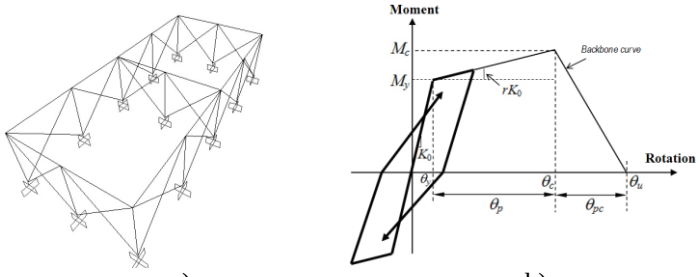

a) b)

Fig. 2: The structural model of school building: a) 3-D model of moment resisting frame with bracing to represent wall, and b) the backbone curve to represent the nonlinear material behavior of RC elements.

2.3. Modeling of the Repeated Earthquakes Ground Motions

The ground motion record is taken from PEER—NGA database and all motions are near fault motion type, as listed in Table 2 and shown in Fig. 3. It is not possible to find the identical seismological parameter as in Sumatran fault earthquake in searching the ground motion record in the database. Therefore, the selection is made only based on the shallow crustal earthquakes on the stiff soil. These selected ground motions are scaled to the design spectra in Indonesian Seismic Code (SNI 1726:2012) [11] based on its response spectrum at the building's fundamental period.

Table 2: List of earthquake ground motions used in this study

No.	Date	Earthquake Name	Mag. (Mw)	Closest. Dist. (km)	Station	PGA [g] (x)	PGA [g] (z)
1	24/04/1984	Morgan Hill	6.2	0.53	Coyote Lake Dam (SW Abut)	1.080	0.814
2	18/10/1989	Loma Prieta	6.9	9.96	Gilroy - Gavilan Coll.	0.414	0.294
3	18/10/1989	Loma Prieta	6.9	3.88	LGPC	0.944	0.886

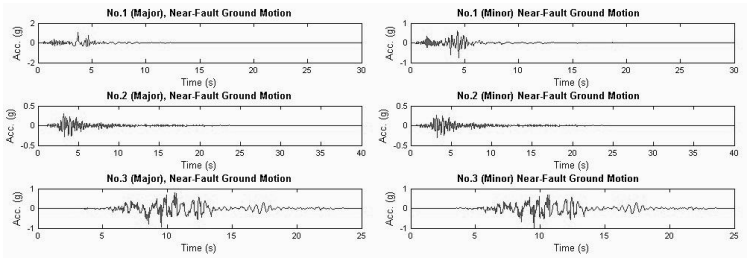

a)

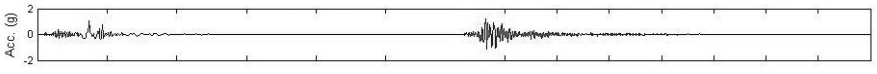

b)

Fig. 3: Near-fault ground motion model: a) major and minor components, b) double events motion model.

The repeated earthquake ground motion presents in the form of the combination of ground motion with single and double events (Fig. 3). The method of assembly is taken from Hatzigeorgiou and Beskos [4]. In this method, the amplitude ratio of assembled ground motion is scaled based on the ratio of peak ground acceleration (PGA), which is governed by magnitude within a consecutive earthquakes sourced from the same seismic region and recorded at the same site. The ratio of PGA is derived using the ratio of empirical attenuation functions, which varied in magnitude. Moreover, an interval motion with zero acceleration of amplitude and 100 seconds of duration length inserts in between two consecutive ground motions [12].

3. Result and Discussion

The model of school building has fundamental period of 0.12 s and 0.11 s for strong and weak directions, respectively. This short period is typical for short structures and would be sensitive to the high frequency ground motion (e.g. near fault ground motion). The result of linear analysis indicates that the school building structures without infilled wall have a poor lateral strength. This strength is significantly increased when the infilled is taking into account in the analysis.

The pushover analysis indicates that the yield deformation of school building model achieves 5.4 cm. The result of nonlinear inelastic response history analysis in form of displacement is listed in Table 3 and 4. These tables explain that the lateral deformation demand significantly increases of up to 24,4% due to repeated earthquakes (double event). It means that the cracked element after a single event of earthquake could be excessively damaged when experiencing the double event of earthquakes.

Table 3: Displacement and ductility demands of the school building in Balige under single event of earthquake.

Earthquake No.	Roof Displacement [cm]	Ductility demand
1	13.3	2.5
2	15.5	2.9
3	14.2	2.6

Table 4: Displacement and ductility demands of the school building in Balige under repeated earthquake.

Earthquake no. in sequence	Roof Displacement [cm]	Ductility demand	Deformation increment
1-2	16.8	3.1	24.4%
2-3	19.1	3.5	20.7%
1-3	17.5	3.2	23.1%

It shows that the single event of earthquake makes some of the infilled brick walls damage and few columns and beams experience plastic hinge. This condition is almost similar for 3 type of selected ground motions. The number of structural elements experiencing plastic hinge are increased after the second event motion occurred (repeated earthquake case). In this case, all of the infilled brick walls are damaged and plastic hinges are indicated on the most of columns. The increment of damage condition is quite significant, which is indicating the school building is sensitive to the repeated ground motion. The short period of ground motion is most probably has an important role in damaging the short period building. Therefore, a proper design code is needed for constructing the single story building near the Sumatran fault, particularly in detailing the rebar of column and beam elements.

4. Conclusion

This study investigates the deformation and damage of the single story school building near the Sumatran fault under the repeated ground motions. The result concludes that the repeated earthquake can increase the ductility demand of the school building built on the stiff soil of up to 24.4%. The damage after the repeated ground motion is found to be significantly increased in comparison with the damage due to single event of earthquakes. All of the infilled brick wall and the beam element are found to be totally damage after experiencing the repeated ground motions. Plastic hinges are exhibited in the most of column due to the double event of earthquakes, whereas only few of columns are experienced it when the single event of earthquake occurred. In order to avoid any casualties, the repeated earthquake shall be considered in Indonesian seismic code.

5. Acknowledgements

This research is fully funded by Directorate General of Higher Education, Ministry of Education and Culture, through the Penelitian Desentralisasi Hibah Bersaing under the contract with no. 70/II.3-AU/UMSU-P3M/C/2014. This support is much appreciated.

6. References

[1] A.S. Elnashai, J.J. Bommer, and A. Martinez-Pereira. Engineering implications of strong-motion records from recent earthquakes. *Proceeding of the 11th European Conference on Earthquake Engineering*. 1998

[2] D. Muria Vila, and A.M. Toro Jaramillo. Effects of several events recorded at a building founded on soft soil. *Proceedings of 11th European Conference on Earthquake Engineering*, Paris, 1998.

[3] C.Amadio, M. Fragiacomo, S. Rajgelj. The effects of repeated earthquake ground motions on the non linear response of SDOF systems. *Earthquake Engineering and Structural Dynamics* 2003; **32**(2):291-308.

[4] G.D. Hatzigeorgiou, and D.E. Beskos. Inelastic displacement ratios for SDOF structures subjected to repeated earthquakes. *Engineering Structures.* 2009; **31**(11):2744-2755.

[5] A.Faisal, T.A. Majid, G.D. Hatzigeorgiou. Investigation of story ductility demands of inelastic concrete frames subjected to repeated earthquakes. *Soil dynamics and earthquake engineering.* 2013; 44(1):42 -53.

[6] A.Aryanto. *Kinerja portal beton bertulang dengan dinding pengisi bata ringan terhadap beban gempa*. Tesis Magister, Institut Teknologi Bandung, 2008.

[7] M.N. Fardis. *Seismic design, assessment and retrofitting of concrete buildings: based on EN-Eurocode 8* (Vol. 8). New York: Springer. 2009.

[8] F. Zareian, H. Krawinkler. *Simplified performance-based earthquake engineering*. Report No. 169, John A. Blume Earthquake Engineering Center, Stanford University, 2009.

[9] Applied Technology Council (ATC). *Effects of strength and stiffness degradation on the seismic response of structural systems*, Report No. FEMA P440A, Washington, DC, 2009.

[10] L. Ibarra, and H. Krawinkler. *Global collapse of frame structures under seismic excitations*. Report No. 2005/06, Pacific Earthquake Engineering Research Center, University of California, Berkeley, 2005.

[11] Badan Standardisasi Indonesia. *Tata cara perencanaan ketahanan gempa untuk struktur bangunan gedung dan non gedung*. Jakarta. 2012.

[12] G.D. Hatzigeorgiou. Ductility demand spectra for multiple near- and far-fault earthquakes. *Soil dynamics and earthquake engineering.* 2010; **30**(4):170-183.

ISBN 979-458-758-3
Proceedings of the 3rd International Conference on the Geohazard Information
Zonation and 5th Seminar & Short Course of HASTAG (GIZ2014-HASTAG5)
Organized by UMSU, HASTAG, USM
Medan, Indonesia, October 20-22, 2014

The Use of Volcanic Ash of Mount Sinabung Eruption as the Substitution of Fine Aggregate in Making Batako (Mass-Produced Brick)

Rahmi Karolina[1], Syahrizal[2], M.Agung Putra[3]Tito Agung Prasetyo[4]

[1]*Lecturer of Civil Engineering Department, University of Sumatera Utara*
Jl. Perpustakaan No. 1, Kampus USU, Medan
E-mail: rachmie_caroline@yahoo.co.id
[2]*Lecturer of Civil Engineering, University of Sumatera Utara*
Jl. Perpustakaan No. 1, Kampus USU, Medan
E-mail: rizal_ar@ymail.com
[3]*Lecturer of Civil Engineering Department, University of Sumatera Utara*
Jl. Perpustakaan No. 1, Kampus USU, Medan
E-mail:agung13handana@gmail.com
[4]*Student of the Department of Civil Engineering, University of Sumatera Utara,*
Jl. Perpustakaan No. 1 Kampus USU Medan
Email: tyo_tito89@yahoo.com

Abstract. The initial idea of writing this research was the use of natural materials from Mount Sinabung eruption which could function as the substitute of natural material, used for making concrete. This idea was strengthened by the chemical content which is found in the volcanic ash of Mount Sinabung which contained 74.3% of SiO_2, 3.3% of AL_2O, and 1.79% of CA O in sand and cement obtained from the Research and Industrial Standardization Center. The research used volcanic ash as the substitution of fine aggregate with the variation of 0%, 5%,, 10%, 15%, 20%, and 25%, within a 28 day-treatment, cylinder testing devices, and batako. The analysis and method of the research were referred to the SNI 03-0349-1989 standard. The result of the analysis showed that the use of volcanic ash in batako with the variation of 0% at the average compressive strength of 166.90 kg/cm^2, 5% at the average compressive strength of 173.72 kg/cm^2, 10% at the average compressive strength of 207.14 kg/cm^2, and 15% at the average compressive strength of 130.97 kg/cm^2 had met the quality standard I of SNI 03-0349-1989 with the average compressive strength of 100 kg/cm^2. The result of the maximum of split tensile strength showed that the variation was 10% of the average split tensile strength was 12.93%, and in the testing of water absorption in the variation of 0%, 5%, 10%, 15%, 20%, and 25%showed that the maximum value of water absorption was 4.142% which had met SNI 03-0349-1989 standard with the average maximum of water absorption quality I of 25%. It could be concluded that the volcanic ash of Mount Sinabungcould be used as batako mixture at the maximum of composition of 10%.

Keywords: Glass Volcanic Ash, Absorption, Compressive Strength, Tensile Strength

1. INTRODUCTION

Mount Sinabung, which is called*DelengSinabung* in Karonese, is one of the active volcanoes in the world; it belongs to the geological type of *Statovolkano*. Mount Sinabung eruption increased to the level of 4 (Alert) on November 24, 2013 since it spat out black, thick smokescreen, followed by sand rain and volcanic ash which covered thousands of hectares of farmers' crops under the radius of six kilometers so that more than 20 thousand people had to be evacuated.

This condition constituted the background for the use of volcanic ash material of Mount Sinabung eruption as the alternative for the substitution of the materials usually used for concrete. The idea was strengthened with the chemical content in the volcanic ash which had the same content as the one in sand and cement (SiO_2, AL_2O_3, and CA O) obtained from the Research and Industrial Standardization Center, Medan. The testing material which would be used was batako (mass-produced brick).

Batako is building material which consists of stones. Its hardening is not through kilning; it is shaped by the mixture of sand, cement, and water at the ratio of 1 cement : 7 sand. It can also be added by other additives and is molded

through the process of compaction so that bars are shaped in a certain size. The process is not through kilning or placed in a damp place and protected from direct sunlight or rain. It is molded in such a way that it meets the requirement and can be used as the substitution of brick for a wall.

The increasing demand for batako in the market will increase the need of the main raw material for it, particularly sand and cement. The availability of these materials is influenced by their location; in the mountainous terrain, the availability of sand is minimal since it is dominated by big gradation of materials. This condition has encouraged technicians to develop a material which could substitute or decrease the need for the construction materialin order to reduce the cost of raw material without reducing the quality of the products. One of the alternatives which can be used to substitute sand and cement is volcanic ash as the additive for batako.

The objective of the research was to find out whether batako, made from volcanic ash, met the qualification of quality I and quality II and to identify each optimum percentage of volcanic ash which met the requirements of the minimum of compressive strength of massive batako, according to SNI-3-0349-1989 standard.

This research was expected to be the reference and information about the planning and developing building construction, particularly in batako industry and about the difference in using alternative material of volcanic ash with or without using it from the visual standpoint, water absorption, compressive strength, split tensile strength, and the implementation which could be used as the reference for feasible use of alternative material and of volcanic ash in batako mixture.

2. RESEARCH METHOD

2.1 Materials

Batako is usually made of sand, cement, and water. In this research, the materials used to make batako were cement, water, sand, and volcanic ash. The following was a glimpse of information about the materials which were used in making batako.

1. Semen Portland

Cement was created by a scientist, Joseph Aspidin in 1784. He was an English bricklayer who succeeded in making cement from the calcinations of limestone. In its process, the limestone and loam were ground to melt.The compound was then kilned in a furnace until the process of decomposition of dried limestone and carbon-dioxide. Dried limestone would react to other compounds to shape clinkers.

SNI 15-2049-2004 defines Portland cement as hydraulic cement which is made by grinding Portland cement slag which consists of calciumsilicate with its hydraulic characteristic along with additives which comprises of one or more calcium sulfate compounds and can be added by other additives.

Portland cement and pozzolan Portland cement are used in making batako, and since they are used for construction, they should have the quality which is in line with accuracy so that they can be used effectively. Cement will act fast when it is mixed with waterso that it will be cement paste. It is not hardened because of drying but because of the reaction of chemical hydration. Therefore, batako should always be wet to ensure that it is properly hard. The hydration reaction releases heat which is called hydration-heat. The amount of heat depends on the type of cement, the fineness of grinding, and the water. This heat development can cause a crack during the cooling.

The cement used in the experiment was Andalas cement in 50 kg packaging.

2. Sand

Aggregate (which does not react) is mixed materials for batako which are bound by cement paste. Sand and gravels are used as aggregate since they have economical. They are naturally found is shallow water (floating) or located at the bottom of the river and as the remnants when ice melts.

The most important characteristic of aggregate (stones, gravels, sand, and others) is its crushing strength, and its resistance to collision which can affect its bound to cement paste, porosity, and the characteristic of water absorption. All of them will affect the resistance to congealment process in the winter and chemical aggression and resistance to shrinkage.

The sand used in the research was taken from Binjai. The examination included:

a. Analysis on sand strainer;
b. Examination on the weight of fine aggregate;
c. Examination on the organic content (*colorimetric test*) in fine aggregate;
d. Examination onspecific gravityin the cement and the volcanic ash;
e. Examination on the mud contentand the fine aggregate clay content.

3 Water

Water constitutes the material for shaping batako. It is functioned to make chemical reaction possible in cement to be bound, to make it hardened, to wet aggregate, and to be used as mixing lubricant in order to make it easy in the process of making batako. It is also used to make the mixture become thick porridge and as the material for causing

reaction in other materials to harden. Therefore, it is highly needed in the implementation of the process. Without it, material construction will not be feasible properly and completely.

The water which was used as the mixing material came from the Engineering Material Laboratory of the Department of Civil Engineering, Faculty of Engineering, University of Sumatera Utara.

4 Volcanic Ash

Volcanic ash is the mineral of volcanic stones, including glass material which is as big as sand and gravels with 2 mm (1/2 inch) in diameter from volcanic eruption. These minute ash particles can have section less than 0.001 mm ($1/25.000^{th}$ of an inch). It is very hard and cannot be dissolved in water so that it is often abrasive and slight corrosive, and it can deliver electricity when it is wet.

The types of mineral in the volcanic ash depend on the chemical magma of the erupting volcano, by considering that the abundant element in magma is silica (SiO_2) and oxygen. Various kinds of magma from volcano eruption are often explained by the parameter of its silica. Eruption which comes from low energy basalt (basalt: dark frozen stones and fine particles which come from the frozen lava of a volcano) produces specific dark ash which contains 74.3% of silica (SiO_2), 3.31% of aluminum (AL_2O_3), and 1.79% of calcium as (CAO)

Table 1. Chemical content ofvolcanic ash of Mount Sinabung eruption

No.	Parameter	Result	Unit	Method
1	Silica as SIO_2	74,3	%	Gravimetric
2	Aluminum as AL_2O_3	3,31	%	Calculation
3	Calcium as CAO	1,79	%	Trimetri

(Source: ResearchandIndustrial Standardization Center Medan, Examining Laboratory, the Ministry of Industry)

In this research, the volcanic ash material which was used for batako was obtained from Mount Sinabung, about 4,600 meters from its top.

2.2 Planning for Mixing

In order to calculate the amount of need of each material, the examination of the specific gravity of each material was conducted so that the composition of the materials from the volume of the testing device mold was calculated. The following is the composition of the need for the materials for the making of testing devices:

Table 2. Calculation ofthe Need forBatako Testing Devices

VARIATION	=	WEIGHT OF CEMENT + (WEIGHT OF SAND – WEIGHT OF VOLCANIC ASH)					1.20	
0%	=	3,660	+	14,137	-	0	=	17,797.20 gr
5%	=	3,660	+	14,137	-	566.16	=	17,231.04 gr
10%	=	3,660	+	14,137	-	1,132.32	=	16,664.88 gr
15%	=	3,660	+	14,137	-	1,698.48	=	16,098.72 gr
20%	=	3,660	+	14,137	-	2,264.64	=	15,532.56 gr
25%	=	3,660	+	14,137	-	2,830.80	=	14,966.40 gr

Table 3. Calculation of the Need forCylinder Testing Devices

VARIATION	=	WEIGHT OF CEMENT + (WEIGHT SAND – WEIGHT OF VOLCANIC ASH)					1.20	
0%	=	2,424	+	9,364	-	0	=	11,787.86 gr
5%	=	2,424	+	9,364	-	374.99	=	11,412.87 gr
10%	=	2,424	+	9,364	-	749.99	=	11,037.88 gr
15%	=	2,424	+	9,364	-	1,124.98	=	10,662.89 gr
20%	=	2,424	+	9,364	-	1,499.97	=	10,287.89 gr
25%	=	2,424	+	9,364	-	1,874.96	=	9,912.90 gr

2.3 Designing of Testing Devices

The design for mixing of the material in arranging batako was the ratio of 1cement : 7 sand. The size of the testing device from outside view and the testing of absorption were made by using batako testing device of 40 x 20 x 10 cm. Cylinder testing device of 15x30 cm with a 10x10 cm batako piece were used to test the compressive strength, and a 15 x 30 cm cylinder testing device was used to test the pull strength. The variation of the adding of volcanic ash was done by reducing the amount of sand from 0%, 5%, 19%, 15%, 20%, and 25% of the weight of sand.

2.4Treatment of Testing Device

Some tips for the treatment of each testing device are as follows:

1. For batako testing device, keep batakofrom direct sunlight and rain in order that the fastening of the paste does not loose. Batako should be treated in 28 days by soaking the testing device in the soaking tub and keep the room temperature in the Engineering Material Laboratory of the Department of Civil Engineering, Faculty of Engineering, University of Sumatera Utara stable.
2. For cylinder device, the treatment of cubic testing devicewas done by soakingit in thespecial soaking tub in the EngineeringMaterial Laboratory of the Department of Civil Engineering, Faculty of Engineering, University of Sumatera Utara.

2.5Testing the testing Device

Some tips for testing each testing device are as follows:

1. The testing of slump value was done by using Abrams' pyramid, piercing iron, and pedestal. The mixing process was done manually.
2. The testing for the size and the outside view was done by using a 40 x 20 x 10 cm batako testing device with a sliding bar. The testing was donewhen batako was 28 days for all variations.
3. The testing for absorption was done by using a 40 x 20 x 10 cm batako testing device with an oven and a scale. The testing was done when batako was 28 days for all variations.
4. The testing for compressive strength and pull strength was done by using a 15 x 30 cm cylinder testing device with a compression machine. The testing was done when batako was 28 days for all variations.

3. RESULT AND DISCUSSION

3.1 Visual Testing

1. Outside View Testing

Table4. Result of Visual Examination

Explanation	Batako Variation					
	Normal Batako	Volcanic AshBatako 5%	Volcanic AshBatako 10%	Volcanic Ash Batako15 %	Volcanic Ash Batako20 %	Volcanic Ash Batako25 %
1. Surfaces						
a. Flatness	flat	flat	flat	flat	flat	flat
b. Rift	none	none	none	none	none	none
c. Smoothness	smooth	smooth	smooth	smooth	smooth	smooth
2. Edges						
a. Right angle	angle	angle	angle	angle	angle	angle
b. Acuity	incisive	incisive	incisive	incisive	incisive	incisive
c. Strength	strong	strong	strong	strong	strong	strong

The result of the examination showed that the use of volcanic ash as the substitution of fine aggregate from various variations in this research, produced batako which had flat surface, not rift, smooth and no cavity, and had met the requirement of outside view, according to SNI 03-0349-1989.

2. Sectional Size Examination

After the outside view had been examined, the examination on the dimension and section which met the provision of SNI 03-0349-1089 was done by using the average of five pieces of complete batako. A 1 mm accuracy of bar as the measurement instrument was used at least 3 (three) times in different places according to the length, width, and thickness of the testing device.

The result of the analysis of the deviation of batako sizefrom various variations of volcanic ashwas as follows:

Table5. Result of Visual Examination

Mixing Composition	Length (mm)		Width (mm)		Thickness (mm)	
	Testing Device	SNI 0349-89	Testing Device	SNI 0349-89	Testing Device	SNI 0349-89
NormalBatako	1.2	5.0	1.1	2.0	1.4	2.0
Volcanic Ash Batako 5%	0.7	5.0	1.7	2.0	0.6	2.0
Volcanic Ash Batako 10%	0.5	5.0	1.0	2.0	1.3	2.0
Volcanic Ash Batako 15%	1.4	5.0	1.1	2.0	1.1	2.0
Volcanic Ash Batako 20%	1.6	5.0	0.9	2.0	1.6	2.0
Volcanic Ash Batako 25%	1.3	5.0	1.3	2.0	1.8	2.0
Average Deviation (%)	1.123		1.190		1.313	

The batako had met the requirement of SNI 03-0349-1989 standard because the volcanic ash had nearly the same particles as those of cement; it could penetrate the sieve No. 200 , and the additives for volcanic ash could fill the cavity among the sand which causedbatako to be solid so that its surfaces became flat.

From the result of the examination, it was found that the condition of the shape and the section did not indicate significant difference; but, since the batako was made manually, its solidity was not uniformed. Besides that, the density of the pores in batako would highly influence the solidity of its composition.

3.2 Absorption Testing

The result of water absorption testing in batako was listed in Table 6. From the tested batako composition, it was found that the biggest water absorption in batako occurred in normal batako and in 0% of volcanic ash batako at the absorption value of 4.142%, and the smallest absorption in batako occurred in 15% of volcanic ash batako at the absorption value of 3.109%.

The requirement of water absorption, according to SNI 03-0349-1989, was below 25% of water absorption for quality I level batako. Thus, it was one of the 5 variations which had met the requirement of water absorption, according to SNI 03-0349-1989.

Table 6. The comparison betweenthe average water absorptionand quality requirement

Mixing Composition	Water Absorption (%)		Quality Level
	Testing Device	SNI 03-0349-1989	
NormalBatako	4.142	25	I
Volcanic Ash Batako (5%)	4.011	25	I
Volcanic Ash Batako (10%)	3.520	25	I
Volcanic Ash Batako (15%)	3.109	25	I
Volcanic Ash Batako (20%)	3.383	25	I
Volcanic Ash Batako (25%)	3.172	25	I

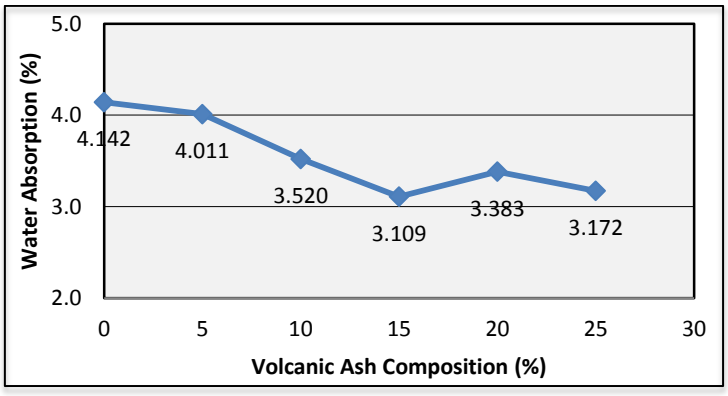

Picture 1. Graph ofCorrelation between Batako Absorption andVolcanic Ash

3.3 Compressive Strength Testing

The recapitulation of the result of batako compressive strength of six types of the experimented mixturewas in the following table:

Table7. Comparison between the average compressive strengthand quality requirement

No.	Mixing Composition	Compressive Strength (kg/cm2)		Quality Req.
		Testing Device	SNI 03-0349-1989	
1	Volcanic Ash Batako (0%)			
	Cube 10x10x10	68.00	40	III
	Cylinder 15x30 (Treatment)	166.90	100	I
	Cylinder 15x30 (Without Treatment)	136.43	100	I
2	Volcanic Ash Batako (5%)			
	Cube 10x10x10	69.33	40	III
	Cylinder 15x30 (Treatment)	173.72	100	I
	Cylinder 15x30 (Without Treatment)	141.20	100	I
3	Volcanic Ash Batako (10%)			
	Cube 10x10x10	70.00	70	II
	Cylinder 15x30 (Treatment)	211.01	100	I
	Cylinder 15x30 (Without Treatment)	142.57	100	I

No.	Mixing Composition	Compressive Strength (kg/cm2)		Quality Level
		Testing Device	SNI 03-0349-1989	
4	Volcanic Ash Batako (15%)			
	Cube 10x10x10	70.67	70	II
	Cylinder 15x30 (Treatment)	130.97	100	I
	Cylinder 15x30 (Without Treatment)	140.52	100	I
5	Volcanic Ash Batako (20%)			
	Cube 10x10x10	63.33	40	III
	Cylinder 15x30 (Treatment)	106.87	70	II
	Cylinder 15x30 (Without Treatment)	138.47	100	I
6	Volcanic Ash Batako (25%)			
	Cube 10x10x10	61.33	40	III
	Cylinder 15x30 (Treatment)	108.23	70	II
	Cylinder 15x30 (WithoutTreatment)	131.65	100	I

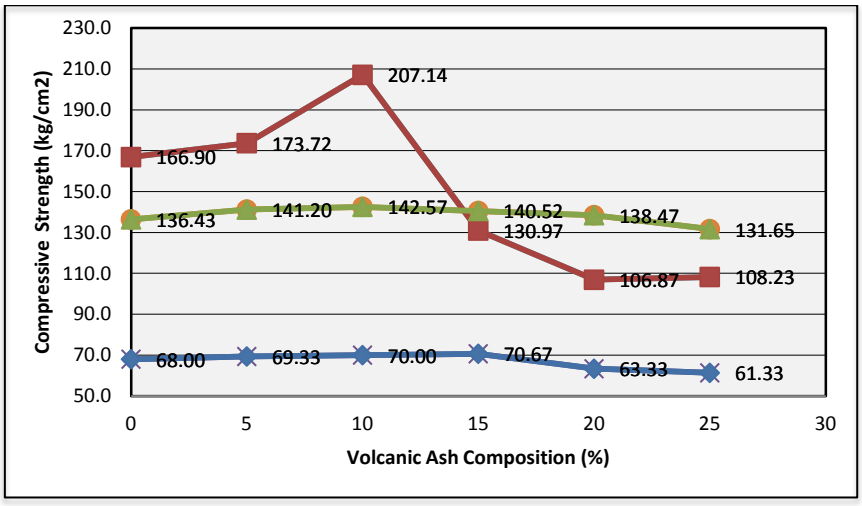

Picture 2. Graph ofthe Correlation between batako Compressive Strength andGlass Powder Content

Graph 4.4 showed significant difference between the result of compressive testing, based on the tests on shape and concrete treatment method. The value of the testing of concrete compressive strength for cylinder testing device with treatment indicated the increase in the value of the maximum of concrete compressive strength in Volcanic Ash Batako at the mixing composition of 10% at the value of the average compressive strength of 207.14 kg/cm^2 and it decreased to 130.97 kg/cm^2.

According to SNI 03-0349-1989, Volcanic Ash Batako of 0% till 25% with treatment belonged to quality I level, Volcanic Ash Batako of 5% with the average compressive strength of 86.54 kg/cm^2 belonged to quality II level, and Volcanic Ash Batako of 10% with the average compressive strength of 105.12 kg/cm^2 belonged to quality I level.

Based on the compressive strength data and graphs, it was found that volcanic ash batako of 10% with treatment was the best composition and the maximum of compressive strength. This increase in compressive strength was because volcanic ash was domineered by silica arrangement material (SiO^2) which had the superiority as the filling material. Empty cavity in the cement particles would be filled with micro-silica so that it functioned as mechanical property and increased its durability. Meanwhile, the decrease in compressive strength in Volcanic Ash Batako of 15% was caused by excessive volcanic ash composition. The consequence was that the mixture was not homogenous, the cement volume as a fastening material was not maximal in fastening the aggregate in arranging batako because it was not followed by the addition of cement and the need for water, and its workability decreased because water absorption was excessive. This condition was strengthened by visual observation of cylinder testing device of split tensile testing in the fragment of cylinder testing device in volcanic ash which could not be mixed well with other aggregates.

3.4 *Briquette*Pull Strength Testing

Table8. The Result the Average Split Pull Strength Testing

No.	Mixing Composition	Pull Strength (kg/cm^2)
1	Normal Batako(0%)	
	Cylinder 15x30 (Treatment)	9.91
	Cylinder 15x30 (Without Treatment)	8.92
2	Volcanic Ash Batako (5%)	
	Cylinder 15x30 (Treatment)	7.83
	Cylinder 15x30 (Without Treatment)	4.95
3	Volcanic Ash Batako (10%)	
	Cylinder 15x30 (Treatment)	12.83
	Cylinder 15x30 (Without Treatment)	11.39
4	Volcanic Ash Batako (15%)	
	Cylinder 15x30 (Treatment)	1.72
	Cylinder 15x30 (WithoutTreatment)	1.32
5	Volcanic Ash Batako (20%)	
	Cylinder 15x30 (Treatment)	1.14
	Cylinder 15x30 (Withoout Treatment)	0.75
6	Volcanic Ash Batako (25%)	
	Cylinder 15x30 (Treatment)	1.01
	Cylinder 15x30 (Without Treatment)	0.82

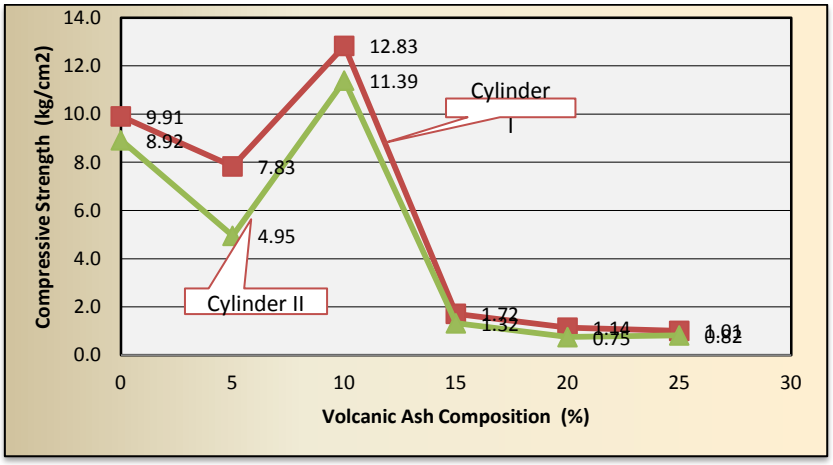

Gambar 3. Graph of the Correlationbetween Batako Pull Strengthand Volcanic Ash Composition

The above graph showed thatthe value ofthe highest pull strengthwas involcanic ash Batako of 10% with the treatment of 12.83 kg/cm^2. Meanwhile,the lowest pull strengthwas in the volcanic ash Batako of 20% without treatmentof0.75 kg/cm^2. Volcanic ash Batakoof 10% was the longest pull strengthbecause the addition ofvolcanic ashto the mixture was over.

3.5 The Best Composition

The best composition was drawn from the result of the comparison of the requirement of quality VI mixing composition, molded as cylinder and batako testing devices with SNI 03-0349-1989 standard.

The result of the best composition was the compressive strength for cylinder testing device with treatment at the mixing composition of 10% with the average compressive strength of 207.14 kg/cm^2. According to SNI 03-0349-1989 quality standard, it belonged to compressive strength Level I at the minimal average of 100 kg/cm^2 and composition.

In the average pull strength of 12.83 kg/cm^2 and the average water absorption of 4.142%, according to SNI 03-0349-1989, water absorption below 25% belonged to quality level Ibatako.The deviation of the average length was 1.123 mm, the deviation of the average width was 1.190 mm, the deviation of the average thickness was 1.313 mm, but they still met the measurement requirement which was in line with SNI 03-0349-1989 standard.

4. CONCLUSION AND SUGGESTION

4.1 Conclusion

From the result of the research and the discussion, it could be concluded that

a. the factor of cement water in batako mixture highly influenced the quality of batako. The higher its f.a.s., the lower its concrete quality; but if the use of the f.a.s. was reduced, the quality of the concrete would be better although the processing would be difficult because the making of batako in this research was done manually. Cement water used in this research was 40%.
b. from the visual test, it was found that the surface of batako was average in each section because the volcanic ash which had nearly the same particles as the cement could fill the cavity of the sand so that batako became more solid which caused the surface of batako flat.
c. the use of batako volcanic ash as an additive by replacing some of its weight could increase its absorption. The maximum of absorption in batako in this research was 4.142%.
d. Based on the compressive strength data and graphs, it was found that batako volcanic ash of 10% with treatment was good composition and obtained the maximum of compressive strength. The increase in compressive strength was because volcanic ash was domineered by silica arrangement material (SiO_2) which was superior as filling material.
e. From the result of the research above, it was found that volcanic ash could be used as an additive in making batako.

3.4 Suggestion

Based on the conclusion and the discussion above, it is recommended that

a. in order to obtain batako maximal compressive strength, volcanic ash with the composition of 10% should be used, and the treatment of concrete should be done by soaking it.
b. in order to obtained good quality, accuracy, planning, work method, equipment, and selecting the materials should be done properly, according to the guidelines.
c. There were a lot of limitations in the research; therefore, the next researchers should consider the following things:

   1). Selecting the materials highly influences the quality of batako which will be examine; mud content in sand can decrease the quality of the concrete which will need more cement;

   2). Chemical content in the volcanic ash should be examined so that the chemical content in the glass minute powder can be detected.

   3). Need for water as the reaction agent between cement and aggregates should be detected. This research was focused on the condition of soil moisture mixing so that determining and controlling f.a.s. was not done.

   4). Specific machine in making batako should be used so that maximal result can be obtained. Since the equipment used in the research was not adequate, the process of making batako was done manually so that it took a long time and the quality of batako was not similar and maximal.

5. REFERENCES

[1] Departemen P.U.(1989), *SNI 03-0349-1989 Bata Beton untuk Pasangan Dinding*, Balitbang,Jakarta.

[2] Departemen P.U.(2004), *SNI 15-2049-2004Semen Portland*, Balitbang,Jakarta.

[3] Departemen P.U. (2002), *SNI 03-2491-2002Metode Kuat Tarik Belah Beton*, Balitbang,Jakarta

[4] Mulyono, Tri. (2004). *Teknologi Beton*. Penerbit Andi: Yogyakarta.

[5] Nugraha, Paul. danAntoni. 2007. *TeknologiBetondan Material, PembuatanBetonKinerjaTinggi.*Yogyakarta: Andi Offset.

[6] Tjokrodimuljo, K. 1992. *TeknologiBeton*. Yogyakarta: Gramedia.

[7] Priantoro, Soerjandani. 2012. *Pemanfaatan Abu VulkanikGunungMerapiSebagaiAlternatifCementitiousUntukCampuranPembuatanBahanBangunan.*Surabaya: UniversitasWijayaKusuma Surabaya.

[8]Kusumadhana,Ivandre.2012.*PenggunaanabuvulkanikGunungMerapiuntukbahantambahpembuatangentengbetonditinjaudarikualitasfisikdanmekanik,* Malang: UniversitasNegeri Malang.

[9] Muldiyanto, Agus. 2012. *AnalisispemakaianabuvulkanikGunungMerapiuntukmengurangipemakaian semen padacampuranbetonmutukelas II.* Semarang :Universitas Semarang, 27 Juni 2012

[10]Setyawan,TriHanaYuli. 2012. *Penggunaanabuvulkanik Gunung Merapi untuk pembuatan batako ditinjau dari efisiensi biayaproduksi*. Malang: UniversitasNegeri Malang.

[11]Wahyuni,E.I.2012. Penentuankomposisi Kimia Abu ulkanindariErupsiGunungMerapi.*JurnalMalusiadanLingkungan,* (Online), Vol. 19. No.2, (hhtp://lib.law.ugm.ac.id, diasestahun 2012).

ISBN 979-458-758-3
Proceedings of the 3rd International Conference on the Geohazard Information
Zonation and 5th Seminar & Short Course of HASTAG (GIZ2014-HASTAG5)
Organized by UMSU, HASTAG, USM
Medan, Indonesia, October 20-22, 2014

The Utilization Of Can Waste As Fibre And The Addition Of Fly Ash To Mechanical Characteristic Of Concrete

Nursyamsi [1] and Luhut Parulian Bagariang [2 +]

[1] Lecturer, Department of Civil Engineering, Universitas Sumatera Utara, Medan, Indonesia
[2] Department of Civil Engineering, Universitas Sumatera Utara, Medan, Indonesia

Abstract. One such effort is the utilization of can waste processed into fibers and coal combustion wastes such as fly ash. Can waste and fly ash can be used as an additive in concrete mixture. In this study, can fiber and fly ash are added in the concrete mixture. Variation I is a normal concrete, variation II with the addition of can fiber by 20%, and variation III with the addition of can fiber by 20% and fly ash by 15% of volume of cement. Tests are conducted in form of slump test, compressive strength, split tensile strength and absorption of concrete. From the test result, it is obtained the increase in the compressive strength, split tensile strength, and absorption. But the biggest improvement is the wet treatment compared to initial wet treatment for 7 days and initial dry treatment for 7 days. The best increase in compressive strength is variation III with 8,333% of normal concrete. Split tensile strength were increased by 18,414% of normal concrete. Concrete absorption decreased by 0,183% and 0,392% of normal concrete.

Keywords: fibre cans, fly ash, compressive strength, split tensile strength, absorption

1. Introduction

In general, concrete is used as a construction material that is often used in building. Due to the amount of the use in concrete, while the constituent materials are limited and expensive, it appears breakthroughs being made to replace the constituent materials without reducing the quality of the concrete itself. One form of these is done by replacing the material with other material such as using waste around us. Thus, these wastes can be used optimally, so as to have a higher value.

Tin cans used are wastes from the former site of food that can be found in the area around where we live such as beverage cans, food, and others. Waste cans need to be utilized more optimally in order to have a higher sale value. One of the waste utilization is by modifying it into a fiber as an ingredient of concrete.

Fiber cans are those derived from waste cans then processed into small fibers of a certain size (Marsudi, 2009 [3]). Previous research has been conducted by Marsudi, 2009 [3], with a length of 10 mm and a width of 1 mm with a compressive strength testing of K-150 and K-450, and research by Nursetiaji Pamungkas 2006, with a length of ± 20 mm and a width of 2 mm with compressive strength testing of K-225. While this research itself goes on the utilization of waste cans as modified fiber 1 x 20 mm mixed as much as 20% of cement volume and fly ash 15% of cement volume on high strength concrete f'c 25 MPa.

Coal fly ash, the fine grained material that is apozzolanic, is a natural or artificial material obtained from coal combustion and heat generation plants. Fly ash itself does not have the ability to bind as well as cement. But with the presence of water and a fine particle size, silica oxide contained in fly ash will chemically react with the calcium hydroxide formed in the cement hydration process and produce a substance that has the ability to bind.

The purpose of this study was to determine the workability of fresh concrete using fiber cans and fly ash as an ingredient added to concrete, as well as to determine the mechanical behavior of concrete using fiber cans and fly ash as an ingredient added to concrete and compared to normal concrete. Mechanical behavior that was studied included: compressive strength, split tensile strength and absorption.

The problems in this study are as follows:

1. Quality of the concrete is f'c 25 MPa
2. A mixed fiber material and fly ash cans

+ *E-mail address*: njnursyamsi@gmail.com

3. The addition of fiber cans and fly ash were 20% and 15% of the volume of cement.
4. Specimens used for compression test, pull apart, and the absorption are a cylinder with a diameter of 15 cm and a height of 30 cm.
5. Curing done by 3 methods: wet, initial wet 7 days, and initial dry 7 days.
6. Testing conducted on the compressive strength of the test specimen 28 days.
7. Tests performed on split tensile test specimens 28 days
8. Absorption tests carried out on test specimens 28 days.

2. Methodology

Material being used is fine aggregates and coarse aggregates (split stone) from quarry Sei Wampu, Binjai and cement used is Portland type 1 – Padang Cement, and water taken from PDAM Tirtanadi, at Construction Laboratory Civil Engineering USU, Medan. Tin fibre used is the one that has been processed into fibre 1x20 mm and fly ash is obtained from PLTU Labuhan Angin. The tools are those to examine fine and coarse aggregates and concrete compressive and tensile testing machine. The mould sizes in cylinder, diameter 15 cm, height 30 cm. Preparation of test specimens are 63 cylinders. It is conducted at the Laboratory of Civil Engineering USU.

3. Result and Discussion

The entire stages of the test objects such as preparation, inspection, casting, as well as the maintenance have been done according to procedure. At this stage the testing is carried out in the Laboratory of Civil Engineering USU. Cylindrical test specimens that have been aged 28 days can be tested their compressive strength, split tensile, as well as the absorption of concrete. Test results obtained is the raw data that must be recalculated and analyzed to determine the effect of added can fiber material and fly ash in the concrete mixture.

Slump Value

The workability of concrete can be seen through slump value. From the figure 1 it can be seen that with the addition of can fiber and fly ash, slump value obtained is also lower. This is because can fiber and fly ash can absorb water, thus making the workability of concrete variation II and III is more difficult than that of normal concrete.

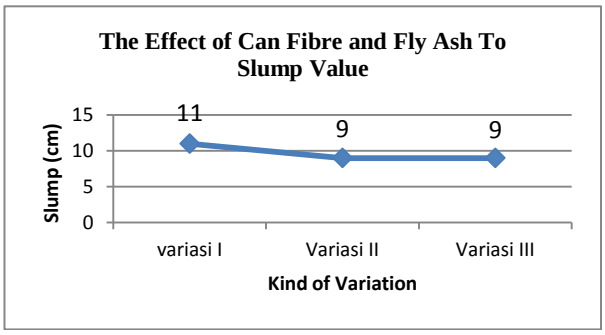

Figure 1. Graphic of Slump Value of Each Variation

Testing of Concrete Compressive Strength

Concrete compressive strength testing conducted at 28th day is intended to get an overview of the improvement of concrete compressive strength by using a can fiber-added material and fly ash.

The results of the compressive strength of each variation can be seen in the figure 2 below.

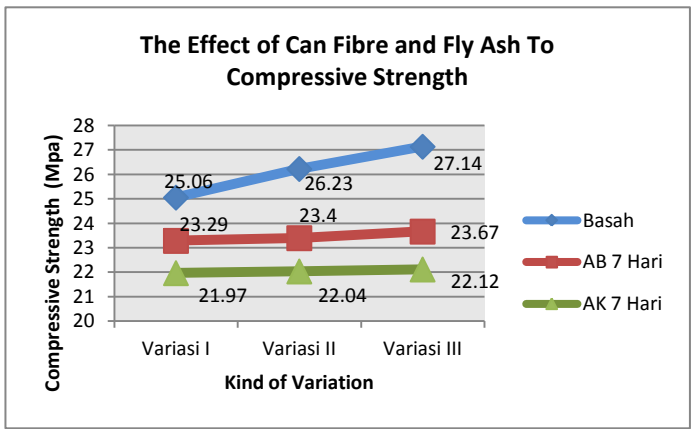

Figure 2. Graphic of Compressive Strength of Each Variation

Based on the compressive strength test results on the test specimen 28th day, it is showed that there is an increase in the strength of the addition of can fiber and fly ash on each curing. In the wet curing, the compressive strength of normal concrete is 25.06 MPa, compressive strength increased in the second variation of 4.666% of the normal concrete. For variation III there is also increase in the compressive strength at 8.333% of normal concrete. At the initial wet curing 7 days, the compressive strength of normal concrete at 23.29 MPa, 7.063% lower than normal in the treatment of wet concrete. However, the compressive strength increased by 0.472% to 1.632% variation II and III to the variation of the normal concrete. At the initial dry curing 7 days, the compressive strength obtained at 21.97 MPa, 12.33% lower than normal concrete in initial wet. But the increase in compressive strength is 0.319% on the second variation and by 0,683% in the third variation of the normal concrete.

Testing of Split Tensile Strength

Testing of concrete tensile strength done at 28th day is intended to overview the value of concrete tensile stress using additives, can fibers and fly ash and the results are compared with normal concrete. The results of split tensile strength of each variation can be seen in figure 3 below

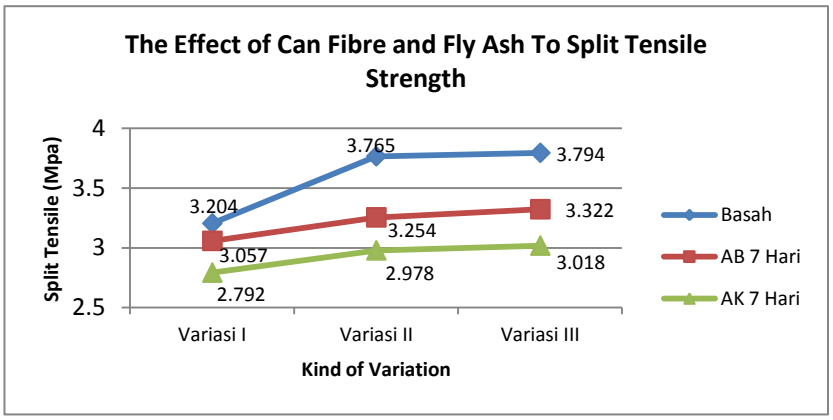

Figure 3. Graphic of Split Tensile of Each Variation

From the graph above, it is showed that the tensile strength of each variation has increased. In the wet curing, split tensile strength of normal concrete is obtained at 3.204 MPa. Variation II gets increase in tensile strength by 17.509% of the normal concrete, while the third variation of split tensile strength increases by 18,414% of normal concrete. At initial wet curing 7 days, split tensile strength of 3,057 MPa obtained, the lower 4.6% of the normal concrete in the wet treatment. But in the second variation has increased by 6,444% and 8.669% in the third variation of the normal concrete. At initial dry curing 7 days, split tensile strength of

2,792 MPa obtained, 12.859% of the normal concrete lower than the wet curing. Variations II, an increase of 6.662% and the third variation increases by 8.095% of the normal concrete.

Testing of Concrete Absorption
Concrete permeability testing is done by soaking the concrete cylinder samples for 24 hours after concrete ages 28 days, intended to get the rate of water infiltration on a wide variety of mixtures compared with normal concrete. The test results can be seen in figure 4 below.

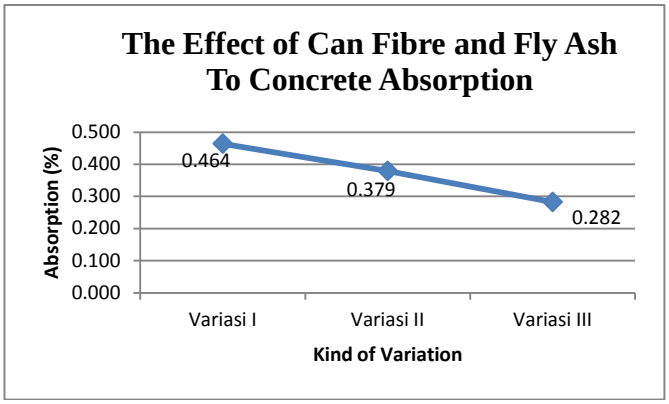

Figure 4. Graphic of Concrete Absorption of Each Variation

From the test results, it is indicated that the normal concrete obtains its absorption values at 0.46%. While variations II and III obtain absorption values at 0.379% and 0.282%. Absorption value of each variation has decreased. This is because can fiber and fly ash are able to fill the empty cavities in the concrete, so that the water absorption of the concrete decreases.

4. Conclusion

From the test results done on the can fibre and fly ash, then some conclusions can be drawn:

1. The use of can fiber and fly ash in concrete mixture with the addition of 20% can fiber (variation II) and 20% can fiber + 15% fly ash (variation III) of cement consumption can decrease the slump value so that the workability of the concrete is reduced.

2. The use of can fiber and fly ash in the concrete mixture can increase the compressive strength of concrete. The most significant improvement is obtained in the wet curing, which increases by 4,669% of the normal concrete on the second variation and increases by 8.3% oft the normal concrete on the third variation. Whereas in the split tensile strength test, the most significant improvement is also obtained in the wet curing, which increases by 17.509% of the normal concrete on the second variation and increases by 18,414% of the normal variation on the third variation. Therefore, can fiber is excellent in improving the quality of concrete, especially on concrete tensile strength.

3. Absorption of concrete also decreases with can fiber and fly ash, because can fiber and fly ash in concrete is able to fill the voids and reduce water absorption. Fly ash can fill the cavity so as to keep the concrete from the relatively high evaporation. From the results of compressive strength and split tensile strength it can also be seen that initial wet curing 7 days compressive strength and split tensile strength of the smallest among treatments early wet and wet treatments 7 days. This is because the initial treatment of dry concrete with 7 days of water shortage in the binding process. As a result, the binding process which occurs is not perfect and have a negative impact on the quality of the concrete itself as reduced compressive strength and tensile strength of concrete.

5. References

[1] Andoyo. 2006. *Pengaruh Penggunaan Abu Terbang (Fly Ash) Terhadap Kuat Tekan dan Serapan Air pada Mortar.* Fakultas Teknik, Universitas Negeri Semarang: Semarang.

[2] Marsudi. 2007. *Kajian Komparatif Kualitas Beton Antara Bahan Tambah Serat Kaleng, Serat Fiber, Serat Kawat Dengan Serat Kaleng dan Serat Fiber yang Berbentuk Pentagonal*. Jurnal Wahana Teknik Sipil, vol.12.No.3.Desember 2007. Semarang.

[3] Marsudi, 2009. *Kualilas Beton Serat Kaleng Proporsi 20% Dimensi 1x10mm Dengan Tinjauan Kuat Tekan K-150 dan K-450 di Banyuwangi Semarang.* Jurnal Wahana Teknik Sipil, volume 14, No.3. Agustus 2009. Semarang.

[4] Maryoto, Agus. 2008. *Pengaruh Penggunaan High Volume Fly Ash Pada Kuat Tekan Mortar.* Jurnal Teknik Sipil dan Perencangan, volume 10, No.2. Juli 2008. Purwokerto.

[5] Mulyono, Tri. 2003. *Teknologi Beton.* Penerbit ANDI. Yogyakarta.
Murdock, L. J, L. M. Brock dan Stephanus Hendarko. 1986. *Bahan dan Praktek Beton, Edisi Ke – 4* . Erlangga. Jakarta.

[6] Nursyamsi. 2005. *Pengaruh Perawatan Terhadap Daya Tahan Beton.* Jurnal Teknik Semetrika, volume 4, No.2. Agustus 2005. Medan.

[7] Sukoyo. 2011. *Rekayasa Peningkatan Karakteristik Beton Dengan Menggunakan Serat* . Jurnal Teknis, vol.6.No. 2. Agustus 2011.Semarang.

[8] SK SNI 03–2491-2002. *Metode Pengujian Kuat Tarik Belah Beton.* Badan Standar Nasional.

[9] SNI. 03-1974-1990. Tentang "*Metode Pengujian Kuat Tekan Beton*".

[10]SNI. 1972:2008. Tentang "*Cara Uji Slump Beton*".

[11]Tjokrodimuljo,K.,1996.*Teknologi Beton*, Nafiri, Yogyakarta.

ISBN 979-458-758-3
Proceedings of the 3rd International Conference on the Geohazard Information
Zonation and 5th Seminar & Short Course of HASTAG (GIZ2014-HASTAG5)
Organized by UMSU, HASTAG, USM
Medan, Indonesia, October 20-22, 2014

Evaluation of the Seismic Strengthening for R/C Frame Building with Soft First Story Using Hysteretic Steel Damper Subjected to Strong Earthquake

Daniel R.Teruna[1], Lukman M[2], Taksiah A. Majid [3], Bambang Budiono [4].

[1] Ph.D student, School of Civil Engineering, Universiti Sains Malaysia, Penang, Malaysia
[2] Lecturer, Dept. of Civil Engineering, Politeknik Negeri Padang, Indonesia
[3]Director, Disaster Research Nexus, School of Civil Engineering, Universiti Sains Malaysia, Penang, Malaysia
[4]Professor, Dept. of Civil Engineering, Institute of Teknologi Bandung, Bandung, Indonesia.

Abstract. This paper investigates the response of R/C frame building with soft first story. The soft first story is characterized by the absence of infill wall on the ground floor. In order to enhance the seismic response of R/C frame building, the yielding damper is incorporated into building on the first story. The finite element method is employed to simulate the response of the frame building subjected to selected strong earthquakes using non-linear time history analysis. The effect of masonry infill on building responses are taken into account using equivalent three-strut model, and the presence of the opening in reduction both stiffness and strength of the masonry infill are also considered. In the finite element modeling, the simplified tri-linear model of stress–strain relationship are used for equivalent strut material, while hysteretic behavior of steel yielding damper is approximated by bilinear model. In addition, the inelastic behavior of beam and column elements with rigid end zone is also adopted. The responses quantities are obtained from nonlinear analysis to be used for assessment the seismic performance of the building under consideration. It also investigates the damage level of the building structure using damage index based on Park and Ang damage model. Finally, the seismic performance of the infilled frame building with and without steel yielding steel dampers in placed are discussed and compared.

Keywords: soft story, infill wall, strut model, steel damper, damage index

1. Introduction

The past experiences show that dramatically changes of the infill area cause the soft story mechanism. Many buildings with first soft story have shown poor performance during earthquakes, and some of them experienced damaged or collapsed during these events. However, these similar buildings are being adopted among architects, because these buildings offer open space, which is usually intended for lobby, parking or retail store. Fig. 1 shows several building with first soft story damaged during earthquakes.

(a) China earthquake 2008 (b) padang earthquake 2009 (c) northridge earthquake 1994

Fig. 1. Example buildings having first soft story collapse after earthquake

Several methods have been proposed in modeling masonry infill, and they are group into two categories: macro model and micro model [9]. In macro model, infill wall was assumed as equivalent strut either single strut method or multi strut method. The advantage of macro modeling is its simplicity in computation process and the use of mechanical properties obtained from the masonry test because the

masonry infill behaves highly nonlinear manner. However, many researchers believed that one single strut model is not sufficient to capture the complex behavior of infilled frame because the interaction of the infill with frame are not apparent if only the two loaded corner of the frame connected though a single strut. The micro modeling is based on finite element method in which the masonry panel and structure frame are divided into several elements. The application of this modeling is more difficult and also too time consuming due to complexity of the model, but it can predict the interaction of the infill with structure more precisely. Kaushik et al. [5] performed comparative study considering different analytical models for masonry infill using experimental results for nonlinear material properties of masonry infill. It was confirmed that 3-strut model can estimate force resultants in R/C members with sufficient accuracy. Furthermore, Ateris [2] have performed nonlinear dynamic time history analysis of four story R/C frame with infill wall opening using Seismostruct and RUAMOKO software. The infill walls are modeled as single strut and multi struts (3-strut). The accuracy of the numerical model is evaluated by comparing the analysis results with the experimental results. It was observed that 3-strut model provides a good fit to experimental results.

There are basically two methods for improving the seismic performance of existing buildings. The first is to reduce the seismic forces impose on the structure by insertion a flexible device between the ground and the structure via a base isolation system and the second is to increase the energy dissipating capacity of the structure by incorporating a passive energy dissipater system. In this paper, the increasing of the energy dissipation capacity of frame using yielding damper is adopted for strengthening the existing building with first soft story.

2. Modeling of Infill Masonry Wall

2.1. Determination of the equivalent strut width submitting

Asteris [1] investigated the complicated behavior of infilled frame under lateral loads using finite element method. It was noted that there are large magnitude of the variation of the contact length between the infill and the frame members, and the frame's contribution to the overall stiffness is affected by the change in its mode of distortion. Fig. 2 shows the general behavior of infilled frame under the lateral load. The width of equivalent diagonal strut is calculated based on FEMA 356 [4].

$$w_s = 0.175 d(\lambda_h h)^{-0.4} \tag{1}$$

where

$$\lambda_h = \left(\frac{E_w t \sin 2\theta}{4 E_c I_c h_w} \right)^{0.25} \tag{2}$$

where d is the diagonal length of the masonry panel, h is the column height, E_w is the modulus of elasticity of the masonry panel, t is the thickness of the masonry panel, $E_c I_c$ is the flexural rigidity of the column, h_w is the height of the masonry panel, θ is angle of the inclination of the diagonal strut with horizontal line. The increasing lateral loads will reduce the length of the contact between masonry infill wall with R/C frame. Park and Paulay [7] proposed the contact length of between infill wall and column or beam as

$$z = \frac{\pi}{2} \sqrt[4]{\frac{4 E_c I_c h_w}{E_w t \sin(2\theta)}} \tag{3}$$

2.2. Three strut model

In the 3-strut model, the masonry infill wall replaced by 3-equivalent pin-jointed diagonal strut having the same thickness as infill wall and having equivalent width as defined in Eq.(1). The joint of strut and beam and column members are shown in Fig. 3. Kaushik et al. [5] proposed simplified stress-strain curves for masonry wall consisting three piece-wise linear segments (Fig. 4). This curve is derived based on experimental results of 84 prism specimens made of masonry brick. In this study, this simplified stress-strain curve is used in the modeling masonry wall as diagonal strut. The effect of opening on the lateral stiffness has been proposed by Asteris [2] through parametric study using finite element method. The stiffness reduction factor is given by

$$\eta = 1 - 2\alpha_w^{0.54} + \alpha_w^{1.14} \tag{4}$$

where α_w is the ratio of the area of opening to the area of infill wall. Furthermore, when calculate the strength of infill wall with opening, the strength reduction factor assume equal to the stiffness reduction factor.

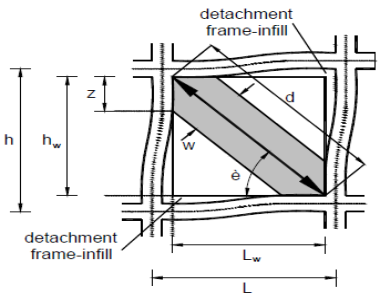

Fig.2 Masonry infill frame sub-assemblage 12)

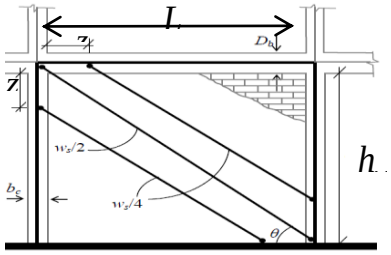

Fig. 3 Three-strut model for masonry infill wall (Kaushik et al. 2008)

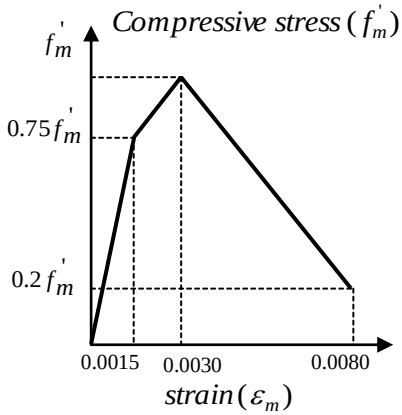

Fig 4. Tri-linear stress-strain model for masonry brick (Kaushik et al. 2007)

3. Modeling of Hysteretic Steel Damper

The primary factor affecting damper elements are elastic stiffness (K_e), yield displacement (d_y), and yiel force (P_y) as reported by Whittaker et al [10]. Therefore, a bilinier model is appropriate to represent of damper device inelastic behavior as depicted in figure 5. The hysteretic energy is dissipated of device in one cycle can be determined from Eq. (5).

$$W_d = 4P_y\,(1-\eta)(\Delta-\Delta_Y) \tag{5}$$

where W_D is area under hysteretic curve and $\eta = K_p / K_e$ is ratio elastic stiffness to Plastic stiffness of the device.

4. Energy Based Cumulative Damage Indices

In order to quantify performance of a structures during earthquake, the drift and damage index are commonly accepted as the performance criteria. The damage index model based on cumulative plastic deformation and maximum hysteretic energy demand has been developed by several researcher [8, 3]. In this paper, damage index model are proposed by Park and Ang [8] as follow:

$$DI = \frac{\delta_m}{\delta_u} + \frac{\beta}{Q_y \delta_u} \sum_{i=1}^{n} \int_0^t dE_i \tag{6}$$

where, δ_m is maximum displacement obtained from non-linear response history analysis for any given earthquake, δ_u is ultimate displacement obtained from non-linear static pushover analysis, Q_y is yield strength of the structure obtained from capacity curve, β is constant to account the effect of cyclic load and structural properties; ranges from 0.05-0.15, E_i is hysteretic energy demand at i^{th} plastic hinge, and n is number of plastic hinges. In this context, the interpretation between damage level and damage index as listed in Table 1.

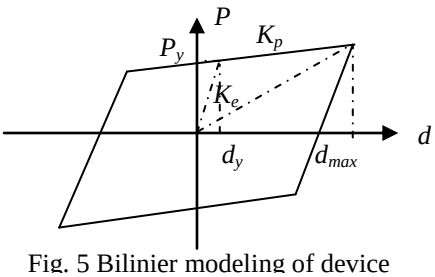

Fig. 5 Bilinier modeling of device

Table 1. Interpretation of damage index

Degree of damage	Damage index	State of structure
No damage	<0.1	Serviceable or localized minor cracking
Minor	0.1-0.25	Minor damage (light cracking throughout)
Moderate	0.25-0.40	Severe cracking, localized spalling
Severe	0.4-1.0	Severe damage (concrete crushing)
collapse	>1.0	Loss of building

5. Numerical Study

5.1. Building Description

The four story R/C building with bare frame at the ground floor and masonry infill walls in the other story are shown in Fig. 5. Fig. 6 presents the strengthening of the structure using yielding damper. The window opening is 1 m x 1.5 m. Design parameters for the structure are summarized as follows

- Concrete strength: $f_c^{'} = 25\ MPa,\ E_c = 23500 MPa$
- Reinforcement steel : $f_y = 400 MPa, E_{st} = 200000 MPa$
- Masonry wall: $f_m^{'} = 4\ MPa,\ E_m = 750 f_m^{'} = 3000 Mpa$
- Dead load: 40 kN/m (1-3 floor); 30 kNm (roof)
- Live load: 15 kN/m (1-3 floor); 12 kN/m (roof).
- Columns size are 400 x 400 mm with main reinforcement using 16D16 mm for 1st and 2nd stories, and 12D16 mm for 3rd and 4th stories. All columns are using stirrup of 3 leg D10 mm (120mm c/c).
- Beam size is 300 x 500 mm (1st -3rd stories), with top rebar: 5 D16 mm, bottom rebar: 3D16 mm.
- Beam dimension for top floor is 250 x 500 mm, with top rebar: 4 D16 mm, bottom rebar: 3 D16 mm. All beams using 2 legs stirrups with D10 mm (120mm c/c).
- Steel bracing is using WF 310 x 117.

5.2 Structural Analysis and Modeling

The finite element analysis of the frame were performed using PERFORM-3D software under 3 (three) acceleration records, i.e. El-Centro, San-Fernando and Tabas scaled to 0.5g. All beams, columns and braces were modeled as one dimensional element. The beam and column elements were modeled as an elastic segment with distributed plastic hinge and rigid end zone element. The rigid end zone was selected a half of column width for beam element and a half of beam width for column element. In the dynamic analysis, Rayleigh damping was constructed, so that the damping ratio is close to 5% over a range of periods from $0.2T_1$ *to* T_1, where T_1 is the first mode period. Furthermore, in order to limit inter-story drift to less than 1%, by adding steel damper with $SR = 12$, yield strength, 900 kN, K_e= 360 kN/mm, and 1% post yield stiffness ratio. The plastic hinge length is given as recommended by Park and Priestley [7]:

$$l_p = 0.08l + 0.022 d_b f_y \qquad (7)$$

where l is the distance between the maximum moment and point of inflection, and d_b is diameter of the longitudinal reinforcement. For discussion purposes, the structure without the interaction infill wall is denoted as MRF, the structure with infill wall using 3-strut equivalent model is denoted as BRF, and the structure with steel damper incorporated to the BRF on the first story is denoted as DRF. Fig. 8 depicted capacity curve from nonlinear static pushover analysis, while Table 1 summarized relevant characteristic of MRF, BRF, and DRF frames. When plotting the capacity curve for DRF by use nonlinear static pushover analysis, the displacement of damper (equal to displacement of first story) is limited to 20 yield displacement.

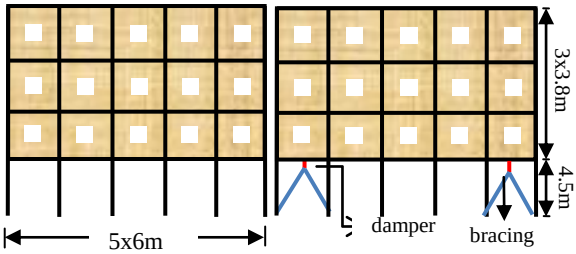

Fig.6 4-story concrete frame

Fig. 7 4-story concrete frame with chevron brace

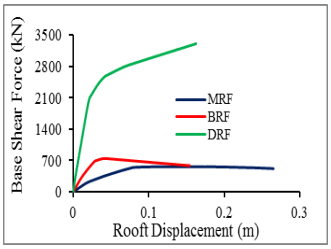

Fig. 8 Evaluation of V_y and Δ_y from capacity curve

Table 2.Characteristic of structures

Frame	Fundamental Period (sec.)	V_y (kN)	Δ_y (m)
MRF	1.23	199	0.018
BRF	0.86	286	0.010
DRF	0.4	2087	0.021

6. Results and Discussion

6.1 Inter-story Drift

The drift is widely used as a response parameter for estimation the seismic performance of a structure subjected to ground motion. Fig. 9 shows the comparison of inter-story drift of MRF, BRF and DRF under 3 selected scaled ground motions. It was found that the inter-story drift on the first story higher than others story. In addition, the effect of infill wall increases the inter-story drift on the first story except for Tabas earthquake. In contrast, the present of infill wall reduces inter-story drift on the others story significantly due to the effect of added stiffness. The improvement of the seismic performance using steel damper on the first story can be observed through the DRF frame. The inter-story drift on the first story is reduced significantly of below 1% as targeted because of the effect of added damping and stiffness. It was also noted that the maximum inter-story drift is occurred under input motion of El-Centro, followed by Tabas, and San Fernando. Furthermore, the earthquake characteristic influences the inter-story drift of the structures as shown in Fig. 10. It was observed that for MRF and BRF structures, the smallest interstory drift is occurred due to San Fernando earthquake followed by Tabas and El-Centro earthquakes. However, for DRF structure, the effect of Tabas earthquake and El-Centro earthquake are almost the same. It can be noticed that for the soft first story structure is characterized by a large drift concentrated on the first story, while the upper story behave as the rigid body. This behaviour can be demonstrated through BRF frame where the inter-story drift above the first story is relatively the same. Consequently, the flexural ductility demand on the column at the first story is larger than their capacity. This phenomenon can also be investigated through the capacity curve, in which MRF and BRF structures exhibit a poor performance due to the soft first story effect. These systems are failed on a small displacement of less than 4% drift that commonly is adopted as a criterion for ductile structure. It can be also demonstrated that both structures (MRF and BRF) show excessive loss stiffness, and lead to premature collapse.

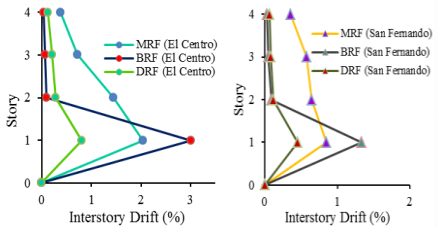

Fig. 9 Interstory drift versus story height

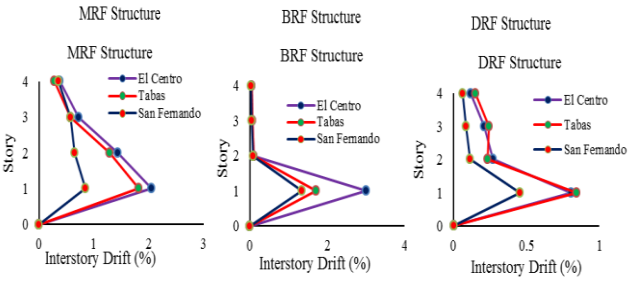

Fig 10. The effect of the earthquake characteristic on the interstory drift

6.2 Input Energy and Hysteretic Energy Demand

Figure 11 and figure 12 present the time history of input energy and hysteretic energy for MRF ,BRF and DRF frames respectively. It is clearly noticed that there are influence of ground motion characteristics and structural properties to the magnitude of total input energy and hysteretic energy . It can be seen that the BRF frame failed under El-Centro and Tabas earlier, since plastic hinge formed on the soft first story with rotation demand higher than rotation capacity. In addition, the input and hysteretic energy under San Fernando ground motion is smaller than El-Centro and Tabas ground motion. This is the reason why interstory drift caused by San Fernando earthquake is lower than the other two earthquakes.

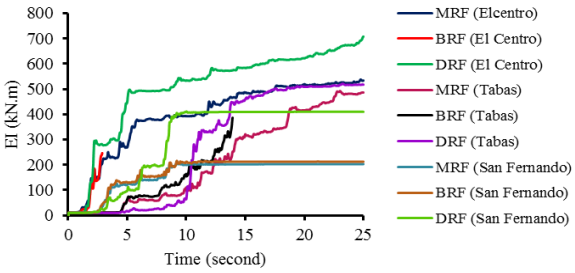

Fig. 11 Time history of input energy

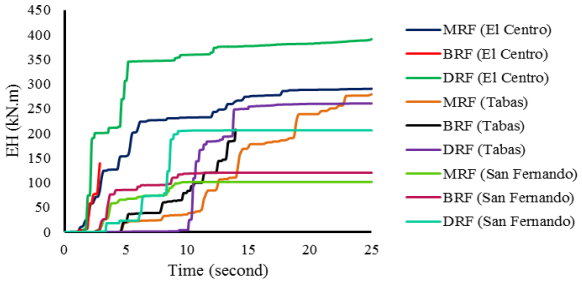

Fig. 12 Time history of hysteretic energy

6.3 Distribution of Inpur and Hysteretic Energy Demand

Many researcher believed that the damage to a structures depend on amount of hysteretic energy dissipated and on its cumulative effect. Figure 13 present the total hysteretic energy components, i.e., dissipated by beams element, columns element, walls and dampers element. For the MRF frame, energy dissipated by beams element larger than columns element. In contrast, most of input energy on the BRF frame absorbed by columns component rather than beams component. The absence of infill wall on the first story (discontinuous in the distribution of stiffness) exhibit the poor behavior on the lateral load carrying system of the structure. This is the reason why BRF frame indicate failure earlier than MRF frame during El-Centro and Tabas earthquake. In addition, for MRF frame in which the largest hysteretic energy demand caused by El-Centro ground motion followed by Tabas and San Fernando. Unlike MRF frame, for BRF frame the hysteretic energy demand under Tabas earthquake larger than El-Centro earthquake and the smallest hysteretic energy demand generated by San Fernando earthquake. Furthermore, DRF frame indicates good behaviour on the lateral load carrying system, although the input energy transmitted into this structure is much higher compare to other systems (MRF and BRF), particularly under El-Centro excitation. This behavior can be attributed to the concentrated a large portion of hysteretic energy demand on the damper devices, only a small portion of the input energy dissipated by main structural component such as: beams and columns. Therefore, building structure incorporated with hysteretic damper during strong earthquake excitation exhibit better performance, i.e. remain elastic or minor damage. Moreover, infill wall of the BRF frame does not play a role in the absorbing of the seismic input energy. On the contary, infill walls element on the first story of the DRF frame have contributed to the energy dissipation. However, energy dissipated by this element are not significant compare to energy dissipated by damper device. Damper device are able to absorb more than 40% of the total input energy. Table 3 shows the distribution of the hysteretic energy through the height of structure. All structural component in each story for MRF frame experienced inelastic deformation, and lead to damage to the structural members. It was also noted that the beams element more suffered than the columns element particularly beams on the lower story. Furthermore, the most important observation that for BRF frame where the damage is concentrated in the first story column as a soft story effect. This phenomena is characterized by significant hysteretic energy dissipated in the columns of the first story. It is clearly demonstrated that the benefits of using a damper on the first story can enhance the seismic performance of the structure as a whole, since most of the input energy is absorbed by damper system.

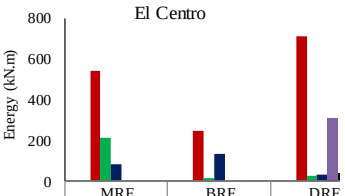

	MRF	BRF	DRF
EI	537.80	246.50	707.8
EH (Beam)	211.28	8.78	20.03
EH (Column)	79.16	130.42	29.85
EH (Damper)			305.1
EH (Wall)			36.13

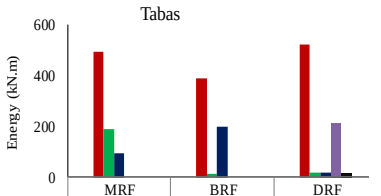

	MRF	BRF	DRF
EI	492.50	386.60	520.90
EH (Beam)	185.95	10.53	17.33
EH (Column)	93.20	197.21	14.93
EH (Damper)			211.07
EH (Wall)			17.83

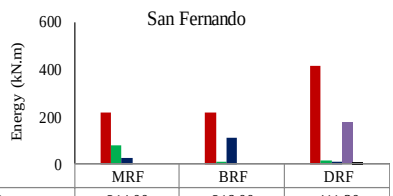

	MRF	BRF	DRF
EI	214.00	216.00	411.30
EH (Beam)	75.13	9.18	14.14
EH (Column)	26.24	110.71	9.53
EH (Damper)			171.76
EH (Wall)			9.83

Figure 14. Comparison of the hysteretic energy among the structural members

Table 3. Distribution of the hysteretic energy vs story height

Story	Component	El Centro			Tabas			San Fernando		
		Hysteretic Energy (kN.m)			Hysteretic Energy (kN.m)			Hysteretic Energy (kN.m)		
		MRF	BRF	DRF	MRF	BRF	DRF	MRF	BRF	DRF
1	Beam	139.17	8.63	15.08	130.42	10.41	11.06	43.61	9.10	9.10
	Column	78.08	130.42	29.85	84.20	197.20	14.93	25.92	110.71	9.53
	Damper	-	-	305.16	-	-	211.07	-	-	171.76
2	Beam	57.52	0.08	4.02	46.34	0.07	4.42	19.14	0.05	3.84
	Column	0.15	0.00	0.00	7.36	0.01	0.00	0.00	0.00	0.00
3	Beam	14.15	0.07	0.93	9.03	0.05	1.85	12.12	0.03	1.19
	Column	0.66	0.00	0.00	1.61	0.00	0.00	0.16	0.00	0.00
4	Beam	0.44	0.00	0.00	0.16	0.00	0.00	0.26	0.00	0.00
	Column	0.27	0.00	0.00	0.04	0.00	0.00	0.16	0.00	0.00
	Wall			36.125			17.827			9.83
	Total	290.44	139.20	391.16	279.15	207.73	261.15	101.37	119.89	205.26

6.4 Interpretation of Damage Level of Structures

Damage level of the building under study can be predicted through response parameters such as : inter-story drift, plastic hinge rotation , cumulative hysteretic energy demand , damage index, and many others parameters. In this study damage index proposed by Park and Ang with $\beta = 0.10$ to be used for predicting the damage level of the structures. Table 4 shows the comparison of the damage level of the structure using damage index and seismic performance based on inter-story drift under three selected earthquake scaled to 0.5g. It can be seen that MRF and BRF frames collapse due to El-Centro and Tabas earthquake. Although, both frames only experienced severe damage under San Fernando earthquake. It was also confirmed that DRF frame shows superior performance under strong seismic excitation, in which the worst condition of the structure indicates just moderate damage. Additional information was noticed that in this case there are correlation between degree of damage and inter-story drift. The higher inter-story drift, the higher the level of damage of the structures.

Table 3. Interpretation of damage level and seismic performance

Frames	El-Centro		Tabas		San Fernando		Inter-story drift (maximum)	
	DI	Degree of damage	*DI*	Degree of damage	*DI*	Degree of damage	*(%)*	Seismic performance
MRF	>1.0	collapse	>1.0	collapse	0.57	severe	2.1	Life safety
BRF	>1.0	collapse	>1.0	collapse	0.64	severe	3.0	Limited safety
DRF	0.40	moderate	0.40	moderate	0.20	minor	0.84	Immediate occupancy

7. Summary and Conclusion

This study emphasizes the importance of considering the interaction of infill walls and structures in seismic performance evaluation of structure, especially when infill wall absence on the first story. By using steel damper incorporated into structure on the first story not only can avoid the premature collapse but also to enhance the seismic performance of the structure with soft first story. Based on observation of the results obtained by nonlinear dynamic analysis, the following main conclusion can be drawn:

- Ground motion excitations scaled to the same PGA does not guarantee produce the similar response parameters of the building under consideration. Because the response of the building are not only influenced by building dynamic properties but also depend on ground motion characteristic, such as duration of motion, Frequency content and intensity parameter (PGA, PGV, others parameters)
- Lateral deformation of the building structure with open space on the first story concentrated at the first story, while others story behave as rigid motion under strong earthquake. This building tend to experienced heavy damage or collapse due to soft story mechanism.
- By using steel damper incorporated into building structure on the first story can enhance seismic performance of the building, and to prevent building collapse prematurely. The selection of stiffness ratio *SR* is primary factor for successful in strengthening of building structure having soft first story.

8. References

[1] Asteris, P.G. *Finite element micro modeling of infilled frames*, Electronic journal of structural engineering .2008, 8:1-11

[2] Asteris, P.G., Gionnopoulos, I.P., and Chrysoustomou, C.Z. *Modeling of infilled frames with openings*, The open construction and building technology journal. 2012 , suppl (1-M6), 81-91

[3] Bojórquez,E.,Reyes-Salaza,A.,Terán Gilmore,A.,andRuiz,S.E. *Energy-based damage index for steel structures*, Steel and Composite Structures.2010 4(4), 343-360

[4] Federal Emergency Management Agency (FEMA). *Prestandar and commentary for the seismic rehabilitation of buildings*. 2000, Rep. No. 356, Washington, D.C.

[5] Kaushik, H.B., Rai, D.C., and Jain, S.K. *Stress and strain characteristics of clay brick masonry under uniaxial compression*, Journal of Material in Civil Engineering. 2007, 19:9, 728-739

[6] Kaushik, H.B., Rai, D.C., and Jain, S.K. *A rational approach to analytical modeling of masonry infills in reinforced concrete frame building*, 14th World Conference on Earthquake Engineering Beijing, China. 2008

[7] Paulay, T., and Priestly , M.J.N. *Seismic design of reinforced concrete and masonry building*.Wiley, 1992

[8] Park, Y.J., and Ang, A.H. *Mechanistic seismic damage model for reinforced concrete*, J. Struct. Eng. ASCE.1985, 111(4), 740-757.

[9] Samolia, D.M. *Analytical modeling of masonry infill*, Acta Technica Napocensis: Civil Engineering & Architecture. 2012, Vol.55(2), 127-136.

[10] Whittaker, AS., Bertero, VV., Thompson, CL., Alonso, LJ. *Seismic testing of steel plate energy dissipation devices*, Earthquake Spectra.1991,7(4), 563–604

[11] Xia, C., Hanson, RD. *Infuence of ADAS element parameters on building seismic response*, Journal of Structural Engineering (ASCE). 1992, Vol.118(7),pp.1903 –1918

ISBN 979-458-758-3
Proceedings of the 3rd International Conference on the Geohazard Information
Zonation and 5th Seminar & Short Course of HASTAG (GIZ2014-HASTAG5)
Organized by UMSU, HASTAG, USM
Medan, Indonesia, October 20-22, 2014

The Effect of Mix Design on Mechanical and Thermal Properties Oil Palm Shell (OPS) Lightweight Concrete

Fahrizal Zulkarnain[1†], Mohd. Zailan Sulieman[2], Eravan Serri[3]

[1]*Department of Civil Engineering, Faculty of Engineering,*
Universitas Muhammadiyah Sumatera Utara (UMSU), Jl. Mukhtar Basri No. 3, Medan, Indonesia
[2,3]*School of Housing, Building and Planning, Universiti Sains Malaysia, Malaysia*

Abstract. This paper discusses the use of oil palm shell (OPS) as lightweight aggregate in lightweight concrete especially in the structure application has been proven by previous researches. As industrial waste material, OPS can be the alternative material to be used in the construction industry. With its advantage as heat resistant material, this study will discuss the potential of OPS as lightweight aggregate with regard to the optimum content of OPS. A total of 15 mix design with 3 different cement/sand ratio (1.7, 1.8, 1.9) and 5 cement content in mix design (300, 350, 400, 450, 500 kg/m³) has been tested. The result showed mechanical and thermal properties for all mix.

Keywords: oil palm shell (OPS) lightweight aggregate, absolute volume, thermal conductivity, specific heat, thermal diffusivity.

1. Introduction

The use of concrete as building material is always in high demand. Good durability and workability of concrete makes it convenient for construction industry players. However, the high density of the concrete will result in increased dead load on building structures because a lot of use of steel reinforced. The use of lightweight aggregate as lightweight concrete is an option to reduce the dead load on a building, especially for high-rise buildings. Normally pumice and perlite are used as lightweight aggregate to produce lightweight concrete and both materials can be found at volcanic area R. (Demirboga & R. Gul, 2003[1]). However, it has not brought much advantage to countries which do not have volcanic environment. The alternative is to use industrial waste material as aggregates for construction.

One of the solid waste products that have increasingly gained researchers' interest is oil palm shell from the processing of oil palm. Oil palm industry is a fast-growing industry and economically it is able to become the backbone of the economy. This industry also produces not only waste from palm oil processing but, all of its parts in palm tree such as fruits, trunks and leaves that can be effectively utilized for producing valuable products. For instance approximately 19 million tonnes of crop residues (empty fruit bunch, fiber and shell) were produced per year (Mustaffa et al, 2011 [2]). It was estimated that over 4.56 million tonnes of oil palm shell are produced annually (Teo et al., 2006 [3] and Sahu et al 2011 [4]) reported that the amount of oil palm shell increases every year because there are more than 270 palm oil mills operating in this country to generate the waste. The growing need for sustainable development has motivated researchers to focus their research on the use of waste or recycled materials in potential construction material.

Oil palm shell is traditionally used as solid fuels for steam boiler to run turbines for electricity (Shafigh et al., 2012 [5]), used to cover the surface of the roads in the plantation area (N. Abdullah et al., 2011 [6]) densified into briquettes (Z. Husain et al., 2002 [7]), used as granular filter material for water treatment (Jusoh et al., 2005 [8]), converted to bio-oil by using pyrolysis process for biomass energy (J. N. Sahu et al.,

† Corresponding author, Tel: +6281361271975; fax: +62616638296
E-mail address: zulkarnain_fahrizal@yahoo.com

2011 [4]), and used in the production of charcoal and activated carbon (Astimar and Ropandi, 2011 [9]). There are a number of studies related to OPS lightweight aggregate concrete especially for lightweight structure. However, there was inadequate information regarding the effect of OPS lightweight aggregate on the thermal properties, porosity, unit weight etc. of these concrete in the technical literature. Previous study only mentions that the OPS lightweight concrete has low thermal conductivity compared to normal concrete. Therefore, an experimental investigation related to effect of OPS on thermal conductivity has been carried out and the results are reported in this article.

2. Experimental Programme

In this study, the materials used are ordinary Portland cement (OPC) with specific gravity of 3.10 type I, river sand with specific gravity, fineness modulus, water absorption and maximum grain size of 2.67, 2.28, 0.98% and 2.36 mm, respectively. OPS are used as course aggregate and the treatment method is as mentioned by previous researcher (Shafigh et al., 2012 [5], U. Johnson Alengaram et al., 2010 [10], M. A. Mannan et al., 2006 [11]). The shells have been left outside the laboratory for 6 months to expose them with natural environment because there might be fibre and oil coating on the surface of fresh OPS. After the exposure, most of the fibres are removed from surface thus reducing the oil coating and other impurities present on the shells. Finally, OPS aggregate were rinsed with potable water to remove the detergent and then dried before being stored in containers. The OPS used has specific gravity, water absorption (24 hour), maximum grain, aggregate impact value and aggregate crushed value of 1.19, 22.1%, 14mm, 3.3% and 2.62% respectively. The OPS need be absorbed in water for 1 hour and left to saturated dry condition before it can be used.

In the experiment, there are 15 mixtures with different 5 cement content (300, 350, 400, 450 and 500 kg/m³) and 3 different sand ratio mix (1.7, 1.8 and 1.9). For lightweight concrete, the amount of cement content specified is in the range of 285–510 kg/m³ (Mindess and Young, 1981 [12]). The mixture proportion is shown in Table 1.0. Effective water/cement ratio is 0.4 and it is constant in all mixture. The mix proportioning was based on the absolute volume. The unit weight of the concrete increased as a result of the increase of cement content used. The OPS was kept in water for 1 hour so that the OPS can absorb water and the effective water/cement ratio is not affected.

To enhance the workability of the mixture, 1.5% of cement weight was used in all mixture. All mixture was prepared in a laboratory mixer with vertical rotation axis by forced mixing. Precautions were taken to ensure it is homogeneous and fully compacted. All specimens were kept in their moulds for 24 hours. After demoulding, they were stored in a water tank until the age of 28 days. At this age, the specimens were taken out of the curing tank and kept in laboratory condition (50% RH at 20°C) until testing day.

3. Test Results And Discussions

The results obtained on mix design are shown in Table 1.0. They are also displayed to some extent in graphical form (figures) and further discussed.

3.1. Workability

As seen in Table 1.0, the mix design result of workability showed the workability of fresh concrete. Bond between aggregate and mortar phase are significantly affected by physical properties and the volume of OPS. This study used the lowest sand ratio (1.7) because it is the minimum amount based on absolute volume design for cement content as low as 300 kg/m³. Mix T1, T2 and T3 with 1.7, 1.8 and 1.9 sand ratios with cement content of 300 kg/m³ show collapse and low workability. A lot of honeycomb is present on cube surface produced from this mix proportion. The bond between aggregate and mortar is very weak because the volume of OPS is high. Therefore mix proportion with cement content of 300 kg/m³ is not acceptable. The workability increased with increased cement content and high sand ratio.

Table 1.0: Mix Design.

Mix Order	T1	T2	T3	T4	T5	T6	T7	T8	T9	T10	T11	T12	T13	T14	T15
Sand Ratio	1.7	1.8	1.9	1.7	1.8	1.9	1.7	1.8	1.9	1.7	1.8	1.9	1.7	1.8	1.9
Cement (kg/m^3)	300	300	300	350	350	350	400	400	400	450	450	450	500	500	500
Sand (kg/m^3)	516	539	570	595	630	666	679	721	760	764	811	854	850	899	951
OPS (kg/m^3)	699	692	678	623	609	592	544	525	508	463	441	423	375	360	335
Water (kg/m^3)	124	124	124	140	140	140	160	160	160	180	180	180	200	200	200
SP (kg/m^3)	4.5	4.5	4.5	5.25	5.25	5.25	6	6	6	6.75	6.75	6.75	7.5	7.5	7.5
Worka-bility(mm)	-	5	10	10	15	15	15	20	20	25	25	30	35	40	50
OPS % (kg/m^3)	42.59	41.92	40.65	36.48	35.22	33.87	30.49	29.05	27.79	24.76	23.44	22.17	19.69	18.37	16.88

3.2. Unit Weight Density

The 28-days unit weight density of OPS concrete shows that all mix have density of below 2000 kg/m^3. The changes in unit weight are shown in Figure 1.0. In average, density of oven dry OPS concrete produced in this study is approximately 8.7%-16% lighter than air dry OPS concrete. The highest gap of density (air dry to oven dry) is seen in T1 mix. The result showed that higher OPS volume will reduce density. Mix T1, T2 and T3 which contained 40% of OPS display a reduction gap of 16% of weight (air dry to oven dry density). Compared to mix T13, T14 and T15, the reduction gap of the density are only 11%, 9.2%, 8.7% respectably with 16% to 20% volume of OPS. The substantial reduction of the unit weight due to air drying is an indication of the presence of large and higher amounts of open pores on the surface.

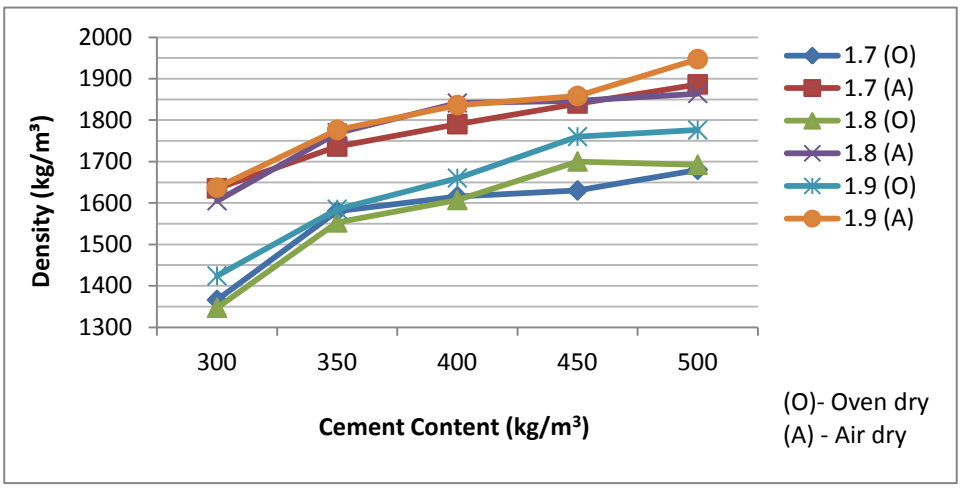

Figure 1.0: Unit Weight Density.

In this table the density, specific heat, thermal diffusivity and thermal conductivity of different samples are categorized according to volume of cement and sand ratio. It is noted that the density of the concrete vary for different samples within each proportion (for the same materials and same mixing ratio). Therefore, the values shown in the table are based on average densities ± a tolerance limit (less than 4%) in order to cover the range of densities as measured for different samples of the same category.

3.3. Compressive Strength

Figure 2.0 shows the effect of cement content and sand ratio on the compressive strength of OPS lightweight concrete. As seen in the figure, compressive strength increased substantially with the increase of concrete

cement content. The lowest strength is produced by T1 mix which is 11.56 N/mm and is still in the range of load bearing strength meanwhile the highest strength is produced by T15 which is 28 N/mm² which is in the range of lightweight aggregate structural concrete strength. When the relationship is shown in figure, it may be concluded that higher OPS aggregate and low cement content will produce low strength. In other words, compressive strength values changed significantly depending on cement content amount.

It can be seen that compressive strength values increase directly proportional to the increase in density values and inversely proportional to the increase in porosity values. In other words, ECACs with high density and low porosity have high compressive strength values. Properties of these constituents affect the properties of concrete. Thus, OPS aggregate will cause high porosity in cement paste and reduced the strength. The air entrainment also contributed to low strength of the concrete.

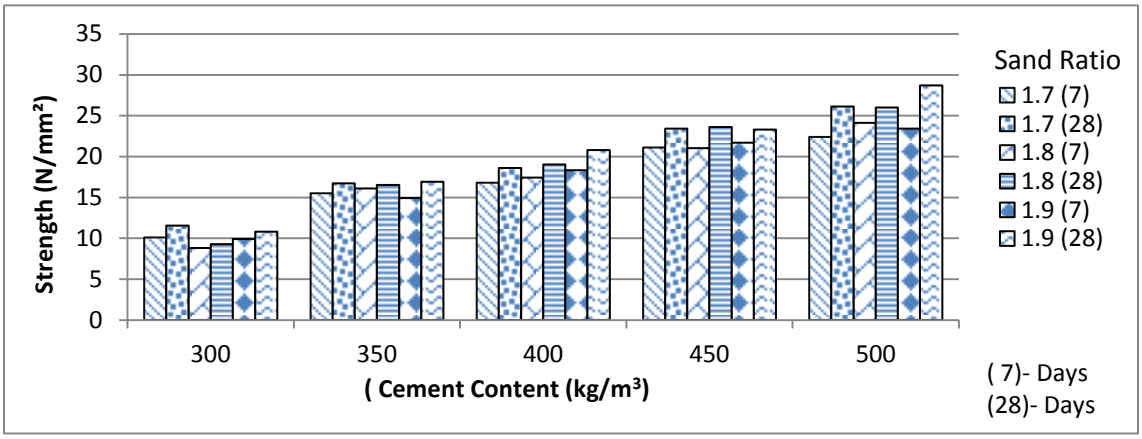

Figure 2.0: Compressive Strength Test Result

a. Thermal Diffusivity

The result of the experiment on thermal diffusivity rate showed that thermal diffusivity increased with increase of cement content of the mix, except for cement content 350 kg/m with sand ratio 1.7 and 1.8., that heat transfer analysis influence by thermal conductivity and volumetric heat capacity therefore, high thermal conductivity will increase the thermal diffusivity. Again in case of OPS volume in mix proportion, the diffusivity of the concrete is less when higher OPS volume is used (300 kg/m³ cement content) compared to when less OPS volume (500 kg/m³ cement content) is used Figure 3.0. Since it is a function of conductivity, specific heat and density, it will vary according to different influences and both conductivity and specific heat increase with moisture content then one might expect a reduced influence on diffusivity (Marshall, 1972 [13]). Hence, thermal diffusivity of concrete is largely influenced by the mineralogical characteristics of the course aggregate (Stephen Tatro, 2006 [14]). The capacity of the aggregate to retain moisture and its chemically stable vesicular and glassy (amorphous) competition are also advantageous. Among other, Stephen points out that the compatibility in relative stiffness between the cement paste and lightweight aggregate is also beneficial for low thermal diffusivities (Stephen S. S., 2006 [15]).

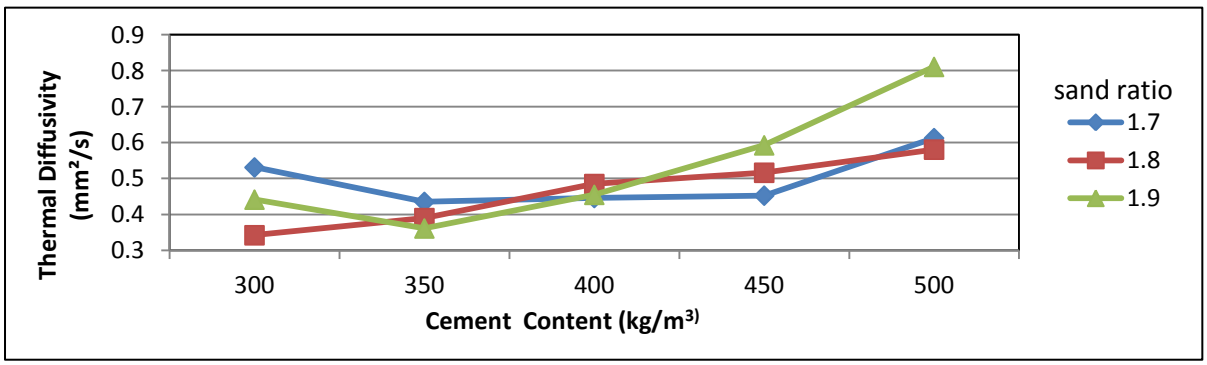

Figure 3.0: Thermal diffusivity test result.

Conclusions

Based on results from objective analysis and research has been conducted on oil palm shell (OPS) lightweight concrete. The main conclusions result of research carried out is as follows:

1. The workability of mix design is categorized as being low especially for mix design using high proportion OPS that have poor workability.
2. Cement/sand ratio 1.8 are the optimum ratio for load bearing strength with low thermal conductivity value.
3. The range of compressive strength for load bearing starts at 350 kg/m³ onwards.
4. Pulse velocity value is of moderate quality except for mix design using 500 kg/m³ cement content that produced good quality concrete.
5. Thermal conductivity that can be categorized as insulation structure is mix design using cement content of 400 kg/m³ and below. According to RILEM the value of thermal conductivity is much less than 0.75 W/mK for load bearing insulation purpose.
6. Specific heat for all mix design showed inconsistencies due to the size, shape and distribution OPS aggregate on concrete. The increase of energy required is due to moisture content of the aggregate.
7. Thermal diffusivity increase when higher cement content is used in mix design.

Acknowledgements

We extend our gratitude to the Research Creativity and Management Office, Universiti Sains Malaysia, for funding this research and to the School of Housing, Building and Planning, Universiti Sains Malaysia for facilitating the field equipments. Specials thanks are also who rendered their timely help to the successful completion of this project research.

References

[1] R. Demirboga & R. Gul. The effects of expanded perlite aggregate, silica fume and fly ash on the thermal conductivity of lightweight concrete. *Cement and Concrete Research*. 2003, (33): 723–727.
[2] W.E.S.B Mustaffa., S. Mehilef., R. Saidur., A. Safari. Biomass energy in Malaysia: current state and prospects. *Renewable & Sustainable Energy Review*. 2011, (15): 3360-3370.
[3] D. C. L., Teo, M. A. M., V. J. Kurian. Structural concrete using oil palm shell (OPS) as lightweight aggregate. *Turkish J. Eng. Env. Sci*. 2006 (30): 251-257.
[4] J. N. Sahu, Faizal Abnisa., W.M.A Daud., W.M.W Husin. Utilization possibilities of palm shell as a source of biomass energy in Malaysia bu producing bio-oil in pyrolysis process. *Biomass and Bioenergy*. 2011 (35): 1863-1872.
[5] Payam Shafigh., M. Z. J., Hilmi Mahmud., Norjidah Anjang Abd Hamid. Lightweight concrete made from crushed oil palm shell: Tensile strength and effect of initial curing on compressive strength. *Construction and Building Materials.* 2012 (*27*): 252–258.
[6] N. Abullah, F.Sulaiman, H.Gerhouser, A.Shariff. An outlook of Malaysian energy, oil palm industry and its utilization of waste as useful resources. *Biomass and Bio energy*. 2011 (35): 3775-3786.
[7] Z. Husain., Z. Zainac., Z. Abdullah. Briquetting of palm fibre and shell from the processing of palm nuts to palm oil. *Biomass and Bioenergy*. 2002 (22): 505-509.
[8] Jusoh A, Noor MJMM, Ghazali AH. Potential of burnt palm shell (BOPS) granules in deep bed filtration. *J Islam Acad Sci*. 2005 (3):143–8.
[9] Astimar A. A. & Ropandi M. Charcoal from palm kernel shells (Hollow plinth carbonisation furnace system), *MPOB information series-June.* 2011. 494.
[10] U. Johnson Alengaram., H. M., Mohd Zamin Jumaat. Development of lightweight concrete using industrial waste material, palm kernel shell as lightweight aggregate and its properties. *Paper presented at the 2010 2nd International Conference on Chemical, Biological and Environmental Engineering*.
[11] M.A. Mannan., J. A., C. Ganapathy., D.C.L. Teo. Quality improvement of oil palm shell (OPS) as coarse aggregate in lightweight concrete. *Building and Environment*. 2006 (41): 1239–1242.
[12] S. Mindess and J.F. Young. *Concrete*. Prentice-Hall, Englewood Cliffs, NJ. 1981.
[13] L. Marhall. The Thermal Properties Of Concrete. *Build Sci.* 1972 (7): 167-174.
[14] Stephen B Tatro. *Thermal Properties. Significance of Tests and Properties of Concrete and Concrete-Making Materials*. ASTM International. West Conshohocken. USA. 2006.
[15] Stephen S.S. *Resistance to fire and high temperature. Significance of Tests and Properties of Concrete and Concrete-Making Materials*. ASTM International. West Conshohocken. USA. 2006.

ISBN 979-458-758-3
Proceedings of the 3rd International Conference on the Geohazard Information
Zonation and 5th Seminar & Short Course of HASTAG (GIZ2014-HASTAG5)
Organized by UMSU, HASTAG, USM
Medan, Indonesia, October 20-22, 2014

ACCELERATION TIME ANALYSIS OF PROJECT WORK ON OPTIMUM STRUCTURE WITH ADDITIONAL COST

Syahrizal[1]
[1] Lecturer of civil engineering department., Universitas Sumatera Utara

ABSTRACT

The construction project is a series of activities carried out only once and generally short-term. Project management is how to ensure that their resources are involved in a construction project can be applied to the construction manager as appropriate. The main purpose of the study was to determine the amount of time that can be accelerated and how much will it cost. The steps that need to be done such as preparing a network with methods of Critical Path Method (CPM), to identify the critical path and non-critical path analysis and calculation of the acceleration of time and project costs. The result of the calculation has shown the implementation of the normal work time for the first floor is 32 day and the normal cost is IDR 707,126,876.90. With the addition of 1 hour of working time, the finishing time is 29.15 days with an increase in cost of IDR 5,191,565.32, and cost slope value is IDR 1,822,816.27 per day. With the addition of 2 hours of working hour, the finishing time is 27.35 days with an increase in cost of IDR 15,101,820.81, and cost slope value is IDR 3,246,891.47 per day. With the addition of 3 hours of working time, the finishing time is 26.23 days with an increase in cost of IDR 25,539,458.68, and cost slope value is IDR 4,426,839.50 per day. With the addition of 4 hours of working time, the finishing time is 25.62 days with an increase in cost of IDR 37,086,554.36 and cost slope value is IDR 3,246,891.47 per day. The addition of working time should be used in critical work (the work that has to be done as soon as possible). If the addition of time is used in all works including non-critical work, it will only increase the cost while the accelerated time is constant.

Keywords : acceleration of the project, critical path method, the optimum cost.

1. Introduction

A good teamwork between owner, consultant and contractor is required in a construction project. In this case, the owner of a project will ensure that the project would follow the scheduled timing. Therefore, a contractor must be able to manage construction project systematically in order to complete the project within the given time and the given budget effectively.

In fact, there will always be discrepancy between the real project timing and the scheduled timing. There are several things that can delay the project implementation; such as, unfavorable weather - rain that forces the workers to stop their work, errors or changes of plan because of delayed material, the lack of supervision that results to errors, or the presence of government regulations especially about traffic that slow down the work, and the influence of the surrounding environment.

The delay of project timing is the responsibility of a contractor as the project manager. If the project timing is dragged for a longer period of time, then the owner of the project will penalize the contractor. For instance, The School Building project, Yayasan Pelita Bangsa, which is located on Jl. Iskandar Muda Medan, Sumatera Utara. It was planned to begin on April 18, 2011 and to be completed by December 12, 2011. In the ninth weeks, dated June 13, 2011, It began to show a delay in the project timing. The project that was supposed to be finished by 15.54%, was only 12.98% complete. It also showed a delay on the following weeks. One of the ways to solve this issue is to add the working time of the workers. The Addition of

working hours can be done by adding in 1 hour, 2 hours, 3 hours and 4 hours. With this analysis, accelerated time can be known and the cost for the acceleration of the project can be calculated.

2. Literature

CPM method (Critical Path Method)

CPM is a method that uses AON (Activity on Node) diagram to determine the critical path of a project. CPM is using estimated duration of a particular activity (deterministic), There are some elements that are used in CPM. They are EET (Earliest Even Time), LET (Last Even Time), total float, free float, and interfering float. EET is the earliest starting point of a project while LET is the latest finishing point of a project.

In CPM method, critical method is used to determine the activity that cannot be delayed, as the delay in the critical activity will cause the delay in the entire project.

Worker Productivity

Productivity is defined as the ratio of output and input, or the ratio of total production and total resource. In a project, productivity ratio is the value that is measured during the construction. It can be categorized as direct labor, direct material, cost, method and tools. The success rate of a project is determined by the effectiveness of resource management. Labor is one of the resources that is not easy to be managed. The cost of each labor varies, depends on each worker's skills; as, different worker has different skills.

Accelerate the Project Time (Crashing Project)

On way to crash a project is to adding the working time of workers. Adding working time is the most often method that is used in project management. It can empower the existing resources in the working environment and would not burst the budget by too much. The normal working hour is 7 hours (starting from 8am to 4pm, with 1 hour break). Overtime is calculated once worker exceed the normal working hour. The addition of working hours can be perform by the addition of 1 hour, 2 hours, 3 hours and 4 hours in accordance to the desired additions.

The decreasing of the labor productivity towards the increasing of working hours can be seen in the picture that shown below:

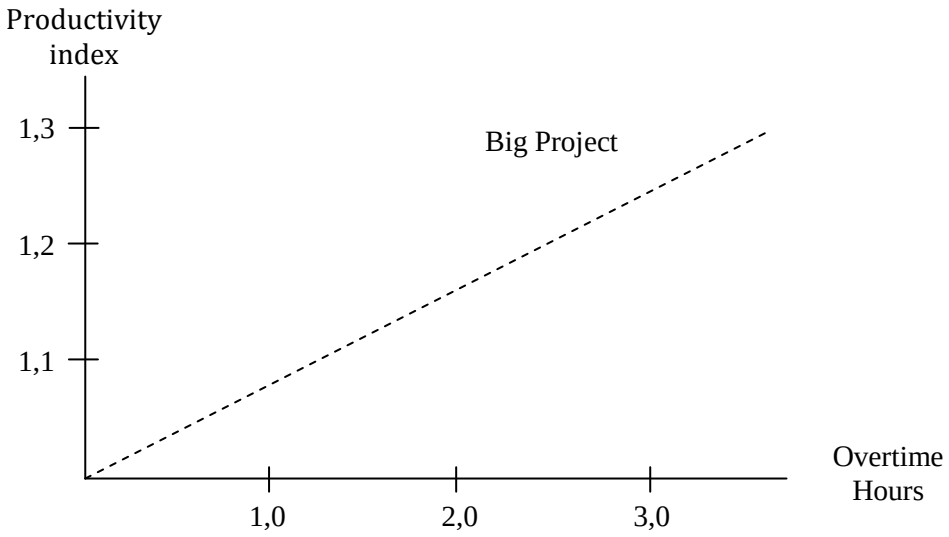

Picture 2. Indicate decreased productivity due to the addition of working hours (sourc: Soeharto,1997)

From the description above can be written as follows :

a. Daily productivity

$$= \frac{\text{volume}}{\text{normal duration}}$$

b. Hourly Productivity

$$= \frac{\text{daily productivity}}{\text{7 hours}}$$

c. Daily productivity after crash

= normal daily productivity + overtime productivity

Atau

= (7 hours x Hourly Productivity)+ (a x b x Hourly Productivity)

Where :

a = work time addition

b = declining coefficient of work time addition productivity

d. Crash duration

$$= \frac{\text{volume}}{\text{daily productivity after crash}}$$

Table 1.coefficient of declining productivity

Overtime hours	Declining productivity index	Work performance (%)
1	0,1	90
2	0,2	80
3	0,3	70
4	0,4	60

Extra wages for worker (crash cost)

With the addition of working time, the cost of labor will increase from the normal cost of labor. Based on Decision Minister of Manpower and Transmigration of the Republic of Indonesia No. KEP. 102 / MEN / VI / 2004, Overtime pay varies, first additional hour will get 1.5 times the normal pay per hour, and the following hour will get 2 times of the normal pay per hour.

It can be formulated as below:

1. Normal Daily wages
   = daily productivity x unit price wages
2. Normal Hourly wages
   = hourly productivity x unit price wages
3. Overtime wages
   = 1.5 x normal hourly wages for the first hour + 2 x n x normal hourly wages for the next hour

   Where : n = the number of extra working hour
4. Crash cost daily workers
   = (7 hours x normal workers cost) + (n x overtime payment hourly)
5. Cost slope (the extra cost to expedite an activity per unit time)

$$= \frac{\text{crash cost} - \text{Normal cost}}{\text{Normal duration} - \text{Crash duration}}$$

Relationship between cost and time

The total cost of a project is equal to direct cost plus indirect cost. Total cost moves in the same direction as the project timing. The longer the project, the higher will the cost be. The relationship between cost and time is shown on picture 2.7. Point A shows a normal point; Point B is shorten point. The line that joins point A and B is called time-cost curve.

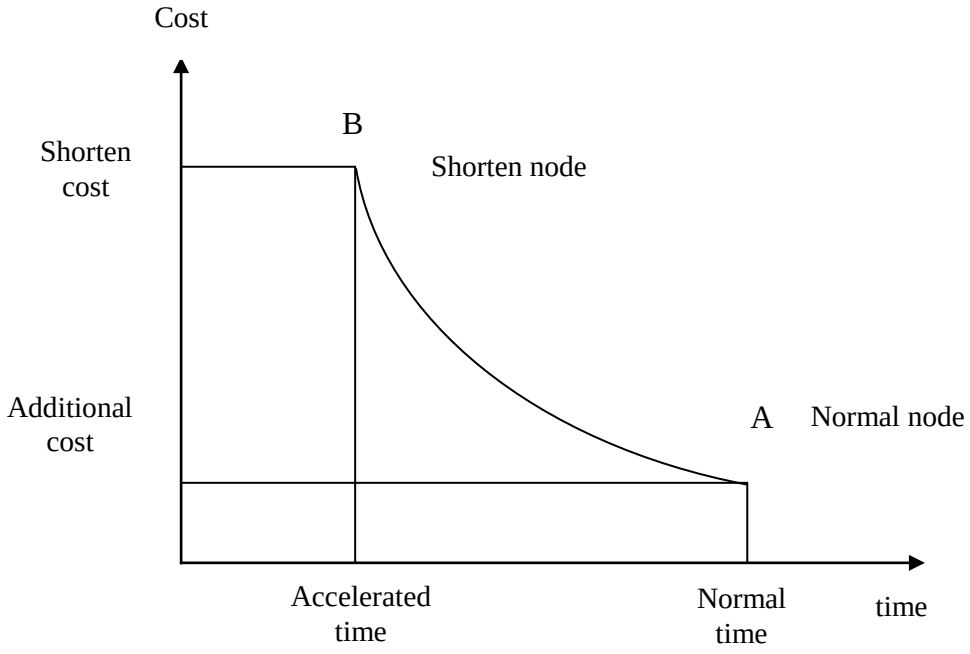

Picture 3. Relationship between time-normal cost and be shorten for one activites (sourc: Soeharto,1997)

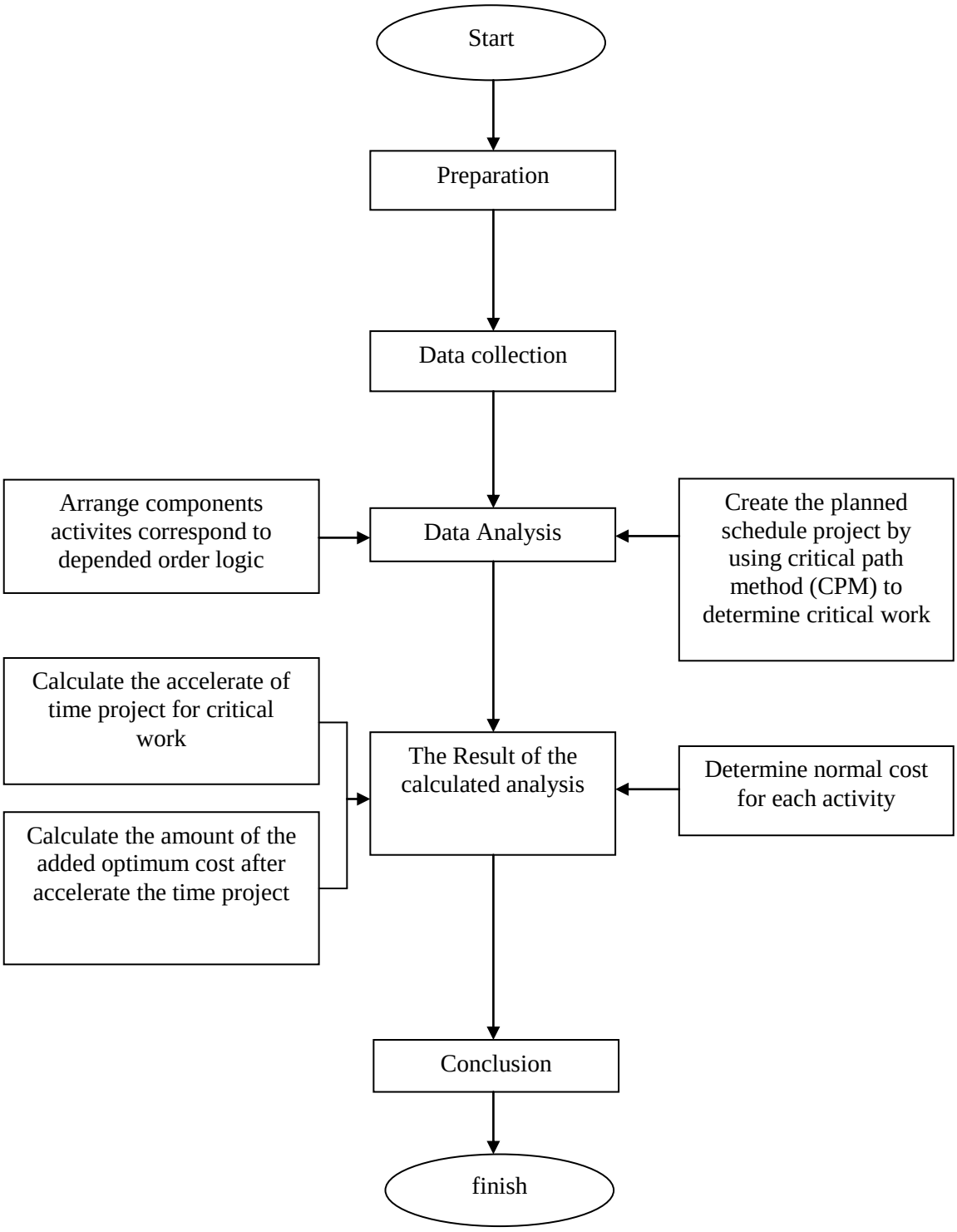

Picture 4. The writing flow chart

Network arrangement

The initial step is to collect data that is required in the project as a research venue, in this case is the S curve and budget. Based on the data we obtained from the S curve. The activity components arrangement is done based on logic dependent order. Next is to reschedule the project by using CPM to determine the activities in the critical path and non-critical path. Then, the project network is made by using the desired method.

The calculation of acceleration time and cost of the project

After the critical work has been obtained, we can gain the normal cost project based on the budget data that has been planned by a contractor. The data can also be used to calculate acceleration of the project by adding work time of 1 hour, 2 hours, 3 hours and 4 hours. After we obtained the acceleration cost of the project, we can then calculate the cost of acceleration and worker time based on the Decision Minister of Manpower and Transmigration of the Republic of Indonesia No. KEP. 102 / MEN / VI / 2004 that the wage increase varied, for the addition of the first hour of work time, workers get extra payment hourly 1.5 times of the normal time, and for the addition of the next hour, the workers get extra payment hourly 2 times of the normal time.

4. The results of the discussion

We can calculate it manually by using Microsoft Excel, which can expedite the calculation. To calculate the used time to finish the project and budget, Critical Path Method (CPM) is used. CPM is a method that use AON (Activity on Node) diagram to determine critical path. AON diagram is an arrow diagram that connects activities in a project together. Critical path connect the beginning and ending activities of a project. As a result, critical path is important to a project flow as a delay in an activity in the critical

path means a delay in the entire project.

Before doing manual calculation, data has to be collected from the companies that were a contractor from study case project, such as; S curve and budget of the project. Below is the brief and systematic step:

1. Collecting required data
2. Create a subjection logic table for each work correspond to existing data
3. Create network diagram by using critical path method
4. Determine the critical path from existing network
5. Calculate the accelerated time project for work at the critical path by adding 4 hours, 3 hours, 2 hours and 1 hour from normal work.

Table 2. dependent work

no	work	Symbol	dependence	Duration (day)
1	Main beam and joist	E1	D5, D6	8
2	Floor t=13cm	E2	B5, E1	7
3	column	E3	D2, D8, E2	6
4	Air condition holder	E4	E3	4
5	Entrance column	E5	E4	4
6	stair	E6	F3	3

Table 3. the result of the added calculation time from 1 hour,2 hours, 3hours and 4 hours for the first floor work

No.	description	The finishing time project (day)	The total of the accelerated time (day)	The budget of the project (IDR)	Added cost (IDR)	Cost slope (IDR)
1	Normal time	32	0	707.126.876,90	0	0
2	Added 1 hour	29,15	2,85	712.318.442,22	5.191.565,32	1.822.816,27
3	Added 2 hours	27,35	4,65	722.228.697,71	15.101.820,81	3.246.891,47
4	Added 3 hours	26,23	5,77	732.666.335,58	25.539.458,68	4.426.839,50
5	Added 4 hours	25,62	6,38	744.213.431,26	37.086.554,36	5.810.226,85

Picture 5. Relationship between time, normal cost and the budget after accelerated for the first floor work

From the graph, we can see that if the finishing time is faster than the normal time, then the cost will be higher than the normal cost. For instance, if the finishing time of the project at level 1 is 32 days and the normal cost is IDR 707,126,876.90. With the addition of 1 hour working time, the finishing time is revised to 29.15days, however the cost become IDR 713,318,422.22. There is an increase of 2.091% from normal cost. With the addition of 3 hours working time, the finishing time is 26.23 days and the normal cost is IDR 722,228,697.71. There is an increase of 3.485% from normal cost. With addition of 4 hours of working time,

the finishing time is 25.62% and the cost is IDR 744,213,431.26. There is an increase of 4.983% from normal cost.

5. Conclusion

Based on the analysis of work acceleration at school building Yayasan Pelita Bangsa on jln. Iskandar Muda Medan, Sumatera Utara, we can conclude that:

The result of the calculation has shown the implementation of the normal work time for the first floor is 32 day and the normal cost is IDR 707,126,876.90. With the addition of 1 hour of working time, the finishing time is 29.15 days with an increase in cost of IDR 5,191,565.32, and cost slope value is IDR 1,822,816.27 per day. With the addition of 2 hours of working hour, the finishing time is 27.35 days with an increase in cost of IDR 15,101,820.81, and cost slope value is IDR 3,246,891.47 per day. With the addition of 3 hours of working time, the finishing time is 26.23 days with an increase in cost of IDR 25,539,458.68, and cost slope value is IDR 4,426,839.50 per day. With the addition of 4 hours of working time, the finishing time is 25.62 days with an increase in cost of IDR 37,086,554.36 and cost slope value is IDR 3,246,891.47 per day.

6. Suggestion

The addition of working time should be used in critical work (the work that has to be done as soon as possible). If the addition of time is used in all works including non-critical work, it will only increase the cost while the accelerated time is constant.

REFERENCES

Andi.(2005).”*Faktor-Faktor Penyebab Rework Pada Pekerjaan Konstruksi”* Civil Engineering Journal, Petra Christian University, Indonesia

Elvianto, Wulfra,I.(2004).*Manajemen Proyek Konstruksi Edisi Revisi*, Andi, Yogyakarta.

Husen,Abrar.(2008).*Manajemen Proyek*, Andi, Yogyakarta.

Lagawan, Gunawan.2007. *Manajemen Proyek Konstruks*. Trisakti University,Jakarta

N.Khaled, H.Ossama.(2012).”A model Of Assessing Maximum Overtime Rate In Labor Subcontracting Practices”. Journal of Construction Engineering and Project Management, KICEM.

Soeharto Imam. (1995).*Manajemen Proyek : Dari Konseptual Sampai Operasional*. Erlangga, Jakarta.

Soeharto Imam. (1998). *Manajemen Proyek : Dari Konseptual Sampai Oprasional Jilid 2*. Erlangga, Jakarta.

GEOTECHNICAL ENGINEERING

ISBN 979-458-758-3
Proceedings of the 3rd International Conference on the Geohazard Information
Zonation and 5th Seminar & Short Course of HASTAG (GIZ2014-HASTAG5)
Organized by UMSU, HASTAG, USM
Medan, Indonesia, October 20-22, 2014

Back Analysis of Slope Failure using Finite Element with Point Estimate Method (FEM-PEM)

Soon Min Ng[1+], Mohd Ashraf Mohamad Ismail[1], Ismail Abustan[1]
[1]School of Civil Engineering, Universiti Sains Malaysia (USM), Engineering Campus, Pulau Pinang, Malaysia

Abstract This paper investigates the slope failure in Precinct 9, Putrajaya, Malaysia by using numerical back analysis method. The catastrophic slope failure was triggered by a cumulative rainfall of 210 mm that occurred 2 days before the occurrence of slope failure. Site investigation that includes borehole sampling was immediately conducted to obtain representative information for the study area. The slope can be divided into 3 layers namely gravelly silt, silt and bedrock. Due to the uncertainty about the actual cause of failure initiation, back analyses have been performed via finite element shear strength reduction method for considering various probable mechanisms. In order to deal with the uncertainty and variability of the soil parameters, the Point Estimate Method (PEM) approach that assumed a normal and uncorrelated distribution was adopted in this study. Analysis results show that the slope failure is mainly influenced by the shear strength of the silt layer where the cohesion and friction angle at failure were 11 kPa and 20° respectively. Besides, the modeled circular slip surface also agrees well with the observed one.

Keywords: Back analysis, slope failure, shear strength reduction, point estimate method.

1. Introduction

The analysis carried out to identify the cause of slope failure in known as back analysis. It can be utilized to determine the shear strength parameters, pore water pressure and other conditions at the time of failure. Generally, back analysis is an effective approach to provide an insight into the underlying failure mechanism and improve the understanding regarding the factors controlling the stability of slopes. One of the advantage of back analysis is it can account for important factors that may not be well represented in laboratory and in-situ tests such as the presence of cracks and pre-existing shear planes within the soil mass [1]. Besides, the scale for back analysis is also much larger compared to the materials that are in at in-situ state [2]. However, there are also some uncertainties in back analysis approach that must be considered. For examples, mechanism of progressive slope failure, information of pore water pressure and the exact slip surface location and geometry [3].

Two methods that can be used to perform back analysis are deterministic and probabilistic method. Deterministic method determines a unique set of parameter such as c and ϕ by considering the factor of safety equals to unity [4]. However, in order to deal with the uncertainties in back analysis, probabilistic method offers a better approach to analyze a multiple sets of parameters simultaneously [5]. The outcomes are numerous combinations of parameters that result in slope failure. Nevertheless, the results of probabilistic method are realistic if the input parameters were correctly statistically characterized [6].

In this paper, a systematic approach of back analysis is proposed using the probabilistic method. The objective of this study is to identify a range of possibilities that cause slope failure from the available information and to determine the suitable parameters that can be used for designing remedial works. The reliability of this approach is demonstrated by applying it to a case study of slope failure in Putrajaya, Malaysia.

+ Corresponding Author. Tel.: +604-5996224; fax: +604-5941009.
E-mail address: soonmin1612@hotmail.com.

2. Project Background

Putrajaya is the third federal territory of Malaysia that serves as the federal administrative centre for the country. It has approximately 49 km^2 of land and was developed due to the congestion and overcrowding in Kuala Lumpur areas. A slope failure that involved 20 m height of man-made slope about 45° occurred on 22nd March 2007 at Precinct 9, Putrajaya. 23 vehicles were buried by the debris and 1000 residents were forced to vacate from their 15 stories apartment which is located 10 m from the failure zone. Prior to the slope failure that occurred at 4.30am, it had been raining heavily in Putrajaya since the evening of 20th March 2007 until the early morning of 22nd.

The slope failure occurred on the western side of a 50m high hill with a 36 million water tank constructed on the crest. The study area is underlain by graphitic quartz mica schist from Kajang Formation. Based on historical site investigation, the rocks in this area consist of interbedded sandstone, shale and actinolite schist [7]. Fig. 1 shows the location of the slope failure in Precint 9, Putrajaya.

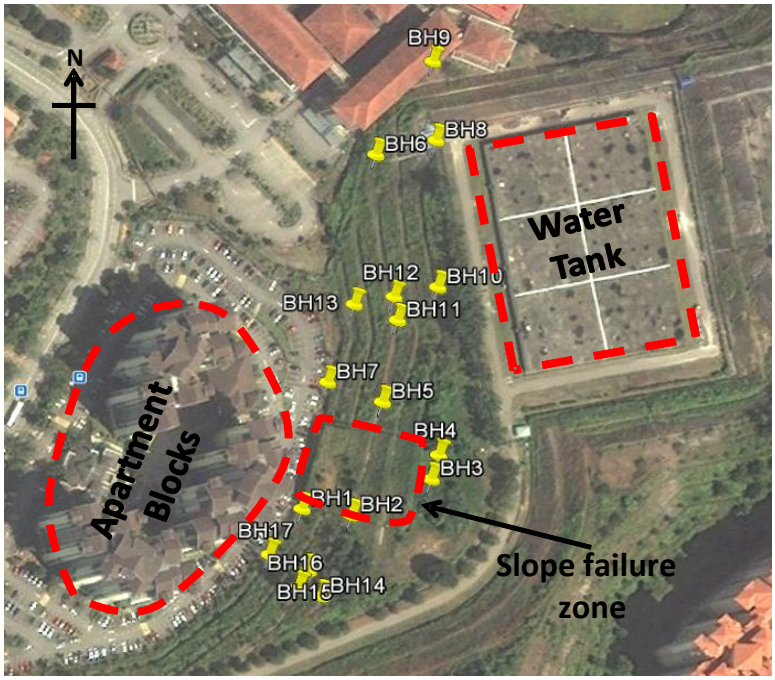

Fig. 1 Location of slope failure and boreholes in Precint 9, Putrajaya

3. Site Investigation

The study commenced with desk study where data collection for hydrological, geological and topographical data were conducted. Rainfall data recorded by a rain gauge station located near to the study area show a high intensity of rainfall of 140mm and 60mm on 20th and 21st March 2007. The rainfall intensity on 22nd March 2007 which is the day of slope failure recorded only 10mm.

A total of 17 boreholes drilling were carried out using rotary wash boring method immediately after the slope failure and their location are as shown in Fig. 1. The purpose of this borehole drilling was to determine the subsurface characteristics of the study area such as depth, groundwater level, lithology, and standard penetration (SPT) value and to collect soil sample for laboratory testing. Standard penetration test (SPT) was conducted in accordance to BS1377: Part 9: 1990 using a self tripping hammer of 63.5kg [8]. Initially, the tests were carried out at 1m interval from the ground surface to a depth of 6m and subsequently at every 1.5m intervals or when change of strata was encountered.

Soil samples were collected in the form of disturbed and undisturbed samples to determine the soil parameters input for back analysis. Rock coring in accordance to BS5930: 1999 was also carried out when a rock layer is encountered [9]. The core recovery ratio (CRR) and rock quality designation (RQD) was recorded for each core run. Groundwater level in each borehole was measured using electric dipmeter when the drilling is in progress and after the completion of the boreholes. The borehole data were then utilized to develop a 3-dimensional multi boreholes logs model as shown in Fig. 2. This 3D model is able to show the types of soil that present in the study area and enable the development of conceptual model that will be used for back analysis.

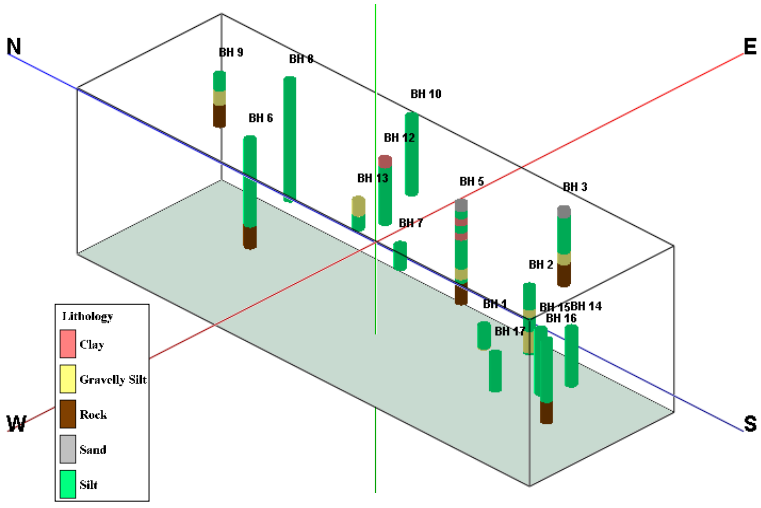

Fig. 2 3-dimensional multi boreholes log

4. Results and Discussions

Generally, the slope consists of 3 layers namely silt, gravelly silt and bedrock. A conceptual model for the slope was developed as shown in Fig. 3. Point estimate method (PEM) developed by Rosenblueth (1975) [10] was used in this study to deal with the probabilistic inputs in slope stability analysis. The principle of PEM is to compute solutions at various estimation points and to combine them with proper weighting in order to get an approximation of the distribution of the output variables. The fundamental assumption to use PEM is all random variables are normally distributed. In this study, the numerical computation for PEM will be solved together with finite element shear strength reduction analysis using *Phase2* software [11].

The input parameters values obtained from laboratory testing that will be used for the analysis are as shown in Table 1. The random variables chosen for probabilistic analysis are cohesion and friction angle for both silt and gravelly silt soil that result in 16 sets of combination. Table 2 shows the factor of safety (FOS) computed with different combination of random variables using PEM method. The results showed that the FOS at unity was produced by cohesion and friction angle of silt soil with the value 11 kPa and 20° respectively. This indicates that the stability of slope is mostly influenced by the silt layer and the slip surface produced match the observed one as shown in Fig. 4.

To verify the results of probabilistic PEM method, a sensitivity analysis was carried out using limit equilibrium (LEM) with Monte Carlo probabilistic method and the results is plotted in Fig. 5. The sensitivity plot agrees well with the results of PEM where the cohesion and friction angle of 10.36 kPa and 19.09° will result in slope failure. The sensitivity plot also shows that the FOS is less sensitive to gravelly silt layer. From this back analysis, remedial work can be designed based on the shear strength parameters of the silt soil computed at the time of failure.

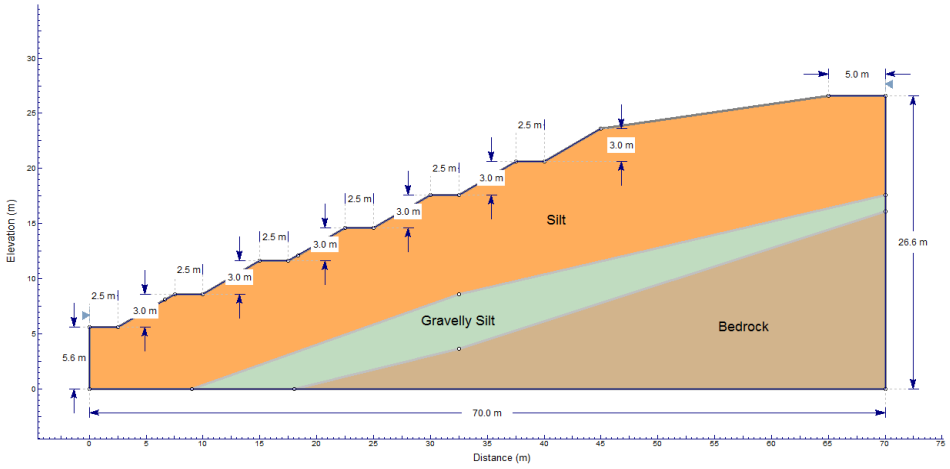

Fig. 3 Conceptual model for the slope

Table 1 Input parameters for stability analysis

Material Parameter	Silt	Gravelly Silt
Soil constitutive model	Mohr Coulomb	
Unit weight [kN/m^3]	18.67	17.79
Cohesion [k.Pa]	14	36
Friction angle [^{o}]	23	18
Hydraulic conductivity [m/s]	1.17 x 10^{-10}	2.42 x 10^{-10}

Table 2 Factor of safety (FOS) with different combination of random variables

Combination No.	Gravelly silt		Silt		Factor of Safety
	Friction Angle (°)	Cohesion (kPa)	Friction Angle (°)	Cohesion (kPa)	
1	21	39	26	17	1.53
2	15	39	26	17	1.53
3	21	33	26	17	1.54
4	15	33	26	17	1.5
5	21	39	20	17	1.28
6	15	39	20	17	1.29
7	21	33	20	17	1.29
8	15	33	20	17	1.31
9	21	39	26	11	1.28
10	15	39	26	11	1.3
11	21	33	26	11	1.29
12	15	33	26	11	1.31
13	21	39	20	11	1.06
14	15	39	20	11	1.06
15	21	33	20	11	1.06
16	15	33	20	11	1.06

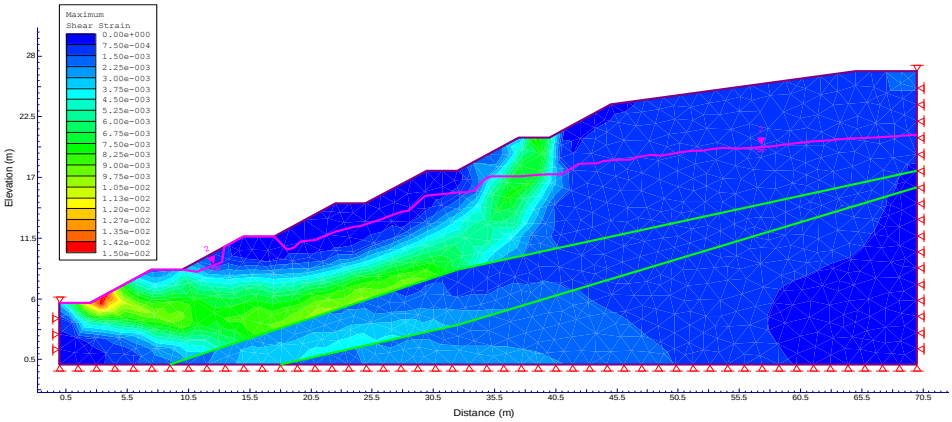

Fig. 4 Slip surface computed with finite element shear strength reduction method

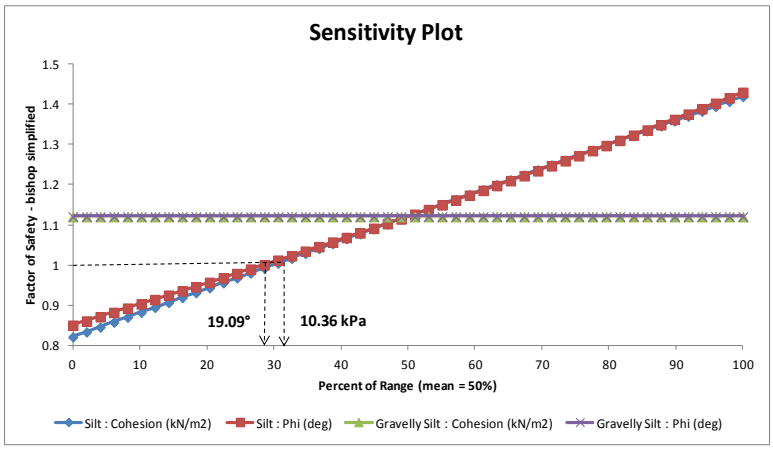

Fig. 5 Sensitivity plot via LEM-Monte Carlo probabilistic method

5. Conclusions

Based on the back analysis carried out, the stability of the slope in Precinct 9, Putrajaya is generally influenced by the silt layer. The shear strength parameters computed at the verge of slope failure are 11 kPa and 20° for cohesion and friction angle respectively. These threshold values can be utilized for remedial works such as installation of slope stabilization measures or designing a new slope under similar geotechnical conditions. This study also shows that the PEM approach is able to deal with the uncertainty and variability in FEM analysis. However, in order to maximize the use of PEM-FEM approach in back analysis, information should be combined from all possible sources such as laboratory testing, field instrumentation, and experience.

6. Acknowledgements

The authors would like to express their appreciation to Universiti Sains Malaysia Research University (RU) Grant (1001/PAWAM/814192) for the financial support to carry out this research. In addition, the authors would also like to acknowledge Putrajaya Corporation and Kumpulan Ikram for the permission to carry out this research at the site and the cooperation given to make this research a success.

7. REFERENCES

[1] Duncan, J. M., and Timothy, D. S. "Soil strengths from back analysis of slope failures." Stability and Performance of Slopes and Embankments II. ASCE, (1993).
[2] Gilbert, R. B., Stephen, G. W., and Eric, L. "Uncertainty in back analysis of slopes: Kettleman Hills case history." Journal of Geotechnical and Geoenvironmental Engineering 124.12 (1998): 1167-1176.
[3] Deschamps, R., and Greg, Y. "Limitations in the back-analysis of strength from failures." Journal of geotechnical and geoenvironmental engineering 132.4 (2006): 532-536.
[4] Jiang, Jing-Cai, and Takuo Yamagami. "A new back analysis of strength parameters from single slips." Computers and Geotechnics 35.2 (2008): 286-291.
[5] Zhang, J., Wilson H. Tang, and L. M. Zhang. "Efficient probabilistic back-analysis of slope stability model parameters." Journal of geotechnical and geoenvironmental engineering 136.1 (2009): 99-109.
[6] Wang, L., Hwang, J. H., Luo, Z., Juang, C. H., & Xiao, J. "Probabilistic back analysis of slope failure–A case study in Taiwan." Computers and Geotechnics 51 (2013): 12-23.
[7] Ahmed, J., Ghazali, M. A., Mukhlisin, M., Alias, M. N. and Taha, M. R.. Effectiveness of horizontal drains in improving slope stability: a case study of landslide event in Putrajaya Precinct 9, Malaysia. Unsaturated Soils: Theory and Practice (2011). Jatisankasa, Sawangsuriya, Soralump and Mairaing. Kasetsart University, Thailand. 753-758p.
[8] British Standard. Methods for test for soils for civil engineering purposes – 1377 Part 9: In-situ Tests. (1990).
[9] British Standard. Code of practice for site investigations – 5930. (1999).
[10] Rosenblueth, E. "Point estimates for probability moments." Proceedings of the National Academy of Sciences 72.10 (1975): 3812-3814.
[11] Rocscience Inc. Phase2 v7.0 – Two-dimensional finite element slope stability analysis. (2008).

ISBN 979-458-758-3
Proceedings of the 3rd International Conference on the Geohazard Information Zonation and 5th Seminar & Short Course of HASTAG (GIZ2014-HASTAG5)
Organized by UMSU, HASTAG, USM
Medan, Indonesia, October 20-22, 2014

Reduction of scour Hazard around Bridge Abutment using Foundation level

Reza mohammadpour [1+], Aminuddin Ab. Ghani [2] Omid Hassan shahi [3]

[1]Post-Doc/ researcher River Engineering and Urban Drainage Research Centre (REDAC), Universiti Sains Malaysia, Engineering Campus, Seri Ampangan, 14300 Nibong Tebal, Penang, Malaysia.

[2]Professor and Deputy Director, REDAC, Universiti Sains Malaysia, Engineering Campus, Seri Ampangan, 14300 Nibong Tebal, Penang, Malaysia.

[3]PhD student Universiti Sains Malaysia, Engineering Campus, Seri Ampangan, 14300 Nibong Tebal, Penang, Malaysia.

Abstract. The scour around piers and abutments is the major damage for bridge which appears during the flood hazard. An experimental study under clear water conditions to investigate the effect of foundation on reduction of local scour at abutment is presented. The complex abutment is included a short rectangular abutment with length of L, which is situated on a larger rectangular foundation. In the testes, the foundation level (Z) was located under initial bed and in different elevation. The results show that topography and depth of local scour is highly sensitive to the foundation size and its level. The minimum local scour at complex abutment was observed in range of $0.8 \leq Z/L \leq 1.2$ with a value between 0.9L and 1.5L. The location of the maximum scour depth is independent of the foundation dimension and its level, which usually occurs in the nose of the complex abutment. The result of this study can be used for protection and reduction of bridge failure due to scour hazard.

Keywords: Local scour; Complex abutment; Short abutment; Scour hazard; Scour reduction.

1. Introduction

The scour around piers and abutments is the major damage for bridge which appears during the flood hazard. Bridges are the main structures in transportation, especially in flood times. One thousand bridges have collapsed over the last 30 years in the United States and 60 percent of those failures are due to hydraulic failure including bridge scour [1]. The Public Department Malaysia (PWD) reported that the major cause of the bridge failure is scour hazard around abutment and pier [2]. The presence of abutments in front of flow may cause a huge change in the flow pattern, and the scour hole develops due to vortices. Development of vortices around the abutment occurs in three parts, in front of, to the side of, and downstream of the abutment.

Most investigations have been carried out on abutments with uniform cross sections (continuous horizontal cross section geometry). Similarly, must scour depth equations in the literature focus on scour around uniform abutments[3, 4]. Melville [5] showed that he local scour at uniform abutment is very sensitive to length of abutment; therefore, the abutment is classified into three groups as short abutment ($L/y \leq 1$), intermediate abutment ($1 < L/y \leq 25$) and long abutment ($L/y > 25$).

Due to geotechnical and financial reasons, actual bridge abutments are built on a foundation (or pile cap) with or without the pile group [6, 7]. Such abutments are named as complex/non-uniform abutments. In Hydraulic Engineering Circular No. 18, the Federal Highway Administration (FHWA) recommended a protection method for abutment as: “The preferred design approach is to place the abutment foundation on scour resistant rock or on deep foundations such as piles” [8]. However, during the flood hazard, the water flow usually erodes the abutment protection (such as ripraps and gabion), and the foundation that is under the stream bed initially will be exposed to flow (Fig. 1). Due to effect of foundation, the flow pattern around the

+ Corresponding author. Tel.: + 60126897332; fax: +6045941036
E-mail address: reza564@gmail.com

complex abutment will be more complicated [9]. However, during the flood hazard, the water flow usually erodes the abutment protection (such as ripraps and gabion), and the foundation will be exposed to the flow (Fig. 1). Then, due to effect of foundation, the abutment is such as complex abutment and estimation of the flow pattern around is more complicated [10].

In spite of using the complex abutment, there is limited information about the local scour at complex abutment. In the literature, just a few studies can be found related to local scour at complex piers [11-14]. If the effects of foundation were integrated into estimation of scour depth at abutment, the conservative approach would be unnecessary. Alternatively, abutment scour failure may be reduced by proper design of the foundation[15].

The main objective of this study is to study experimentally the clear-water local scour at vertical-wall abutment by considering the effects of foundation on scour depth. The short abutments ($L/y \leq 1$) were chosen for all tests. To find the optimum depth of foundation for reduction of the local scour, the foundation was located at different levels. The result of this study can be used for protection and reduction of bridge failure due to scour hazard.

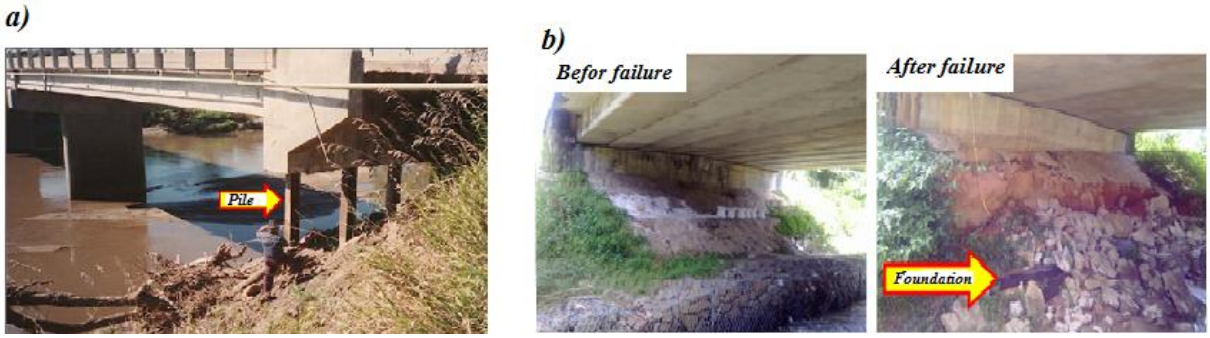

Fig.0: Exposed pile and foundation after erosion of abutment protection
Atlanta metro area (Sturm et al., 2011); b) Kurau River, Perak, Malaysia

2. Experimental Setup

A complex abutment is included a short rectangular abutment which is situated on a larger rectangular foundation. Different dimensions were chosen for complex and uniform abutments. Several sets of experiments was conducted for complex with a different level of foundation (Z). To investigate the effects of foundation on a complex abutment, three foundation locations (cases) were considered depending on the Z level (Fig. 2). In Case I, the foundation level was located below the scour hole. In Case II, the scour depth reached the top of the foundation, and the horseshoe vortices in front of the abutment were weakened by the foundation. In Case III, the foundation top was located within the scour hole. Melville [5] indicated the maximum local scour at uniform abutment is 2L, where L is abutment length. Therefore, it can be concluded that for $Z > 2L$, the complex abutment is similar to uniform abutment (Case I) and in range of $0 < Z \leq 2L$ (Cases II and III), the foundation influences on local scour.

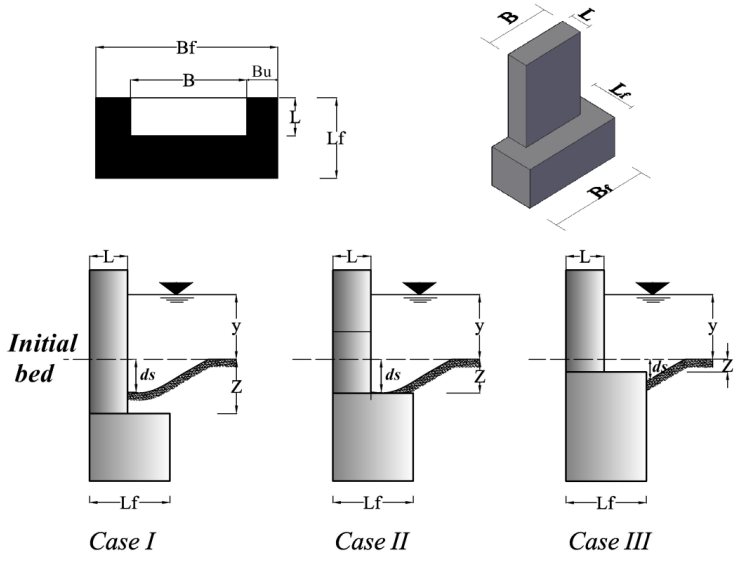

Fig. 2) Three cases for complex abutment below the initial bed

The experiments were carried out in the laboratory flume at REDAC with a 6.0 m long, 0.6 m wide and 0.6 m deep, equipped with a 25 cm deep sediment recess. Several floatable screens were placed at the entrance of the flume to dissipate the flow energy and reduce the turbulence. The flow depth was selected in such a depth that no influence on scour hole (L/y<1). For the experiments, uniform sand was selected with σg=1.2 and d50= 0.60 mm. To maintain the clear water condition, the flow velocity was set close to the critical velocity of sediment (U/Uc ≈1). A long-term experiment was conducted for each abutment until the rate of growth of scour hole reached close to equilibrium scour depth. A point gauge with an accuracy of ±1 mm was used to measure the topography of the scour hole after each run. Totally, seven abutments were chosen for all tests that included three uniform abutments (without foundation) and four complex abutments (Table 1).

Table 1: Abutment-Geometry Characteristics for the Present Study

Experiment No.	*Abutment*	*Foundation*		*Abutment*		*Length ratio*	*Z/L*
		L_f (cm)	B_f (cm)	L (cm)	B (cm)	(L/L_f)	
AB 1	Uniform	-	-	4	8	-	
AB 2	Uniform	-	-	5.5	11	-	
AB 3	Uniform	-	-	7	14	-	
FA 21	Complex	5.5	11	4	8	0.73	0.38,0.88, 1.25
FA 33	Complex	9	18	7	14	0.78	0.43, 0.5,1.0, 1.14,1.29
FA 42	Complex	12	24	5.5	11	0.46	0.55, 0.91, 1.27,1.45
FA 43	Complex	12	24	7	14	0.58	0.43,0.71 1.0,1.14,1.29

3. Result and Discussion

Fig. 3 shows the variation of maximum scour depth ratio (d_s/L) at abutment in terms of the foundation level ratio (Z/L). The results indicate that at short complex abutment, the scour depth depends on both *Z/L* and L/L_f where *L* and L_f are abutment and foundation length respectively. In Case I ($Z/L \geq 2.0$), the elevation of the foundation is under the base of the scour hole; therefore, the scour depth just depends on abutment length (*L*) and the scour hole around the complex abutment is similar to uniform abutments. In Cases II and III, the top of the foundation exposes to scour hole, and the depth of scour is usually smaller than the maximum scour depth for uniform abutment ($d_s<2L$). Starting from a Z/L approximately equal to 2 and subsequently decreasing, the top of the foundation rises to the scour hole, and the depth of scour decreases and reaches a minimum value in range of $0.8 \leq Z/L \leq 1.2$. In this range, the scour depth at complex abutment is between 0.9<ds/L<1.5.

The main causes of the local scour at abutment are the principal vortex and its associated down-flow at upstream of the abutment. As shown in Fig. 3 the location of foundation and its dimension are a main case to decrease the scour depth at complex abutment. Melville and Raudkivi [16] indicated that if the foundation is located above the bed level (*Z/L<0),* in addition to pier, the foundation is a case for another principle vortex and increasing the local scour at complex piers. Even though in this research, the effect of foundation for *Z/L<0* was not considered but since the local scour at abutments and piers are roughly similar, then it can be concluded that the scour depth more increases with an increase in the foundation level above the bed.

In Case II ($1 \leq Z/L < 2$), the principal vortices in front of the abutment are weakened by the foundation and the scour depth is confined by the top of the foundation. In this case, the scour depth is equal to the foundation level (Z); therefore, all points located on the line ds=Z.

In range of 0 <*Z/L<1*(Case III), even though the top of foundation is like an obstacle for the principal vortices produced by the abutment, but the foundation produces another vortex which contributes to increase the local scour. With a decreasing *Z/L*, the foundation rises more within the scour hole and a case to increase the effect of the vortex in front of abutment. Therefore, the relative scour depth (d_s/L) increases with decreasing Z/*L*.

As shown in Fig. 3, the scour depth around a complex abutment is sensitive to the foundation dimension (L_f), and the scour depth decreases with a decrease in the foundation dimension. For instance, the abutment

length is similar both complex abutments of FA 43 and FA 33(L=7 cm, Table 1). For FA 33, with a decrease in the foundation dimension the uniformity of the complex abutment increases. Then, the principal vortices produce by foundation are smaller than those produced by FA43. Consequently, the scour depth for FA 33 is less than those for FA43. Generally, in Case III the scour depth is bigger than the foundation level (d_s>*Z).*

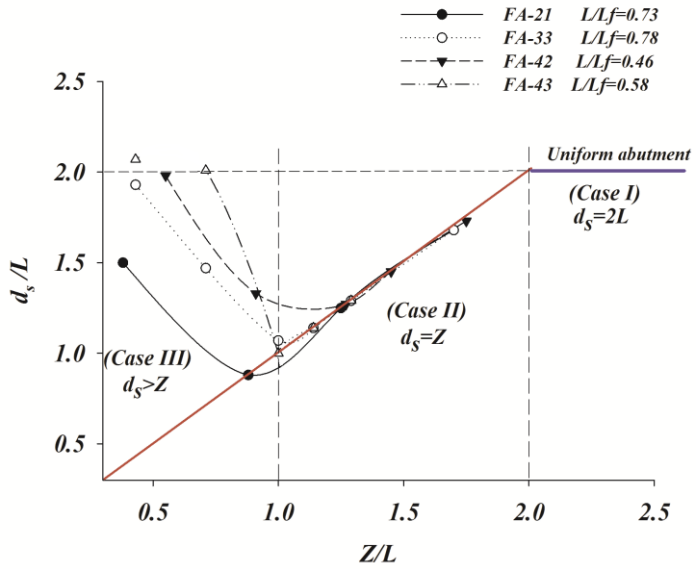

Fig. 3) Scour depth as a function of top elevation of foundation

The experimental observation indicates that although the foundation reduces the effect of principle abutment vortex, but the location of the maximum scour is independent of the foundation dimension and its level and always occurs in the nose of foundation or abutment (Fig. 4). This is due to a maximum shear stress at the nose of complex abutment. The similar result was reported for uniform abutment [12, 17].

Although the location of maximum scour depth is fixed, but topography of local scour around abutment is sensitive to the foundation level. Fig. 4 illustrates the topography of local scour around FA 42 for *Z/L* at 0.91 and 0.55 with same flow conditions. The scour depth ration increases from 1.33 to 1.98 with decreasing Z/L from 0.91 to 0.55 respectively (raising the foundation). There is no sediment deposition in downstream of complex abutment with Z/L=0.55, while the deposition of sediment can be observed for Z/L=0.91. It can be concluded that with raising the foundation within the scour hole, in additional to wake vortex produced by abutment, the foundation also produces another wake vortex which contributes to remove a big portion of sediment in downstream of complex abutment. Consequently, the foundation level influences on both scour depth and topography.

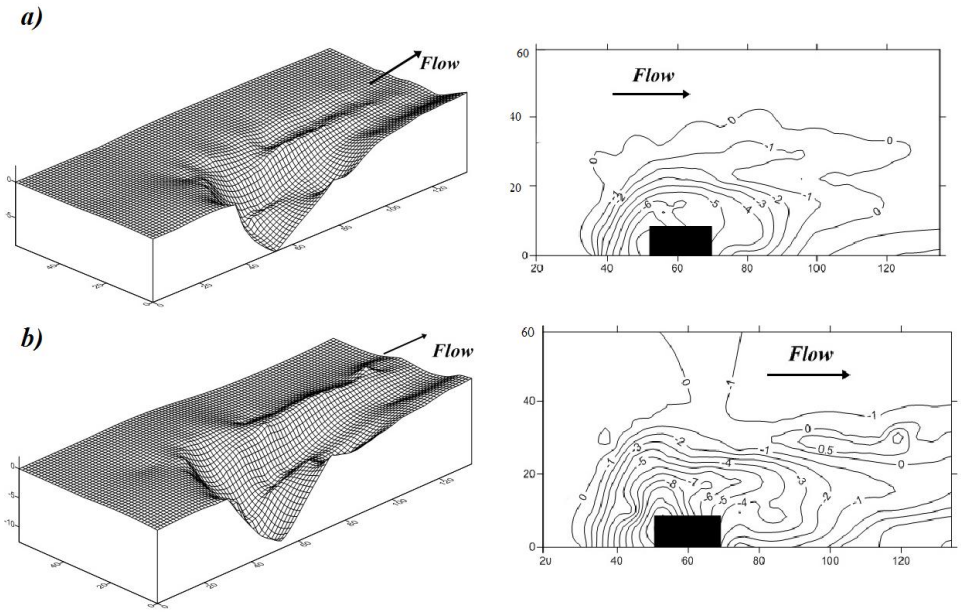

Figure 4: Local scour around complex abutment FA 42 for
(a) Z/L=0.91; (b) Z/L=0.55

4. Conclusion

To find the effect of foundation on reduction of local scour around abutment, a set of experiment was conducted under clear water conditions at complex short abutment ($L/y \leq 1$). All experiments were conducted under threshold conditions and with uniform sediment, where the foundation was located under the initial bed. A range of configurations, including different sizes of abutments and various foundation levels and sizes were considered in the tests. The results show that both scour depth and topography of local scour at complex short abutment is highly sensitive to the foundation size and its level. In range of $0 < Z/L < 2.0$, the foundation is exposed to scour hole and the scour depth is usually smaller than those at uniform abutment. The minimum local scour at complex abutment was observed in range of $0.8 \leq Z/L \leq 1.2$ with a value between $0.9 < ds/L < 1.5$. In this range, the top of foundation is similar to an obstacle for the principal vortices which produced by the abutment, and the foundation decreases the effects of principal vortices. Furthermore, the location of the maximum scour depth is independent to the foundation dimension and its level, which usually occurs in the nose of the complex abutment.

Acknowledgements

The authors would like to thank Universiti Sains Malaysia for the financial support under the RU GA grant.

References

[1] A.M. Shirole, Planning for a comprehensive bridge safety assurance program Transportation Research Board, (1991) 137-142.
[2] P.W.D. Malaysia, Annual Bridge Inspection Manual, in, 1995.
[3] R. Mohammadpour, A. Ab. Ghani, H.M. Azamathulla, Prediction of equilibrium scour time around long abutments, Proceedings of the Institution of Civil Engineers: Water Management, 166 (2013) 394-401.
[4] R. Mohammadpour, A.A. Ghani, H.M. Azamathulla, Estimation of dimension and time variation of local scour at short abutment, International Journal of River Basin Management, 11 (2013) 121-135.
[5] B.W. Melville, Local Scour at Bridge Abutments, J Hydraul Eng-Asce, 118 (1992) 615-631.
[6] B. Ataie-Ashtiani, Z. Baratian-Ghorghi, A.A. Beheshti, Experimental Investigation of Clear-Water Local Scour of Compound Piers, J Hydraul Eng-Asce, 136 (2010) 343-351.
[7] S.E. Coleman, Clearwater local scour at complex piers, J Hydraul Eng-Asce, 131 (2005) 330-334.
[8] E.V. Richardson, Davis, S. R. , Evaluating scour at bridges, in, Federal Highway Administration, Washington,D.C., Hydraulic Engineering Circular No. 18 (HEC-18), 4th Ed., Rep. No.FHWA NHI 01-001, , 2001.
[9] A. Kumar, U.C. Kothyari, K.G. Ranga Raju, Flow structure and scour around circular compound bridge piers – A review, Journal of Hydro-Environment Research, 6 (2012) 251-265.
[10] (!!! INVALID CITATION !!!).
[11] A.C. Parola, S.K. Mahavadi, B.M. Brown, A. ElKhoury, Effects of rectangular foundation geometry on local pier scour, J Hydraul Eng-Asce, 122 (1996) 35-40.
[12] B.W. Melville, S.E. Coleman, Bridge scour, Water Resources Publications, Highlands Ranch, Colo., 2000.
[13] M. Mia, H. Nago, Design Method of Time-Dependent Local Scour at Circular Bridge Pier, Journal of Hydraulic Engineering, 129 (2003) 420-427.
[14] D.M. Sheppard, t. Glasser, SEDIMENT SCOUR AT PIERS WITH COMPLEX GEOMETRIES, in: Pro., 2004 2nd Int. Conf. on scour and Erosion, World Sceientific, Singapore, 2004.
[15] R. Mohammadpour, Effect of Foundation Geometry On Short Abutment Scour, in: REDAC,PhD Thesis, Universiti Sains Malaysia, 2013.
[16] B.W. Melville, A.J. Raudkivi, Effects of foundation geometry on bridge pier scour, J Hydraul Eng-Asce, 122 (1996) 203-209.
[17] F. Ahmed, N. Rajaratnam, Observations on Flow around Bridge Abutment, Journal of Engineering Mechanics, 126 (2000) 51-59.

ISBN 979-458-758-3
Proceedings of the 3rd International Conference on the Geohazard Information
Zonation and 5th Seminar & Short Course of HASTAG (GIZ2014-HASTAG5)
Organized by UMSU, HASTAG, USM
Medan, Indonesia, October 20-22, 2014

Prediction of sand thickness using ordinary kriging

Ahmad Shukri Yahaya[+], Fauziah Ahmad and Lo Yean Tiing

School of Civil Engineering, Engineering Campus, Universiti Sains Malaysia, 14300 Nibong Tebal, Pulau Pinang, Malaysia

Abstract. The objective of the research is to determine the characteristics of sand in Batu Ferringhi, Penang. Then an ordinary kriging model was developed which can be used to predict thickness of sand. A set of data from three different sites in Batu Ferringhi were collected from the site investigation report. There are three main stages in predicting sand thickness. The first stage is to determine the location and coordinate of each boreholes from the three different sites in Batu Ferringhi. The second stage is to obtain descriptive statistics of the thickness of sand. The third stage is to model the sand thickness using ordinary kriging and to obtain the best model. The results show that the best model variogram is the exponential function. Five boreholes were then used for prediction using the best ordinary kriging model. It was found that the prediction is quite accurate.

Keywords: Sand, clay, ordinary kriging.

1. Introduction

Penang is located at the north-eastern coast and constituted by two geographically varying entities which is an island with area of 293 km^2 called Penang Island and a portion of mainland called Seberang Perai having the area of about 755 km^2. Batu Ferringhi is located in Penang island. The development in Penang Island is very rapid because it is one of the most industrialized area in Malaysia. In Penang, the most frequent hazard that always occurs is landslide. Malaysia is a hilly or a mountainous country and the slope failure are a common occurrence. Geologically, this area is also underlain by medium to coarse-grained biotite granite layer with predominant orthoclase and subordinate microcline (Fauziah Ahmad *et al*., 2005). Thus it is important to analyze the soil conditions as well as to predict sand thickness in Penang Island.

Based on the kriging principle, Ishii and Suzuki (1989) presented a simple probabilistic model that evaluates an unknown value of ground thickness and estimation of error for the soil properties at unsampled location in the ground. This model is capable to evaluate the borehole spacing. However, the model required statistical parameters, namely, a correlation distance and variance of soil properties as important data input. The geotechnical database system for Saga Plain, Japan provided the parameters needed. Finally, the exploration spacing for different values of estimation error was suggested for site investigation. A kriging prediction case study was carried out on clay thickness data in Kuala Lumpur (Saffur, 2003). This prediction technique is capable in predicting the clay thickness at an unsampled location provided that the data used were collected at reasonable distances so that it is correlated, for the technique to work. The kriging method was used to estimate the presumed unknown values of sorptivity for a soil under tilled and no-tilled condition in some locations in the 0.5 m × 0.5 m grid distances (Sepaskhah *et al*., 2004). The result shows that the method is capable to estimate the unknown sorptivity of the soil.

This study aims to determine the characteristics of sand thickness in Batu Ferringhi, Penang Island and to predict sand thickness using ordinary kriging so that engineers can use this model to predict sand thickness at unsampled locations.

2. Methodology

The data was obtained from 22 boreholes which were collected from three sites around the area of Batu Ferringhi in Penang Island. The information contained in the report that will be used in the research are location, description of soils, depth of soil and thickness of soil. Batu Ferringhi is located in the northern part of Penang Island as shown in Figure 1. The coordinates of the boreholes are obtained using ArcView GIS software (Lee and Wong, 2001) by plotting the boreholes based on the contour levels in the report and hence the coordinate for each borehole was obtained.

Fig. 1: Map of Penang showing the study location
(Source: Penang map, 2012)

Descriptive statistics for measures of location such as mean, median, minimum and maximum values and for measures of spread such as standard deviation, variance and range were obtained. For predicting sand thickness five variogram models were fitted namely Spherical, Exponential, Gaussian, Linear and Power functions. The best fitted model was chosen based on its objective value. This will provide the values of the parameters of the functions that are range, slope and nugget. The best variogram model was chosen to be used in ordinary kriging (Webster and Oliver, 2000).

3. Results and discussions

The analyses are done using the descriptive statistics to get the typical values that represent the study area. Table 1 below shows the summary of the descriptive statistics for all boreholes in Batu Ferringhi.

Table 1: Summary of descriptive statistics for thickness of sand and clay

	Sand Thickness
Number of boreholes, N	22
Mean (cm)	39.5968
Std. Error of Mean (cm)	8.18758
Median (cm)	27.7750
Std. Deviation (cm)	38.40314
Variance (cm^2)	1474.801
Range	183.63
Minimum (cm)	0.00
Maximum (cm)	183.63
COV	0.96988

From Table 1, the mean for sand thickness is 39.6cm. This shows that the geotechnical profile for Batu Ferringhi is rich with sand. The range of sand thickness is 183.6cm. The value for coefficient of variation (COV) is small (less than one) showing that the variability of sand thickness is small.

The surface plot for sand thickness based on the coordinates of the boreholes is given in Figure 2. From the Figure 2, the bubble plots are the point and the locations of the boreholes with the sand thickness. The bigger the bubble, the greater is the thickness. The surface of the sand thickness indicates that the most thickness area falls between x-coordinate from 253000 to 254000.

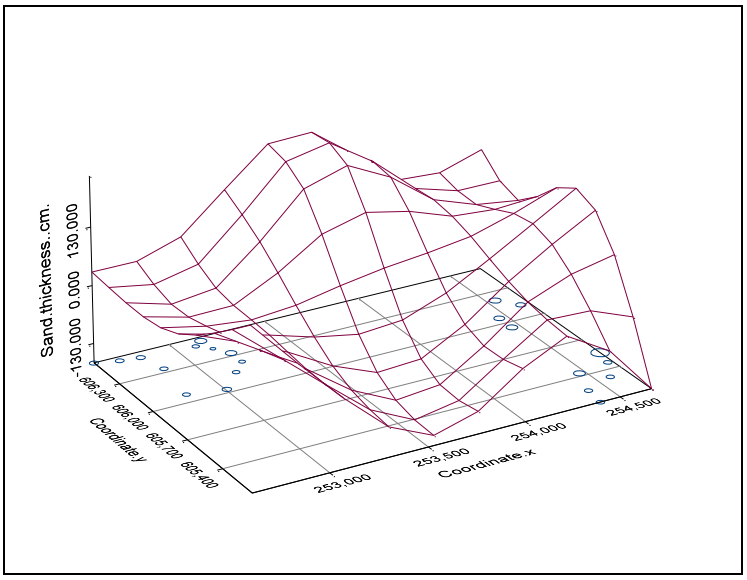

Fig. 2: Surface plot of the sampled points

3.1. Prediction using ordinary kriging

In this case study, 22 samples of sand thickness from Batu Ferringhi were used to carry on the ordinary kriging prediction. The coordinates for the 22 boreholes were obtained by visiting the sites as well as by using the ArcView GIS software.

Empirical variograms were obtained for the sand thickness. Five different variogram models were fitted namely: (a) Spherical (b) Exponential (c) Gaussian (d) Linear and (e) Power functions. The best empirical variogram function was found to be the Power function with range, a = 0.03775782, slope = 1116.63737676 and nugget,C_o=399.35630940.

Due to lack of data, five observations of sand thickness were then taken out randomly in order to predict the thickness of sand, which is assumed, had not been visited. Table 2 shows the five samples used to predict sand thickness.

Table 2: Prediction of sand thickness using ordinary kriging

No.	Borehole no.	x coordinate	y coordinate	Actual thickness (cm)	Predicted thickness (cm)	Percentage accuracy
1	1	253205	606232	8.50	10.28	79.1
2	7	252862	606336	18.90	20.08	93.8
3	13	252825	606480	29.70	30.27	97.0
4	18	252614	606531	30.15	30.69	98.2
5	5	254412	605270	20.40	21.50	94.6

Table 2 shows the predicted sand thickness for the five locations, which was assumed, had not been visited. The percentage accuracy for the prediction varies from 79.1%

until 98.2%. Four out of five locations were accurately predicted with percentage accuracy more than 90% which were borehole 7, 13, 18 and 5. The sand thickness at borehole number 1 was not predicted reasonably well (percentage accuracy of 79.1%).

4. Conclusion

The research is to analyze the thickness of sand at Batu Ferringhi, Penang Island. These are based on site investigation reports of project developments done during recent years. The study concentrates on the results of statistical analyses on the data.

The characteristics of sand are described and analyzed based on information from a total of 22 samples. The descriptive statistics were calculated to determine the sand profile around the area. It was found that the mean sand thickness is 39.6cm and the variability of sand thickness in Batu Ferringhi was very small.

The best variogram model was found to be the Power function with range, a = 0.03775782, slope = 1116.63737676 and nugget, C_o = 399.35630940. This variogram model was used to obtain the ordinary kriging model. Predictions of sand thickness at five chosen points were found to be accurate. Thus it will enable engineers to predict with good accuracy the sand thickness using the developed model.

5. Acknowledgements

The authors would like to acknowledge the Universiti Sains Malaysia for funding this research through the Research University grant scheme and Minitry of Education Malaysia through Exploratory Research Grant.

6. References

[1] K. Ishii and M. Suzuki. Stochastic finite element analysis for spatial variations of soil properties using kriging technique. In : *Proceedings of ICOSSAR '89, the 5th International Conference on Structural Safety and Reliability, Part II*, Aug 7-11 1989, San Francisco, CA, USA. America : America Society of Civil Engineers. pp. 1161-1168.

[2] S. Saffur. *Analysis of site classification for Kuala Lumpur's ground assessment*. 2003, MSc thesis, University Sains Malaysia.

[3] Fauziah Ahmad, Ahmad Shukri Yahaya and Mohd Ahmadullah Farooqi. Characterization and Geotechnical Properties of Penang Residual Soils with Emphasis on Landslides, *American Journal of Environmental Sciences*, 2006, 2(4): 121-128.

[4] A.R. Sepaskhah, S. H. Ahmadi and A.R. Nikbakht Shahbazi. Geostatistical analysis of sorptivity for a soil under tilled and no-tilled conditions. *Journal of American Society of Civil Engineers*. 2004, 83(2):237-245.

[5] Penang map (2012) available at http://www.welt-atlas.de/karte_von_penang_6-151 (accessed 01/01/2012).

[6] J. Lee and D.W.S. Wong. *Statistical analysis with ArcView GIS*. 2001. New York : John Wiley.

[7] R. Webster and M. Oliver. *Geostatistics for environmental scientists*. 2000. Chichester: John Wiley and Sons.

ISBN 979-458-758-3
Proceedings of the 3rd International Conference on the Geohazard Information
Zonation and 5th Seminar & Short Course of HASTAG (GIZ2014-HASTAG5)
Organized by UMSU, HASTAG, USM
Medan, Indonesia, October 20-22, 2014

Analysis of Thickness of Sand and Silt in Penang Island

Fauziah Ahmad[1+], Ahmad Shukri Yahaya[1] and Kong Chun Sian[1]

[1]School of Civil Engineering, Engineering Campus, Universiti Sains Malaysia, 14300 Nibong Tebal, Pulau Pinang, Malaysia

Abstract. The soil contents for sand and silt are important in the development of project. Twelve locations containing 112 boreholes data in the Penang Island were collected and a database was set up. These boreholes logs were taken from site investigation reports by the Public Works Department, Penang Island. The database was set up for five sub-districts in Penang Island. Descriptive statistics was carried out on the thickness of sand and silt in these five sub-districts. Analysis of variance (ANOVA) was used to determine whether there are significant different in the thickness of sand and silt between the five sub-districts. All the analyses were carried out as case studies involving sand and silt thickness for Penang Island. Based on the results of the analyses, the mean of sand in five sub-districts were almost the same. District 11 – Teluk Kumbar is the area which contained the least sand if compared to other districts. For the thickness of silt, the results can be divided into two groups. These two groups were divided base on the mean value obtained from each sub-district.
Keywords: Sand, Silt, ANOVA test.

1. Introduction

Penang Island lie off the northwestern coast of Peninsula Malaysia with an area of about 293 km^2. Penang has evolved from a trading centre to a manufacturing centre. Penang has begun the industrialization program in 1972 with the establishment of the first Free Trade Zone in Malaysia. It has attracted both foreign and local companies which have established projects in Penang. Hence many construction activities had been completed in this island ranging from small projects, such as condominiums, hotels, housings, highways and stadiums to mega projects such as the Penang bridge and the Sultan Abdul Halim bridge. In Penang, the most frequent hazard that always occurs is landslide. Malaysia is a hilly or a mountainous country and the slope failure are a common occurrence. Thus it is important to analyze the soil conditions in Penang Island.

Fauziah Ahmad *et al*. (2006) has described in detailed about the characteristics, nature, structural features, engineering behaviour and field properties of soil samples in Penang Island. They found that the soil around Penang Island is either silty, clayey or sandy. Fauziah Ahmad *et al*. (2010) have determined the rating scale of two areas in Penang Island and found that 12% of the areas have high environmental risk. Chu et al. (1997) report reveals that the coastal area in the north and south of Penang Island is of rocky type and partially sandy beach. Based on aerial photographs, topography and coastal map and field observation works, they pointed out some results which can be visually compared with the TiungSAT-1 image (Abdul Hadi *et al.*,2000).

This study aims at comparing the thickness of sand and silt between sub-districts of Penang Island to determine whether there are significant differences in their thickness.

This will help engineers and policy makers make appropriate decisions in the future development of Penang Island.

2. Methodology

The site investigation (S.I.) reports were collected from the Public Works Department, Penang. The data comes from 112 boreholes which were collected from 12 sites. The soil explorations of the sites were for the development of projects such as residential housing schemes, retaining wall, higher buildings and so on. The S.I. reports were produced from the year 1999 until the year 2004. These reports contain important information that had been extracted such as purpose of the project, water level, date drilled, depth of borehole, description of different layers and types of soils and rock, thickness of different layers and types of soils and rock, standard penetration test (SPT) of different layers and types of soils.

In this case, the locations were from five districts out of 18 districts in Penang Island. They are District 11-Teluk Kumbar, District 12-Bayan Lepas, District 13-Paya Terubong, District 17-Batu Feringghi and District 18-Tanjung Tokong. The location of the study area is given in Figure 1.

Fig. 1: Map of Penang (Source: Penang map, 2012)

Table 1 shows in detail the five sub-districts, the number of boreholes and the number of project sites. A total of 12 project sites and 112 boreholes were used in the analysis.

Table 1: Description of project sites and number of boreholes

Number	Sub-districts	Number of Project Sites	Number of Boreholes
1	Mukim 11-Teluk Kumbar	1	25
2	Mukim 12-Bayan Lepas	3	19
3	Mukim 13-Paya Terubong	2	17
4	Mukim 17- BatuFeringgi	4	26
5	Mukim 18-Tanjong Tokong	2	25
	Total	12	112

3. Results and discussions

The summary of the descriptive statistics for sand is shown in Table 2. The mean thickness of sand ranged from 3.38m to 6.56m among the five sub-districts. The lowest mean thickness is in District 11 – Teluk Kumbar which is 3.38m, followed by District 12 – Bayan Lepas is 5.02m, District – 17 Batu Ferringhi is 6.05m, District 13 – Paya Terubong is 6.09m and District 18 – Tanjong Tokong is 6.56m. The variability of the sand thickness is low. District 18 – Tanjong Tokong has high sand thickness because it is near to the sea. Sand has high infiltration, lose water quickly and can be a good drainage system. It is a suitable place for development especially for roads and building.

Table 2 : Descriptive statistics for sand thickness in the five sub-districts

Sub-districts	No. of Observations, n	Mean (m)	Variance, (m^2)	Standard Deviation (m)	Minimum thickness (m)	Maximum thickness (m)
District 11 – Teluk Kumbar	4	3.38	2.06	1.44	1.50	4.50
District 12 – Bayan Lepas	18	5.02	14.63	3.83	0.15	13.20
District 13 – Paya Terubong	17	6.09	14.25	3.77	0.30	14.70
District 17 – Batu Ferringhi	24	6.05	14.38	3.79	0.30	14.90
District 18 – Tanjong Tokong	25	6.56	21.51	4.64	2.10	23.00

Table 3 shows the summary of the descriptive statistics for silt among the five sub-districts. District 10, District 13 and District 15 have mean thickness of silt which is less than 8.00 m. The standard deviations of the data were calculated too for measuring the variability of the mean values. Here, the standard deviation is small compared to the mean. Thus, the variability among the districts is small. The minimum thickness of silt was found in District 13 (0.30m) and maximum silt thickness is obtained at District 11 (19.50m).

Table 3 : Descriptive statistics for silt thickness in the five sub-districts

Sub-districts	No. of Observations, n	Mean (m)	Variance (m^2)	Standard Deviation (m^2)	Minimum thickness (m)	Maximum Thickness (m)
District 11 – Teluk Kumbar	22	8.15	31.84	5.64	0.50	19.50
District 12 – Bayan Lepas	10	4.57	5.59	2.36	1.50	9.00
District 13 – Paya Terubong	9	4.57	12.09	3.48	0.30	9.80
District 17 – Batu Ferringhi	15	6.49	15.00	3.87	1.50	15.00
District 18 – Tanjong Tokong	5	10.04	24.83	4.98	4.00	15.00

The analysis of variance (ANOVA) test (Ahmad Shukri Yahaya *et al*., 2008) was done to determine whether there are significant differences in the mean sand and silt thickness between the five sub-districts. The results of the ANOVA test shows that there is no significant difference in the thickness of sand between the five sub-districts (F-statistic = 0.801 and p-value = 0.528). For the thickness of silt, the ANOVA test shows that there is a significant difference between the five sub-districts (F-statistic = 2.350 and p-value = 0.065). Duncan's Multiple Range test was performed to determine the different groups. The first group is District 12, District 13, District 11 and District 17 which have no significantly differences in the mean thickness of silt. The second group is District 11, District 17 and District 18 which have no significantly differences in the mean thickness of silt. However, the mean thickness of silt for group 1 is greater and is significantly different than the mean thickness of silt for group 2.

For silt, District 11 – Teluk Kumbar and District 18 – Tanjong Tokong have higher silt thickness compared to the other districts. The size particle for silt is smaller than sand but it has more plasticity and cohesively. Existing sand and silt in soil helps in selecting the type and depth of foundation which are suitable for a structure. Frictional force between soil and the pile shaft helps support the structure loading. Thus, it is important to determine the total sand and silt thickness in soil.

4. Conclusion

The research is to analyze the thickness of sand and silt in Penang Island. These are based on site investigation reports of project developments done during recent years. The study concentrates on the results of statistical analyses on the data. To have a complete database of characteristics of soil is necessary to plan for future development in Penang Island.

The soils characteristics are described and analyzed based on information from a total of 112 boreholes logs collected. Five sub-districts were considered. The descriptive statistics were calculated to determine the soil profile around the area. District 18 – Tanjong Tokong has high mean sand thickness and therefore it is a suitable place for development especially for roads and buildings.

For silt, District 11 – Teluk Kumbar and District 18 – Tanjong Tokong have higher mean silt thickness compared to the other districts. The size particle for silt is smaller than sand but it has more plasticity and cohesively. Existing sand and silt in soil helps in selecting the type and depth of foundation which are suitable for a structure. Frictional force between soil and the pile shaft helps support the structure loading. Thus, it is important to determine the total sand and silt thickness in soil.

One way Analysis of Variance test was applied to test whether the mean thickness between the sub-districts are equal or not. From the results of the analyses, conclusions of thickness of sand and silt in Penang Island can be interpreted. The thicknesses of sand in the five sub-districts were found not to be significantly different. However, the means of silt thicknesses between the five sub-districts are not equal. Thus, Duncan's Multiple Range Test has been carried out. The result shows that silt thickness among the five districts is significantly different. Thus, the thickness of silt between the sub-districts is not equal between them.

5. Acknowledgements

The authors would like to acknowledge the Universiti Sains Malaysia for funding this research through the Research University grant scheme.

6. References

[1] Abdul Hadi Abd Rahman, Mohamad Zaki Ibrahim and Yajesh V. Ramachandram. Coastal Sedimentation and Recent Coastalline Changes Along the Seberang Perai. *Proceedings of the Geological Society of Malaysia Annual Geological Conference 2000*, 8 – 9 September 2000.

[2] Ahmad Shukri Yahaya, Amran Ahmed, Darmesah Gabda, Chin Su Na, 2008. *Problems and Solutions in Statistics for Engineers and Scientists*. 2008. Pearson Prentice-Hall, 299 pp.

[3] L.H. Chu, H.P. Ong, P.P. Sinjeng, A.A. Kadir, K.M. Slar and C.S. Ismail. An Investigation of Malaysia Granitic Rocks as Suitable Source of Feldspar. *Journal of Asian Earth Sciences*. 1997, 15 : 477-488.

[4] Fauziah Ahmad, Ahmad Shukri Yahaya and Mohd Ahmadullah Farooqi. Characterization and Geotechnical Properties of Penang Residual Soils with Emphasis on Landslides, *American Journal of Environmental Sciences*, 2006, 2(4): 121-128.

[5] F. Ahmad, A.S. Yahaya, M.M. Ali, WNAM Hussain. Environmental Risk Assessment On Hill Site Development In Penang, Malaysia: Recommendation On Management System, *European Journal of Scientific Research*. 2010, 40(3):318-340.

[6] *Penang Map* available at: http://malaysia-maps.com/penang/ (accessed 01/01/2012).

ISBN 979-458-758-3
Proceedings of the 3rd International Conference on the Geohazard Information
Zonation and 5th Seminar & Short Course of HASTAG (GIZ2014-HASTAG5)
Organized by UMSU, HASTAG, USM
Medan, Indonesia, October 20-22, 2014

Solidification Potential of Fine-grained Dredged Marine Soils : Water-binder Ratio Effects

Amira Azhar [1], Chee-Ming Chan [2] and Ahmad Tarmizi Abd Karim [1]

[1] Faculty of Civil and Environmental Engineering,
Universiti Tun Hussein Onn Malaysia (UTHM), Malaysia

[2] Faculty of Engineering Technology,
Universiti Tun Hussein Onn Malaysia (UTHM), Malaysia

Abstract. Dredging activities are important to ensure safe navigation of ships and vessels at Ports, Harbors, and navigational channels. DMS is a valuable resource even though not commonly practice. The use of dredged material has a major contribution to make to sustainable development and can reduce the quantities of primary resource needed for activities such as construction and habitat creation. Solidification is a method that aims to improve the engineering properties of soil such as soil strength. Soil stabilization involves the use of stabilizing agents or binder materials in soft soils to improve its geotechnical properties such as compressibility, strength, permeability and durability. The fine-grained DMS sample collected from Marina, Melaka was used in this study. According to Unified Soil Classification System (USCS), the DMS was classified as high plasticity clay (CH). The amount of DMS that will be mixed with the binders was calculated based on water-binders (water-cement) ratio. Calculation for the amount of binders (OPC and BA) for each mixture was calculated from mass of dry sample and moisture content of the sample. The water binder ratios of the samples are 1, 3 and 5. Unconfined compressive strength tests were performed to determine stability of the solidified samples to withstand overburden loads and to determine the increment of strength. The water-binder ratio gives high impact on the increment of the DMS strength. As the water-binder ratio decrease, the DMS strength will increase. Curing days also give effects to strength of the samples. The result shows that strength increase with respect to time.

Keywords: dredged marine soils, solidification, water-binder ratio

1. Introduction

Dredging activities are important to ensure safe navigation of ships and vessels at Ports, Harbors, and navigational channels. Dredging activities generates large volumes of dredged marine soils (DMS). DMS consist of clean gravel and sands or contaminated fine-grained soils. The fine-grained soils may pose high risks to human health and the environment [1][2]. Contaminants in DMS can be stabilized or removed by treatment techniques to make it suitable for reuse [3].

Dredged marine soils are a valuable resource even though not commonly practice. The use of dredged material has a major contribution to make to sustainable development and can reduce the quantities of primary resource needed for activities such as construction and habitat creation. Some countries do already make extensive use of dredged material, for example in Japan in 2003 more than 90% of dredged material was used [4].

Solidification is a method that aims to improve the engineering properties of soil such as soil strength. There are two types of stabilization that are commonly used nowadays that are mechanical stabilization and chemical stabilization. Soil stabilization involves the use of stabilizing agents or binder materials in soft soils to improve its geotechnical properties such as compressibility, strength, permeability and durability. The components of stabilization technology include soils and binders. The binders used normally are cementitious materials[5]. The factors that affect the physical properties of mixing of soil-cement are including the soil type, quantity of cement, degree of mixing, curing time and dry density of the compacted mixture[6].

Solidification binders are materials that form cementitious composite materials when in contact with water or in the presence of pozzolanic minerals that reacts with water. The material used for cementitious material is also known as binder. The commonly used binders are cement, lime and fly ash [5]. Ordinary portland cement (OPC) is a mechanical additive that can be used for soil solidification. OPC is a common type of fine powdery cementitious building material. When mixed with water and sand (or gravel) it turns into masonry mortar (or concrete). After a series of complex internal reactions (hydration), the mixing will sets like a stone.

Bottom ash is produced as a result of burning coal in a dry bottom pulverized coal boiler. It consists of non-combustion materials. Raw bottom ash is a granular material that consists of a mix sand, stone, glass, porcelain, metals, and ash from burnt materials. The non-combustion material from a dry bottom boiler consists of 20 % of bottom ash. Generally, bottom ash is a porous, glassy and is dark gray material with a grain size similar to that of sand or gravelly sand.

Successful modern soil stabilization techniques are necessary to assure adequate subgrade stability, especially for weaker or weaker soils [7]. The increase of cement content and curing time caused significant improvement of unconfined compressive strength as well as stiffness of the treated clay [8].

2. Materials and Methods

2.1. Materials

Two types of fine-grained dredged marine soils (DMS) were used in for this study. The characteristics of DMS samples were shown in Table 1. The first DMS sample used in this study was derived from Marina, Melaka. According to Unified Soil Classification System (USCS), the DMS was classified as high plasticity clay (CH). The second DMS sample was derived from Tok Bali, Kelantan. This soil was classified as low plasticity silt (ML).

Table 1: Physical and Chemical Properties of Dredged Marine Soil

Properties	**Marina**	**Tok Bali**
Moisture content (%)	142.97	92.23
Liquid limit (%)	65.00	36.90
Plastic limit (%)	50.46	25.83
Plasticity index (%)	14.54	11.07
Particle density (%)	2.56	2.41
Loss on ignition	9.49	4.78
pH	8.32	8.51
Soil classification	CH	ML

** CL = Highly plasticity clay ML = Low plasticity silt

The binders used in this study were ordinary portland cement (OPC) and bottom ash (BA). Portland cement was used as cementing agent in this study. OPC used in this study is Portland Fly Ash cement with a high-quality silica rich coal fly ash. Type II OPC was used in this study. Bottom Ash (BA) was used in this study in order to reduce the usage of cement in solidified soils. Bottom Ash was obtained from Tanjung Bin, Johor. Table 2 summarised the properties of the binders.

Table 2: Properties of Binders

Properties	**Binders**	
	Cement (OPC)	**Bottom Ash**
Moisture content (%)	Free from moist	Negligable amount of moist
Particle density	1.26	2.30
pH	12.35	9.17

2.2. Methods

The original DMS sample was mixed thoroughly by using the mixer and stored for 24 hours to ensure the sample was homogenous. While cement, fly ash and bottom ash was dried in oven to ensure moisture free and kept at tight container. The amount of DMS that will be mixed with the binders was calculated based on water-binders (water-cement) ratio. Calculation for the amount of binders (OPC and BA) for each mixture was calculated from mass of dry sample and moisture content of the sample. The water binder ratios of the samples are 1, 3 and 5. Amount of OPC and BA are different based on the ratio calculation. Table 3 show the percentage amount of the OPC and BA used. Even though the DMS samples have different moisture content, the strength of admixed samples is identical as long as water/binder ratio is the same.

Table 3: Percentage of amount of OPC and BA

Water-binders ratio	Percentage of Cement (%)	Percentage of Bottom Ash (%)
1	100	0
3	75	25
5	50	50
	25	75

The mixing of DMS with binder was done after DMS was stored for 24 hours. All of DMS samples were then mix together with the binders at a time. The mixture was first mixed using hand then proceeds with food mixer for 5 minutes. The steps were repeated until all cement and bottom ashes were fully mixed with DMS. The test used in this study is unconfined compression tests (UCS). Unconfined compression test was conducted according to BS 1377-7:1990, Clause 7. The sample was then compacted in three layers inside cylindrical split mould. The cylindrical mould used is 38 mm diameter and 76 mm height. After finished the moulding, the weight, diameter and height of the samples was measured. The samples were then wrapped with the plastic wrapper to ovoid the loss or gain of the moisture content. The samples then stored in plastic container and air cured at room temperature (25 ± 5°C) for 3, 7, 14, 28 and 56 days.

3. Result and Discussion

Unconfined compressive strength tests were performed to determine stability of the solidified samples to withstand overburden loads. Other than that, it is used to determine the improvement in strength characteristics. The degree of reaction between soil-binder mixture and hardening rate also can be predicted from unconfined compressive strength test. Figure 1 show the effect of curing day on unconfined compressive strength based on water-binder ratio (w/b). The water-binder ratio gives high impact on the increment of the DMS strength. As can be seen in Figure 1, the sample with w/b=1 has the highest strength. For w/b=1 with 100% of OPC, the graph can be seen increase rapidly starting day 3 and stagnant after day 14 until day 56. The same increment can be seen for sample w/b=1 with 75%OPC + 25% BA and for sample with 50%OPC + 50%BA. For the 25%OPC + 75%BA, the sample increase continuously.

For w/b=3, the sample with 100% of OPC, 75%OPC + 25% BA, 50%OPC + 50%BA and 25%OPC + 75%BA have slightly increase from day 3 until day 56. From the pattern of these three graphs it can be estimated that, the strength will be increase even after 56 days. Although the strength of the sample with w/b=3 is lower compared to samples with w/b=1, but it is good enough for solidified sample. As for w/b=5, the graph shown that the strength increase steadily from day 3. It was observed that, as the water-binder ratio decrease, the strength increase rapidly. The strength of the sample with w/b=1 is too high for solidified sample. It is due to the excess design and not economical since large amount of cement and bottom ash used. The ratio for w/b to the DMS is about 1:1. It is not suitable to be used in construction since it will consume large amount of money.

Curing days also give effects to strength of the samples. The result shows that strength increase with respect to time. As the time increase the strength also increases. Initially the gain in strength in high but it started to level after day 14. As the age of the sample increases, the different in strength of each sample tends to gets smaller. Generally, it can be observed that, longer period of curing time results in greater strength

gain. The improvement of the strength of solidified soils is due to the hardening of the cement. The binders or cementitious materials can stabilized soils and modified their properties. This is due to the cation exchange, flocculation and pozzolonic reactions. Hydration agents in the cement will increase the strength of DMS samples [9].

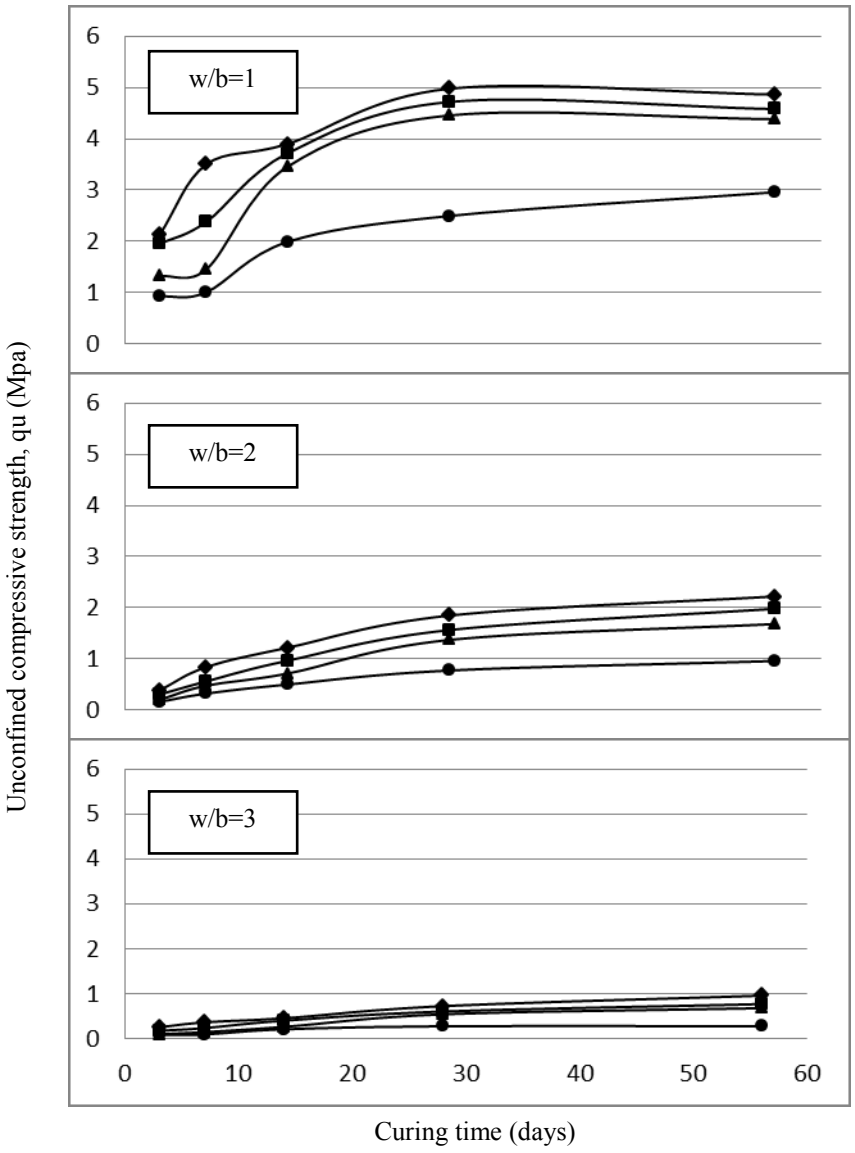

Figure 1: Effects of curing day effects on unconfined compressive strength

4. Conclusion

The water-binder ratio gives high impact on the increment of strength of dredged marine soils (DMS). It was observed that, as the water-binder ratio decrease, the strength increase rapidly. Curing days also give effects to strength of the samples. The result shows that strength increase with respect to time. As the age of the sample increases, the different in strength of each sample tends to gets smaller. Generally, it can be observed that, longer period of curing time results in greater strength gain. The improvement of the strength of solidified soils is due to the hardening of the cement. For further study, more variable on the percentage of the binders should be used.

5. Acknowledgement

Special thanks goes to Jabatan Laut Malaysia and Malaysian Maritime & Dredging Corporation Sdn. Bhd (MMDC) for giving us access to the sampling site. Besides that, we also would like to thanks RACE Vot 1115 and Geran Insentif Penyelidik Siswazah (GIPS) for financial support.

6. References

[1] B. Rekik, and M. Boutouil, "Geotechnical properties of dredged marine sediments treated at high water/cement ratio," Geo-Marine Letters

[2] [8] A. Maher, W.S. Douglass, F. Jafari and J. Pecchioli, "The Processing and Beneficial Use of Fine-Grained Dredged Material: A Manual for Engineers," January 2013.

[3] CEDA, "Dredging and Environment: Moving Sedimenets in Natural System," CEDA information paper, December 2009

[4] CEDA, "Dredged Material as a Resource : Options and Constrain," CEDA information paper, June 2010

[5] G.P. Makusa, Soil Stabilization Methods and Materials in Engineering Practice. Luleå University of Technology, 2012

[6] E.J. Yoeder, Principles of Soil Stabilization: Technical Report, 1957

[7] Tim E.Kowalski and Dale W. Starry, Jr. Wirtgen America, Inc (2007). Characterization and improvement of soils and materials session. Annual Conference of the Transportation Association of Canada Saskatoon, Saskatchewan.

[8] [6] A. H. M. Kamruzzaman, S. H. Chew and F. H. Lee(1998). Engineering behaviour of cement treated Singapore marine clay. Department of Civil Engineering, National University of Singapore, Paper 1190.

[9] A.K. Ahmad Tarmizi, A.L. Ab. Aziz and T. Mohd Raihan, " The Remediation of lead contaminated soil by the solidification/stabilization method" Proceeding of KUiTTHO Research Seminar, Kolej Universiti Tun Hussein Onn, Malaysia 2005

ISBN 979-458-758-3
Proceedings of the 3rd International Conference on the Geohazard Information
Zonation and 5th Seminar & Short Course of HASTAG (GIZ2014-HASTAG5)
Organized by UMSU, HASTAG, USM
Medan, Indonesia, October 20-22, 2014

Landslides Hazard Map in Malay Peninsula by Using Historical Landslide Database and Related Information

Satoshi Murakami [1], Tay Lea Tien [2], Rohayu Bte Che Omar [3], Tomomi Nishigaya [1],
Nazirah Aziza [4], R. Roslan [3], I.N.Z Baharuddin [3], Habibah Hj Lateh [4], and Naoki Sakai [5]

[1] Urban & Civil Engineering, Ibaraki University, Japan
[2] School of Electrical and Electronic Engineering, Universiti Sains Malaysia, Malaysia
[3] Civil Engineering, Universiti Tenaga Nasional, Malaysia
[4] School of Distance Education, Universiti Sains Malaysia, Malaysia
[5] National Research Institute for Earth Science and Disaster Prevention, Japan

Abstract. Recently, slope disaster has occurred in regions around urban area and along highways in Malay Peninsula. The disaster is a major factor that disturbs the sustainable development in the country. It is important to understand high potential regions of landslide and to predict slope disaster based on geotechnical and geological engineering for a sustainable development. Historical data of slope disaster helps us to understand the regional characteristics of landslide and the mechanism. The purpose of this study is to develop a historical landslide database in Malay Peninsula. The database can be available on GIS. The developed historical landslide database has been used with related information to landslide on GIS for investigation of characteristics of landslide in Malay Peninsula. In order to evaluate the hazard of slope failure in the whole Malay Peninsula, the spatial relationships between locations of historical landslides and the related information with slope failure have been investigated. Finally, the locations of historical landslide events are plotted on the proposed hazard map for confirming the applicability.

Keywords: landslide, database, historical record, hazard map, GIS

1. Introduction

Recently, slope disaster has occurred in regions around urban area and along highways in Malay Peninsula [1]. The disaster is a major factor that disturbs the sustainable development in the country. It is important for sustainable development unit to understand high potential regions of landslide and to predict slope disaster based on geotechnical and geological engineering. Historical data of slope disaster helps us to understand the regional characteristics of landslide and the mechanism. Although we can use some reports of regional landslide in Malay Peninsula, there is no available historical database of landslides in whole of the Malay Peninsula.

The purpose of this study is to develop a historical landslide database in Malay Peninsula that can be available to spatial analysis on GIS (Geographic Information System). First of all, historical landside that should be included in a database has been defined because there are enormous of landslide in the whole Malay Peninsula and their types are from small scale to large one. Subsequently, historical records of landslides have been collected from national reports, technical papers, newspapers and so on related to slope disaster. And then, the historical landslides have been digitized as database on GIS. After that, the developed historical landslide database has been used with related information to landslide on GIS for investigation of characteristics of landslide in Malay Peninsula. Finally, in order to confirm the applicability of the landslide hazard map proposed in the previous study, the locations of historical landslide events are plotted on the map.

+ Satoshi Murakami. Tel.: +81-294-38-5174; fax: +81-294-38-5174
E-mail address: murakami@mx.ibaraki.ac.jp

2. Development of Historical Landslide Database in Malay Peninsula

2.1. Definition of landslide in this study

There are enormous of landslide in the whole Malay Peninsula and their types are from small scale to large one. Therefore, historical landside that should be included in a database has been defined as social impact is high. Figure.1 shows a concept of major and minor landslide problems.

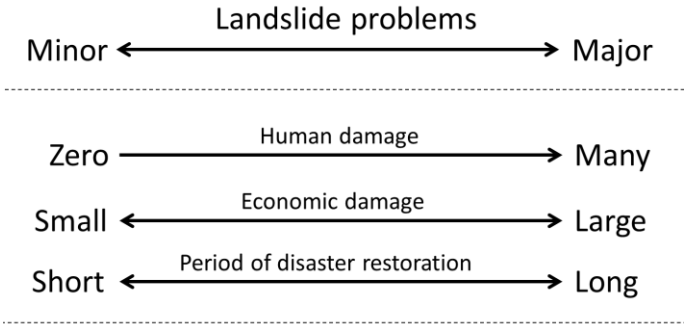

Fig. 1: A concept of major and minor landslide problems

2.2. Development of historical landslide database in Malay Peninsula

In order to develop historical landslide database in Malay Peninsula, historical records of landslides have been collected from national reports, technical papers, newspapers and so on related to slope disaster [2, 3, 4, 5, 6, 7] in the previous study [10].

88 historical landslides have been collected and historical landslide database has been developed. The contents of historical landslide database are location name, city, date, location (a latitude/longitude information), and situation of disaster. However, same events of landslides could not be identified the locations. Locations of 37 landslide events have been identified. All the locations of 37 landslides have been checked by using an aerial photograph and they have been modified from the locations of a stricken area to them of collapsed slopes as shown in Fig. 2.

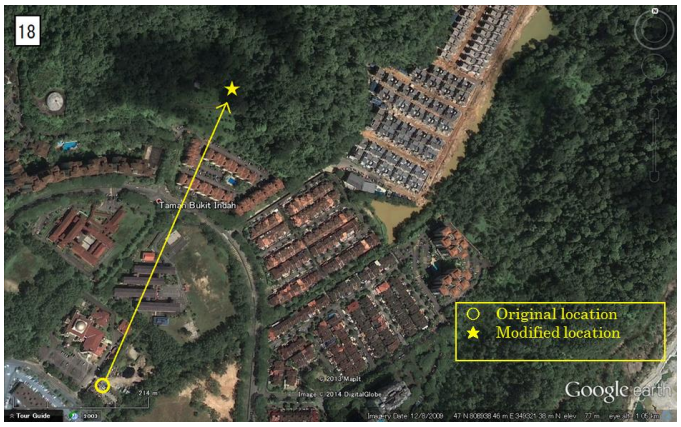

Fig. 2: An example of a modified location of a landslide

In the present study, the historical landslide database has been added with 35 events that are sites at the steel tower of power transmission line and along the road. As the added data have information of locations, it was easy to import to the historical landslide database. Figure 3 shows the locations of historical landslides in Malay Peninsula. Historical landslide map shows most historical landslide events concentrate in Kuala Lumpur, Ipoh, and Cameron Highland. On the other hand, there is less historical data in the middle-eastern and southern side of Malay Peninsula. The reason may be that collected historical data is not enough to cover over the whole of Malay Peninsula. So it is necessary to keep collecting historical landslide data. However, the present historical landslide database informs us some knowledge for understanding landslides in Malay Peninsula as next chapter.

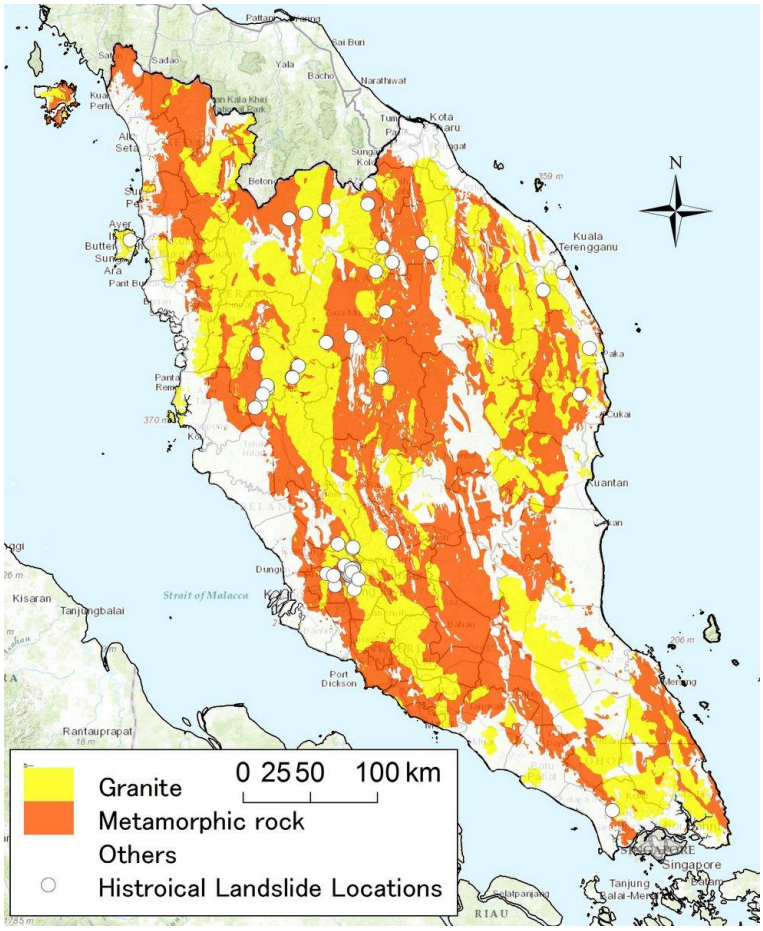

Fig. 3: Locations of historical landslide on a geological map

3. A Spatial Analysis by Using Landslide Database

One of factors of landslide is ground properties of slope. Especially, kind of soils and rocks consisting slope is very important to understand slope failure. Figure 3 shows a geological map and the locations of landslides in the developed historical landslide database. The geological map has been reclassified into granite, metamorphic rocks and the others based on geological maps supplied by USM (Universiti Sains Malaysia) and Geological Survey of Japan.

Granites and metamorphic rocks have a wide distribution in Malay Peninsula as Fig.3. The figure shows that all the locations of historical landslides have occurred on the categories.

Granite has large mineral particles in plutonic rocks and it is generally hard and high density. However, the strength decreases with changing to clay mineral due to the weathering by affected surface water and ground water. In addition, the void between minerals expands and irregular micro-cracks in the rock increase with changing temperature because the component minerals have different coefficient of expansion. Therefore, granite changes to weathered granite by the influence of weather condition. So, strength of granite decreases with progressing the weathering and stability of slope also decreases.

On the other hand, metamorphic rock made from igneous, plutonic and sedimentary rocks by a metamorphism caused by heat and pressure. Metamorphic rock contains schistosity in the structure of rock. It is known that metamorphic rock also affect by the weathering [8]. So, strength of metamorphic rock decreases with progressing the weathering and stability of slope also decreases.

It seems that tropical rain forest climate in such as Malay Peninsula accelerates the weathering of granites and metamorphic rocks [9]. Therefore, the historical landslide database as shown in Fig.3 indicates that it is important to investigate not only topography and weather but also the weathering of rocks for understanding landslide hazard in Malay Peninsula.

4. Applicability of Landslide hazard map in Malay Peninsula

A landslide hazard map has been proposed in the previous study [11]. The mapping method is very simply and uses regional characteristics of kinds of rocks as shown in Fig.3, rainfall and humidity. In order to confirm the applicability of the mapping method, all the locations in historical landslide database have been plotted on the landslide hazard map.

The landslide hazard map and all the locations of historical landslides are shown in Fig. 4. Figure shows that almost all the locations of historical landslides are plotted on the high risk zone. It is necessary to collect more historical landslide events and the related information with high accuracy because the spatial resolution of the map is low. But it seems that the map is available to evaluate landslide hazard.

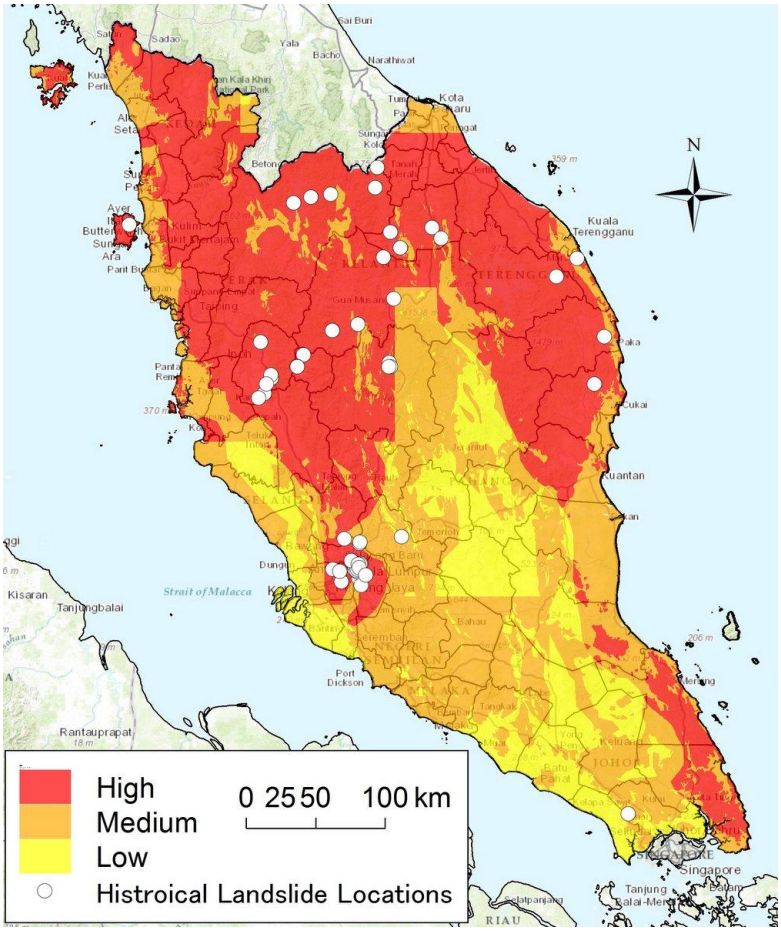

Fig. 4: A landslide hazard map proposed in the previous study and the locations of historical landslide events

5. Conclusion

The purpose of this study is to develop a historical land slide database in Malay Peninsula. The database can be available on GIS. The developed historical landslide database has been used with related information to landslide on GIS for investigation of characteristics of landslide in Malay Peninsula.

The main conclusions are as follows;

(1) A historical landslide database has been developed by collecting from national reports, technical papers, newspapers and so on related to slope disaster. And the database has been upgraded by adding 35 events that are sites at the steel tower of power transmission line and along the road. The historical landslide database can be available to use on GIS (Geographic Information System).

(2) It seems that tropical rain forest climate in Malay Peninsula accelerates the weathering of granites and metamorphic rocks. Therefore, the historical landslide database indicates that it is important to

investigate not only topography and weather but also the weathering of rocks for understanding landslide hazard in Malay Peninsula.

(3) The landslide hazard map proposed in the previous study shows that almost all the locations of historical landslides are plotted on the high risk zone. The proposed map is available to evaluate landslide hazard.

6. Acknowledgements

This research was supported by Japan Science and Technology Agency (JST)/Japan International Cooperation Agency (JICA), Science and Technology Research Partnership for Sustainable Development (SATREPS), and Ministry of Education, Malaysia (Grant number 203/PJJAUH/6711279). Some of historical landslide data have been supplied by Malaysian Public Works Department. Kind help and advice on this study form Mr. Suhaimi Jamaludin (Malaysian Public Works Department) and Mr. Koay Swee Peng (Universiti Sains Malyasia) are also highly appreciated.

7. References

[1] Asian Disaster Reduction Center, *Malaysia Country Report 2008*, http://www.adrc.asia/countryreport/MYS/2008/malaysia2008.pdf#search='malaysia+countory+report+2008' (2013/10/29 references)

[2] H. Sasahara, Landslide disater in Malaysia, *SABO (Organ of Sabo and landslide technical Center)*, 2006, 85: 10-17. (in Japanese)

[3] H. Mizuno and N. Osanai, Typhoon Committee Establish : a flash flood and sediment-related disaster forecasting/warning system in a pilot project area in cooperation with DPP component and spread to other area, *Technical Note of NILIM(National Institute for Land and Infrastructure Management)*, 2010, 570: 42. (in Japanese)

[4] A. Hashim, Malaysia Country Profile, *Malaysian Meteorological Department*, 2010.

[5] EM-DAT: *The OFDA/CRED International Disaster Database – www.emdat.be*, Université Catholique de Louvain, Brussels (Belgium)

[6] T. A. Ooi and W. H. Ting, Report on Some Major Geotechical Disasters in Malaysia, *Proc. International Conference on Geotechnical Engineering for Disaster Mitigation & Rehabilitation*, 2005 :151-164.

[7] N. K. Yeong, Rainfall-Induced Landslides in Hulu Kelang Area, Malaysia, *Final Year Project, UTAR*, 2012.

[8] T. Yamamoto and M. Suzuki, Material Properties and Some Problems of Weathered Sangun Metamorphic Rocks, *J. Japanese Geotechnical Society*, 2005, 53(6): 19-21. (in Japanese)

[9] B. B. K. Huat, Tropical Residual Soils Engineering, *A.A. Balkema Publishers, a member of Taylor & Francis Group plc*, 2004: 15.

[10] S. Murakami, T. Nishigaya, Tay Lea Tien, N. Sakai, Habibah Hj Lateh, and Nazirah Azizat, Development of Historical Landslide Database in Malay Peninsula, *Proc. 2nd IEEE International Symposium on Telecommunication Technologies (ISTT2014)* (submitted)

[11] T. Nishigaya, S. Murakami, and N. Sakai, Hazard Mapping of Slope Failures in Malay Peninsula by Using a Historical Map of Slope Disaster, *Proc. 2nd IEEE International Symposium on Telecommunication Technologies (ISTT2014)* (submitted)

ISBN 979-458-758-3
Proceedings of the 3rd International Conference on the Geohazard Information
Zonation and 5th Seminar & Short Course of HASTAG (GIZ2014-HASTAG5)
Organized by UMSU, HASTAG, USM
Medan, Indonesia, October 20-22, 2014

Effect of additive to the moisture content at different decomposition level of peat

Junita Abd Rahman[1] and Chee-Ming Chan[2]

[1]Faculty of Civil and Environmental Engineering, Universiti Tun Hussein Onn Malaysia, 86400, Batu Pahat, Johor, Malaysia

[2]Faculty of Engineering Technology, Universiti Tun Hussein Onn Malaysia, 86400, Batu Pahat, Johor, Malaysia

Abstract. The decomposition of peat soil is largely influence by its fiber content. The fiber has a high potential to retain water thus make peat soft and tender. The high water content owned by peat soil, is one of the reason of its easily compressible and low shear strength. Hydration water in soil was studied to understand the effect of additive in helping to reduce the water content of peat soil. Mixtures of peat soil with OPC and peat soil with bottom ash (BA) were tested using cone penetration limit method. The effect of BA in controlling peat water content was analyzed and compared with widely known hydration agent, ordinary portland cement (OPC). OPC was found to be effective to minimize the amount of water in peat soil. The hydration reaction between calcium in OPC with water to form C-S-H gel has lessen the amount of water in the mixture. On the other hand, the presence of BA does not show a significant decrease of water in the mixture. However, thixotropic effect was observed at day 3 for mixture of BA and peat soil at all decomposition level.

Keywords: Peat, ordinary portland cement (OPC), bottom ash, cone penetration, moisture content, thixotropic.

1. Introduction

The decomposition of peat soil is largely influence by its fiber content. The less decompose will give a bigger size of fiber and known as fibric peat soil. The fiber has a high potential to retain water thus make peat soil soft and tender. The high water content owned by peat soil, is one of the reason of its easily compressible and low shear strength.

Fabric peat soil (F) generally retained more water, if compared to hemic (H) (moderately decomposed) and sapric (S) (most decomposed) peat soil. Thus, the amount of hydration agent should be applied to the peat soil must be differ. According to Mitchell and Soga (2005), there are three types of water that presence naturally in soil. Based on the binding forces acting on the water molecules in the soil matrix, soil–water can be classified into: 1) hydration water; 2) bound water; and 3) free water. Hydration water is chemically bound water which is an integral part of soil minerals. Bound water refers to those water molecules physically bound in the vicinity of soil particles (double layer) by adhesive forces. Free water is the loosely held water which is controlled by surface tensional forces and gravity. In conventional soil mechanics, pore water in the soil matrix is comprised of bound water and free water.

Hydration water in soil was studied to understand the effect of additive in helping to reduce the moisture content of peat soil. Additive that commonly use in peat soil treatment is ordinary portland cement (OPC). The hydration reaction between OPC and soils leads to initial gain in strength as the cementation product is formed due to drying up of water.

Bottom ash (BA) was introduced in this study to know its potential in controlling peat soil water content. BA is currently a waste product of coal power plant. Therefore, any usage of BA is considered as cost wise. Bottom ash is normally porous and contain high minerals especially quartz. The particle size is varies starting from as big as aggregates to the size of fine sand. The high value of silica and alumina in bottom ash is a key for pozzolan that will takes place with the presence of water and calcium hydroxide. Through x-ray fluoresence analysis, calcium presence in peat soil is around 0.54 % of total mass of dry peat soil. The effect of BA in controlling water content in peat soil is to be compared with widely known hydration agent, OPC.

2. Method

2.1. Peat soil sampling

Three types of peat soil was excavated at a maximum of 1.3 m depth at Pontian, Johor. Peat soil was physically and visually identified its decomposition level according to von post scale [2]. All samples were kept in tight container with plastic cover at the top of the peat soil to prevent moisture loss to the ambient. The containers were then placed in a curing chamber and ready for mixing step. A basic physical and chemical properties test of peat soil were conducted.

2.2. Preparation of sample - Peat soil

Three types of peat soil at different decomposition level namely fibric, hemic and sapric were used in this study. Wet peat was sieved passed through 2 mm sieve size. The peat was mixed thoroughly by hand for about 3 minutes. This was to ensure that only homogenous wet peat was used for mixing. The peat sample was mixed using food mixer at low speed for 1 minute followed by medium speed for another 4 minutes. The mixer was stopped and the material was scraped off the paddle and sides of the bowl before resuming mixing for another 3 minutes. This process was completed in duration of 8 minutes. EuroSoilStab (2002) suggesting 10 minutes of blending to achieved sufficiently uniform dispersion mixture. The peat was ready for mixing process.

2.3. Cement

The cement was first oven dried to ensure moisture free and kept in tight container. The amount of cement was calculated based on dry weight of peat soil.

2.4. Bottom ash

Bottom ash (BA) was gained from local coal power plant at Pontian, Johor. Variety of sizes owned by BA was recorded, starting from aggregates to fine sand. BA was first oven dry at 105^{o}C for 24 hours. BA was then sieve at 2 mm and kept in airtight container. The 2 mm size and below was chosen to be used in this study because the BA still consist of porous materials and some may have pozzolan effect. Furthermore, bigger size may cause misleading of cone penetration reading as the cone might penetrate on the aggregates, not the mixture.

2.5 Mixing

The OPC or BA was added to the soils as per one scoop at a time. The mixture was first mix using hand before continue using food mixer for 5 minutes. The steps were repeat until all OPC or BA was fully mixed with the soils. The hydration process of cement is almost immediately and can last for 24 hours [3]. The mixture must be moulded into specific test specimen right after mixing before the cementation takes place where the sample hardens. The calculation of the mixture was based on the dry weight of soils (Eq. 1);

$$Mass\ of\ dry\ peat = \frac{Mass\ of\ water}{Moisture\ content} \quad (1)$$

It can be reverse calculated to find the mass of wet soils needed for the mixing as (Eq. 2);

$$M_1 = \left(\frac{Moisture\ content}{100} \times M_2\right) + M_2 \quad (2)$$

where;

M_1 = Mass of wet soils
M_2 = Mass of dry soils

The amount of OPC and BA used were based on dry mass of peat soil. The mixture of the samples prepared is as in Table 1.

Table 1 Mixing portion

Fabric, Hemic, Sapric	200 g of dry peat									
OPC, BA	5	10	15	20	25	30	35	40	45	50

2.6. Cone penetration test

Cone penetration test was used in this study to understand the mixture behaviour. The higher penetration recorded will represent the lower stiffness of the sample and vice versa. The samples were filled into cone penetration equipment for cone penetration test. The cone was penetrating into the sample and left for 5 seconds. The reading of penetration in cm was recorded. 3 consecutive reading were taken for each samples.

2.7. Moisture content tests

30 g of samples were taken out from mixture after one hour of mixing and heated at 105 ^{o}C for 6 hours. Samples were then weight. The different between the wet samples and dry samples will be calculated to find its moisture content. The moisture content was measured at Day 0 (D_0) and Day 3 (D_3) of the mixture.

3. Results and discussions

3.1. Basic physical and chemical properties of peat and hydration agent

Basic physical and chemical properties were determined using simple laboratory test as in Table 2.

Table 2 Basic physico-chemical properties of peat and OPC

Properties	Samples					Standard
	Fabric	Hemic	Sapric	OPC	BA	
Moisture content (%)	883	393	602	Moisture free		BS1377 Part 2 :1990
Cone penetration (%)	321	184	255	-	-	BS1377Part 2 :1990
Specific gravity	1.10	1.58	1.18	1.26	2.30	BS1377Part 2 :1990
Fiber content (%)	68.2	37.6	21.0	-	-	ASTM D1997-91
pH	3.27	3.82	3.37	12.3	9.17	BS1377Part 2 :1990
Loss of Ignition	0.97	0.97	0.97	-	-	BS1377Part 2 :1990
Bulk Density	9.20	9.21	9.21	-	-	BS1377Part 2 :1990

3.2 Effect of additive to the peat at different decomposition level

The cone penetration test has been conducted to all types of mixtures. All mixtures were tested for D_0 and D_3. D_0 was chosen to look into the fresh condition before any reactions take place. Horpibulsuk found that fewer than 7 days, only early stage of hydration happens [4]. This is the reason of considering curing times when a study on soil stabilization is to be conducted. While D_3 was chosen as to look into hydration effect if there is any. The patterns of the stiffness of mixture for all three types of peat (Fig.1) with OPC and BA were compared.

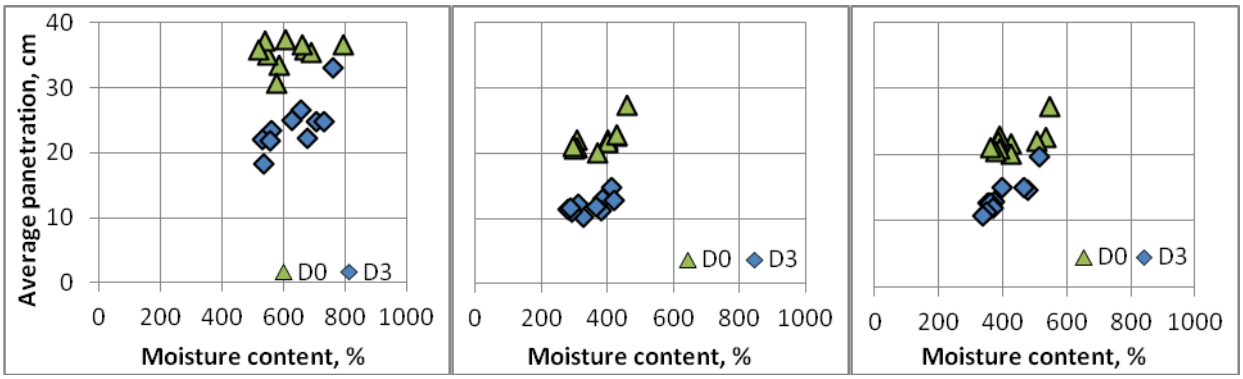

Fabric Hemic Sapric

Fig. 1Average penetration for mixture of peat and OPC

All three types of peat, when mixed with OPC have loss its water content. This is due to hydration process. The main product of hydration is $Ca(OH)_2$ where calcium was gained from the OPC while OH is the part of the water in the soil, particularly peat. The consumption of the water to produced $Ca(OH)_2$ which also

known as C-S-H gel effect the stiffness of the mixture. The higher amount of C-S-H gel present the lower the penetration values.

Generally, increment of 5 % of OPC in the mixture did not give any significant trend. The cone penetration and moisture content reading shows that there are ranges for the mixtures. All treated samples were found stiffer at D_3 if compared with D_0.

For fabric peat, the range of penetration at D_0 was found at 30 - 40 cm while at D_3 it reduces to 17 - 27 cm. The water content for fabric peat was initially high which is 883 %. The high amount of water gives a scatter pattern to the cone penetration test.

Unlike fabric peat, hemic peat shows more uniform reading for all types of mixtures. At D_3, all cone penetration gives typical reading with ranges of 10 - 15 cm of penetration at moisture content of 250 - 450 %. This is mainly because of the low moisture content of hemic peat which is 393 %. Less water can be consumed to form C-S-H gel resulting not much different in reading even for increasing amount of OPC in the mixtures.

Sapric peat, with moisture content of 602 %, shows almost same pattern with hemic peat at D_0. A different in pattern can be seen for D_3 where the penetration of the mixtures has a wide range, which is 6 - 19 cm. The moisture content was found lessen at D_3 with the range of 350 - 550 %. As the initial moisture content of sapric peat is moderate, the water to be consumed by calcium in OPC is there. It is the main key to understand the reason of variety of stiffness recorded by cone penetration test.

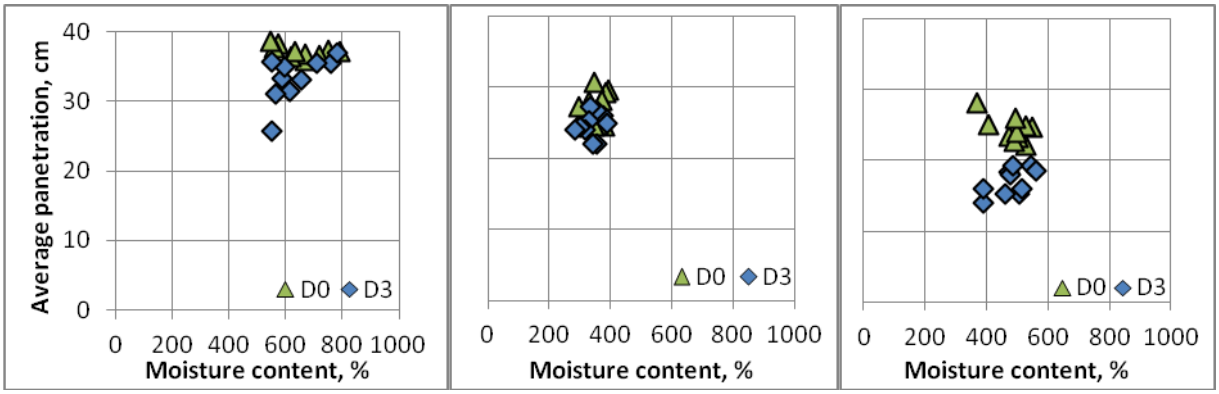

Fabric Hemic Sapric

Fig. 2 Average penetration for mixture of peat and BA

Bottom ash, as a porous material, may provide spaces for water and soil particles to be trapped in. The stiffness of the mixtures (Fig. 2) were found to be affected a bit with the presence of bottom ash but the moisture content of the mixture, even at D_3 was found at almost the same value with reading recorded at D_0.

No hydration reaction occurs that consume the water in the peat. The dehydration process, which is defined as loss of water to environment was also at minimum percentage. The stiffness gained by the mixtures explains the possibility of BA to fill the porous void within peat fiber. Some finer particles of peat also may fill the porous spaces in BA as in Fig. 3. This shows that BA is not a dehydration agent but may act as filler in soil treatment.

The pozzolanic reaction which resulting in strengthening the soil skeleton [5] may occur with the presence of BA in peat but the longer curing times is needed to confirm such reaction which normally 28 days.

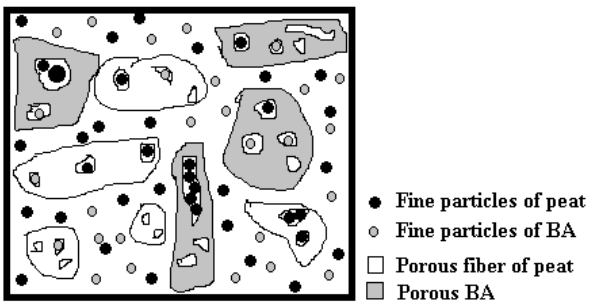

Fig. 3 Illustration of fine particles filling porous spaces in BA and peat

Thixotropy effect was observed in mixture of peat and BA. In geotechnical engineering, thixotropic hardening is, after softening by remolding, the process of time-dependent return to a harder state under constant water content or volume conditions [6]. As the finer particles in peat filling the porous spaces in bottom ash, the cured samples were found higher in density. Self compaction of particles in the mixtures happens due to gravitational force which pushes the less dense water to the upper part of the container (Fig.4). When sample of mixture of peat-BA was open at D_3, water can be observed clearly. A few drops of water was normally comes out easily from the container. This phenomenon is known as bleeding. This answer the stiffer mixture gained on D_3 even though no reaction occurs between peat and BA.

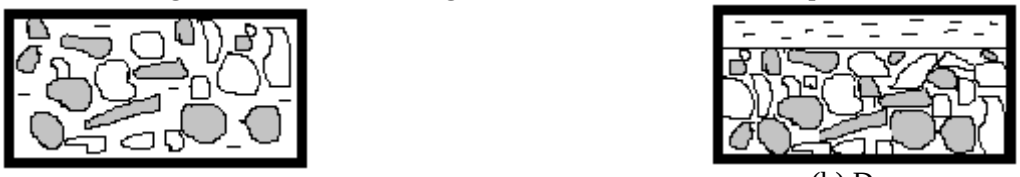

(a) D_0 (b) D_3

Fig. 4 Illustration of peat-BA mixture

4. Summary

The reaction between OPC and hydration water in peat shows that OPC is always the most practical additive for controlling water content during peat treatment. As for comparison, BA is not suitable to be used as dehydration agent but it is good to work as filler. The pozzolanic reaction may happen when peat is mix with BA but the study should be extend to 28 days to confirm the hypothesis.

5. References

[1] J. K. Mitchell and K. Soga, *Fundamentals of soil behavior*, third ed., Wiley, New York. (2005)

[2] L. Von Post and E. Granlund, Södra Sveiges torvtillgangångar I. *Peat resources in southern Sweden*. Sveriges geoliska undersökning. (1926)

[3] O. Alawode and O. I. Idowu, Effects of Water-Cement Ratios on the Compressive Strength and Workability of Concrete and Lateritic Concrete Mixes. *The Pacific Journal of Science and Technology. Vol. 12*. Number 2. 99-105. (2011)

[4] S. Horpibulsuk, *Strength and Microstructure of Cement Stabilized Clay*, *Scanning Electron Microscopy*, Dr. Viacheslav Kazmiruk (Ed.), ISBN: 978-953-51-0092-8, InTech, Available from: http://www.intechopen.com/books/scanning-electron-microscopy/strength-and-microstructure-of-cementstabilized-clay. (2012)

[5] D.T. Bergado, L.R. Anderson, N. Miura and A.S. Balasubramaniam, Soft ground improvement in lowlands and other environments. *ASCE press*, ISBN10 # 784401519. (1996)

[6] Seng, S. and Tanaka, H. Properties of very soft clays: A study of thixotropic hardening and behavior under low consolidation pressure. Soils and Foundations Vol. 52(2). 335–345.(2012)

ISBN 979-458-758-3
Proceedings of the 3rd International Conference on the Geohazard Information
Zonation and 5th Seminar & Short Course of HASTAG (GIZ2014-HASTAG5)
Organized by UMSU, HASTAG, USM
Medan, Indonesia, October 20-22, 2014

Interactions between the survival of *Escherichia coli* and the physico-chemical properties in Malaysia dredged marine soils

Nurasiah Anuar [1], Chee-Ming Chan [2] and Angzzas Sari M. Kassim [3]

[1] Faculty of Civil and Environmental Engineering, UTHM, Parit Raja, 86400, Johor
[2,3] Faculty of Engineering Technology, UTHM, Parit Raja, 86400, Johor.

Abstract. Knowing the survival of *Escherichia coli* (*E. coli*) is important in evaluating the fecal contamination level in dredged marine soils. The significant factors in the survival of *E. coli* in dredged marine soils are important to know because marine soils can act as reservoir for bacteria. The soils physico-chemical properties are likely to affect the survival of bacteria. In fact, the relationship between soil characteristic such as type of soil, particle sizes, pH, moisture content and organic matter were related with the pattern of bacteria concentration. A study was conducted on the physico-chemical properties of marine soils samples dredged from two different dredging sites in Peninsular Malaysia. The results of the present study show that physico-chemical properties of the dredged marine soil measured varied among two dredging sites. The soils with finer fraction, high in pH, moisture content and organic matter appear to have high concentration of bacteria

Keywords: *Escherichia Coli*, Malaysia dredged marine soils, soil physico-chemical properties,

1. Introduction

Dredging is a necessary activity in civilization development which involves the excavation of marine soils from the bottom of waterways. The marine soils excavated are known as dredged marine soils (DMS). Million cubic meters of marine soils was dredged every year. This is due to the continuous demand for maintenance. For instant, the maintenance dredging project at Marina Melaka dredged about 120 000 cubic meter of marine soils [1]. In Malaysia, DMS are often deposited offshore, thoughtless to reuse.

The marine soils could be contaminated by human activities including untreated discharge from near shore population which contains various organic and inorganic chemicals with potential risk on aquatic organism and human as well [2]. The contaminants in the dredged marine soils include oil and grease, pesticides and microbial agents. Among these contaminants, microbial agents are a major problem. Pathogens such as *Escherichia coli (E. coli)* can lead to severe diseases and possible death [3].An epidemiology study revealed the most frequently used indicators of fecal contamination; *E. coli* was better than coliforms [4]. Instead of indicating the presence of fecal contamination, *E. coli* also used to indicate the presence of pathogenic microorganisms [5].

It is important to know that not all water body is the same. Thus, the marine soils physico-chemical properties and microorganisms survival will be different. Several study found that distribution of bacteria were depends on the soils physico-chemical properties. The objectives of the present study were to examine the physico-chemical properties of dredged marine soils and to study the concentration of the indicator bacteria, *E. coli* in the soils.

2. Materials & Methods

Field site description and sampling procedure

The dredged marine soils sample was obtained from dredging work at Marina Melaka and Tok Bali. The soils was dredged at a depth of 3.5m and packed in sampling bags and maintained at 4ºC before analysis. The sampling site were chosen as shown in Fig. 1.The sampling sites were chosen based on schedule of dredging work in East Malaysia by Jabatan Laut Malaysia.

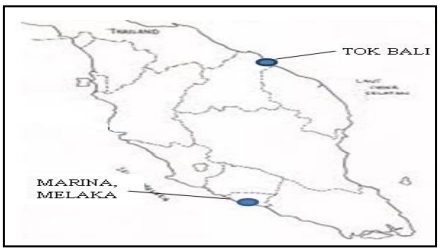

Fig. 1: Location of dredging sites

Marine soils physico-chemical analysis

The marine soils were mixing manually to provide a homogeneity condition. The pH values of sediment were measured by mixing sediment and distilled water in 1:1 ratios. The pH value was taken after 30 minutes by inserting the probe in sediments solution [6]. The pH of samples was measured using the Eutech Instruments probe. The analysis of particle size, organic matter, and moisture content were conducted according to the British Standard 1377:1990.

Bacteria enumeration

Sediment solution was prepared by mixing soils samples with sterilized distilled water at ratio 1:1. Once the supernatant of the sediment solution was retrieved, it was processed for isolation using Chromocult Coliform Agar (CCA). Samples were collected with sterile 1-ml pipettes and enumerated by spread plating onto Chromocult agar. All cultures plates were incubated for 24 hours at 37ºC before colony forming unit were counted [9]. The number of colonies was counted with between 30 and 300 colonies present, utilizing colony counter. The number of colonies with blue to violet were counted and recorded as the Colony Forming Unit per milliliter (CFU/ml)

3. Results and discussions

The marine soils from Marina Melaka and Tok Bali contain a mixture of clay, silt, sand and gravel in different proportions (Table 1). Overall, both soils contain high percentage of clay and low percentage of gravel. However, it appears that Marina Melaka samples has high percentage of silt with low percentage of sand while Tok Bali marine soils have low percentage of silt and high percentage of sand. Oliver [7], found that 65 % of *E. coli* was associated with soil particle less than 2 µm in diameter. *E. coli* was also observed to show greater adhere to silt and clay than sand particles [8].

Table 1: Particle size and soil type of dredged marine soils

	Marina Melaka	***Tok Bali***
Clay (%)	66	59
Silt (%)	18	8
Sand(%)	9	20
Gravel (%)	3	5
Liquid limit (%)	95.80	36.90
Plastic Limit (%)	34.40	25.83
Plasticity index (%)	61.40	11.07
Soil type	Highly plasticity clay	Low plasticity silt

Soil structure depends on the association between soil particles (sand, silt, and clay) in which aggregates of different sizes are formed [10]. According to the Unified Soil Classification System (USCS), the fine-grained soil was classified according to the plasticity. The classification criteria are based on the relationship between Liquid Limit (LL) and Plasticity Index (PI). The relationship was determined from the plastic chart. Based on the USCS, the marine soil from Marina Melaka was placed in highly plasticity clay categories. The marine soil from Tok Bali then categorized as low plasticity silt. According to Sessitich [11], the number of bacteria was most high in the smaller size silt and clay fraction. Therefore hypothetically, DMS from Marina Melaka is expected to have high numbers of *E. coli*.

pH value of the DMS from both sites was found to be in the alkaline range. Yet, the pH value has shown slightly changes in both dredging areas with the value 8.36 and 8.32 (Table 2). According to Rousk [12], bacteria populations in soil decline at low pH level and were growing fastest at pH above 7. Hypothetically, the pH recorded in this present study was suitable for bacteria growth. The moisture content from the Marina Melaka and Tok Bali dredging sites were from 151.79 % and 74.03 %. The Low moisture content may limit microbial activity by lowering intracellular water potential [13]. High number of bacteria was determined in soils with high moisture content [14] suggesting, that Marina Melaka DMS may have a high number of bacteria than Tok Bali samples.

Table 2: pH value and moisture content in marine soils

Properties	Marina Melaka	Tok Bali
pH	8.36	8.32
Moisture content	151.79	74.03

The result shows that organic matter was high in Marina Melaka sample (Table 4.3). Dafini [15] discovered the relation between the textures of sediment with organic matter content. It was reported that higher organic matters was found associated with the finer fraction of sediment. The same trend was also observed in this study where lower organic matter was found in Tok Bali sample which has higher silt particles than the Marina Melaka sample.

Table 3: Organic matter in marine soils

Properties	Marina Melaka	Tok Bali
Organic matter (%)	8.32	4.78

Soils appear to serve as a hospitable environment for bacteria survival due to the availability of organic matter [16]. Soil microorganisms play a significant role in the decomposition of organic matter. It was formed by metabolic action of the organisms [17]. In order to obtain carbon and energy from the sediment organic matter, the bacteria has to degrade organic macro-molecules such as proteins and nucleic acid to simpler substrates. Thus, organic matter provides food for microorganisms in the soil through decay or decomposition of plant and animal residue [18]. Therefore, the high organic matter in marine soils could be the result of high concentration of bacteria.

Table 4: Concentration of *E. coli* in dredged marine soils

Samples	***Bacteria concentration (CFU/ml)***
Marina Melaka	1.70×10^5
Tok Bali	2.00×10^2

Data obtained on the bacteria concentration in marine soils for both locations is shown in Table 4. The higher numbers of *E. coli* was found in Marina Melaka samples. Such differences in the bacteria concentration could be related with the varieties in physico-chemical characteristics among the soils samples. The result of the present study was corresponded with the findings of the other study that reported the influence of soils particle size, pH, moisture content as well as organic matter content with the bacteria concentration level [19]. The soils with finer fraction, high in pH, moisture content and organic matter appear to have high concentration of bacteria.

4. Acknowledgement

The research for this project was financially supported by Ministry of Higher Education under Research Acculturation Collaborative Effort (RACE) grant. We would like to thank Universiti Sains Malaysia (USM) for collaboration and helpful input. We also would like to thank Jabatan Laut Malaysia and Universiti Tun Hussein Onn Malaysia (UTHM) for the technical support.

5. References

[1] Jabatan Laut Malaysia, 2013.

[2] P. Vervaeke, S. Luyssaert, J. Mertens, E. Meers, F.M.G. Tack, & N. Lust, (2003) Phytoremediation propects of willow stand on contaminated sediment: a field trial. *Environmental Pollution*, 126 (2003), pp. 275 – 282.

[3] C. Mulligan, M. Fukue, & Y. Sato. *Sediments Contamination and Sustainable Remediation*. New York: IWA Publishing. 2010

[4] L. Fewtrell, & J. Batram, (2001) Water Quality: Guidelines, standards and health. *World Health Organization Water Series*, pp. 20-21

[5] R.A. Blaustein, Y. Pachepsky, R.L. Hill, D.R. Shelton, & G. Whelan .(2013). *Escherichia coli* survival in waters: Temperature dependence. *Water research*, 47, pp. 569-578.

[6] F.L. Singleton, R. Attwell, S. Jangi, and R.R. Colwell, "Effect of temperature and salinity on *Vibrio Chlorae* growth," Applied and Environmental Microbiology, Vol. 44, pp. 1047- 1058, Nov 1982

[7] D.M. Oliver, C.D. Clegg, A.L. Heathwaite & P.M. Haygarth ,(2007). Preferential attachment of Escherichia coli to different particle size fraction of an agricultural grassland soil. *Water, Air, Soil Pollution*, 185, pp. 369-375.

[8] A.K. Guber, Y.A. Pachepsky, D.R. Shelton, & O. Yu, (2007). Effect of bovine manure on fecal coliform attachment to soil and soil particles of different sizes, *Applied and Environmental Microbiology, 73*, pp. 3363-3370.

[9] M.A. Arshad, P. Bakar, and M. Samingin, " Integration of fisheries into coastal area management: Case of Semerak Lagoon,"

[10] Tisdall J.M. & Oades J.M. (1982). Organic matter and water stable aggregates in soils, *Journal of Soil Science,33*, pp. 141-163.

[11] Sessitch A., Weilharter A., Gerzabek M.H., Kirchmann H. & Kandeler E. (2001). Microbial population structures in soil particle size fractions of a long-term fertilizer field experiment, *Applied and Environmental Microbiology*, 67(9), pp. 4215-4224.

[12] Rousk J., Brookes P.C. & Baath E. (2009). Contrasting soil pH effects on fungal and bacterial growth suggest functional redundancy in carbon mineralization. *Applied and Environmental Microbiology*, 75(6), pp. 1589-1596.

[13] Stark J.M. & Firestone M.K. (1995). Mechanisms for soil moisture effects on activity of nitrifying bacteria. *Applied and Environmental Microbiology. 61(1),* pp. 218-221.

[14] Stres B., Danevčič T., Pal L., Fuka M.M., Resman L., Leskovec S., Hacin J., Stopar D., Mahne I. & Mandic-Mulec I. (2008). Influence of temperature and soil water content on bacterial, archaeal and denitrifying microbial communities in drained fen grassland soil microcosms. *Federation of European Microbiological Societies, 66*, pp. 110-122.

[15] Dafini M., Ramya K.D., Jimly C.J. & Rosamma P. (2013). Heterotrophic bacterial and fungal diversity in the inner shelf sediments of central west coast of India. *Advance in Applied Science Research, 4(4),* pp. 490 – 500.

[16] Alam M.W. & Zafar M. (2013). Spatial and temporal variation of *Escherichia coli* in water and soil with relation to water parameters at the estuary of Karnafuly River, Bangladesh. *Journal of Bacteriology Research, 5(1),* pp. 1-8.

[17] Mirsal I.A.. Soil Pollution: Origin, Monitoring & Remediation. 2nd Ed.German: Springer. 2008

[18] Arnosti C., Jorgensen B.B., Sagemann J. & Thamdrup B. (1998). Temperature dependence of microbial degradation of organic matter in marine sediments: polysaccharide hydrolysis, oxygen consumption, and sulfate reduction. *Marine ecology progress series, 165,* pp. 59-70.

[19] Hossain M.Z., Aziz C.B. & Saha M.L. (2012). Relationship between soil physico- chemical properties and Total Viable bacteria counts in Sunderban Mangrove Forests, Bangladesh, *Journal of Biological Science*. 21(2), pp. 169-175.

ISBN 979-458-758-3
Proceedings of the 3rd International Conference on the Geohazard Information
Zonation and 5th Seminar & Short Course of HASTAG (GIZ2014-HASTAG5)
Organized by UMSU, HASTAG, USM
Medan, Indonesia, October 20-22, 2014

Determination of Landslide Trigger Points by using Infinite Slope Stability Chart

Mohammad Radzif Taharin, Fauziah Ahmad, and Ahmad Shukri Yahaya

School of Civil Engineering, Engineering Campus,
UniversitiSains Malaysia,
14300 NibongTebal, Pulau Pinang, Malaysia

Abstract. The objective of the research is to determine the landslide trigger points in Kundasang, Sabah. Then the factor of safety (FOS) was developed by using the groundwater:landslide depth ratio. A set of data from two different sites in Kundasang were collected from the site investigation report. There are three main stages in determining the landslide trigger points.The first stage is to determine the location and coordinate of each boreholes from the two different sites in Kundasang. The second stage is to obtain descriptive statistics of the geotechnical characterization which includes internal angle of friction (Φ'), cohesion (c'), and groundwater level (m). The third stage is to determine the factor of safety of landslide by using Strength to Slope Ratio (SSR) in Infinite Slope Stability Charts. Boreholes with high groundwater level will be selected due to the criteria in the Infinite Slope Stability Charts. Results will be determined by the FOS value, 1.

Keywords: Groundwater level, Slope Stability, Factor of Safety.

1. Introduction

Sabah is located at the north of Borneo Island, East Malaysia and adjacent to another state in Malaysia, which is Sarawak, and close to two other countries, which areIndonesia (Kalimantan) and Brunei. The area of the Sabah state is 73,620 km^2. Kundasang is located at the toe of the Mount of Kinabalu, which is the highest peak in South East Asia, and part of the Crocker Range, and also the connecting road between west coast and east coast of Sabah. Due to its popularity as a tourist attraction area, the development of holiday resorts has been very rapid in Kundasang area. However, due to the landslide occurrence, the development needs to be planned properly to avoid any unnecessary losses due to the landslide. In most of the landslide cases in Malaysia, clay content has been one of the major factors. The unique of this Kundasang area, is that the clay content is very low, compare to other types of soil. And groundwater level is quite high at the certain area.

Based on the previous study, Farooqi et al.(2005) presented a correlation of how clay can be determined as a major factor of the landslide in Batu Feringghi, Penang. The angle of internal friction is correlated with cohesion, which showed that relationship between these two parameters in positive-negative relationship. However, in the area, which clay existence is very minimal and the cohesion is zero, this relationship could not be used to describe the factors of landslide event, such as in Kundasang. Due to the high groundwater level, minimal percentage of clay existence and zero cohesion value, a simple method need to be adapted in order to determine which are the points that have a very high possibility to trigger the landslide (Das, 2002). Conforth (2005) has developed a chart for infinite slope analysis for slope stability, where the landslide:groundwater ratio (h:z) is emphasized as the main factor for the charts, which can also provide the slope angle (β) value, before determining the factor of safety (FOS) value. The unique of this chart is that the failure value of FOS is 1. Any FOS value, which is approximate to 1 is considered the less safe area.

This study aims to determine the points of boreholes in the studied area, which has potential to trigger the landslide in Kundasang, so in the future, engineers can use this method to determine which area need to have more priority to avoid landslides.

+ Corresponding author. Tel.: +6088320000 ext 3099; fax: +6088320348.
E-mail address:radzif1@gmail.com.

2. Methodology

The data was obtained from 24 boreholes which were collected from two sites around the area of Kundasang in Sabah. The information contained in the report that will be used in the research are locations, description of soils, depth of soil and groundwater level.Kundasang is located in the northern part of Crocker Range National Park in Sabah as shown in Figure 1.

Fig. 1: Map of Sabah showing the study location
(Source:enton-1malaysia.blogspot.com, 2010)

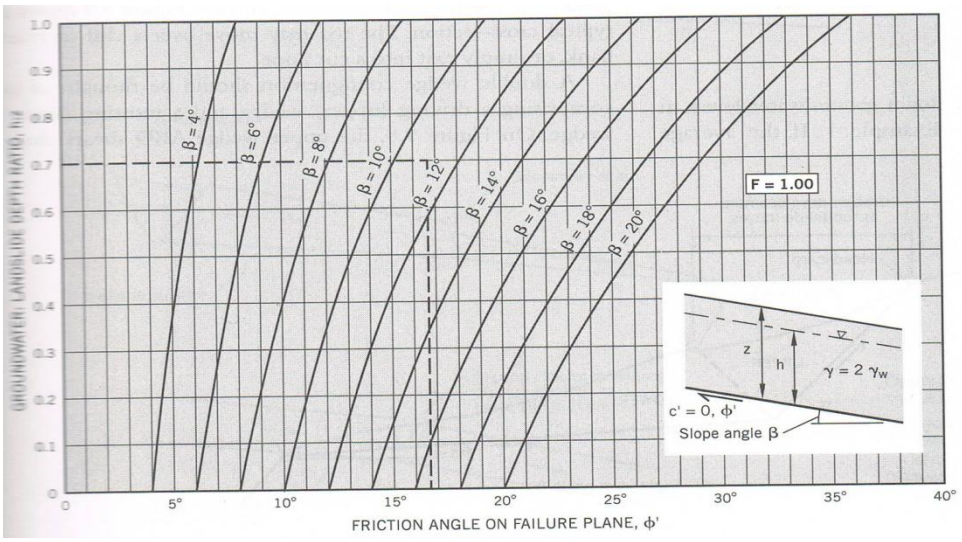

Fig. 2: Infinite Slope Analysis. Determination of Φ' on failure plane based on slope angle β and groundwater/landslide depth ratio.
(Source: Conforth, 2005)

For this study, two landslides area has been chosen to be reviewed for case studies, which are Zen Garden as case study 1 and KM79.9 as case study 2. Area with high groundwater level is more likely to trigger the landslides (Cho, 2010). In this research, the boreholes with the higher groundwater level were chosen as a landslide trigger points, due to the criteria in The Infinite Slope Analysis chart (Fig. 2), which shows the groundwater: landslide depth ratio (h:z) can be used to determine the slope angle β, when the slope failure occurred. This charts can also been use for determining the angle of internal friction, Φ' at the failure area, given the slope angle, β and the h:z ratio were provided.

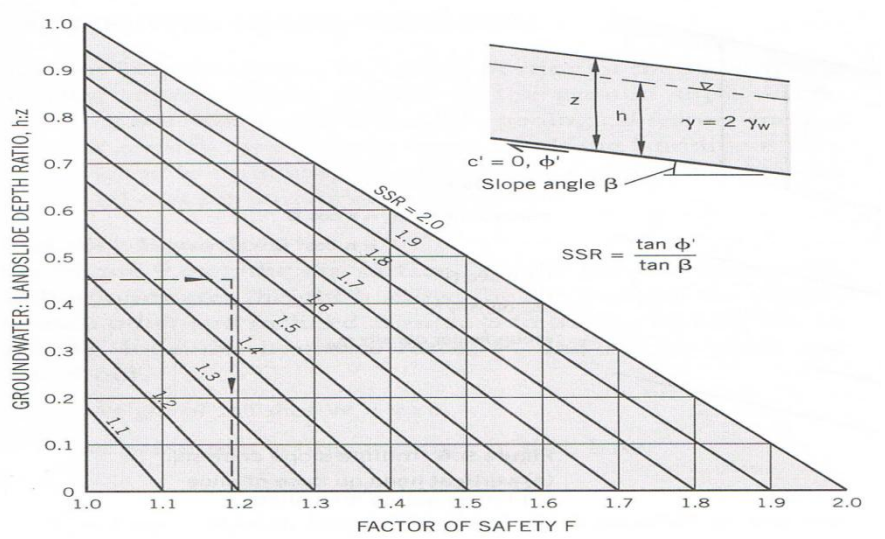

Fig. 3: Infinite Slope Analysis. Determination of factor of safety F for known groundwater:landslide depth ratio (h:z) and known shear strength:slope inclination ratio (tan Φ'/ tan β).

(Source: Conforth, 2005)

For this case study, the slope angle β could be determined since the groundwater level and the internal angle of friction, Φ' are known. Only boreholes with increase value of groundwater level will be chosen due to the h:z ratio to be used in both charts (Rao, 2012). Value of β is obtained to show when the slope fail (F = 1).

In order to cross validate this value, the second Infinite Slope Analysis chart (Fig.3) can be used. This chart can be use to determine the slope factor of safety by h:z ratio and Strength-Slope Ratio (SSR), which can be obtain by inserting theΦ' andβ value for determination by Equation (1):

$$SSR = \frac{\tan \Phi\prime}{\tan \beta} \qquad (1)$$

With the SSR value and h:z value, factor of safety, F, could be determined to confirm the value of β, which was obtained from Fig.2.

3. Results and discussions

The analyses are done using the descriptive statistics to get the typical values that represent the study area. Figure 4 and Figure 5 below show the summary of the descriptive statistics for all boreholes in Kundasang.

In both figures (Fig. 4 and Fig. 5), the chart is showing the depth of the boreholes from the ground surface, and the groundwater level from the bedrock. Note that only few boreholes were filled with groundwater, and the level is different from one to another. Reduced level is showing the ground surface heights from the sea level.

From Fig. 4, only three boreholes that have groundwater level from the bedrock, which are BH1, BH7, and BH11.Since BH11 is been determined as rock, only data from BH1 and BH7 is considered. These data is shown in Table 1 before proceed with the charts. And the cross-validated data is shown in the Table 2. From Fig.5, data from ABH2 and ABH4 were chosen and both of these boreholes went through the same process. The data is shown in Table 3before using the first chart, andthe cross-validated data is shown in the Table 4.

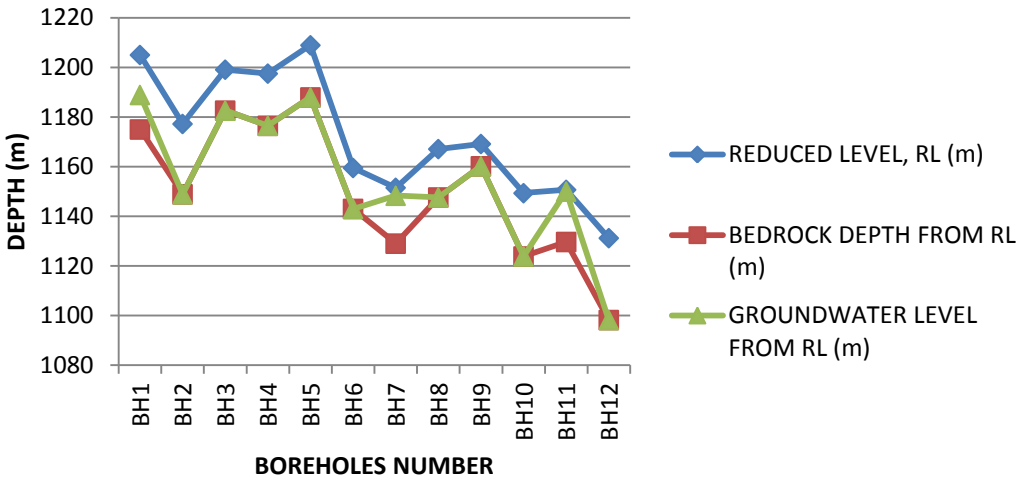

Fig. 4: Boreholes number and depth at Zen Garden (Case study 1)

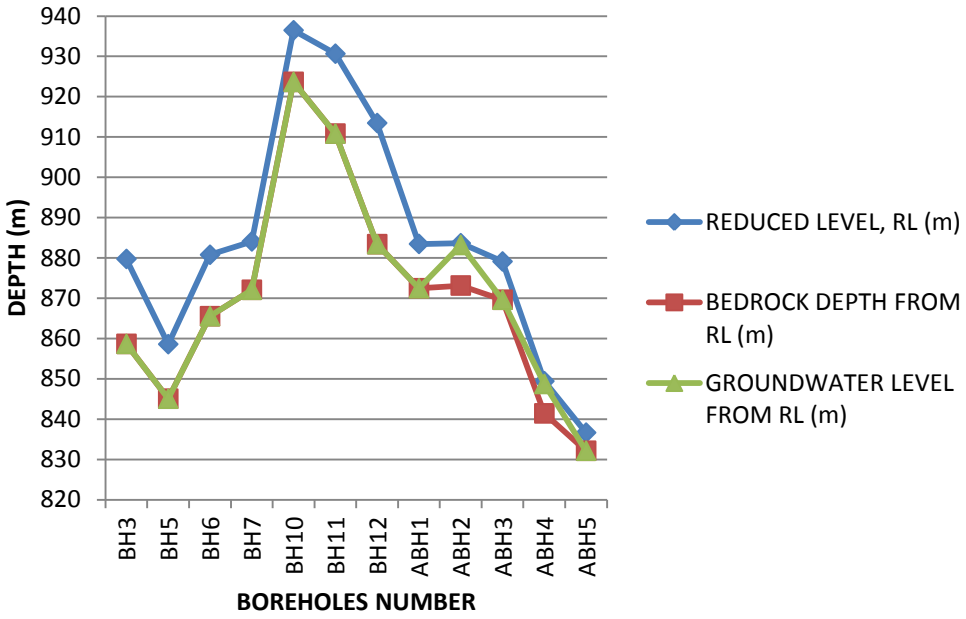

Fig. 5:Boreholes number and depth at KM 79.9 (Case study 2)

Table 1: Properties of boreholes selected in Zen Garden

Boreholes	Borehole Depth, h (m)	Groundwater Level, z (m)	h:z ratio	Angle of Internal Friction, Φ' (°)	Slope Angle, β (°)	Factor of Safety, F
BH1	30	13.9	0.463	18.98	15	1
BH7	22.5	19.3	0.858	22.78	13.5	1

After obtaining the β values, the cross check could be done by determining the SSR value, and obtain the factor of safety, F through the second chart in Fig. 3.

Table 2: Crosscheck the factor of safety, F by using the chart in Fig. 3

Boreholes	h:z ratio	SSR value	Factor of Safety, F
BH1	0.463	1.28	1.01
BH7	0.858	1.75	1.01

Table 3: Properties of boreholes selected in KM79.9

Boreholes	Borehole Depth, h (m)	Groundwater Level, z (m)	h:z ratio	Angle of Internal Friction, Φ' (°)	Slope Angle, β (°)	Factor of Safety, F
ABH2	10.5	10.05	0.957	11.38	6	1
ABH4	8	7.3	0.913	10.58	5.8	1

Table 4: Crosscheck the factor of safety, F by using the chart in Fig. 3

Boreholes	h:z ratio	SSR value	Factor of Safety, F
ABH2	0.957	1.91	1.01
ABH4	0.913	1.84	1.01

4. Conclusion

The research is to analyze the connection between the elevation of groundwater level and the factor of safety at slope. These are based on site investigation reports of project developments done during recent years. The study concentrates on the results of statistical analyses on the data.

The factor of safety on the slopes tends to reduce due to the elevation of the groundwater level (Michalowski, 2009). In one slope area, there are only few boreholes that have elevated groundwater level. However, these few boreholes are the one which could trigger the landslide. The slope angle could be determined through this research and the differences of factor of safety; F value is very small, which is 1%.

With these infinite slope analysis charts, the factor of safety, F and the slope angle, β, could be determine if one of them is available. This research could help the engineers in determining which areas need to be given priority for remedial works in the future.

5. Acknowledgements

The authors would like to acknowledge the Universiti Malaysia Sabah (UMS), Research University Grants of Universiti Sains Malaysia (USM), Jabatan Kerja Raya (JKR) for providing these data for this research.

6. References

[1] Enton-1malaysia.blogspot.com, Maps of Sabah, 2010.
[2] Fauziah Ahmad, Ahmad Shukri Yahaya and Mohd Ahmadullah Farooqi. Characterization and Geotechnical Properties of Penang Residual Soils with Emphasis on Landslides, *American Journal of Environmental Sciences*, 2006, 2(4): 121-128.
[3] D. H. Conforth, Landslides in Practice, 2005, New York; John Wiley and Sons.
[4] B.M. Das. Principles of Geotechnical Design, 2001. New York; Thomson.
[5] N.S.V.K. Rao, Foundation Design, 2012. New York;John Wiley and Sons.
[6] R. L. Michalowski. Critical Pool Level and Stability of Slopes in Granular Soils, Journal of Geotechnical and Geoenvironmental Engineering, ASCE, 2009.135: 444-448.
[7] Sung Eun Cho. Probabilistic Assessment of Slope Stability That Considers the Spatial Variability of Soil Properties, Journal of Geotechnical and Geoenvironmental Engineering, ASCE, 2010.136: 975-984.

ISBN 979-458-758-3
Proceedings of the 3rd International Conference on the Geohazard Information
Zonation and 5th Seminar & Short Course of HASTAG (GIZ2014-HASTAG5)
Organized by UMSU, HASTAG, USM
Medan, Indonesia, October 20-22, 2014

Landslide Hazard Mapping of Penang Island Using Poisson Distribution with Dominant Factors

Lea Tien Tay [1], Mutasem Sh. Alkhasawneh[1] , Habibah Lateh [2], Md Kamrul Hossain [2], Anton Abdulbasah Kamil [2]

[1] School of Electrical and Electronic Engineering, USM Engineering Campus, 14300 Nibong Tebal, Penang, Malaysia
Email: tay@usm.my
[2] School of Distance Education, Universiti Sains Malaysia, 11800 Penang,Malaysia

Abstract—Landslides in Malaysia are mainly triggered by rainfall. However, there are many other landslide causative factors which are related to landslide event in Malaysia. One of them is topographical factor which plays an important role in the landslide susceptibility analysis. This paper presents landslide hazard mapping using dominant factors with Poisson Distribution approach and the study area is Penang Island of Malaysia. Landslide hazard map of Penang Island is generated by taking into account of twenty-two landslide causative factors, including fourteen topographic factors. After considering all twenty-two factors for landslide hazard mapping, the analysis is repeated with removing one factor at one time to determine the dominant landslide-causative factors. Eleven dominant factors are selected from the twenty-two factors. Landslide hazard map was segregated into four categories of risks, i.e. Highly hazardous area, Hazardous area, Moderately hazardous area and Not hazardous area. The maps was assessed using ROC (Receiver Operating Characteristic) based on the area under the curve method (AUC). Landslide hazard map produced by including all 22 factors has an accuracy of 77.75%. By removing 11 irrelevant factors and employing only 11 dominant factors, the generated hazard map achieves better performance with accuracy of 79.20%.

Keywords—Poisson Distribution, Geohazard, Hazard Mapping, Landslide

1. Introduction

Landslide is a geological phenomenon involving movement of mass of rock, deep failure of slopes or debris flows due to soil erosion. Landslides cause infrastructure damages, destroy properties and even claim human lives. Landslides happen rather frequently in Malaysia due to the heavy rainfall especially during annual monsoons mainly known as Southwest Monsoon from late May to September, and Northeast Monsoon from November to March. Damages due to landslides have been high from 2000 to 2009 [1]. It is difficult to predict a landslide event in space and time, however an area may be classified into different categories based on the level of potential hazard due to mass movement [2]. The identification of high risk areas is important in landslide prediction and warning system. Penang Island is chosen as area of interest in landslide hazard analysis in this research work as it has suffered numerous damages due to landslide in recent years. There have been many studies on landslide hazard evaluation using Geography Information Systems (GIS) and various analysis techniques. Probabilistic methods have been applied to achieve promising result in landslide hazard analysis [1], [3], [4], [5], [6]. In this study, Poisson distribution was applied to produce the landslide hazard map for Penang Island.To the best of our knowledge, the Poisson distribution has been used for landslide hazard mapping for the first time in our previous study [7].

+ Corresponding author. Tel.: + (604-5996082); fax: +(604-5941023).
E-mail address: (tay@usm.my).

2. STUDY AREA

The study area chosen in this research work is Penang Island (Fig. 1) due to its frequent landslide occurrences over the years. Penang is one of the 13 states of Malaysia and it is located on the North West of Peninsular Malaysia. It is bounded to the north and east of the state of Kedah, to the south of the state of Perak and to the west of Strait of Malacca. Penang consists of the island of Penang and a coastal strip on the mainland known as Province Wellesley. In this paper, the island of Penang is considered for landslide analysis and mapping. The island covers an area of 285 km^2 and is separated from the mainland by a channel. It is located on the geographical coordinates of $5^o15'N$ to 5^o $30'N$ latitudes and 100^o $10'E$ to 100^o $20'E$ longitudes. Elevation of the terrain ranges from 0 to 820 meters above sea level and slope gradient ranges from 0^o to 87^o. Penang Island is affected by fault lines that run from north to south mainly in the centre of the island. Land-cover of Penang Island consists mainly of swamp, plantation, forest, grassland and urban area. Major vegetation types are forest and fruit plantation. The average amount of rainfall varies from 2254 to 2903 mm annually.

Fig. 1. Penang Island (Google map).

Data collection of Penang Island database was carried out. Topographical, geological and various images of Penang Island were obtained from various government departments in Malaysia including Malaysia Meteorological Department (MMD), Department of Irrigation and Drainage (DID), Department of Agriculture (DOA), Minerals and Geoscience Department (JMG), Department of Survey and Mapping Malaysia (JUPEM) and Penang Geography Information System Center (PeGIS). Landslide occurrence points in Penang Island were also collected and transformed into spatial database for probabilistic landslide susceptibility analysis. Most landslides in Penang Island happened at the mountainous terrain which locates in the center of the island. These landslides consist of mainly shallow rotational debris slides and debris flows. Identification and mapping of a suitable set of landslide-causative facts having relationship with the slope failures requires prior information of the main causes of landslide [8]. In order to apply the probabilistic methods, data sets of landslide-causative factors were collected and developed as spatial database. In this research work, twenty two landslide-causative factors were considered in the computation of the landslides probability. From topographic database, digital elevation model (DEM) was constructed with a resolution of 10-meter. DEM provides the elevation of the study area. Elevation was used to calculate the slope angle, slope aspect, plan curvature, profile curvature, tangential curvature, longitudinal curvature, cross section curvature, general curvature, total curvature, diagonal length, surface area, surface roughness and rugosity [9]. Distance from drainage and distance from road were computed from drainage map and road map each available in digital map respectively. Van Westen et al. [10] suggested that buffer zones for line features, such as, rivers and roads should be set to 50 m. Similarly, distances from fault lines of Penang Island were calculated and divided into 100 m intervals. Soil texture database of the island includes sand, clay and urban land. Land use map consists of 17 classes of land cover and vegetation cover map consists of 14 classes of vegetation types. Geology map, tabling the types of rocks and granites of Penang Island is used as one of the

landslide-causative factors. Rainfall or precipitation is the triggering factors of landslide as it saturates soils and slops away debris and rocks, causing landslides to happen. There are only several rain gauge stations in Penang Island. Therefore, interpolation method was used to prepare the precipitation map. Using 29 years of historical rainfall data (1980-2008), statistical distribution of the accumulated average precipitation was prepared using inverse weight distance interpolation method.

3. Methodology

Thirteen topographical factors were extracted from DEM, i.e. slope angle, slope aspect, plan curvature, profile curvature, tangential curvature, longitudinal curvature, cross section curvature, general curvature, total curvature, diagonal length, surface area, surface roughness and rugosity. Detailed works on the factors extraction can be found in [9]. Besides topographical factors, there are eight landslide-causative factors considered in this research work as well. They are land cover, vegetation cover, distance from road, distance from stream, distance from fault line, geology, soil texture and rainfall precipitation.

Landslide hazard evaluation using probabilistic method has been proven to be very useful in the landslide prediction. The advantages of this method include its high efficiency, low cost, easy implementation and better interpretation of the relationships between landslides and landslide-causative factors. In probabilistic method, the weightages of each factor are calculated based on landslide density for certain classes [11]. These weightages represent the importance of each factor to occurrence of landslide and are used to produce landslide hazard index.

Poisson distribution is a discrete distribution [12]. It is very useful in ecological studies. In this study, Poisson distribution is used for "landslide" which is a geological event. The distribution function for the Poisson distribution is defined as

$$P[X] = \frac{\exp(-\theta) * \theta^{X}}{X!} \quad (1)$$

To estimate probability of one landslide under a characteristic, Poisson distribution is simplified as follows:

$$P[x = 1] = \exp(-\theta) * \theta \quad (2)$$

where $\theta = \frac{Number \quad of \quad Landslide}{Total \quad Number \quad of \quad Observesion}$

Higher value of the probability for a characteristic shows high risk of landslide occurrence.

Landslide hazard index is computed by summing up the probability of landslide in term of Poisson distribution of various factors as follows:

$$LHI = P_1 + P_2 + ... + P_N \quad (3)$$

Where P = Poisson probability value of each factor.

First of all, all the twenty-two factors were considered in the landslide hazard analysis using the Poisson distribution. The landslide hazard map was generated and the assessment was carried out using ROC (Receiver Operating Characteristic) to check the accuracy of this output map. Secondly, the analyses were repeated by removing one factor at one time. The results were assessed with ROC to determine the dominant landslide-causative factors. If the accuracy declines when one particular factor is removed, that particular factor is a dominant factor in landslide hazard analysis. On the other hand, if the accuracy increases when a factor is removed, that factor is irrelevant. The irrelevant factors should be removed. The importance of each factors is ranked based on the accuracies obtained. Finally, the selected dominant factors are used in the probabilistic method for landslide hazard analysis to produce the final landslide hazard map.

4. Verification and Discussion

In our analysis, ROC method was employed to verify the efficiency and accuracy of the landslide hazard mapping. Two assumptions are necessary to verify the maps. First assumption is that landslides are related to spatial information such as slope gradient and slope aspect, and the second assumption is that the future landslides will be affected by triggering factor such as rainfall [13]. Both assumptions are fulfilled in this study. Verification by ROC is carried out by first

sorting the landslide hazard indexes (LHI) in a descending order. The ordered indexes are then divided into 100 classes and set on y-axis, with accumulated 1% intervals on x-axis [1]. The resulting graph shows a line curve that explains how well the model and factors predict future landslide [13]. The accuracies of the prediction models is represented by the area under the curves and it is one of the commonly used accuracy statistics in natural hazard assessments [13].

Table 1 shows the results obtained from the assessment of the landslide hazard map produced using all twenty-two factors and also the maps produced by removing one factors at one time. The accuracies of the landslide hazard maps are presented in percentage. If the accuracy of the produced map decreases when one particular factor is removed, this particular factor is a dominant landslide-causative factor. One the other hand, if the accuracy of the produced map increases by removing a particular factor, that factor is unimportant in landslide hazard analysis. Therefore, those unimportant factors should be removed to produce a hazard map with better accuracy. Based on the results in Table 1, eleven dominant factors are selected and they are distance from distance from drainage, rugosity, height, slope gradient, diagonal length, surface area, distance from fault line, rain, aspect, geology and soil texture. The unimportant factors are plan curvature, tangential curvature, cross section curvature, vegetation, total curvature, distance from road, general curvature, profile curvature, landuse, longitudinal curvature and surface roughness. The factors are arranged in the level of their importance in landslide analysis in Table 1, from the most important factor (distance to drainage) to the two least important factors (tangential curvature and plan curvature)

Table 1: Accuracies of landslide hazard map produced by using all factors and also removing one factor at one time

Number of factors considered	Factors removed	Accuracy (%)
22	None	77.75
21	Distance from drainage	77.34
21	Rugosity	77.49
21	Height	77.53
21	Slope gradient	77.55
21	Diagonal length	77.57
21	Surface area	77.59
21	Distance from fault line	77.61
21	Rain	77.61
21	Aspect	77.66
21	Geology	77.68
21	Soil texture	77.72
21	Surface roughness	77.72
21	Longitudinal curvature	77.78
21	Landuse	77.8
21	Profile curvature	77.81
21	General curvature	77.84
21	Distance from road	77.85
21	Total curvature	77.85
21	Vegetation	77.91
21	Cross section curvature	77.98
21	Tangential curvature	78.00
21	Plan curvature	78.00

Figure 2 shows the accuracies of landslide hazard maps produced with lesser number of factors from 22 to 6. Firstly, the most unimportant factor is removed. It is followed by removing two unimportant factors until 16 factors are removed based on the sequences of their irrelevancy in Table 1. The accuracies increase by removing more unimportant factors. However, the accuracies reduces when important factors are removed too. Landslide hazard map produced using Poisson distribution method achieves an accuracy of 77.75% when all twenty-two factors are considered. When 11

unimportant factors were removed, the final hazard map has best accuracy of 79.20% using Poisson distribution with the eleven dominant factors.

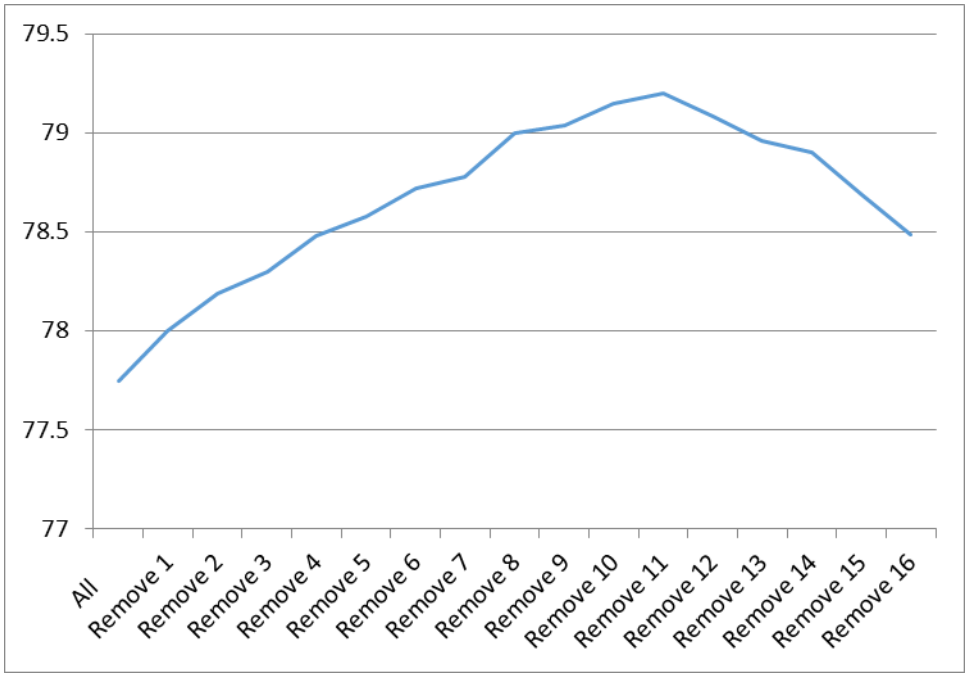

Fig. 2. Accuracies of the landslide hazard maps produced by removing increasing number of factors

Landslide hazard mapping is done by classifying LHI (landslide hazard index) into several categories of risks. In this study, the indexes are classified into 4 groups: Highly hazardous for the highest 10% of the indexes (90-100%), Hazardous for the next 10% (80-90%), Moderately hazardous for the next 20% (60-80%) and Not hazardous for the remaining 60% (0-60%). ROC curves illustrate how well the prediction models fit the data of landslide-causative factors with landslide occurrences to predict future landslides. Figure 3 shows the landslide hazard maps produced using Poisson distribution with all twenty-two factors and with eleven dominant factors. Red color represents "Highly hazardous" areas, green color indicates "Hazardous" areas, blue color represents "Moderately hazardous" areas and "Not hazardous" areas are represented by white color.

5. Conclusion

There are a lot of housing and development in the mountainous areas of Penang Island due to the limitation of flat land. This creates a scenario where landslide warning system is required to warn people of impending landslides on hazardous area. Prediction models such as statistical or probabilistic methods are simple approaches which have been proven to produce promising results in landslide prediction. In this paper, landslide hazard maps of Penang Island were produced with Poisson distribution using twenty-two landslide-causative factors available and also eleven dominant factors. The accuracy of the produced landslide hazard map improves when eleven dominant factors are used in the landslide hazard analysis as compared to the map produced using all twenty-two factors. The produced maps are useful as part of the guidelines in the sustainable land use planning and future development.

Acknowledgments

The authors would like to thanks the sponsorship from Ministry of Education Malaysia (MOE) under FRGS Top-Down research grant. The authors would also like to thank the Minerals and Geosciences Department Malaysia and Department of Irrigation and Drainage Malaysia for the data used in this research.

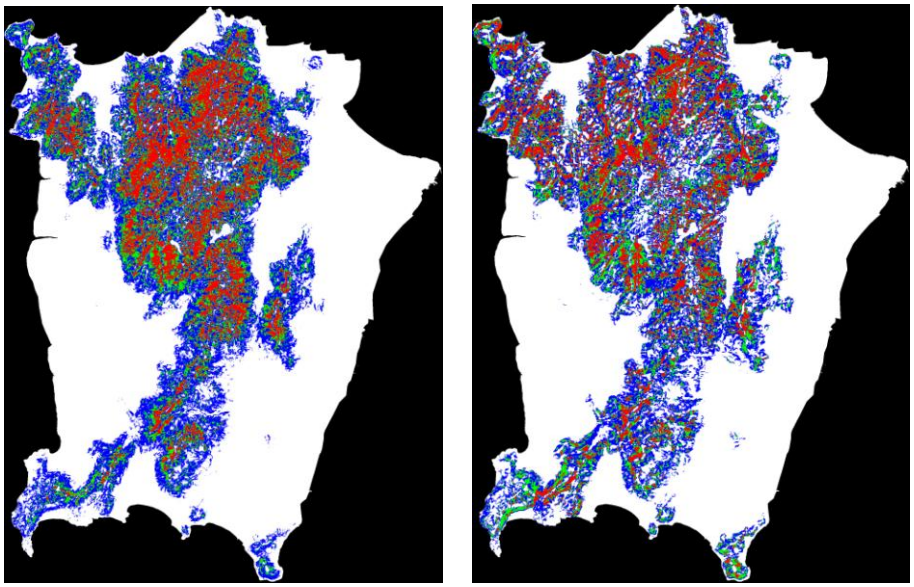

(a) (b)

Fig. 3. Landslide hazard maps produced using Poisson distribution (a) with all twenty-two factors, (b) with eleven dominant factors.

References

[1] B. Pradhan and S. Lee, "Delineation of landslide hazard areas on Penang Island, Malaysia, by using frequency ratio, logistic regression, and artificial neural network models," in Environmental Earth Sciences, Volume 60, Number 5, 1037-1054, 2010.

[2] D. J. Varness, "Landslide hazard zonation: a review of principles and practice," in *Nat Hazards*, 3:63, 1984.

[3] S. Lee and J. A. Talib, "Probabilistic landslide susceptibility and factor effect analysis," in *Environ. Geol*., 47, pp 982-990, 2005.

[4] A. K. Saha, P. R. Gupta, I. Sarkar, M. K. Arora and E. Csaplovics, "An approach for GIS-based statistical landslide susceptibility zoning-with a case study in the Himalayas" in *Landslide*, 2(1), pp. 61-69, 2005.

[5] K. W. Lim, L. T. Tay, H. Lateh, "Landslide Susceptibility Mapping of Penang Island using Probabilistic Method and Logistic Regression", IEEE International Conference on Imaging Systems and Techniques (IST 2011), 17-18 May 2011.

[6] Lea Tien Tay, Habibah Lateh, "Landslide Hazard Mapping Using Probabilistic Approaches: A Case Study of Penang Island, Malaysia", *Caspian Journal of Applied Sciences Research*, 2 (AICCE'12 & GIZ'12), pp. 140-144, 2013.

[7] Lea Tien Tay, Habibah Lateh, Md Kamrul Hossain, Anton Abdulbasah Kamil, "Landslide Hazard Mapping Using a Poisson Distribution: A Case Study in Penang Island, Malaysia", *Landslide Science for a Safer Geoenvironment*, Springer International Publishing, pp. 521-525.

[8] F. Guzzetti, A. Carrarra, M. Cardinali, P. Reichenbach, "Landslide hazard evaluation: a review of current techniques and their application in a multi-scale study, Central Italy," in *Geomorphology*, 31, pp 181-216, 1999.

[9] Mutasem Sh. Alkhasawneh, Umi Kalthum Ngah, Lea Tien Tay, Nor Ashidi Mat Isa, "Determination of importance for comprehensive topographic factors on landslide hazard mapping using artificial neural network", *Environmental Earth Sciences*, DOI 10.1007/s12665-013-3003-x, 2013.

[10] C. J. Van Westen, N. Rengers, R. Soeters, "Use of geomorphological information in indirect landslide landslide susceptibility assessment," in *Natural Hazards*, 30, pp 399-419, 2003.

[11] M. L. Suzen and V. Doyuran, "A comparison of the GIS based landslide susceptibility assessment methods: multivariate versus bivariate," in *Environmental Geology*, 45, pp 665-679, 2004.

[12] Frank A. Haight, Handbook of the Poisson Distribution. New York: John Wiley & Sons.

[13] C. F. Chung, A. G. Fabbri, "Probabilistic prediction models for landslide hazard mapping," in *Photogrammetric Eng Remote Sens*, 65(12), pp 1389-1399, 1999.

ISBN 979-458-758-3
Proceedings of the 3rd International Conference on the Geohazard Information Zonation and 5th Seminar & Short Course of HASTAG (GIZ2014-HASTAG5)
Organized by UMSU, HASTAG, USM
Medan, Indonesia, October 20-22, 2014

Stability Analysis of Masonry Structure in Angkor Ruin Considering The Construction Quality of The Foundation

Ryota Hashimoto [1+], Tomofumi Koyama [2], Mamoru Kikumoto[3], Toru Saito[3] and Mamoru Mimura[1]

[1] Kyoto University, Kyoto, Japan
[2] Kansai University, Osaka, Japan
[3] Yokohama National University, Kanagawa, Japan

Abstract. Angkor ruin, one of the World Cultural Heritage in Cambodia includes many masonry structures in danger of collapse due to geotechnical problems. The foundation of the Angkor monuments is artificial soil embankment, so-called "rammed earth", and its compaction quality affects significantly on the stability of the buildings. In this paper, to investigate the influence of the compaction quality of the rammed earth numerically, stability analyses of an actual building in Angkor (Prasat Suor Prat N1 Tower) were performed with NMM-DDA code, which is a discontinuum based numerical method. In order to treat the different mechanical behavior of rammed earth with different density (void ratio), the subloading modified Cam-clay model, a constitutive model for saturated overconsolidated soil, was also applied. The simulations were performed in two cases changing the initial density (void ratio) of the rammed earth, and then, its effect on the stability of the structure was discussed based on the simulation results.

Keywords: Masonry structure, Angkor, Numerical simulation, NMM-DDA

1. Introduction

Today, Angkor ruin (JSA [1]), a World Cultural Heritage in Cambodia, contains large numbers of the masonry structures in danger of collapse because of geotechnical problems. For instance, many buildings are tilted due to uneven settlement of the foundation ground as shown in Fig. 1. This uneven settlement is often caused by the structural characteristics of the buildings. Fig. 2 is a schematic figure of the foundation of the Angkor monuments. Masonry blocks are stacked on the artificial soil embankment, so-called "rammed earth", directly. Hence, the deformation and/or failure of the foundation due to the building self-weight will cause the deterioration of the upper structure immediately. Since the strength and stiffness of rammed earth depend on its quality of compaction significantly, it can be inferred that the construction condition of the rammed earth affect the stability of the structures.

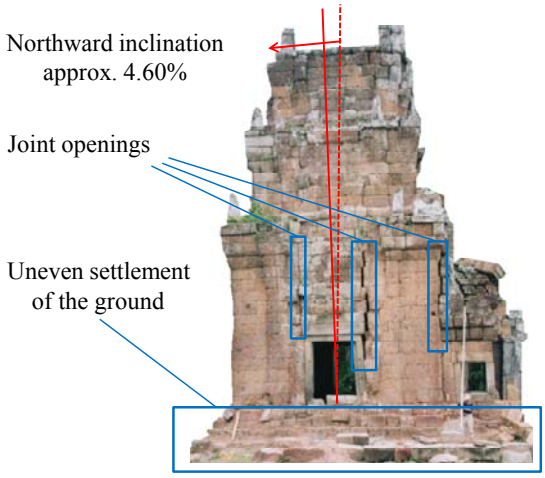

Fig. 1: Prasat Suor Prat N1 Tower in Angkor before restoration (West side view)

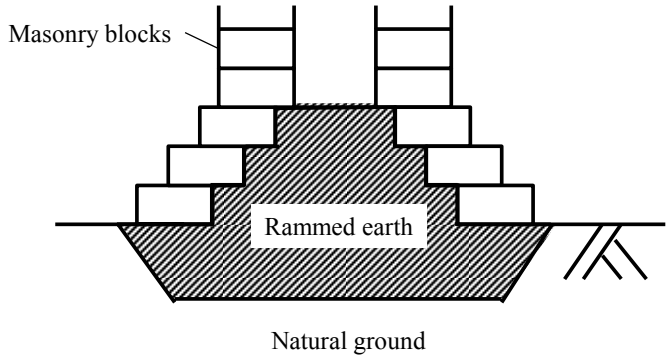

Fig. 2: Schematic diagram of the foundation in Angkor

+ Corresponding author. Tel.: +81-75-383-3306; fax: +81-75-383-3307.
E-mail address: hashimoto.ryouta.57u@st.kyoto-u.ac.jp

In this paper, to investigate the influence of compaction quality of the rammed earth on the stability of the masonry structure, numerical simulation of Prasat Suor Prat N1 Tower in Angkor (Fig. 1) was carried out using NMM-DDA (Miki et al. [2], Hashimoto et al. [3]), a discontinuum based numerical method. The simulations were carried out for two cases with different initial density (void ratio) of the rammed earth, and the differences between the simulation results were discussed.

2. Basic Theory of NMM-DDA

NMM-DDA is a discontinuum based numerical method which was developed combining NMM (Numerical Manifold Method, Shi [4]) and DDA (Discontinuous Deformation Analysis, Shi and Goodman [5]). Similarly to the original DDA and NMM, the formulation of NMM-DDA is based on the principle so-called the minimization of potential energy (Miki et al. [2]). The total potential energy for the whole system can be expressed as:

$$\Pi_{sys} = \Pi_{sys}^{\mathrm{d}} + \Pi_{sys}^{\mathrm{m}} + \sum_{B,i}\sum_{E,j}\Pi_{i,j} \tag{1}$$

The first and second terms on the right side of Eq. 1 are the potential energy for DDA and NMM parts, respectively (which is exactly same as DDA and NMM alone). The third term represents the potential energy for the contacts between a DDA block i and a NMM element j. Based on Hamilton's principle, from the stationary condition of Eq. (1), equation of motion in NMM-DDA can be derived as Eq. 2.

$$\mathbf{M}\ddot{D} + \mathbf{C}\dot{D} + \mathbf{K}D = \mathbf{F} \tag{2}$$

where $\mathbf{M}$ is the mass matrix, $\mathbf{C}$ is the viscosity matrix, $\mathbf{K}$ is the stiffness matrix, and $\mathbf{F}$ is the external force vector. D, $\dot{D}$ and $\ddot{D}$ are the displacement, velocity, and acceleration of DDA blocks and the nodes of NMM elements, respectively. In the process of deriving the stationary condition, the first and second terms of the right side in Eq. (1) are minimized in terms of the displacement variables of the DDA blocks (D^{d}) and the NMM elements (D^{m}), respectively same as DDA and NMM alone. The third term, specific to NMM-DDA, is minimized in terms of both D^{d} and D^{m}. Consequently, in the formulation of NMM-DDA, only defining the potential energy for the contacts between DDA blocks and NMM elements is newly required. The detailed explanations for the theory of NMM-DDA and derivation of the contact sub-matrixes can be seen in the references (Miki et al. [2]). The original NMM-DDA code treats only linear elastic material, however, elasto-plastic NMM-DDA code was also developed by Hashimoto et al. [3].

3. Subloading Modified Cam-clay Model

To evaluate the deformation/failure processes of the rammed earth, a constitutive model for overconsolidated soil should be used. Hashimoto et al. [3] introduced the subloading modified Cam-clay model (Hashiguchi [6]), a elasto-plastic model for overconsolidated soil, into NMM-DDA.

The yield function of the subloading modified Cam-clay model is expressed as follows:

$$f = \frac{\lambda-\kappa}{1+e_0}\left[\ln\left(\frac{p}{p_0}\right) + \ln\left\{1+\left(\frac{\eta}{M}\right)^2\right\}\right] - \frac{\rho_0-\rho}{1+e_0} - \varepsilon_v^p = 0 \tag{3}$$

where λ is the compression index, κ is the swelling index, e_0 is the initial void ratio, p and p_0 are the present and initial mean principal stress, respectively, and η is the stress ratio (=q/p). ρ is the parameter of overconsolidation expressed as follows;

$$\rho = e_{\mathrm{N}} - e \tag{4}$$

where e is the present void ratio, and e_{N} is the void ratio on Normal Consolidation Line under the same stress condition. Thus, when a soil is in overconsolidated state, $\rho > 0$, and in normally consolidated state, $\rho = 0$. ε_v^p is the plastic volumetric strain. Defining the evolution rule of ρ as

$$\frac{d\rho}{1+e_0} = -G(\rho)\left|d\varepsilon_{ij}^p\right| = -G(\rho)\left|\frac{\partial f}{\partial \sigma_{ij}}\right|\Lambda \tag{5}$$

$$G(\rho) = a\rho^2 \ (a\text{: parameter of dissipating overconsolidation}) \tag{6}$$

and considering the associated flow rule and Prager's compatibility equation, elasto-plastic stiffness tensor can be derived.

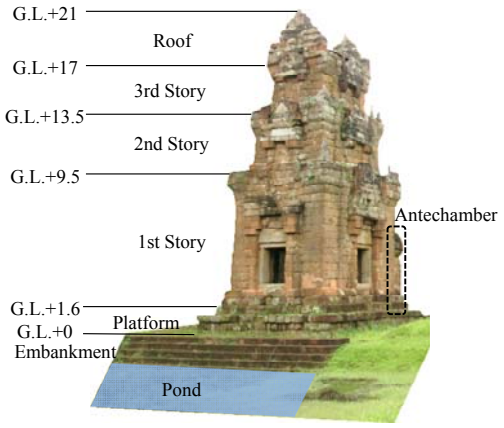

Fig. 3: Outward appearance of Prasat Suor Prat N1 Tower (after restoration)

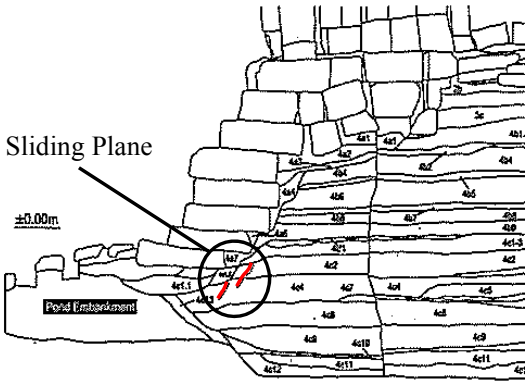

Fig. 4: Trench cross section inside the rammed earth and the observed shear plane

4. Overview of Prasat Suor Prat N1 Tower

In this study, as an objective of the simulation, Prasat Suor Prat N1 Tower was selected. The N1 Tower is a masonry structure in Angkor which had been in danger of collapse due to geotechnical problems, and the restoration project was conducted by Japanese Government Team for Safeguarding Angkor (JSA) from 2002 to 2005. Outlines of the N1 Tower and damages before the restoration are described below.

The N1 Tower consists of the main tower and the antechamber (see Fig. 3). The antechamber faces south and the bathing pond is located to the north of the N1 Tower. The main tower is composed of the platform, three stories (the 1st, 2nd and 3rd) and roof. The main material of the building is laterite blocks and sand stones are partially used. As shown in Fig. 2, the foundation ground of the Tower consists of two parts: natural ground and rammed earth. Natural ground is clayey soil and rammed earth is sandy soil.

The damages before the restoration are summarized as follows (see Fig. 1) (JSA [1], Iwasaki et al. [7]).

- The tower inclined 4.96%/2.84º toward northwest (4.60%/2.63º toward north from west side).
- Some blocks fell down due to the inclination of the tower.
- Some critical joint openings were observed in the upper and lower platform and along the wall of the tower (especially, around the windows).

Above mentioned damages may be caused by uneven settlement of the foundation ground. Therefore, it is necessary to consider the interaction between masonry building and foundation ground for the stability analysis using accurate stress redistribution of masonry blocks. The following issues may be related to the uneven settlement of foundation ground.

- A sliding toward the bathing pond by cutting slope and uneven soil pressure (Fig. 4).
- Stress concentration due to weathered laterite blocks and/or changes of the stress transmission paths.
- Changing mechanical properties of foundation ground due to rain water infiltration and wet-dry-cycle.

Since the N1 Tower is a typical building deteriorated due to the deformation of the rammed earth, it would be an appropriate example to observe the influence of the compaction quality of the rammed earth.

5. Stability analysis of Prasat Suor Prat N1 Tower

5.1. Outline of the Simulation

Fig. 5 shows the numerical model of Prasat Suor Prat N1 Tower (in 2-D, plane strain condition), which was created based on the sketch from west side view after restoration. The masonry blocks, which may possibly collapse during the simulations, were modelled by DDA and the foundation ground which consists of rammed earth and natural ground was modelled by NMM. This enabled to focus on the large displacement of the blocks (include joint openings) and the local distribution of stress/strain in the foundation ground simultaneously. The displacements in both normal and horizontal directions, and only horizontal direction were fixed along the bottom and side edges of the analytical domain, respectively. All masonry blocks were modelled as linear elastic body, and the subloading modified Cam-clay model (Hashiguchi et al. [6]) was applied to the foundation ground (for both natural ground and compacted soil layer). The material properties used for the simulations are summarized in Table 1. These values except the critical state stress ratio M of the natural ground were determined from laboratory tests for soil samples obtained from the site, and M of

the natural ground was set assuming that the internal friction angle $\phi = 30°$. Table 2 shows the joint properties used in the simulations.

Initial stress of whole ground was obtained from the self-weight analysis. Initial void ratio of the natural ground was set assuming the normally consolidated state. In order to investigate the effect of compaction quality, two different initial void ratios of the rammed earth were set (called Case A and B, see Table 3). In Case A, the rammed earth is assumed to be compacted with optimum water content and the value of the initial void ratio is based on the compaction test, and Case B is a looser compaction case.

During the simulations, only the self-weight of the masonry blocks was applied, and the simulations were continued until the displacements of the blocks became stable.

Table 1: Material properties

	Masonry block	Rammed Earth	Natural ground
Constitutive model	Linear elastic	Subloading modified Cam-clay	
Unit weight: γ [kN/m^3]	30	18	18
Elastic modulus: E [kPa]	1.0×10^6	-	-
Compression index: λ	-	0.0580	0.0782
Swelling index: κ	-	0.00484	0.00711
Poisson ratio: ν	0.2	0.3	0.3
Critical state stress ratio: M	-	1.37	1.2
Void ratio on normal consolidation line at p=98 [kPa]: e_{NC}	-	0.700	0.478
Parameter of subloading surface: a	-	25	100

Table 2: Joint properties

	Value
Normal direction penalty stifness [kN/m]	5.0×10^5
Shear direction penalty stiffness [kN/m]	5.0×10^3
Surface friction angle [°]	36
Open-Close criterion	1.0×10^{-5}
Close-Open criterion	1.0×10^{-8}
Assumed maximum displacement ratio	0.001

Table 3: Simulation cases

Case	Initial void ratio of rammed earth	Note
A	0.399	Compacted with optimum water content ratio
B	0.500	Looser case

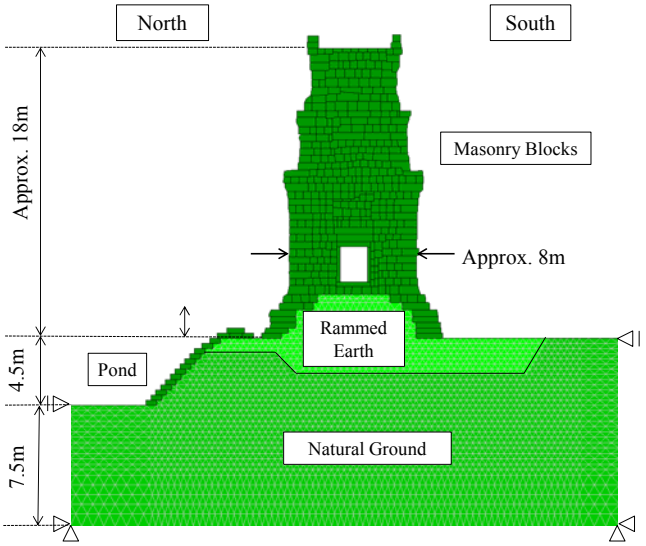

Fig. 5: Analytical domain (2D, plane strain condition)

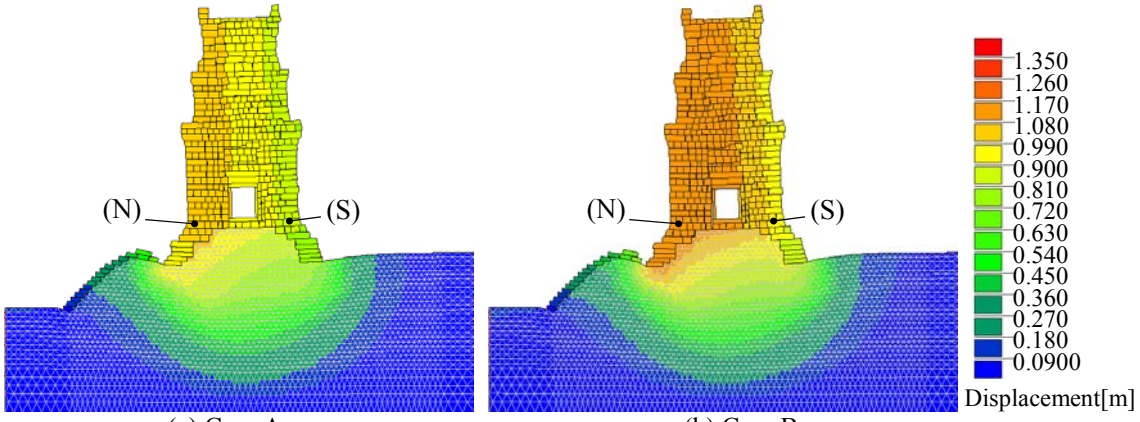

(a) Case A (b) Case B

Fig. 6: Distribution of the vertical displacement at the end of the simulation

5.2. Simulation Results

Firstly, the distributions of the vertical displacement at the end of the simulation in two cases are shown in Fig 6. These figures obviously show the following facts.

- Northern side of the tower settled larger in both cases as observed before the restoration.
- The settlement of Case B (looser case) is larger.

Table 4: Differential settlement and northward inclination of the tower

Case	Differential settlement [m]	Inclination of the tower [%]
A	0.165	2.36
B	0.195	2.76

The differential settlement between the north and south sides of the tower, and the northward inclination of the tower for each case are summarized in Table 4. These values were calculated from the coordinates of block (N) and (S) in Fig. 6 at the end of the simulation. In addition to the settlement itself, both the differential settlement and the inclination of the tower became larger in Case B.

These results imply that the compaction quality of the rammed earth has much influence on the stability of the structure. This means that controlling the compaction quality of the rammed earth during the restoration process is significantly important for the permanent conservation of the Angkor monuments.

6. Conclusions

In this paper, NMM-DDA with the subloading modified Cam-clay model was applied to the stability analyses of Prasat Suor Prat N1 Tower in Angkor. The simulations were carried out in two cases with different initial density (void ratio) of the rammed earth. From the simulation results, the influence of construction quality of the rammed earth on the stability of the structure was investigated. The findings obtained from this study are summarized as follows.

- Inadequate compaction of rammed earth causes the increase of the differential settlement and the inclination of the tower.
- Controlling the compaction quality of the rammed earth is significantly important for the permanent conservation of the Angkor monuments.

In the future, to apply the NMM-DDA to the design process of the restoration method for Angkor monuments, following subjects should be researched.

- Accumulating the data of the mechanical properties of the in-situ soil.
- Coupled stress-flow behavior in the foundation ground such as rainwater infiltration and its effect of mechanical behavior of the tower.

7. Acknowledgement

This work was supported by JSPS KAKENHI, Grant-in-Aid for JSPS Fellows, 26-77. The authors are really grateful to Dr. Shigeru Miki, Kiso-Jiban Consultants Co., Ltd, Dr. Takeshi Sasaki, Suncoh Consultants Co., Ltd., and Dr. Mitsuharu Fukuda, Taisei Geo Tech, for their valuable comments and suggestions.

[1] Japanese Government Team for Safeguarding Angkor (JSA). *Report on the conservation and restoration work of the Prasat Suor Prat Tower*. OGAWAINSATSU Co., Ltd.. 2005.

[2] S. Miki, T. Sasaki, T. Koyama, S. Nishiyama & Y. Ohnishi. Development of coupled Discontinuous Deformation Analysis and Numerical Manifold Method (NMM-DDA). *Int. J. Computational Methods*, 2010, **7**(1): 1-20.

[3] R. Hashimoto, T. Koyama, M. Kikumoto, S. Yamada, M. Araya, Y. Iwasaki & Y. Ohnishi. Stability analysis of masonry structures in Angkor Thom, Cambodia using elasto-plastic NMM-DDA with subloading Cam-clay model. In: *Proc. of the 47th US Rock Mechanics/Geomechanics Symposium*. 2013, paper No.13-362 (CD-ROM).

[4] G.H. Shi. Manifold Method of material analysis. *Trans. the 9th Army Conf. on Applied Mathematics and Computing*, 1991, **92**(1). U.S. Army Research Office.

[5] G.H. Shi & R.E. Goodman. Two Dimensional Discontinuous Deformation Analysis. *International Journal for Numerical and Analytical Methods in Geomechanics* 9. 1985, pp. 541-556.

[6] K. Hashiguchi & M. Ueno. Elastoplastic constitutive laws of granular material. Constitutive Equations of Soils, In: S. Murayama and A.N. Schofield (eds.). *Proc. of 9th Int. Conf. Soil Mech. Found. Engrg., Spec. Ses. 9*, Tokyo. JSSMFE. 1977, pp. 73-82.

[7] Y. Iwasaki, M. Fukuda, K. Nakagawa, A. Akazawa, I. Shimoda & T. Nakagawa. Geotechnical Aspects of the N1 Tower, Prasat Suor Prat, Angkor Thom, Cambodia. *Advanced Materials Research*, 2010, Vol. 133-134: 113-118.

ISBN 979-458-758-3
Proceedings of the 3rd International Conference on the Geohazard Information Zonation and 5th Seminar & Short Course of HASTAG (GIZ2014-HASTAG5)
Organized by UMSU, HASTAG, USM
Medan, Indonesia, October 20-22, 2014

Evaluation of Rainfall Induced Instability of Tumulus Mounds

Mai Sawada[1], Mamoru Mimura[1] and Mitsugu Yoshimura[2+]

[1]Department of Urban Management, Graduate School of Engineering, Kyoto University, Japan
[2]Soil and Rock Engineering Co. Ltd, Japan

Abstract. Rainfall induced instability of a tumulus mound is one of the most serious damages to tumuli. Evaluation of water infiltration and the induced instability of tumulus mounds is an important geotechnical mission for the conservation of tumuli. This paper deals with the evaluation of rainfall infiltration into the unsaturated mound and the induced instability and damage of Kengoshizuka Tumulus. Rainfall induced failure took place in the severely embrittled surface of the mound in the rainy season of 2012. The embrittled layered structure and geotechnical properties of the mound are investigated by in-situ and laboratorytests and considered in the analytical model for the evaluation. The factor of safety in terms of slope stability is calculated using the analytically estimated degree of saturation of the mound and the experimentally obtained strength parameters of the sliding surface. The results of the evaluation quantitatively show the instability of the tumulus mound induced by rainfall.

Keywords:historical geo-relics, slope stability, rainfall infiltration, seepage flow analysis

1. Introduction

Tumuli are tombs for ancient emperors and district rulers constructed in various parts of Japan from the third to the seventh centuries.Tumulus mounds usually consist of densely compacted earth mounds and have chambers for coffins inside. The structure and construction method of a tumulus are characterized by the period and region in which the tumulus was constructed. Some tumuli have cultural heritages such as burial accessories and mural paintings in the chambers. Tumuli have been conserved as historical geo-relics which provide us important historical knowledge.

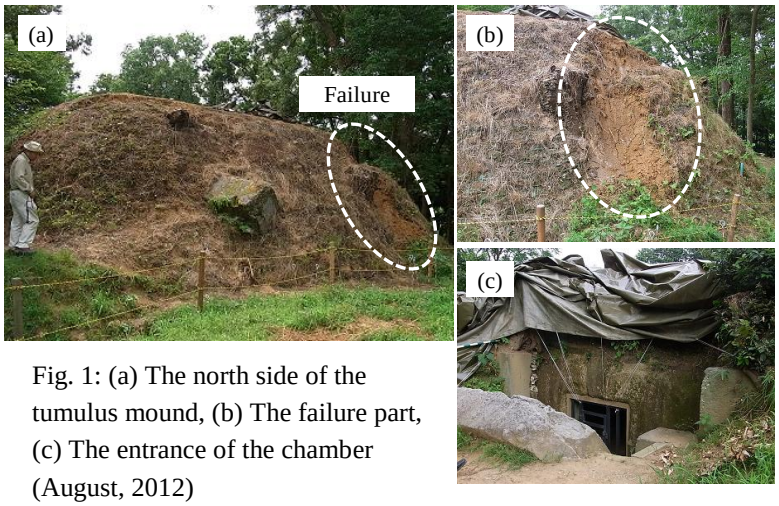

Fig. 1: (a) The north side of the tumulus mound, (b) The failure part, (c) The entrance of the chamber (August, 2012)

Tumuli, however, have been damaged by exposure to natural environment and man-caused destruction such as weathering, earthquakes, tomb robbery, urban development, etc. This paper deals with harmful rainfall infiltration into tumulus mounds which inducesslope failure. The weight of the surface layer of a tumulus mound increases, meanwhile the shear strength of the sliding surface decreases with rainfall infiltration into the mound. These instability factors induced by rainfall infiltration lead to slope failure. Water seeps deeply into the mound through the failure part andthe hydrothermal environment in the chamber changes. Because of this, mural paintings in the chamber are finally damaged by fungi and insects. Evaluation of water infiltration and the induced instability of tumulus mounds is hence an important geotechnical mission for conservation of tumuli.

[+]Mai Sawada. Tel.: +81-75-383-3306; fax: + 81-75-383-3307.
E-mail address:sawada.mai.43u@st.kyoto-u.ac.jp.

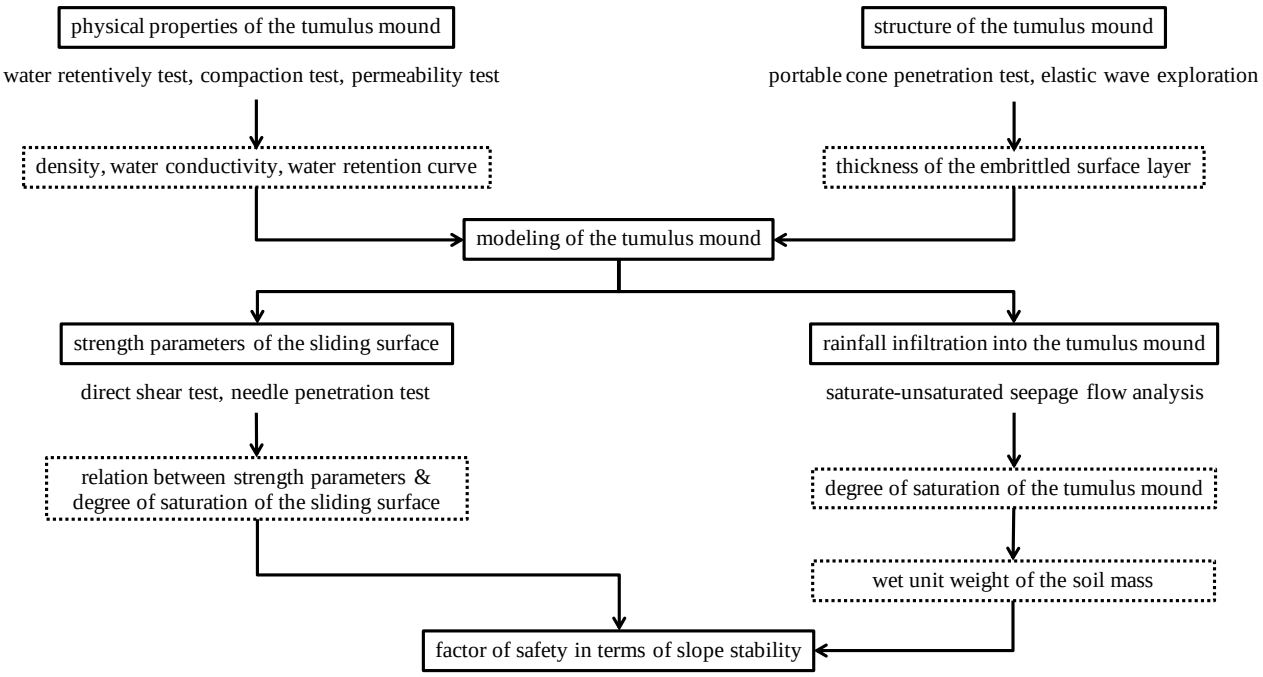

Fig. 2: Procedure of the evaluation of rainfall infiltration and the induced instability of the tumulus mound

Rainfall induced failure took place in the severely embrittled surface of the mound of Kengoshizuka Tumulus, in Asuka village, Takaichi country, Nara prefecture, in the rainy season of 2012 (Fig. 1). The tumulus was constructed in the seventh century and added to tentative UNESCO World Heritage lists in 2006 as a part of "Asuka-Fujiwara: Archaeological sites of Japan's Ancient Capitals and Related Properties".The present study discusses the evaluation of rainfall infiltration into the unsaturated mound and the induced instability of KengoshizukaTumulus. Fig. 2 shows the procedure of the evaluation.

2. TheLayeredStructure of The Tumulus Mound And GeotechnicalProperties of The Soil Layers

The tumulus mound consists of densely compacted decomposed granite soil layers called Hanchiku. The surface of the mound, however, has been embrittled mainly because of repetitive propagation and die of plants. The investigation of the layered structure of the mound and the physical, hydraulic and mechanical properties of the soil layers is important in modelling of the tumulus mound.

Fig. 3 shows plan and cross-section views of the tumulus mound. Elastic wave exploration and portable cone penetration test are conducted on the two lines shown in Fig. 3. The results on Line1 are shown in Fig. 4. Five points named A to E shows the measuring points of portable cone penetration test. The results of elastic wave test shows that shear wave velocity changes at a depth of 50 to 100 cm from the ground surface. The shear wave velocity in the surface layer is lower than that in the underlying layer. Around at the boundary ofshear wave velocity, the penetration resistance reaches 500 kN/m^2. The

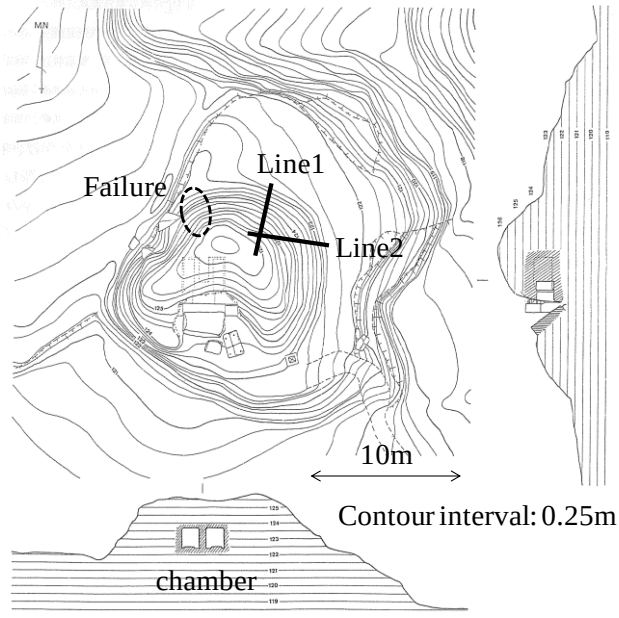

Fig. 3: Plan and cross-section views of Kengoshizuka Tumulus [1]

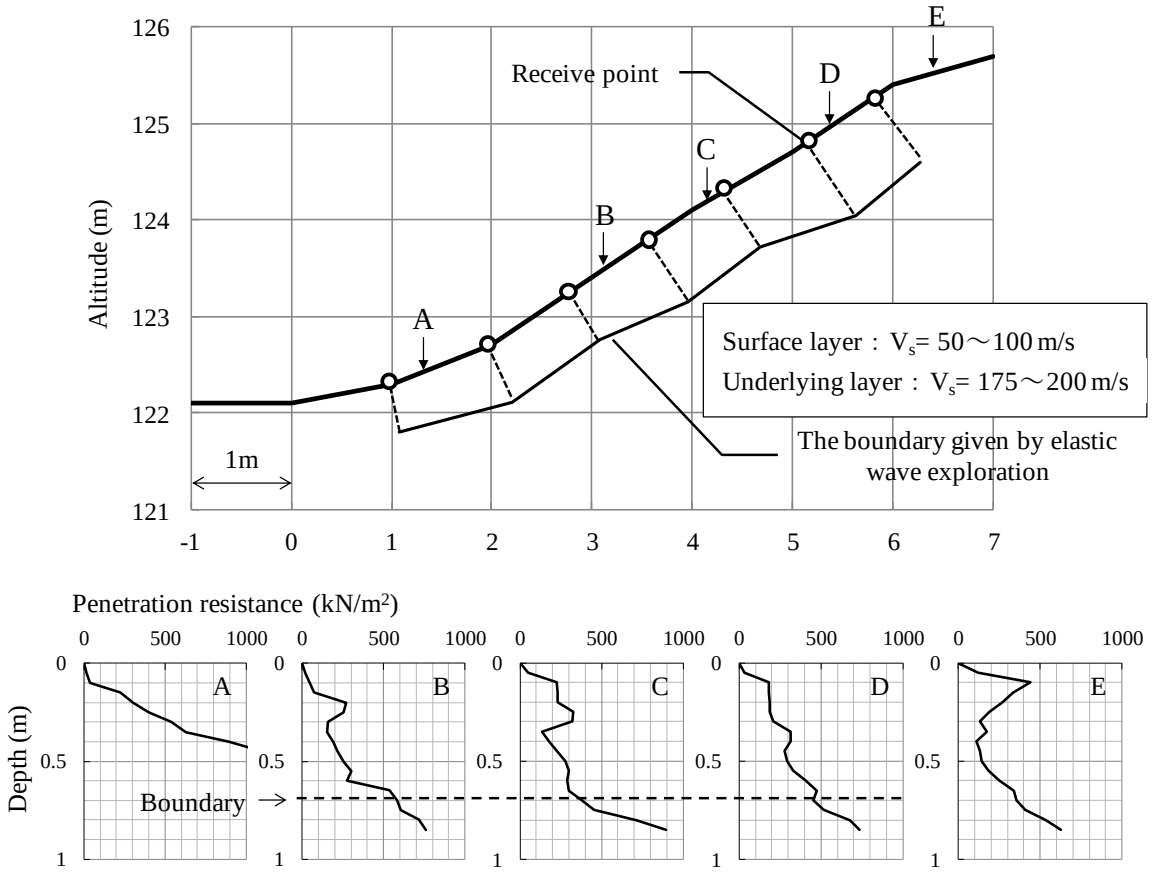

Fig. 4: The results of elastic wave exploration and portable cone penetration on Line1

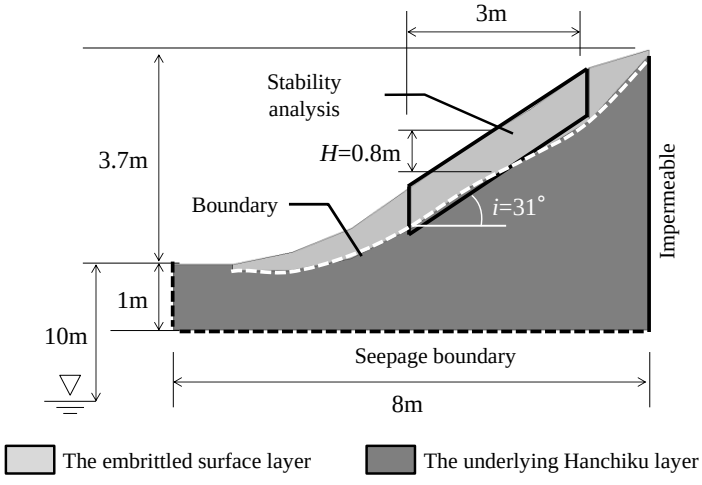

	Embrittled surface	Underlying Hanchiku
Dry density (g/cm³)	1.23	1.29
Natural water content (%)	29	
Degree of saturation (%)	65	71
Hydraulic conductivity (cm/s)	3.3×10^{-3}	3.3×10^{-4}

Fig. 5: The adopted model for the evaluation

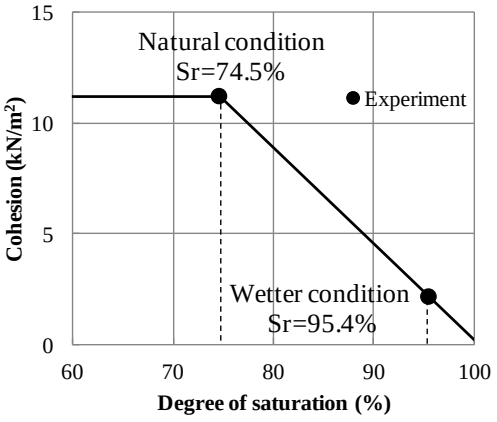

Fig. 6: Experimentally obtained relation between cohesion and degree of saturation

results on Line2 show the same tendency with those on Line1.

These results of in-situ tests provide the analysismodel shown in Fig. 5. The tumulus mound consists of the embrittled surface layer and the underlying Hanchiku layer.The densities of the two layers are assessed

by a relation between density of the mound soil and compaction energy. The former studies on the density of tumulus mounds concluded that tumulus mounds wereconstructed by manual laborwhich equivalents tothe compaction energy level of 0.1 to 0.2 x E_c (Proctor's compaction energy E_c=550kJ/m^3)[2, 3]. Here, the embrittled surface and underlyingHanchiku layers are assumed to have dry densities with 0.1 xE_c and 0.2 xE_c, respectively. The permeability of the embrittled surface isassumed to be higher than that of the underlyingHanchiku layer consideringthat plants provide cracks and voids to the surface of the mound. The soil water characteristic curves of the two layers refer to those of decomposed granite soilobtained by Takeshita et.al. [4].

The failure is assumed to occur at the boundary of the two layers. The strength parameters of the sliding surface are evaluated by a series of direct shear test on specimens under both natural and wetter conditions and needle penetration test on the excavated surface of the tumulus mound.The details are discussed by Sawada et al. [5].The experimentally obtained relation between cohesion and degree of saturation of the sliding surface is shown in Fig. 6.

3. Evaluation of Rainfall Infiltration Into The Tumulus Mound And Slope Stability

The rainfall infiltration into the tumulus mound is evaluated by saturate-unsaturated seepage flow analysis using FEM [6]. The rainfall infiltration into the tumulus mound is evaluated during seven days from 16th to 22nd June, 2012. The amount of rainfall during the period is shown in Fig. 10. The initial condition is adjusted to the measured water content of the tumulus mound by providing appropriate amount of prior rainfall and subsequent seepage period. Here, 3.33mm/hr x 30day-prior rainfall and subsequent 200day-seepage period are adopted. Distributions of degree of saturation of the mound during the seven days are shown in Fig. 7.The seepage water flows along the boundary of the two layers and the degree of saturation at the boundary increases day by day. This is because the permeability of the underlyingHanchiku layer is lower than that of the embrittled surface layer.The results of seepage flow analysis and in-situ tests shown before suggest that the boundary is vulnerable to failure.

The factor of safety in terms of slope stability of the tumulus mound is given by Eq.1. Here, let *H*, *i* and *c*be the depth, gradient and cohesion of the sliding surface, respectively. The angle of shear resistance of the sliding surface is assumed not to contribute to the safety factor. The stability analysis area is designatedin Fig. 5.The experimentally obtained relationshown in Fig.6 gives *c*. The degree of saturation obtained by seepage flow analysisgives the wet unit of

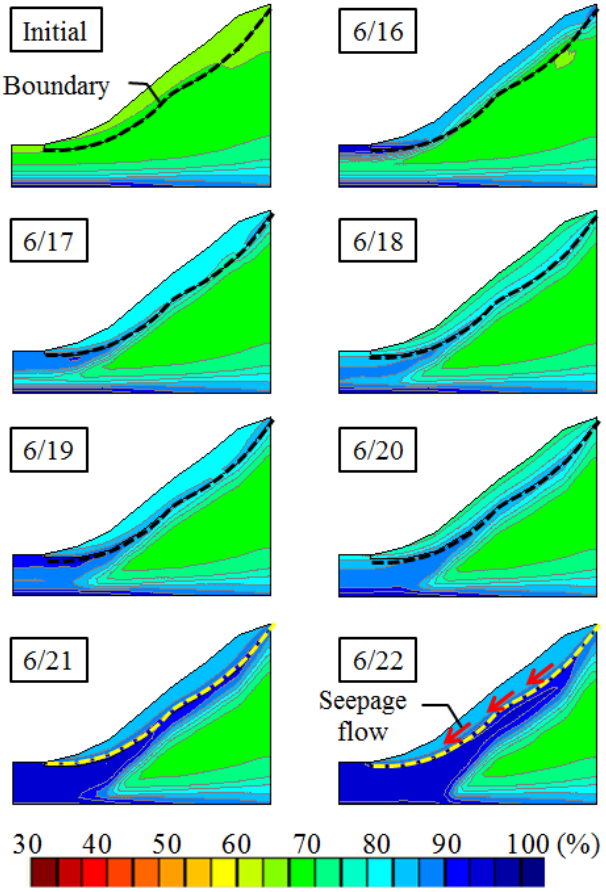

Fig. 7: The distributions of degree of saturation of the tumulus mound from 16th to 22nd June, 2012

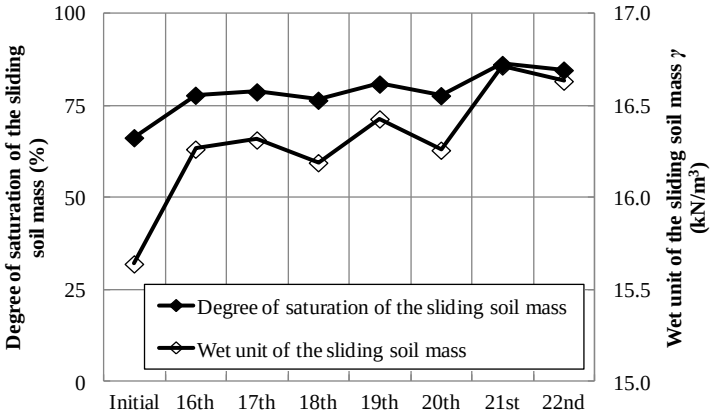

Fig. 8: Degree of saturation and wet unit of the sliding soil mass

the sliding soil massγ. Fig. 8 and Fig. 9 show γ and $c$during the seven days,respectively.The calculated safety factors are shown in Fig. 10. The safety factor continues to decrease and goes below to 1.0 on June 21st. This result explains the rainfall induced failure occurred in 2012.

$$F_s = {}^{c}/_{\gamma H \sin i \cos i} \quad (1)$$

4. Conclusion

The evaluation of rainfall infiltration into the unsaturated mound and the induced instability of the Kengoshizuka Tumulus are discussed.The results of in-situ tests show that the density and strength of the embrittled surface layer of the tumulus mound are lower than those of the densely compacted underlying layer. Based on this, the analysis model with the layered structure of the mound is adapted to the evaluation and the physical, hydraulic and mechanical properties of the soil layersare assessed. The rainfall infiltration into the mound is estimated by seepage flow analysis. The slope stability is evaluated using the analytically estimated degree of saturation of the mound and the experimentally obtained strength parameters of the sliding surface. The results of the evaluation quantitatively show the instability of the tumulus mound induced by rainfall.

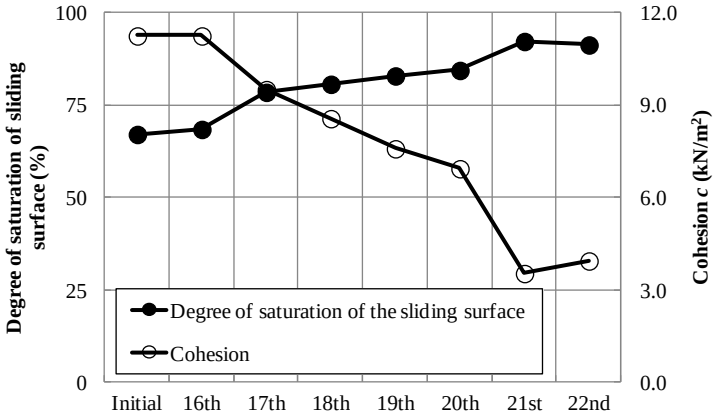

Fig. 9: Degree of saturation and cohesion of the sliding surface

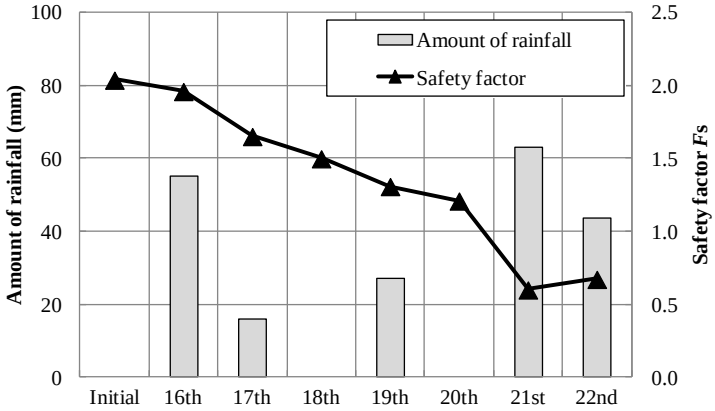

Fig. 10: The amount of rainfall and the calculated safety factor

[1] Asuka Village Board of Education. Excavation report in Kengoshizuka Tumulus, *Research report of cultural herigtage in Asuka village*. 2013, **10**: pp. 18-64 (in Japanese).

[2] M. Mimura & M. Yoshimura. Geotechnical contribution for conservation of compacted tumulus mounds, *Proc. 14th ISSMGE*. 2011.

[3] M. Sawada, M. Mimura & M. Yoshimura. Characterization of geotechnical properties for reconstruction of archeological excavations –case study of Higashinomiya Tumulus–, *Proc. Workshop ATC 19, 18th ICSMGE*. 2013.

[4] Y. Takeshita& I. Kohno. A method to predict hydraulic properties for unsaturated soils and its application to observed data, *Ground and Construction*. 1993, **11(1)**: pp.95-113 (in Japanese).

[5] M.Sawada, M. Mimura & M. Yoshimura. Evaluation of rainfall induced instability of tumulus mounds for the conservation of tumuli based on geotechnical engineering, *J.JSNDS*. 2014 (in press, in Japanese).

[6] K. Akai, Y. Ohnishi &M. Nishigaki. Finite element analysis of saturated unsaturated seepage in soil, *J. JSCE*. 1977, **264**: pp. 87-96 (in Japanese).

GEOLOGY AND SEISMOLOGY ENGINEERING

ISBN 979-458-758-3
Proceedings of the 3rd International Conference on the Geohazard Information
Zonation and 5th Seminar & Short Course of HASTAG (GIZ2014-HASTAG5)
Organized by UMSU, HASTAG, USM
Medan, Indonesia, October 20-22, 2014

On the Selection of Ground-Motion Prediction Equations Compatible with Peninsular Malaysia Region for Sumatran Subduction In-slab Earthquakes

Azlan bin Adnan [1, +], Abdollah Vaez Shoushtari [1], Noor Sheena Herayani Binti Harith[1,2]

[1] Faculty of Civil Engineering, Universiti Teknologi Malaysia, 81310, Johor Bahru, Malaysia
[2] School of Engineering and Information Technology, Universiti Malaysia Sabah, 88450 Kota Kinabalu, Sabah, Malaysia

Abstract. Although Peninsular Malaysia is located in a low-seismicity region, the medium to high rise structures could be vulnerable to distant earthquakes generated by Sumatran fault and Sumatran subduction seismic sources. In addition, seismic design has not been specifically considered in the building design codes of the region. Therefore, it is rational to assess the seismic hazard of the region to apply appropriate seismic designs for the existing and future structures. The most comprehensive method recommended by design codes is Probabilistic method in order to do Seismic Hazard Analysis (i.e. called PSHA). The key component required in any seismic hazard analysis is employing an appropriated set of Ground-Motion Prediction Equations (GMPEs). This paper has attempted firstly to drive new GMPE for Peak Ground Acceleration (PGA) using data recorded in Peninsular Malaysia due to Sumatran subduction in-slab earthquakes. Secondly, the study has presented a classification among the new derived GMPE and other four GMPEs proposed for subduction in-slab earthquakes of different regions through a comparative study based on the PGAs recorded in Peninsular Malaysia. The goal of the classification was to introduce the GMPEs which were the most compatible with the region. The results of the present study are applicable for seismic hazard analysis in Peninsular Malaysia.

Keywords: Ground-motion prediction equation, Sumatran subduction in-slab earthquake, Peninsular Malaysia

1. Introduction

Generally speaking, seismic designs have not been considered in low-seismic regions of Southeast Asia, as these regions have never experienced any severe damages due to earthquakes. Kuala Lumpur, the capital of Malaysia, could be a good example of these regions. Even though it is located in a low-seismic region, it could be vulnerable to distant earthquakes. The active Sumatran seismic sources that could affect this city are located more than 300 km away. The number of felt events is increasing due to the rapid construction of high-rise buildings in this city [1]. Even though earthquakes have never caused any structural damage in Kuala Lumpur, the effects of even a moderate level of ground motion would be enormous because of the large population taking place in the structures that have not been designed for earthquake loads [2].

In view of the Probabilistic Seismic Hazard Analysis (PSHA), Adnan et al. [3] and Petersen et al. [4] obtained the Peak Ground Acceleration (PGA) across Peninsular Malaysia with the values of 20-100 gal and 40-120 gal with 10% probability of exceedance over 50 years (i.e., 475-year return period), respectively. Pan and Megawati [5] calculated the PGA values of 29.5 and 12.7 gal with the same return period for Kuala Lumpur and Singapore, respectively. In a recent study, Nabilah and Balendra [6] found that the PGA in Kuala Lumpur with 10% and 2% probabilities of exceedance over 50 years had the values of 16.5 and 23.4 gal, respectively. One of main reason behind these different results is the selection of unsuitable Ground-Motion Prediction Equations (GMPEs).

Sumatran seismic sources consist of three discrete zones, the Sumatran fault, the Sumatran subduction interface, and the Sumatran subduction in-slab. Since these seismic zones have three different rupture mechanisms, three sets of GMPEs must be derived for the earthquakes generated by these seismic sources.

[+] Corresponding author. Tel.: (+6)0197551665, (+6)075531581.
Email Address: azelan_fka_utm@yahoo.com; vsabdollah@gmail.com

This paper has attempted firstly to drive new GMPE for horizontal Peak Ground Acceleration (PGA) using data recorded in Peninsular Malaysia due to Sumatran subduction in-slab earthquakes. Secondly, the study has presented a classification among the new derived GMPE and other four GMPEs proposed for subduction in-slab earthquakes of different regions, through a comparative study based on the recorded PGAs in Peninsular Malaysia.

2. Regional Tectonic Setting

The Sumatra and Java Islands in the Indonesian archipelago are on the Eurasian plate, which rests on top of the subducting Indian-Australian plate (Fig. 1). The Indian-Australian and the Eurasian plates converge to form the Sunda trench. The convergence is nearly perpendicular to the trench axis in south of Java, but it becomes more oblique in southwest of Sumatra. Based on hypocentral distributions and earthquake focal mechanisms, the subducting plate in Sumatra dips less than 15 degrees beneath the outer arc ridge (interface part), and the dip angle steepens to about 50 degrees under the volcanic arc (in-slab part) [7, 8].

The Sumatran fault is 250 km away from the northeast side of Sunda trench. Geological and geophysical studies identify the fault as a seismically active, right lateral strike-slip fault [9].

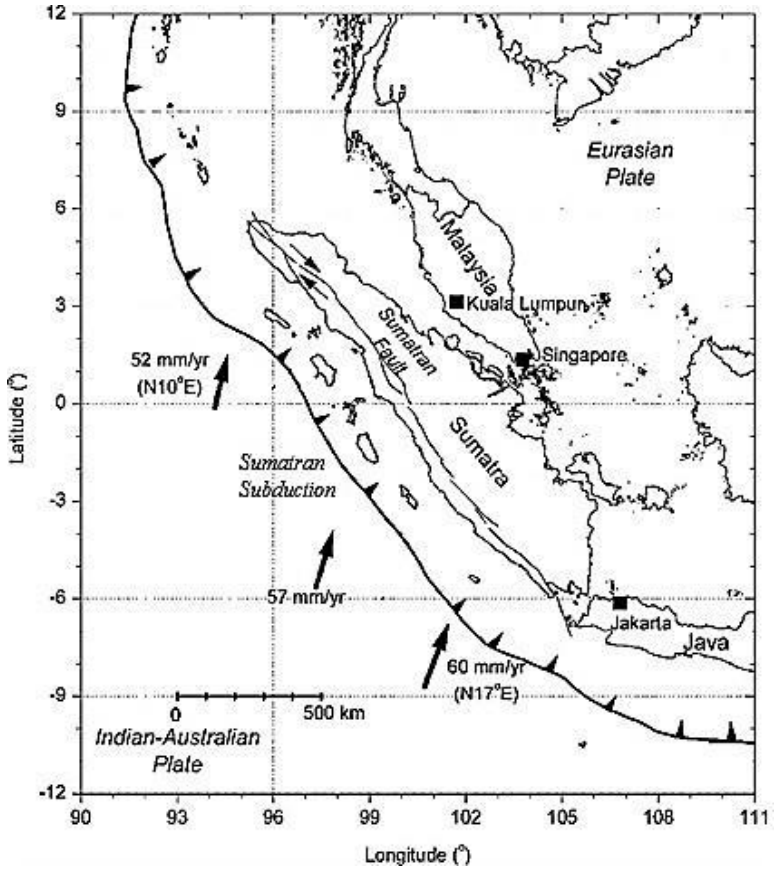

Fig. 1: Tectonic setting of Sumatra Island [10].

3. Sumatran Subduction In-slab Earthquakes Recorded in Peninsular Malaysia

Since 2004, the Malaysian Meteorological Department (MMD) has installed a network of seismic stations in Malaysia. The network is comprised of 28 three-component and real time stations. Twelve seismic stations of this network are located on granite, meta sediment, sandstone and rocky sites (i.e. NEHRP site class B with shear-wave velocity values; 760 m/s$<V_S\leq$1500 m/s) in Peninsular Malaysia.

The Sumatran subduction in-slab earthquakes from 2006-2012, recorded by the twelve seismic stations are listed in Table 1. The recorded PGAs were between 0.027-1.700 gal. The 37 records due to 5 Sumatran subduction in-slab earthquakes collected in this study had moment magnitudes ranging from 6.1 to 7.6 and hypocentral distances of 327-904 km.

In the present study, in order to classify earthquakes by type (i.e., interface and in-slab events), the method proposed by Atkinson and Boore [11] that it is related to both the focal depth and focal mechanism was used. The trust worthy epicenters, moment magnitudes, focal depths and mechanisms of collected Sumatran earthquakes were obtained from the Harvard Centroid Moment Tensor (CMT) catalogue [12].

Table 1: List of Sumatran subduction in-slab earthquakes recorded in Peninsular Malaysia

Date (Time/UTC)	Lat.	Long.	M_W	H^a (km)	Station	NEHRP Site Class	Soil site condition	R_{hypo} (km)
23/06/2012 (04:34:00)	2.98°N	97.77°E	6.1	104.5	BRSM	B	Rock	466.5
					DTSM	B	Rock	464.0
					FRM	B	Rock	441.5
					GTSM	B	Rock	459.0
					IPM	B	Rock	416.0
					JRM	B	Rock	542.3
					KGM	B	Rock	634.0
					KTM	B	Rock	658.0
					KUM	B	Rock	422.9
05/09/2011 (17:55:00)	2.88°N	97.86°E	6.7	94.6	BRSM	B	Rock	454.5
					FRM	B	Rock	430.5
					GTSM	B	Rock	448.5
					IPM	B	Rock	409.9
					JRM	B	Rock	533.0
					KGM	B	Rock	621.0
					KOM	B	Rock	682.7
					KUM	B	Rock	420.0
					PYSM-B0	B	Rock	435.1
30/09/2009 (10:16:00)	0.79°S	99.67°E	7.6	77.8	BRSM	B	Rock	483.7
					FRM	B	Rock	503.8
					GTSM	B	Rock	526.1
					IPM	B	Rock	620.8
					JRM	B	Rock	611.4
					KGM	B	Rock	517.3
					KOM	B	Rock	551.5
					KTM	B	Rock	785.4
					KUM	B	Rock	689.2
					PYSM-B0	B	Rock	475.6
16/05/2006 (15:28:00)	0.01°N	96.98°E	6.8	13.5	IPM	B	Rock	678.5
					KGM	B	Rock	738.9
					KTM	B	Rock	903.7
					KUM	B	Rock	714.7
01/12/2006 (03:58:00)	3.46°N	99.05°E	6.3	208.4	FRM	B	Rock	354.6
					IPM	B	Rock	327.0
					KGM	B	Rock	542.0
					KTM	B	Rock	540.0
					KUM	B	Rock	341.0

H: Focal depth (km)

4. New GMPE for Sumatran Subduction In-slab Earthquakes

Referring to Fukushima and Tanaka (1990) [13], the following attenuation model was selected in order to drive new GMPE:

$$\log(PGA) = aM_W - bR_{hypo} - \log\left(R_{hypo} + c \times 10^{aM_W}\right) + d + \varepsilon_{\log(PGA)} \quad (1)$$

where PGA is peak ground acceleration in cm/sec^2, M_W is moment magnitude, R_{hypo} is hypocentral distance in km, and a, b, c, and d are regression coefficients. Performing least-square regression analysis released following equation to predict Sumatran subduction in-slab earthquakes:

$$\log(PGA) = 0.504632M_W - 0.000845R_{hypo} - \log(R_{hypo}) - 0.918416 \qquad \sigma_{\log(PGA)} = 0.1895 \tag{2}$$

5. Classification of GMPEs

The description of the GMPEs are summarized and listed in Table 2. The comparison between the PGAs predicted by the GMPEs and the 37 PGAs recorded on rock sites in Peninsular Malaysia are depicted in Fig. 2.

Table 2: Descriptions of the selected GMPEs

Reference (Model designation)	Model description	M_w range considered	Distance (R) definition and range considered
Present study (New GMPE)	Regression of recorded data from Sumatran subduction *in-slab* earthquakes in Peninsular Malaysia.	6.1-7.6	The hypocentral distance, 327-904km
Zhao et al. [14] (ZA06)	Regression of recorded data mainly from crustal and subduction interface and *in-slab* earthquakes in Japan, with supplementary data from earthquakes in western part of the United States and 1978 Tabas, Iran earthquake.	5.1-8.3	The shortest distance to the rupture plane if fault model is available and otherwise is the hypocentral distance, 25-300km
Atkinson and Boore [11] (AB03)	Regression of real recorded ground motion data from interface and *in-slab* earthquakes occurring in subduction zones of Alaska, Chile, Cascadia, Japan, Mexico, Peru and the Solomon islands.	5.0-8.3	The closest distance to the rupture plane, 10-500km
Youngs et al. [15] (YO97)	Regression of recorded interplate earthquakes from different subduction interface and *in-slab* zones.	5.0-8.2	The closest distance to the rupture plane, 10-500km
Lin and Lee [16] (LL08)	Regression of recorded ground motions from both interface and *in-slab* earthquakes of subduction zones in Taiwan and other foreign regions.	5.3-8.1	The hypocentral distance, 15-630km

Figs. 2 shows that at long distances, Lin and Lee [16] and Youngs et al. [15] equations predicted the largest PGA out of the six models, and the predicted PGAs were significantly larger than the recorded ones. As demonstrated by the figure, the PGAs predicted by Zhao et al. [14] equation were approximately close to the observed data compare to the predicted ones based on the equation proposed by Atkinson and Boore [11]. Refer to the Fig. 2, it could be understood that the PGAs predicted by the New GMPE presented in this study, fit well with the recorded data.

6. Conclusions

One of the most significant components required in any seismic hazard analysis is the selection of a set of appropriate Ground-Motion Prediction Equations (GMPEs). The first objective of this study was to drive a new GMPE for horizontal Peak Ground Acceleration (PGA) using data recorded in Peninsular Malaysia due to Sumatran subduction in-slab earthquakes. As the second objective, the study has presented a classification among the new derived GMPE and other four GMPEs proposed for subduction in-slab earthquakes of different regions, through a comparative study based on the recorded PGAs in Peninsular Malaysia.

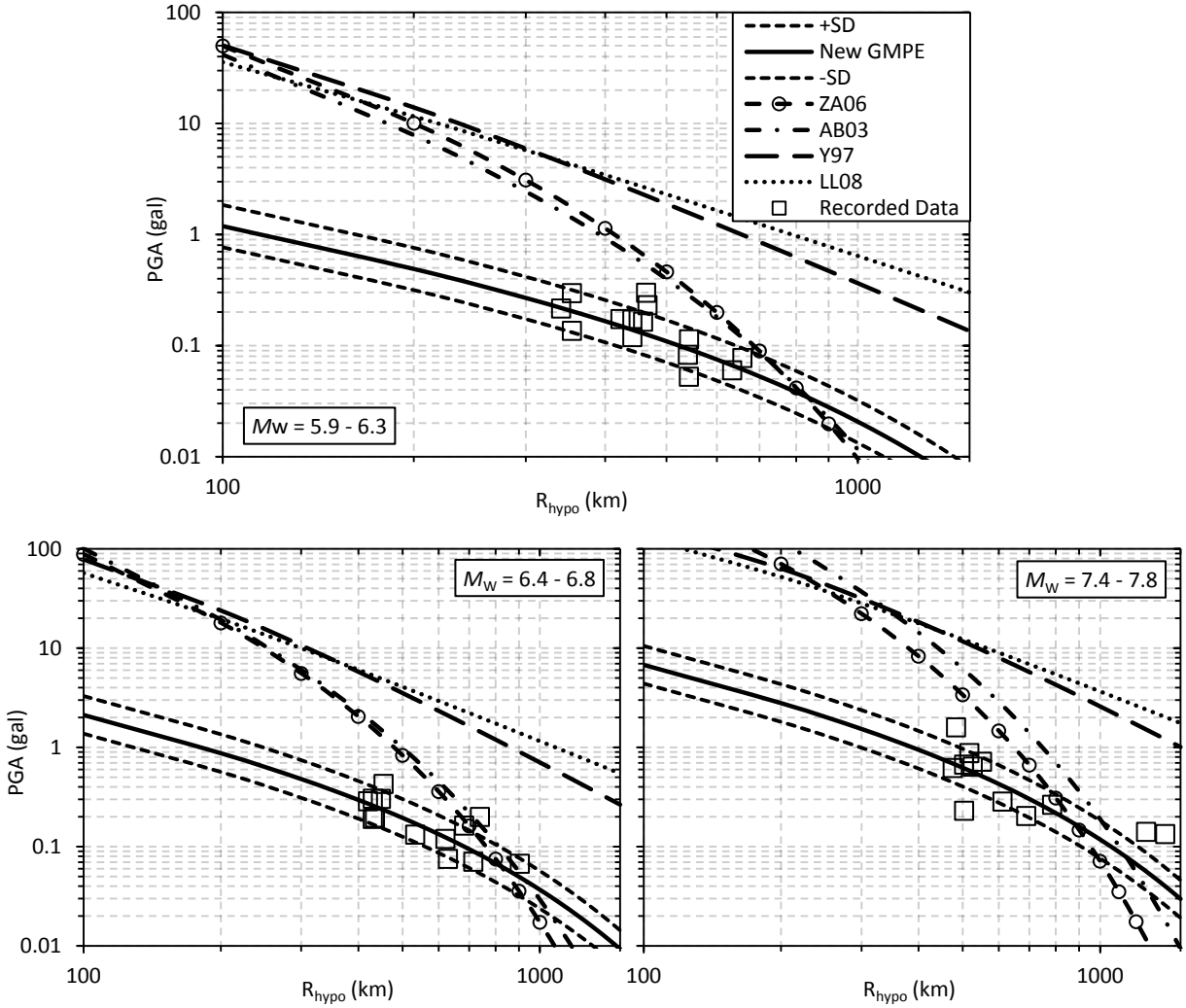

Fig. 2: The 37 recorded PGAs due to Sumatran subduction in-slab earthquakes on rock sites (NEHRP site class B) in Peninsular Malaysia, together with the GMPE of this study and other four ones derived for different subduction zones.

The PGAs predicted by the New GMPE and the response spectral acceleration relations provided by Zhao et al. [14], were found to correlate well with the recorded PGAs. As the PGAs collected in this study were recorded with hypocentral distance of more than 327 km, it should be mentioned that the conclusions about the most compatible GMPE for the region are valid only for distances greater than 327 km. The results of the present study in terms of introducing the GMPEs compatible with the region could be applicable in seismic hazard analysis projects of Peninsular Malaysia.

7. Acknowledgments

This study was financially granted by Universiti Teknologi Malaysia (UTM) and Ministry of Science, Technology, and Innovation (MOSTI) of Malaysia. We thank the contributions of the Malaysian Metrological Department (MMD) for providing Sumatran earthquakes data used in this study.

8. References

[1] Pan, T.C., *Site-dependent building response in Singapore to long-distance Sumatra earthquakes.* Earthquake Spectra, 1997. **13**(3): p. 475-488.

[2] Megawati, K., T.-C. Pan, and K. Koketsu, *Response spectral attenuation relationships for Sumatran-subduction earthquakes and the seismic hazard implications to Singapore and Kuala Lumpur.* Soil Dynamics and Earthquake Engineering, 2005. **25**(1): p. 11-25.

[3] Adnan, A., Hendriyawan, Marto, A., and Irsyam, M., *Development of seismic hazard map for Peninsular Malaysia*, in *Proc. of Malaysian Science and Technology Congress*. 2006: PWTC Kuala Lumpur, Malaysia.

[4] Petersen, M.D., et al., *Probabilistic seismic hazard analysis for Sumatra, Indonesia and across the Southern Malaysian Peninsula.* Tectonophysics, 2004. **390**(1–4): p. 141-158.

[5] Pan, T.C. and K. Megawati, *Estimation of peak ground accelerations of the Malay Peninsula due to distant Sumatra earthquakes.* Bulletin of the Seismological Society of America, 2002. **92**(3): p. 1082-1094.

[6] Balendra, A.B.N.T., *Seismic Hazard Analysis for Kuala Lumpur, Malaysia.* Earthquake Engineering, 2012. **16**(7): p. 1076-1094.
[7] Newcomb, K.R. and W.R. McCann, *Seismic history and seismotectonics of the Sunda Arc.* Journal of Geophysical Yrch, 1987. **92**(B1): p. 421-439.
[8] Fauzi, et al., *Lateral variation in slab orientation beneath Toba Caldera, northern Sumatra.* Geophysical Research Letters, 1996. **23**(5): p. 443-446.
[9] Sieh, K. and D. Natawidjaja, *Neotectonics of the Sumatran fault, Indonesia.* Journal of Geophysical Research B: Solid Earth, 2000. **105**(B12): p. 28295-28326.
[10] Megawati, K. and T.C. Pan, *Ground-motion attenuation relationship for the Sumatran megathrust earthquakes.* Earthquake Engineering and Structural Dynamics, 2010. **39**(8): p. 827-845.
[11] Atkinson, G.M. and D.M. Boore, *Empirical ground-motion relations for subduction-zone earthquakes and their application to Cascadia and other regions.* Bulletin of the Seismological Society of America, 2003. **93**(4): p. 1703-1729.
[12] *Harvard Seismology Centroid Moment Tensor Database. Department of Earth and Planetary Sciences, Harvard University website: http://www.seismology.harvard.edu/CMTsearch.html*.
[13] Fukushima, Y. and T. Tanaka, *A new attenuation relation for peak horizontal acceleration of strong earthquake ground motion in Japan.* Bulletin - Seismological Society of America, 1990. **80**(4): p. 757-783.
[14] Zhao, J.X., et al., *Attenuation relations of strong ground motion in Japan using site classification based on predominant period.* Bulletin of the Seismological Society of America, 2006. **96**(3): p. 898-913.
[15] Youngs, R.R., et al., *Strong ground motion attenuation relationships for subduction zone earthquakes.* Seismological Research Letters, 1997. **68**(1): p. 58-73.
[16] Lin, P.S. and C.T. Lee, *Ground-motion attenuation relationships for subduction-zone earthquakes in Northeastern Taiwan.* Bulletin of the Seismological Society of America, 2008. **98**(1): p. 220-240.

ISBN 979-458-758-3
Proceedings of the 3rd International Conference on the Geohazard Information
Zonation and 5th Seminar & Short Course of HASTAG (GIZ2014-HASTAG5)
Organized by UMSU, HASTAG, USM
Medan, Indonesia, October 20-22, 2014

The Compatible Ground-Motion Prediction Equations with East Malaysia for Shallow Crustal Earthquakes

Noor Sheena Herayani Harith[1, 2 +], Azlan bin Adnan[1], Abdollah Vaez Shoushtari[1]

[1] Faculty of Civil Engineering, Universiti Teknologi Malaysia, 81310, Johor Bahru, Malaysia.

[2] School of Engineering and Information Technology, Universiti Malaysia Sabah, 88450 Kota Kinabalu, Sabah, Malaysia

Abstract. The common features in establish seismic design criteria for buildings, probabilistic seismic hazard analysis requires estimation of ground motion such as peak ground acceleration (PGA). This estimation process needs to use a ground motion prediction equation (GMPE) which provides PGA estimates incorporating a number of earthquake magnitude, distance and other seismic parameters. On the other hand, it is not always easy to assess inside GMPE since they mostly have all reliable parameters of ground motion records to develop a GMPE. Thus, the objective of this paper is to find the suitable existing models four international GMPEs that provide significant estimates at large source-to-site distance evaluated against comprehensive set of PGA compiled. The dataset of 41 observations of earthquake ground motions recorded provided by Malaysian Meteorological Department (MMD) specifically considered from earthquake with magnitude M_W 2.9 to 7.3, fault distance from 10 to 1350 km were plotted and compared to the field records. It was found that the best fitting model of prediction equation proposed by Fukushima and Tanaka (1990) suitable for magnitude 5.0 and above whereas Atkinson and Boore (1997) and Campbell (2003) are suitable for magnitude less than 5.0.

Keywords: Ground motion prediction equation, earthquake, East Malaysia

1. Introduction

A seismic hazard analysis is usually carried out to establish seismic design criteria for building and other critical structures such as nuclear power plant and dams. The analysis depends on the identification of the seismic sources and the estimation of their capacity to produce ground motions. The production of seismic hazard map for East Malaysia could be developed based on earthquake source zones identifiable from earthquake catalogs and ground motion estimation using current developed prediction equations.

Ground motion prediction equation (GMPE) is essential in seismic hazard studies for estimating the ground motions generated by the seismic sources that rely on earthquake magnitude, source-to-site distance, and local site condition. In low seismicity regions, only weak motions are available and the equations selected for the probabilities studies are usually models established from foreign data. Although most ground motion prediction equations have been developed for magnitudes 5 and above, the smaller magnitude often used in probabilistic studies in low seismicity regions. The studies shows in [1] that the magnitude lower than 5 can be contributing to the earthquake hazard.

+ Corresponding author. Tel.: +60197551665; fax: +6075531581.
E-mail address: azelan_fka_utm@yahoo.com; harithsheena@gmail.com.

East Malaysia had rarely experience large earthquake during the past few years. Since 1900 there have been two moderate earthquakes of shallow focal depths were recorded in Sarawak during year 1994 and 2004 of magnitude Mw 5.2. In Sabah, the historical records of moderate earthquakes caused substantial damage to buildings with two well-known event in 1976 and 1991 of magnitude Mw 5.8 and Mw 5.4, respectively. Even moderate magnitude of earthquake can be devastated when it destroyed many buildings and killed one third of the city's population as happened in Morroco during 1960 [2]. Hence, there is a need for reliable predictions of ground motion equation over the whole magnitude range in low seismicity region such as East Malaysia.

Prediction equation models developed from other regions of the world can be adopted if there is no reliable ground motion prediction equation as analyzed by many researchers ([3], [4], [5], [6], [7], [8] and [9]). The chosen of ground motion prediction equation must represent the geological and seismological attributes of the region with containing a wide range of magnitude and source-to-site distance. The prediction equation that suitable for stable continental region is implemented in this study to determine the most suitable attenuation function by comparing PGA estimates from four ground motion prediction equation to a number of records available from Malaysian Meteorological Department (MMD) recorded.

2. Ground Motion Data

East Malaysia located on the island of Borneo and beside of affected by earthquakes located in the Straits of Macassar, Sulu Sea and Celebes Sea, this state also have experienced earthquakes from local origin faults that delineated over East Malaysia. In this study, the information of earthquake database is dependent on the data gathered by Malaysian Meteorological Department (MMD). After the devastating event of Sumatra earthquake on December 2004, Malaysian Meteorological Department (MMD) has installed the instrument recording on earthquake activities throughout Malaysia. The PGA values of earthquake data recorded by 26 stations around Malaysia has been corrected and filtered appropriately from year 2004 to 2012. The epicenter locations, date, time, and moment magnitudes of those 41 events of shallow crustal earthquakes were obtained from Harvard Central Moment Tensor Catalog (Fig. 1). The site conditions at the MMD recording stations are categorized into soil type B or rock site based on shear wave velocity in the top 30 meter of the ground (V_{s30}).

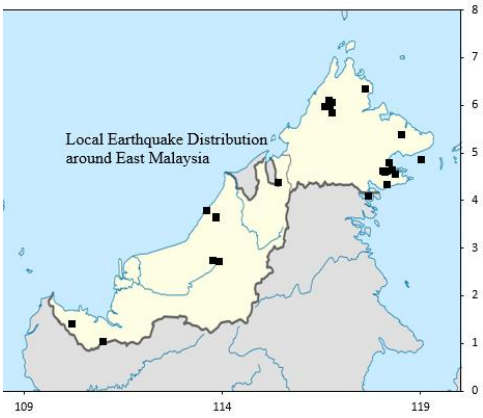

Fig. 1: Earthquake events distribution map in East Malaysia

The earthquake events considered in this study only from shallow crustal earthquakes since East Malaysia being affected by this type of fault. The distribution of records with respect to moment magnitude (M_W) and hypocenter distance (R_{hypo}) is shown in Fig. 2(a). Ground motion records used in this study were obtained from earthquake M_W between 2.9 to 7.3 and recorded at R_{hypo} ranging from 10 to 1350 km. The earthquake data is categorized as low-to-moderate earthquake. Higher proportion of data is clustered at long distances as few of the events have epicenters located in Minahassa Peninsula and Sumatra fault. Fig. 2(b) shows the distribution of maximum PGA values between two horizontal components over distance. However, the particular data recorded is lack of small earthquakes at close distance, therefore the near source ground motions for small events will not be constrained by observations. Records used in this study have PGA ranging from 0.0039 gal to 6.368 gal.

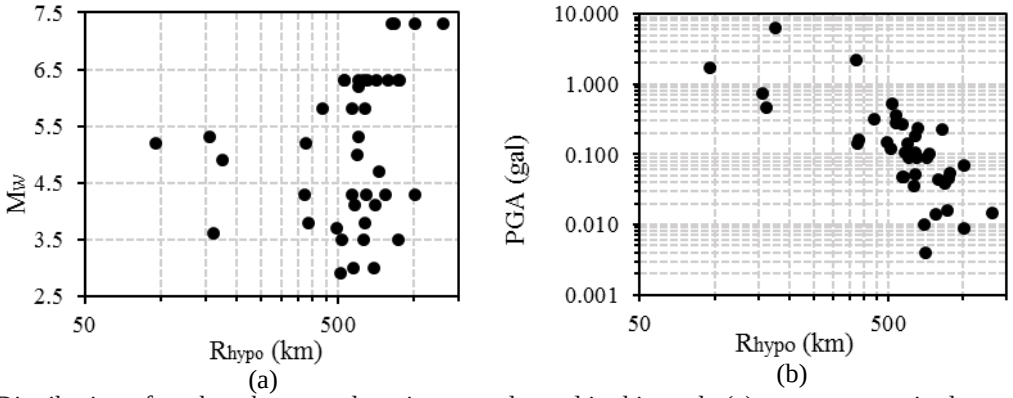

Fig. 2: Distribution of earthquake ground motion records used in this study (a) moment magnitude versus distance; and (b) peak ground acceleration versus distance.

3. Ground Motion Prediction Equation (GMPE)

Various ground motion prediction equations (GMPE) that become available made it possible to choose the GMPE that suits East Malaysia region where each model is to be compared to the corresponding records. The analysis is carried out with four well-known GMPE models. The models were selected due to the criteria in magnitude and distance. The different type of distance measures are treated as hypocentral distance (R_{hypo}) together with the range of magnitude as shown in Table 1.

The first model is the Fukushima and Tanaka [10] model, which was calibrated from rock, hard, medium and soft soil ground on the basis of earthquake data in Japan and other countries. The second model is Dahe et al. [11] which derived from rock and soil from of strong earthquake recordings in Central America. The third model examined is Atkinson and Boore [12] that developed using stochastic simulation of ground motion for low seismicity and stable continental region of eastern North America. The forth equation investigated is by Campbell [13] which used combination of stochastic and theoretical methods developed from western North America on hard rock. These models were developed using different sets of ground motion records and used records at distance less than 500 and 1000 km. These limiting distance represent the applicable ranges of distance where the models provide reliable estimates of ground motions which is acceptable for long distance and low seismicity earthquake.

Table 1: Ranges of suitable attenuation models from stable region

Ground Motion Prediction Equation (GMPE) Model	**Reference**	**Distance Type**	**Distance Range [14]**	**Magnitude Type**	**Magnitude Range**
Fukushima and Tanaka [10]	FT90	R_{epi}	0 – 300	M_{JMA}	4.6 – 8.2
Dahle et al. [11]	DS95	R_{epi}	6 – 490	M_W	3.0 – 8.0
Atkinson and Boore [12]	AB97	R_{hypo}	10 – 500	M_W	4.0 – 7.5
Campbell [13]	C03	R_{rup}	0 – 1000	M_W	5.0 – 8.2

4. Comparison of Ground Motion Prediction Models and Recorded Data

PGA estimated by attenuation models for East Malaysia regions are compared to actual records on rock sites as shown in Fig. 3. These actual earthquake recording were plotted into Mw=2.7 and 7.6 for comparison. Throughout all magnitude range, the attenuation functions except Fukushima and Tanaka [10] predicts large PGA than the observed PGAs. Although the Dahle et al. [11] attenuation function was to cover far-field and low magnitude earthquakes, it is over predicts the observed PGAs for magnitude less than 3.1 and give consistent trend of magnitude 3.2 and 5.1. The equation prediction by Atkinson and Boore [12] and Campbell [13] yield a similar trend with the recorded PGA for magnitude between 2.7 and 5.1 at longer distance. Among the four models, the Fukushima and Tanaka [10] gives the prediction equation rate for distance 10 – 1350 km and fits the observed data from magnitude 5.2 and above.

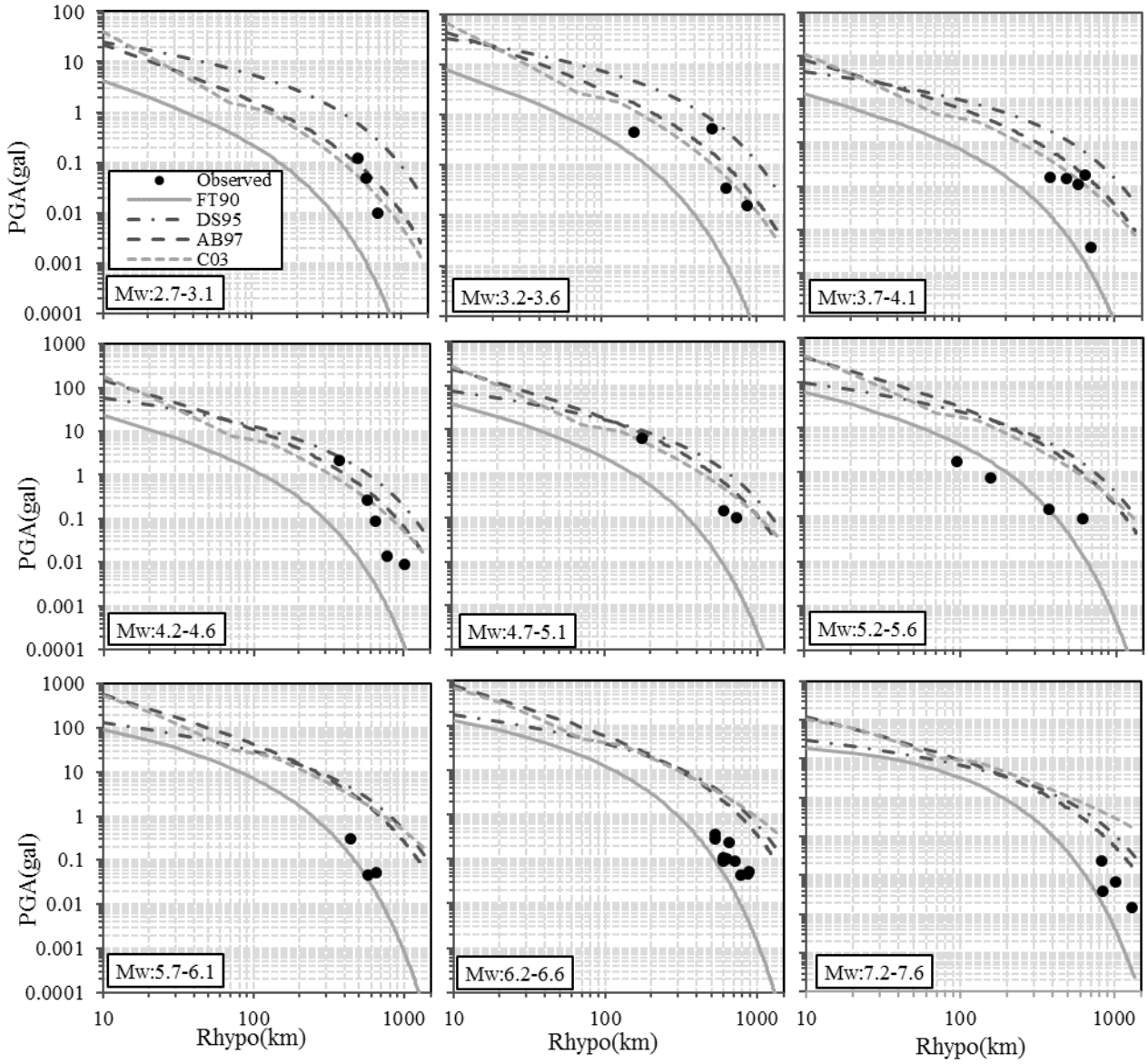

Fig. 3: Comparison of attenuation curves with new developed attenuation models and recorded PGA for rock sites in East Malaysia from shallow crustal earthquakes.

Some ground motion prediction equations show a good ability to predict and fits the observation data. The model of Dahle et al. [11] performs roughly higher PGA at low magnitude. Conversely, the model of Atkinson and Boore [12] and Campbell [13] performs data observations correctly for magnitude less than 5.0. The Fukushima and Tanaka [10] model reflecting the observation correctly for the magnitude higher than 5.0. The results show that the observation recorded from small to large earthquakes are varies for the earthquake condition in East Malaysia.

5. Conclusion

Based in the database used in this study, suitable ground motion prediction equation (GMPE) for estimating PGA on rock sites in East Malaysia due to shallow crustal earthquake are Atkinson and Boore [12] and Campbell [13] for magnitude less than 5.0 and Fukushima and Tanaka [10] for magnitude more than 5.0. The new GMPE specifically for East Malaysia could be developed if more earthquake data recorded from small to large magnitude at close distance are available.

6. Acknowledgments

This study was financially granted by Universiti Teknologi Malaysia (UTM) and Ministry of Science, Technology, and Innovation (MOSTI) of Malaysia. We thank the contributions of the Malaysian Metrological Department (MMD) for providing Sumatran earthquakes data used in this study.

7. References

[1] Beauval, C., Tasan, H., Laurendeau, A., Delavaud, E., Cotton, F., Guéguen, Ph., and Kuehn N., *On the Testing of Ground-Motion Prediction Equations against Small-Magnitude Data.* Bulletin Seismological Society America, 2012: p. 1-45.

[2] Paradise, T.R., *Perception of earthquake risk in Agadir, Morocco: A case study from a Muslim community.* Global Environmental Change Part B: Environmental Hazards, 2005. **6**(3): p. 167-180.

[3] Pan, T.-C. and K. Megawati, *Estimation of peak ground accelerations of the Malay Peninsula due to distant Sumatra earthquakes.* Bulletin of the Seismological Society of America, 2002. **92**(3): p. 1082-1094.

[4] Kracke, D.W. and R. Heinrich, *Local seismic hazard assessment in areas of weak to moderate seismicity—case study from Eastern Germany.* Tectonophysics, 2004. **390**(1): p. 45-55.

[5] Garcia, J., et al., *Seismic hazard map for Cuba and adjacent areas using the spatially smoothed seismicity approach.* Journal of Earthquake Engineering, 2008. **12**(2): p. 173-196.

[6] Chintanapakdee, C., Naguit, M. E., and Charoenyuth, M., *Suitable Attenuation Model for Thailand*, in *The 14th World Conference on Earthquake Engineering (14WCEE)*. 2008: Beijing, China.

[7] Gaspar Escribano, J.M., et al., *Towards a new seismic hazard assessment in Spain.* 2010.

[8] Faisal, A., et al., *Influence of large dam on seismic hazard in low seismic region of Ulu Padas Area, Northern Borneo.* Natural Hazards, 2011. **59**(1): p. 237-269.

[9] Kumar, B.L., G.R. Rao, and K.S. Rao, *Seismic Hazard Analysis of Low Seismic Regions, Visakhapatnam: Probabilistic Approach.* J. Ind. Geophys. Union (January 2012), 2012. **16**(1): p. 11-20.

[10] Fukushima, Y., T. Tanaka, *A new attenuation relation for peak horizontal acceleration of strong earthquake ground motion in Japan.* Bulletin Seismological Society America, 1990. **80**: p. 757-783.

[11] Dahle, A., Climent, A., Taylor, W., Bungum, H., Santos, P., Ciudad Real, M., Linholm, C., and W. Strauch, & Segura, F. *New spectral strong motion attenuation models for Central America.* in *Proceedings of the Fifth International Conference on Seismic Zonation*. 1995. Nice, France.

[12] Atkinson, G.M., Boore, D. M., *Some Comparisons Between Recent Ground-Motion Relations.* Seismological Research Letters, 1997. **68**(1): p. 24-40.

[13] Campbell, K.W., *Prediction of Strong Ground Motion Using the Hybrid Empirical Method and Its Use in the Development of Ground-Motion (Attenuation) Relations in Eastern North America.* Bulletin of the Seismological Society of America, 2003. **93**(3): p. 1012-1033.

[14] Simons, W.J.F., et al., *A decade of GPS in Southeast Asia: Resolving Sundaland motion and boundaries.* Journal of Geophysical Research: Solid Earth, 2007. **112**(B6): p. B06420.

ISBN 979-458-758-3
Proceedings of the 3rd International Conference on the Geohazard Information
Zonation and 5th Seminar & Short Course of HASTAG (GIZ2014-HASTAG5)
Organized by UMSU, HASTAG, USM
Medan, Indonesia, October 20-22, 2014

Northern Uemachi Flexure Zone investigated by borehole database and Numerical Simulation

Naoto Inoue [1], Naoto Kitada [1] and Keiji Takemura [2 +]

[1] Geo-Research Institute
[2] Institute for Geothermal Sciences Kyoto University

Abstract. The subsurface flexure structure of the Uemachi Fault, which runs in the center of Osaka City, Japan, with N-S trend, was investigated based on numerous borehole database and numerical simulation, which was considered fault movements. The simulation result represents an actual layer profile, which was confirmed by borehole database.

Keywords: borehole database, fault structure, flexure zone and fault displacement

1. Introduction

The Uemachi fault zone locates in the center of the Osaka City with N-S trend. The Uemachi fault is buried reverse fault and forms the flexure zone. Lifelines and constructions should consider the displacement of the Uemachi Fault Zone. In this region, the detection of geomorphological approach is difficult because of several regression of transgression of sea. Many organizations have carried out investigations of fault structures. Various surveys have been conducted, such as seismic reflection survey in and around Osaka (Fig. 1). Many borehole data for the constructions have been collected and the borehole database has been constructed. The database provides the high-quality subsurface structural information with several geological borehole data.

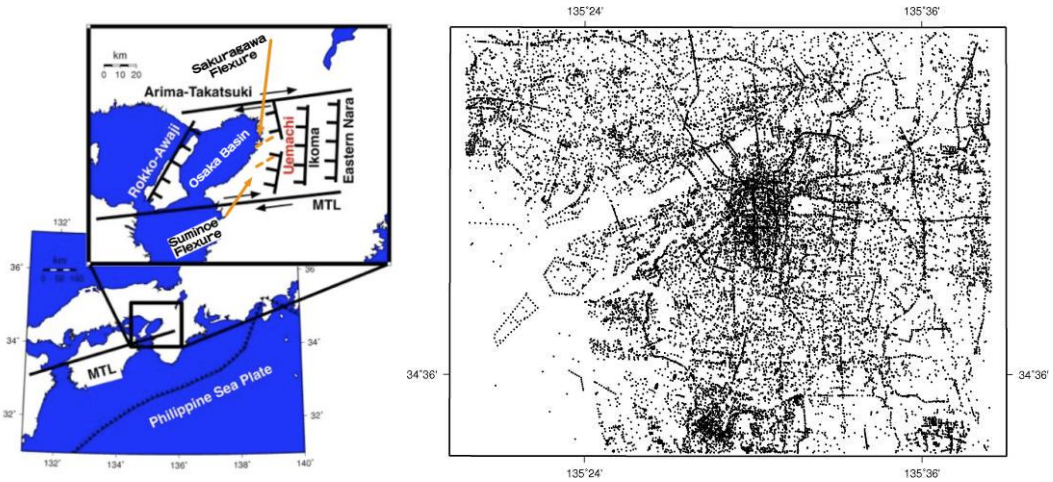

Fig. 1: Left: Tectonic setting of Uemachi fault. Right: Location of Uemachi Fault and survey lines and borehole points.

+ Corresponding author. Tel.: +81-6-6539-2975; fax: + 81-6-6578-6253.
E-mail address: naoto@geor.or.jp.

In this study, we introduce the structures based on the borehole database. We examined the structures with the result of the numerical simulation.

2. Data and Method

2.1. Borehole data

The many borehole data have been interpreted by compared with several geological investigated borehole and extend the lithological and geological information in lateral direction. Fig. 2 shows the example borehole profile across the Uemachi fault (Kansai Geo-informatics Network [1]).

The distribution of interpreted marine clay layers was investigated. Fig. 3 shows gradient of the top on Ma10 above 1 degree. The contour of the basement also shown (Inoue et al. [2]).

Fig. 2 and Fig. 3 indicate the flexure structures on the west side of the Uemachi fault. Furthermore, several layers on the eastern side of the Uemachi fault dips towards the east side. In the next section, we

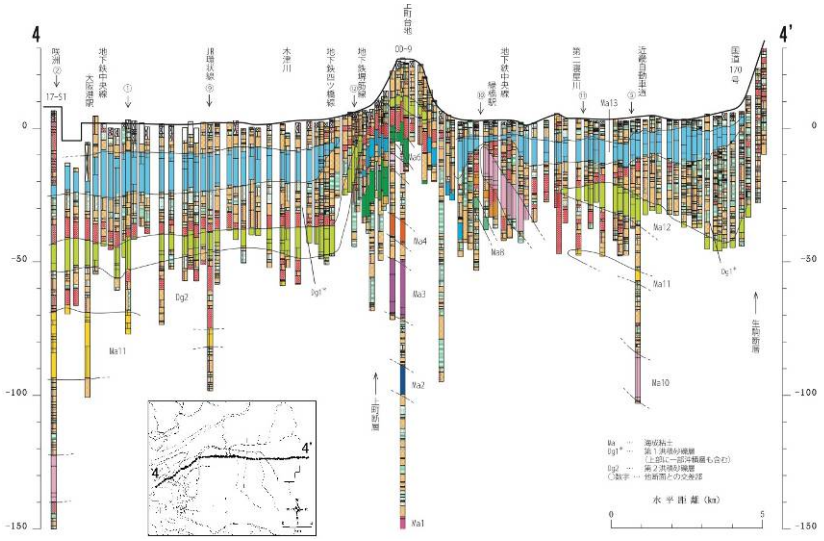

Fig. 2: Borehole database profile across the Uemachi Fault (Kansai Geo-informatics Network [1]).

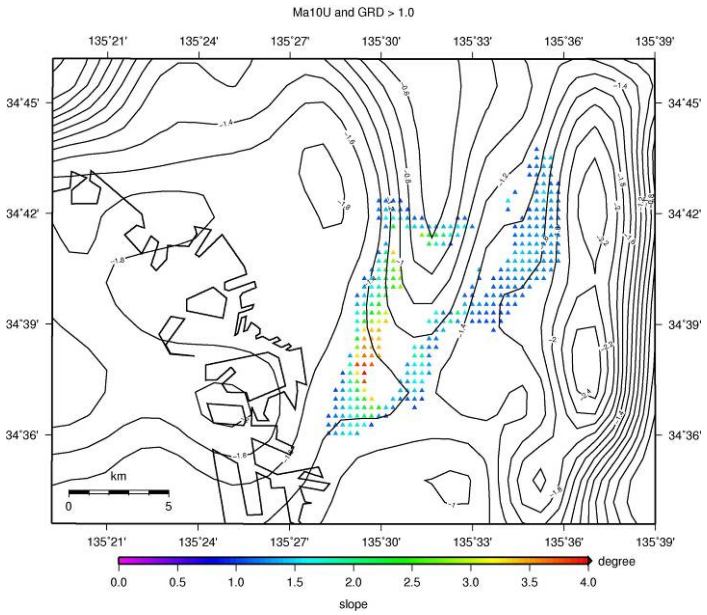

Fig. 3: Distribution of flexure zone of Uemathi fault (Inoue et al. [3]). The contour of the basement also shown (Inoue et al. [2]) in km.

investigate the distribution of the marine clay due to the fault structure based on numerical simulation.

2.2. Numerical Simulation

Various numerical simulations have been carried out to investigate the development of buried reverse fault in soft sediment (e.g. Lin et al. [4]). The movement of the basement is given as wall movement in many numerical simulations (see Fig. 4 case 2). We carried out two cases of the simulations as shown in Fig. 4. The Comprehensive Research on the Uemachi Fault Zone reported that the dip of the Uemachi fault is 50° to 60°. Ishiyama [5] reported the 40°. We simulated low and high fault dip angle (30 ° and 60°). The total slip of the basement is 200m. The model was divided into 500 x 500 m. The Drucker-Prager and elastic model were used for the sediment and basement, respectively. The physical property is shown in Table. 1. We used Pylith code [6] for the simulation.

Table. 1 Physical property

basement		(elastic model)
Density	[km/m3]	2,700
Vs	[km/sec]	3,300
Vp	[km/sec]	5,500
sediment		(elastic-plastic model)
Density	[km/m3]	1,900
Vs	[km/sec]	900
Vp	[km/sec]	1,900
Friction angle	[degree]	40
Cohesion	[Pa]	75,000

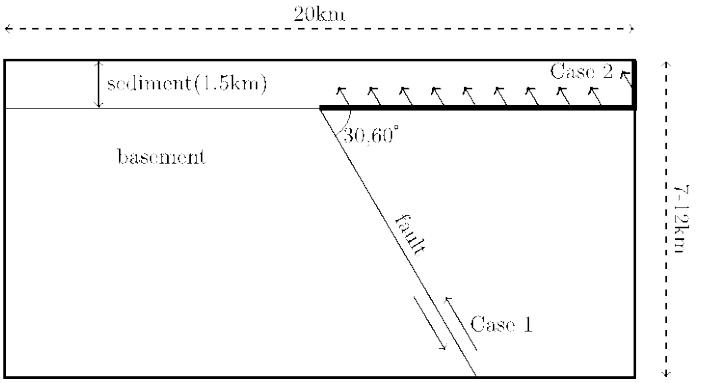

Fig. 4 Model Setting

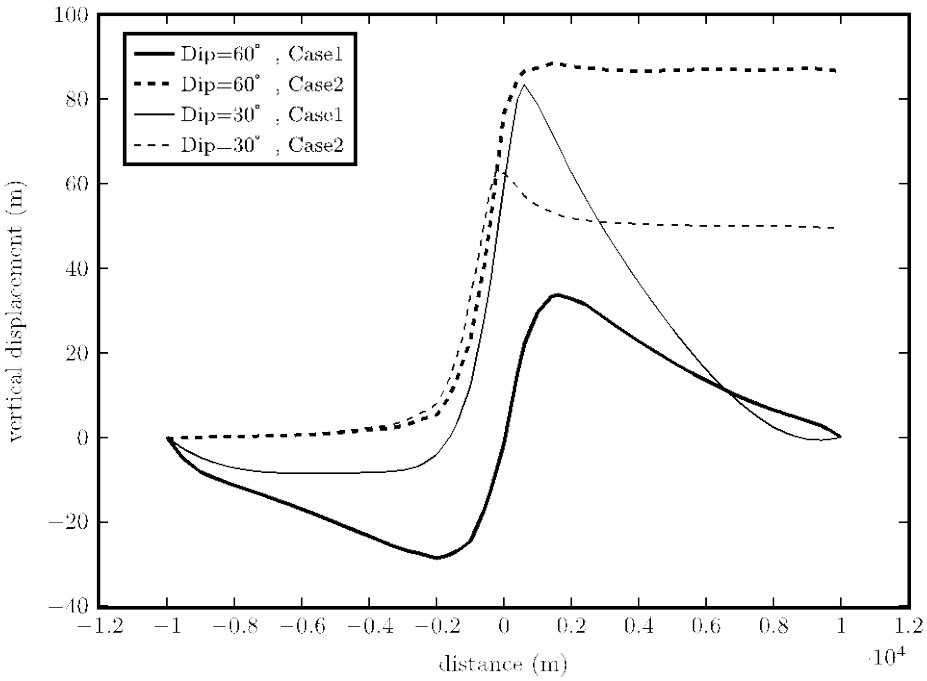

Fig. 5: FEM Result

3. Concluding Remarks

Fig. 5 shows the simulation result. The profiles shown the displacement at z=-50m. The case1 represents the flexure structure of marine clay on the west side of the fault and also represent the dipping to the east on the east side of the fault. The result of the low dip angle model is similar to the borehole profile in the northern part of the Uemachi fault (Fig. 2). The flexure structures were examined based on the borehole data around the Uemachi fault. The layers show the flexure structures on the west side of the fault and show the dipping to the east on the east side of the fault. We carried out 2 kinds of the Numerical simulation of the blind reverse fault. The simulation with fault movement shows the good agree with the actual distribution of the marine clay derived from borehole data.

4. Acknowledgements

This research is partly funded by the Comprehensive Research on the Uemachi Fault Zone (from FY2010 to FY2013) by the Ministry of Education, Culture, Sports, Science and Technology (MEXT).

5. References

[1] Kansai Geo-informatics Network. Geo-informatics for Geological and Geotechnical Researches of Kansai Ground - Osaka Plain and Osaka bay -, 2007, pp. 354.

[2] N. Inoue, N. Kitada, Y. Itoh, K. Takemura, and K. Nakagawa. Integrated study of high resolution geophysical and geological information of Osaka Bay, Southwest Japan, Journal of Asian Earth Sciences, 2003, Vol. 22, p. 1–11.

[3] N. Inoue, N. Kitada, and K. Takemura. Uemachi Fault deformation zone mapping with borehole database, Japan Association for Quaternary Research Meeting Abstract, 2012, p. GP-10.

[4] M.-L. Lin, C.-F. Chung, and F.-S. Jeng. Deformation of overburden soil induced by thrust fault slip, Engineering Geology, 2006, Vol. 88, No. 1–2, p. 70 - 89.

[5] T. Ishiyama. Geometry and kinematics of the Uemachi and Ikoma fault zones beneath Metropolitan Osaka, central Japan, Active Fault and Paleoearthquake Researches, 2003, Vol. 3, p. 145–155.

[6] B. Aagaard, S. Kientz, M. Knepley, L. Strand, and C. Williams. PyLith User Manual Version 1.9.0, www.geodynamics.org, 2013,

ISBN 979-458-758-3
Proceedings of the 3rd International Conference on the Geohazard Information
Zonation and 5th Seminar & Short Course of HASTAG (GIZ2014-HASTAG5)
Organized by UMSU, HASTAG, USM
Medan, Indonesia, October 20-22, 2014

Consideration about Subsurface structure of Uemachi Fault using geotechnical borehole database in Osaka, Japan

Naoko KITADA [1], Naoto Inoue [1], Keiji TAKEMURA [2] and Muneki MITAMURA[3]

[1] Geo-Research Institute
[2] Department of Geosciences, Graduate school of Science, Kyoto University
[3] Department of Geosciences, Graduate school of Science, Osaka City University

Abstract. In Osaka, Uemachi Fault is one of the famous active faults. It across the center of Osaka and lies in N–S direction mainly and is more than 40 km in length. Pliocene to Quaternary sediment "Osaka Group" and terrace sediment are found to be deposited in the Osaka Plain. These sediment are very thick layers over 1000m therefore, fault structure are appeared as flexure zone (only vending the strata) and hidden the fault displacement around the surface.

In this study, we try to show the flexure zone around central Osaka area using borehole database and decided the site of borehole drilling site and carried out the survey in order to decide the displacement rate of Uemachi fault. Sakuragawa flexure and Suminoe flexure are considered the secondary fault of Uemachi fault system. These are NE-SW trend and only several km lengths. Database show the Sakuragawa flexure wind in the plain. We carried out the drilling the borehole and sampling the core samples in the Sakuragawa flexure zone. The result of compare with the neighbor area, the average displacement speed indicates more active the Sakuragawa flexure rather than Uemachi fault zone.

Keywords: Osaka Plain; active fault; borehole database; marine clay; surface structure; fault activity

1. Introduction

The Uemachi Fault in Osaka is an important active fault that controls tectonics and sedimentation in the Osaka Basin. It across the center of Osaka and lies in N–S direction mainly and is more than 40 km in length. The sediments that cover this basin are over 1000 m thick and, start to subsidence of the basin and aggradation from 3.5 Ma (Kitada et al., 2011 [1]). Cyclic climate change has occurred since 1.3 Ma, with at least 15 layers of marine clay having been deposited in central Osaka during warm intervals. The stratigraphy of this sedimentary sequence, known as the Osaka Group, has been summarized for upland areas on the basis of correlation of marine clay beds and volcanic ash layers.

2. Characteristics of Uemachi fault and borehole database

In Osaka, Uemachi Fault is important active fault control the tectonic movement of sedimentation of Osaka basin. Pliocene to Quaternary sediment "Osaka Group" and terrace sediment are found to be deposited in the Osaka Plain and Holocene marine clay layers (Ma13) are covered these plains in order to sea level change. Fifteen layers of marine clay beds are deposited due to the cyclic sea level changes during glacial retreats. These sediment are very thick layers over 1000m therefore, fault structure are appeared as flexure zone (only vending the strata) and hidden the fault displacement around the surface（Fig.1）. The up side on the fault (east side) is modified by erosion and urban development however, many seismic reflection surveys information the fault trace line on a piecemeal basis. One of the subway construction project across the fault, are carried out the many borehole drilling survey around the fault. It is the good case to understand the subsurface structure around fault. The active fault survey is almost done by the seismic reflection survey. However the surface structure is very complicated and difficult to estimate the folding structure. The result of this study along the subway, these marine clay layers are correlated using tephra and microfossil analysis. Fault displacement is resolved by the 600m flexture zone. These flexture zone need

attention of amplified the seismic wave not only the fault displacement. From 2010, Project of focus investigations for Uemachi fault start and in this program, to make clear the distribution of this flexture zone, we use borehole database of KG-Net.

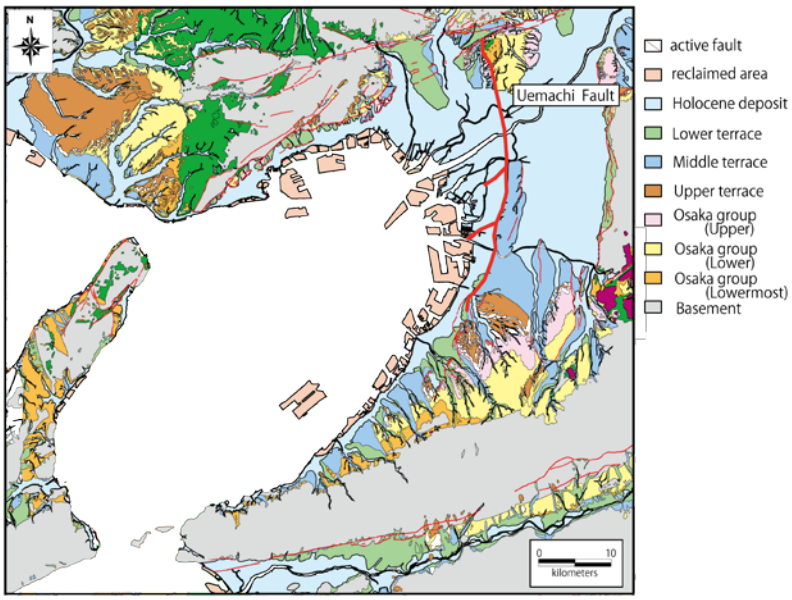

Fig 1: Geological and tectonic map of area around Osaka Area
(Active fault map in urban area, 1996 [2])

In the Osaka basin, about 60,000 borehole data was collected and in the Uemachi fault zone, about 2000 borehole data can used to study about subsurface structure (Fig 2). Geological subsurface structure in the Osaka basin is considered about delta deposit area (lowland) and sometimes in the marine environment due to the sea level change. Figure 3 shows the cross sections of the Osaka basin. Blue and green strata show the marine clay layers. Uemachi uphill were formed by the structural movement of Uemachi fault. The seismic profile shows the displacement of the top of the basement rock over several hundred meters (Fig.4).

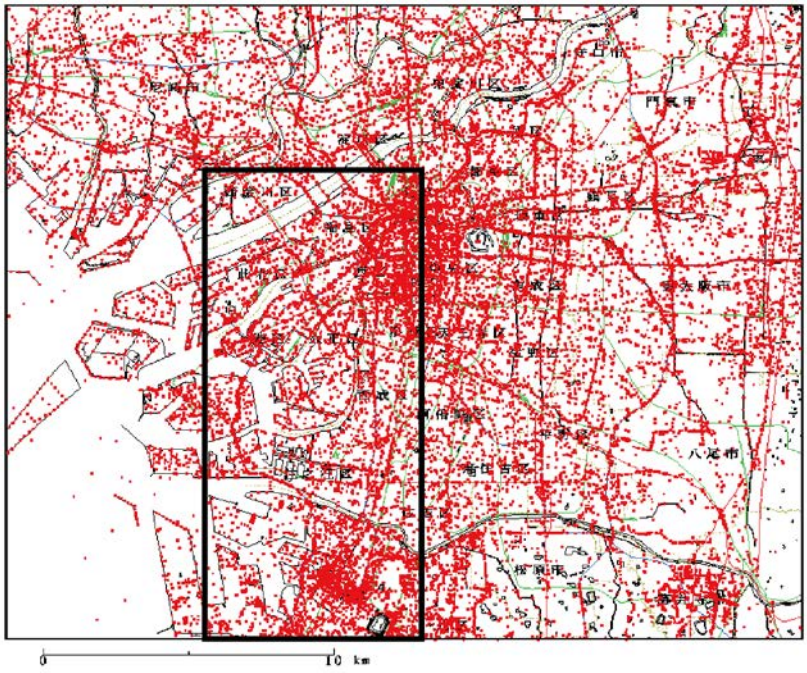

Fig 2: Distribution of borehole database in the Osaka Basin
Square shows the study area.

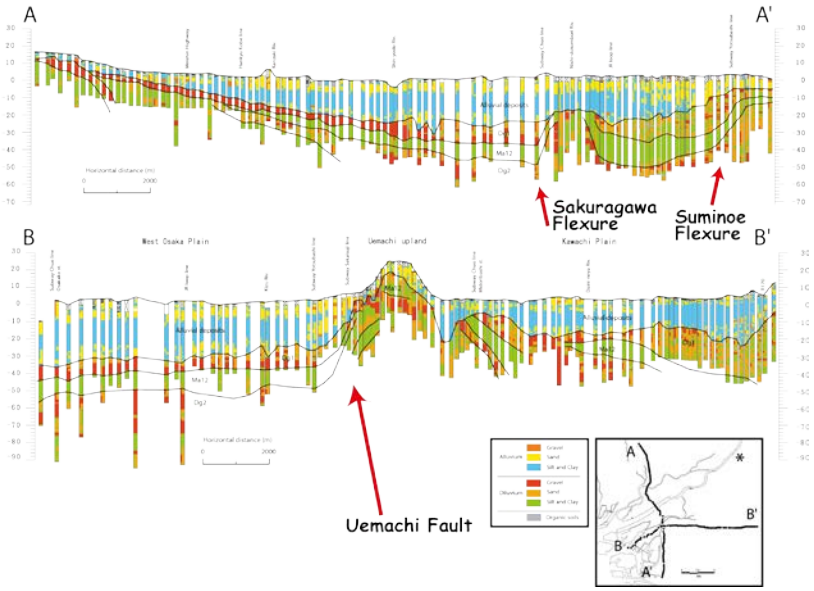

Fig 3 Geological cross section across the Osaka plain [3]

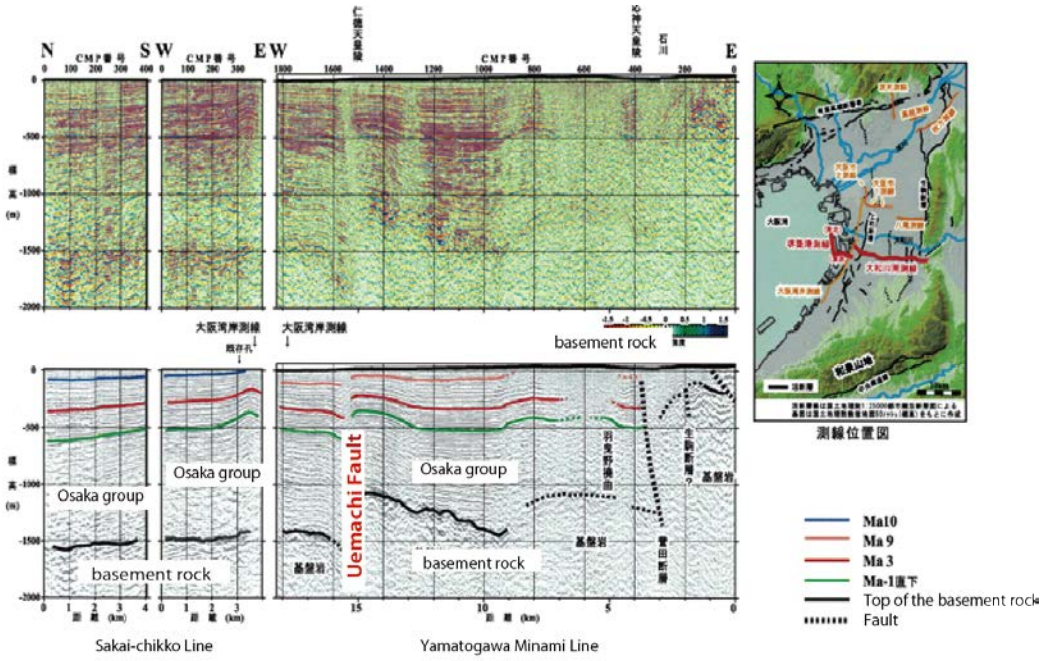

Fig 4 Sceismic profile inth Osaka basin [4]

3. Subsurface structure around Uemachi fault and result

We first examined the borehole data along the seismic reflection line and then considered the surrounding area. An example of this analysis is shown in Figure 5, which highlights the fact that the buckling is expressed particularly well in the marine clay layers. An Upper Pleistocene marine clay (Ma12) is a good indicator of the flexure zone. We constructed many cross sections in and around the fault zone and classified the deformation form into three categories around the flexure zone. First, Ma12 marine clay layers were folded and were recognized on both the up and down sides of the flexure. Second, Ma12 marine clay layers appeared to be folded, but did not continue toward the hanging wall. Third, old marine clay, which was folded or displaced, was observed. An example of the correlate between seismic profile and borehole data shows in Fig 5. The results of this study allowed us to map the distribution of folding in a zone in the west of the Osaka area. Folding can be classified into three types: (1) Ma12 folding, (2) Ma12 folding that does not continue toward the hanging wall, and (3) folding or displacement of

old marine clay. Ma12 marine clay is folded near the flexure, but the hanging-wall side appears to be denuded. Type (3) is distributed around Uemachi in upland areas, but the Ma13 and Ma12 layers are not found in these areas; therefore, it is difficult to estimate later activity along the Uemachi Fault [5] (Fig 6).

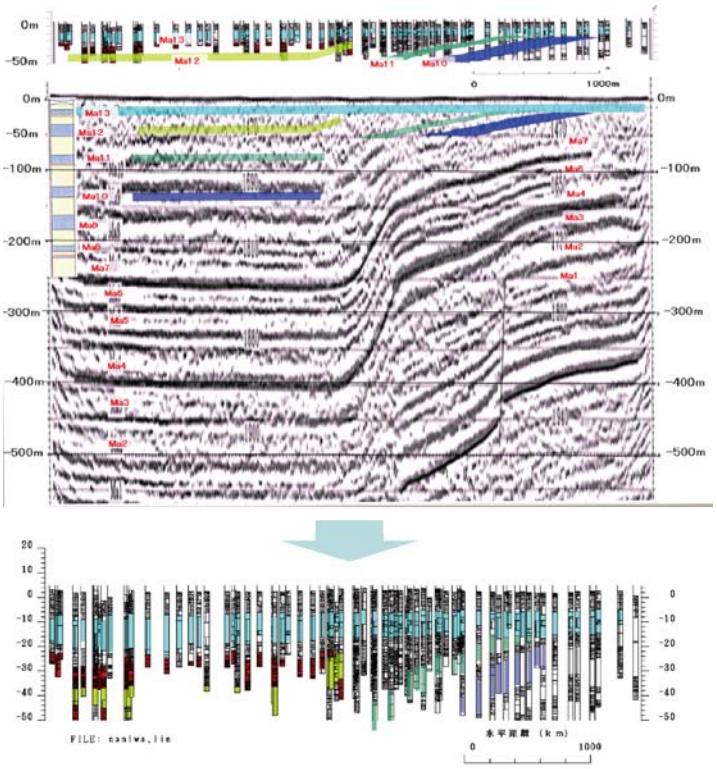

Fig 5 An example of compare seismic profile and borehole data

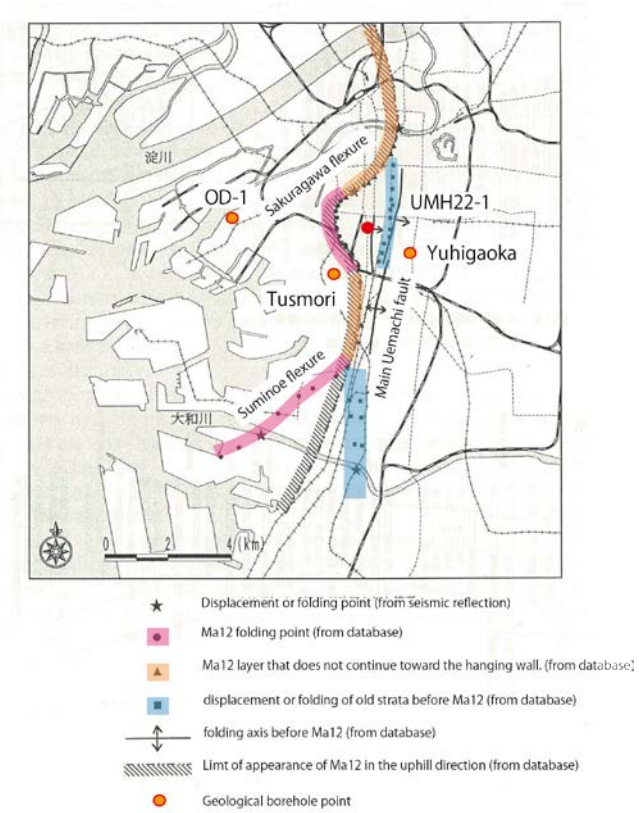

Fig 6: Distribution of flexure zones (Kitada et al, 2012)[5]

In this time we correlate more borehole data before and show the detail the folding zone in the Osaka basin. Figure 7 show the folding zone map in Osaka basin. Folding zone include Ma12 (pink zone) is the positively resent activity because the Ma12 (about 12,500 years before) sediment is folding. These zone are NE-SW direction not N-S. It might be changed the stress direction in the Osaka basin.

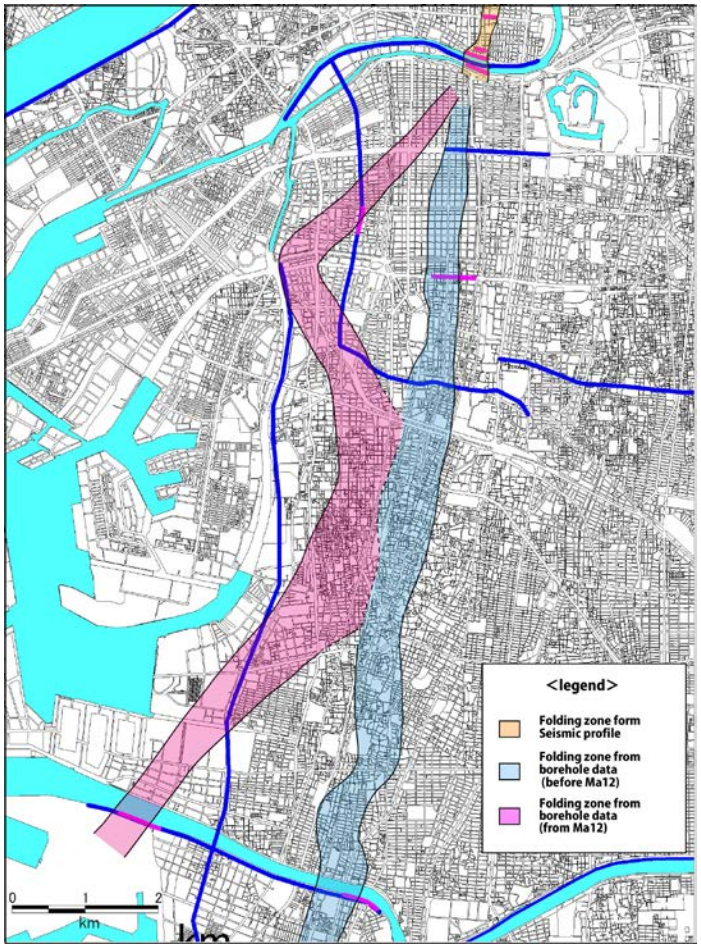

Fig 7 Distribution of the folding zone of Uemachi Fault

4. Acknowledgements

This research is funded by the integrated research project for the Uemachi active fault system in FY2011 by MEXT.

5. References

[1] Naoko KITADA, Naoto INOUE, Keiji TAKEMURA, Kouji FUKUDA and Tsuyoshi EMURA (2011）:Subsurface structure model around Kansai Airport according to re-interpretation of borehole data based on result of KIX18-1 core. *Advances in Ground Technology and Geo-Information*. Kok-Kwang Phoon, Siang Huat Goh & Rui Fu Shen (ed.)，137-142.

[2] GEOLOGICAL SURVEY INSTITUTE, "1:25,000 Active fault map in urban area," *Geological survey report* D.1, No. 524,333,502.

[3] Geo-database Information Committee of Kansai (2007): *"Shin Kansai Jiban (Ground of Kansai Area – Osaka Plain to Osaka Bay-*), p. 296.

[4] Osaka Prefecture (2004): Structural explorations in the Osaka Plain. *digest repot*, 74pp.

[5] Naoko KITADA, Naoto INOUE, Keiji TAKEMURA, Muneki MITAMURA (2012): Consideration of subsurface structure using a geotechnical borehole database in Kansai area, Awan International Conference on Civil Engineering (AICCE'12) Geohazard Information Zonation (GIZ'12), 691-698.

ISBN 979-458-758-3
Proceedings of the 3rd International Conference on the Geohazard Information
Zonation and 5th Seminar & Short Course of HASTAG (GIZ2014-HASTAG5)
Organized by UMSU, HASTAG, USM
Medan, Indonesia, October 20-22, 2014

Geological Models and Geotechnical Models – Lessons from Development of Japan-wide Geotechnical Ground Models -

Hiroaki Todo [1] and Koji Yamamoto [2]

[1] Overseas Department, Kiso-Jiban Consultants Co., Ltd., Tokyo, Japan
[2] Geo-Informatics Engineering Group, Geo-Research Institute, Osaka, Japan

Abstract. On October 15, 2010, the Japanese Geotechnical Society (JGS) released sets of geotechnical ground models for 6 cities on the internet. At the end of 2014, the public release would grow to 34 cities, and by 2017 the models of additional 40 cities would join the line-up. Hundreds to thousands of individual ground models constitute a database of ground models for a city, which is a part of the nation-wide ground model databases. Each model covers an area of 250 m by 250 m in plan and to a depth of less than 100 m from the ground surface, and was built by using data from various geotechnical information databases. The paper discusses one issue arising from rapid expansion of the model construction in number of cities. The issue is 'relationship between geological models and geotechnical models.' Although they are different concepts, their differences are often overlooked as they are similar.

Keywords: Digital geotechnical information database, ground models, urban geo-informatics, hazard map

1. Introduction

Japan has more than 100 geotechnical information databases published since 1960 by various organizations in the form of printed media, compact disks, and the internet. Those databases are, however, diverse in terms of format, data contents, accuracy, data construction, input methods, distribution methods, up-dating methods and frequency, and subscription fees [1]. It is thus difficult for the public to compose appropriate data from various databases and comprehend the ground conditions at desired locations. In 2006 the JGS studied the way to integrate those geotechnical information databases and to publish them on the internet in consolidated, harmonized, and unified ways, so that the public can easily access and understand ground conditions anywhere in Japan. Subsequently the JGS started building their own ground models using then available geotechnical information databases and published the first version of the geotechnical ground models for 6 cities on the internet on October 15, 2010 [2]. The published ground models expanded into more cities year-by-year reaching to 34 cities at the end of 2014. During the 8 years of the development, it becomes apparent that even geotechnical specialists have difficulties in properly interpreting the data from these databases. The paper aims at improving the interpretation of the data through systematic approach by making distinction between geological models and geotechnical models.

2. Geotechnical Databases in Japan

Before 'the Access to Government Information Act' was in force in 2001, there were already about 100 geotechnical information data bases (GIDB) in Japan and they were published mostly by private hands [3]. Figure 1, the locations of typical geotechnical information databases, shows that most of the databases cover small areas of one or two cities while others enclose large areas containing several prefectures.

The construction of the GIDBs in Japan started around 1960 in large metropolises like Tokyo, Osaka, and Nagoya. They are a sort of borehole data books, and are basically compilations of borehole data and soil cross sections. The construction of the databases has spread to all over Japan and has continued up to today. The advance of digital technology and its growing availability stimulated the shifting from paper-based databases to digital databases. With the rapid development of computer hardware, storage technology, and GIS technology, the databases expanded their coverage from city or prefecture size to much greater areas.

Such databases covering several prefectures are regional geotechnical information databases (RGIDBs) published by the local chapters of the JGS [4]. There are 7 RGIDBs covering such large areas. Compact

disks (CD) or digital versatile disks (DVD) are common media to provide the data except Hokuriku and Tohoku, where the data are distributed on the internet. Only the members who pay annual membership fee can purchase the data of Hokuriku, Tohoku, Kansai, and Shikoku, and receive updated data, while anyone can buy the databases of Hokkaido, Kanto, and Kyushu, but there is no update in these databases until a new version is published.

After 'the Access to Government Information Act' was in force, disclosure of the borehole data by municipalities and prefectural governments increased. Ministry of land, infrastructure, transportation, and tourism also started publishing the geotechnical data on the internet, named as Kuni-Jiban.

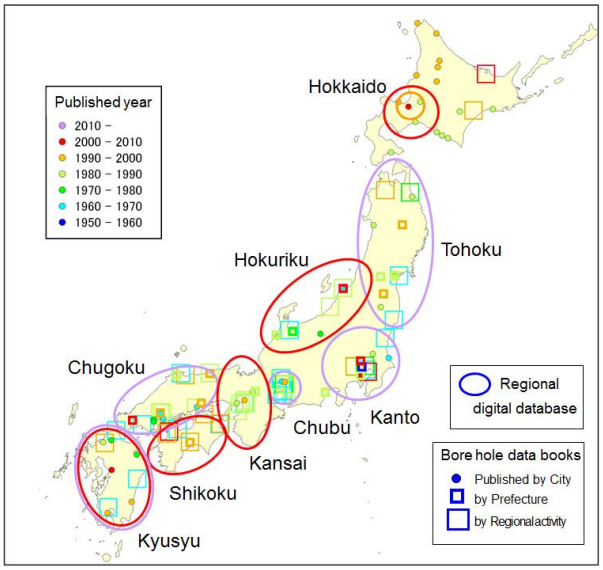

Fig. 1: Locations of Typical Geotechnical Information Databases in Japan (as of July 2014)

3. Development of Japan-wide Geotechnical Ground Models

In July 2006 a 5-year, nationwide, inter-agency project, the Integrated Geophysical and Geological Information Database, started, led by the National Research Institute for Earth Science and Disaster Prevention (NIED), with the participation of the National Institute of Advanced Industrial Science and Technology, the Public Works Research Institute , Tokyo University, Tokyo Institute of Technology, and the JGS. The Special Coordination Funds for Promoting Science and Technology (SCFPST) under the Ministry of Education, Culture, Sports, Science and Technology, Japan, financed the project [5].

The JGS's mission in the project was to link the existing geotechnical databases that the Society's local chapters took part in their construction, maintenance, and administration. For this purpose, the JGS set up a work team. After a year of discussion, the work team's answer to 'the linking the existing geotechnical databases' was to make ground models throughout Japan by interpreting all the available raw data from the existing databases. The system is called Nation–Wide Electronic Geotechnical Database Systems (NEGDS), which is essentially a collection of ground models with each model representing the ground of 250m by 250m in plan to a maximum depth of 100 m. The proposed systems can digitally construct, save, modify, and display the models and the information contained there can be viewed and downloaded from the internet.

The reasons for building the ground models rather than merely linking the existing databases through the internet are as follows with details given elsewhere [1].

(1) The existing databases are very much different in their construction, systems, data structures, data contents, and data quality. It is very difficult to link such variety of databases with different contents and systems.

(2) The condition that the research results funded by the SCFPST have to be open to the public makes many operators of the databases difficult to participate to the systems because all the data linked to the systems have to be eventually disclosed. The problems associated with the free disclosure are:-

- Some data had been supplied with prior confidential agreement not to disclose the data due to ownership of the data, copy rights, and information on private properties.
- Some data had been supplied with the conditions that data can be used for research only, and cannot be released to the public.
- The databases were sold with fee.

(3) The work team did not have authority over other independent database operators and could not force them to link their databases to a new system the work team was going to develop. The systems should be such that the other independently operated databases would willingly join.

Building the ground models can skip the above problems related to simply linking various databases. As of July 2014, the models cover 34 cities as shown in Figure 2 and all the models will be published by the end of the year.

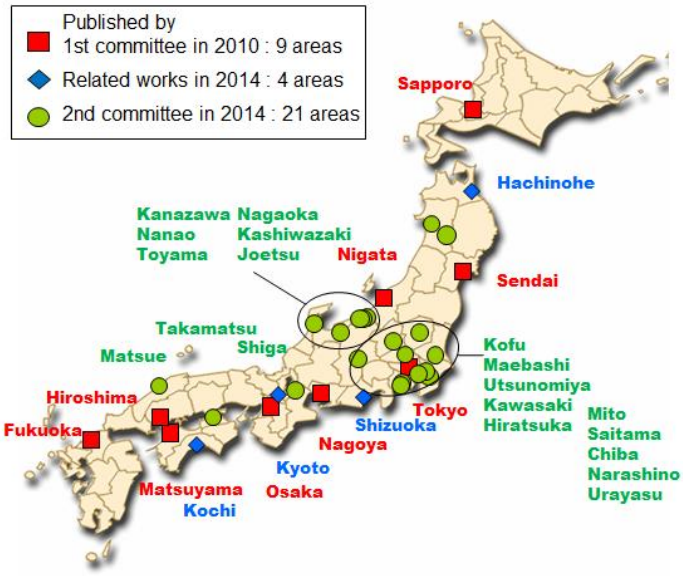

Fig. 2 Areas of Ground Models Ready for Publication as of July 2014 together with Earlier Publication

4. Construction Method of One Ground Model

The construction procedure of a model is as follows [1]:

(1) To use a standard 250 m grid map published by Geographic Survey Institute of Japan.

(2) To select the location for the model to be constructed.

(3) To construct a ground model using borehole data available nearby in consideration of topography and geology. For making the ground model, the software developed by the work team is available to assist construction of a ground model from the existing digital databases.

One should not simply make the model by selecting one borehole inside the area, but should build the model in consideration of surrounding ground conditions. The model thus represents average ground conditions in the area, not the ground condition at the center of the area.

5. Pitfalls during Construction of Japan-wide Geotechnical Ground Models

Anyone can easily construct a ground model of a particular location of 250 m by 250m area using the software developed by the work team based on the data from digital geotechnical databases at hand. Although the user manual of the software emphasizes geological, topographical and engineering interpretation for the construction of the models, the authors have observed that this statement is taken lightly by many who make the models with little training. The authors sometimes observe that geotechnical models, constructed straight away using the software with little reference to local geology, are assessed later if they conform to available published geological models such as geological cross sections. This practice is against the intent of the user manual of the software and the development team of Japan-wide geotechnical models. The geotechnical ground models should be built while referring to local geology, topography, and geotechnical engineering properties.

Rapid expansion of the coverage areas to many cities is the cause for lacking well-trained volunteers. While anyone can construct the models very easily using the software with the borehole data in and around the target area, the requirement for the geological, topographical and engineering interpretation is vague without standardized procedures.

Another reason for this unintended practice is that the software requires inputting soil types (clay, sand, etc.) but is incapable of handling geological classification (Holocene, Pleistocene, etc.) of each soil layer. Similarly, the software needs to differentiate between natural ground and man-made ground. For example, man-made sandy ground and natural sandy deposits are both classified as sand by the software, while their potential for liquefaction during earthquakes is very much different.

The present software cannot produce the ground models where no data is available, because the ground models are constructed based on the borehole data within and around the target area of 250 x 250m. However, the models can be constructed with reasonable accuracy at such blank areas if geological models such as contour maps of the base of the Holocene deposits are available.

6. Geological Models versus Geotechnical Models

In every-day practice, geotechnical engineers usually use the geological models and geotechnical models in the following ways. The information contained in each model is commonly as in Table 1.

- Geological models; soil cross sections are first made based on topographic map, survey drawings, boreholes data, sounding results, and other information. Contour maps of the bottom of soft clay layers are often made.
- Geotechnical models; ground models are constructed for the evaluation of bearing capacities and settlements based on the geological models and soil test results.

Table 1 Information Contained in Geological Models and Geotechnical Models

Geological Models	Geotechnical Models
Geological layers and thickness	Soil layers and thickness
Geological age	Groundwater levels
Geomorphology	Geotechnical properties
Sedimentation environment	SPT N-values
Sedimentation sequence	Strength, compressibility, permeability, etc.
Sea level changes	
Volcanic ash key beds	
Contour maps (bottom of Holocene)	

7. Recommendations

The authors perceive the necessity of creating a standard/guideline procedure for the geological and topographical interpretation. A draft procedure is proposed below taking an example from the lower reach of the Tama Gawa River:

(1) To set up a local team of specialists who have good knowledge of local ground conditions. The team should consist of geo-engineers, geologists, and specialists for topography and geomorphology because geotechnical engineers are generally weaker in interpreting topography and geology compared to geologists and geo-morphologist. A list of member has to be submitted to the central development team of Japan-wide geotechnical models.

(2) To construct geological models first before making geotechnical models in order to better represent the ground conditions. This should be clearly stated in the user manual of the software.

(3) To understand topographic conditions by investigating literatures
- Topographic features as shown in Figure 3
- Micro-topography classification map including past meander of the rivers as shown in Figure 4
- Liquefaction record map ([7] for example)
- Recent topographic change such as reclamation and large scale land development

(4) To understand geological history and sedimentation environment by investigating literatures
- Geological map as shown in Figure 5
- Published geological history and sedimentation environment
- Collection of published geological cross sections such as Figure 6
- Collection of published contour maps of various geological formations
- Collection of other geological literature

(5) To understand groundwater level by collecting published information

(6) To try to comprehend the ground conditions at a particular location to be modeled
- To draw geological cross sections for the area to be modeled
- To identify geological formations to be present at the area
- To draw contour lines for the top of the tertiary formations, the top of the Pleistocene deposits, the bottom of the Holocene deposits, the engineering base level such as SPT N-values of 30 or 50, such as shown in Figure 7

(7) To cross check the identified geological formations with their geotechnical engineering properties (for example, soft clay should have high natural water contents).

(8) At this stage, the software is introduced to make the ground models. The first step is to relate the soil types given in each borehole log to the geological formations. For example, each soil type is labeled as Tertiary formation, Pleistocene deposits, Holocene deposits, or the engineering base formations. This process, the most difficult part, requires discussions and judgment by specialists.

(9) Now, it is ready to make models using the software.

The authors also consider important for undergraduate and graduate students majoring geotechnical engineering to learn quaternary geology, sedimentology, and geomorphology, among others.

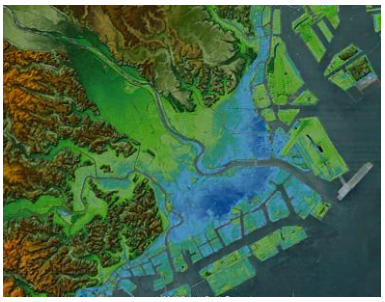

Fig. 3 Topographic Features

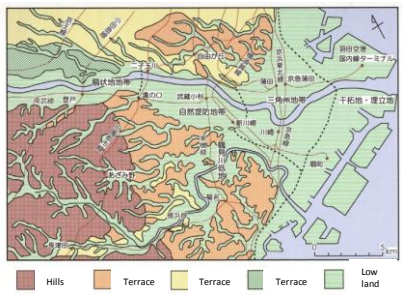

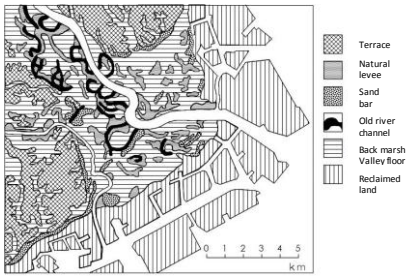

Fig. 4 Topographic Classification (Figs. 4 to 7, Reference to [6])

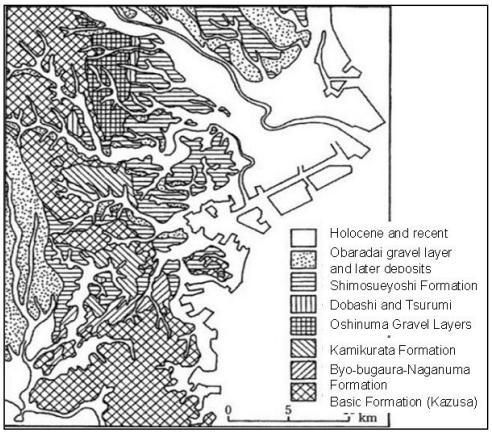

Fig. 5 Geological Map

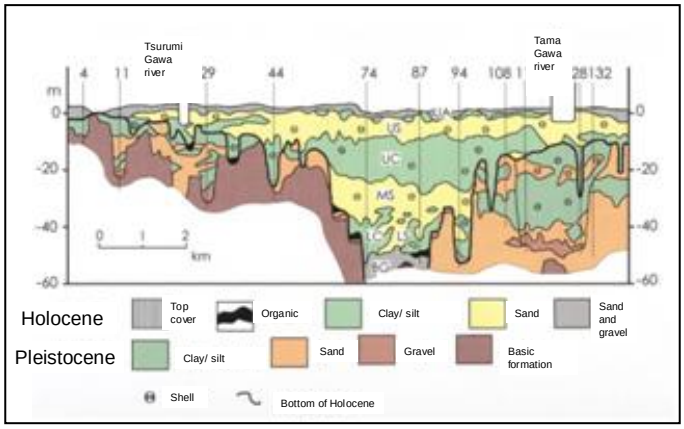

Fig. 6 Geological Cross Section

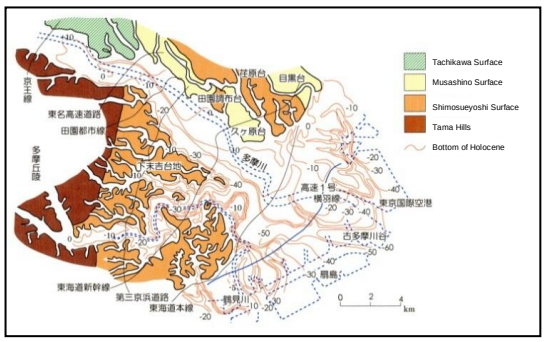

Fig. 7 Contour Lines of Bottom of Holocene

8. References

[1] Todo H., Yamamoto K., Mimura M., and Yasuda S.. Japan's Nation–Wide Electronic Geotechnical Database Systems by Japanese Geotechnical Society, *Geotechnical and Geological Engineering*, Published online 07 November 2012, Springer, 10.1007/s10706-012-9562-x

[2] Japanese Geotechnical Society. *Nation–Wide Electronic Geotechnical Database Systems*. 2010, http://www.denshi-jiban.jp/ (written in Japanese)

[3] Todo H. and Mimura M. Recent Developments of Geotechnical Databases in Japan. *Proceedings of the International Symposium on Geo-informatics and Zoning for Hazard Mapping*. December 2009, Kyoto, Japan

[4] Todo H., Yamamoto K., Wakabayashi R.. Regional Geotechnical Information Databases in Japan and Funding Methods. *AWAM International Conference on Civil Engineering & Geohazard Information Zonation*, *Caspian Journal of Applied Sciences Research, 2012*.Available online at http://www.cjasr.com

[5] National Research Institute for Earth Science and Disaster Prevention. *Integrated Geophysical and Geological Information Database*, http://www.chika-db.bosai.go.jp/ (2006), (written in Japanese)

[6] Kanagawa Group, Japanese Geotechnical Society, *The Ground of Great Kanagawa*, Gihodo Press, 2010 (written in Japanese)

[7] Wakamatsu K., *Liquefaction Record Map in Japan*. University of Tokyo Press. 2011 (written in Japanese)

HIDROLOGY AND CLIMATE CHANGE

ISBN 979-458-758-3
Proceedings of the 3rd International Conference on the Geohazard Information
Zonation and 5th Seminar & Short Course of HASTAG (GIZ2014-HASTAG5)
Organized by UMSU, HASTAG, USM
Medan, Indonesia, October 20-22, 2014

Development of Windstorm Database System for Wind Damages in Malaysia

Wan Chik, F.A [1], Che Deraman, S.N.A [1 +], Noram, I.Ramli[1], Muhammad, M.K.A [1], Majid, T.A [2] and Zulkarnain, N.Z[1]

[1, 2] Disaster Research Nexus, School of Civil Engineering, Universiti Sains Malaysia,
14300 Nibong Tebal, Penang, Malaysia.
[2]Coordinator, Disaster Research Nexus, School of Civil Engineering,Universiti Sains Malaysia,Penang,Malaysia

Abstract. Damage, losses and social problem are casualties that could create by this natural disaster. All natural disasters including those related to wind have enormous socio-economic implications in terms of the sustainability of the human habitat and built environment No complete database gathered on previous wind storm occurrence in Malaysia to study the past trend of event. A systematic wind database must be created in order to manage, to display and store the wind data. The objective of this research is to produce windstorm occurrence map and to compare wind damage with terrain category as stipulated in MS 1553:2002.

Keywords: windstorm occurrence, database, terrain category, land use

1. Introduction

Almost every year some part of Malaysia will experienced of roof damages caused by the windstorm. In Malaysia, the wind database system must be improved in order to make the information becomes more efficient and flexible. The requirement of a database system that uses the latest software is needed that can give good information to user and public regarding the windstorm events that happen nowadays. A database is an integrated collection of data records, files, and other objects. A DBMS allows different user application programs to concurrently access the same database. DBMSs may use a variety of database models, such as the relational model or object model, to conveniently describe and support applications. It typically supports query languages, which are in fact high-level programming languages, dedicated database languages that considerably simplify writing database application programs [1].

Wind data is the essential study element for wind researcher in either in meteorological field or renewable energy. Indeed, a reliable wind data also one of the aspects studies before wind system been built. However, Malaysia, there is lack of reliable and accurate wind data which present on spatial [2]. Until to date, there is no conclusive statistics that relate to the scenario of this disaster that could be referred as a whole in Malaysia are readily available. When integrating data coming from multiple different sources we are faced with the possibility of inconsistency in databases. A systematic wind database must be created in order to manage, to display and store the wind data. The current data with respect to wind data in Peninsular Malaysia is being kept in the form of news and attribute files. It will be very beneficial and time saving if a proper wind data database system is introduced to local authority.

2. Methodology

2.1. Windstorm occurrence map

The study area also included Peninsular Malaysia but the raw data is compared by year 2007 to 2012. For Peninsular Malaysia, the data collection is from news report. In this study, the data were summarized general features of the windstorm occurrences scenario of the date, location, regions, number of damaged/injured/dead, cost, structure damage, and references. The coordinate system WGS corroborated by

+ Corresponding author. Tel.: + 6045996201 fax: +6045941009
E-mail address: farah_alwani@yahoo.com

Kelab Ukur Malaysia. The finding of the coordinate of damage area is done by using Google Earth and Google Map.

Preparation of the map for the studied region was done by adding layer to Peninsular Malaysia map using the GIS software. The map is produced by divide the data by month and number of damage houses. To develop the windstorm occurrence map is by import the XYZIDRIS (ASCII XYZ) file. Establishing shape files (point, line and polygon) where performed by GIS software. The result obtained will be compared with MS1553:2002[3]. The outcome map will be compare with terrain category in MS1553:2002 Section 4 Clause 4.2.1 under terrain category definitions. The windstorm occurrence map will overlay with land use map using database query in GIS in order to get terrain category due to windstorm location.

3. Result and Discussion

This sub-section will discuss result using GIS software on wind damages mapping. This includes data collection, data extraction for Peninsular Malaysia since year 2002 to 2012 and detail data for Penang in year 2012 only. Data collected are called raw data whereby all the information are based on general features of the windstorm occurrences scenario of the date, location, region, number of damaged, injured, dead, cost, structure damage, and references.

3.1. Windstorm occurrences

Figure 4.1 shows the windstorm occurrence based on number of damages during the study years between years 2007 to 2012. Number of cases of windstorm occurrence in Peninsular Malaysia between the study years, the occurrences shows slightly increases from years 2007 to 2012. From this study, the total number of windstorm occurrences in Peninsular Malaysia between the study periods is 74 cases. In six years data period, it shows that the highest number of occurrence is in year 2012 which is 21 occurrences, followed by year 2011 (16 cases), year 2009 (12 cases), year 2008 (10 cases), year 2010 (9 cases) and the lowest number of occurrence is in year 2007 by 6 occurrences. Kedah state represents a maximum number of occurrences, 19 cases in six years data. Meanwhile the minimum number of occurrences is 3 cases where is Melaka and Penang state. The graph denotes that there is no data recorded in Kuala Lumpur State due to some circumstances.

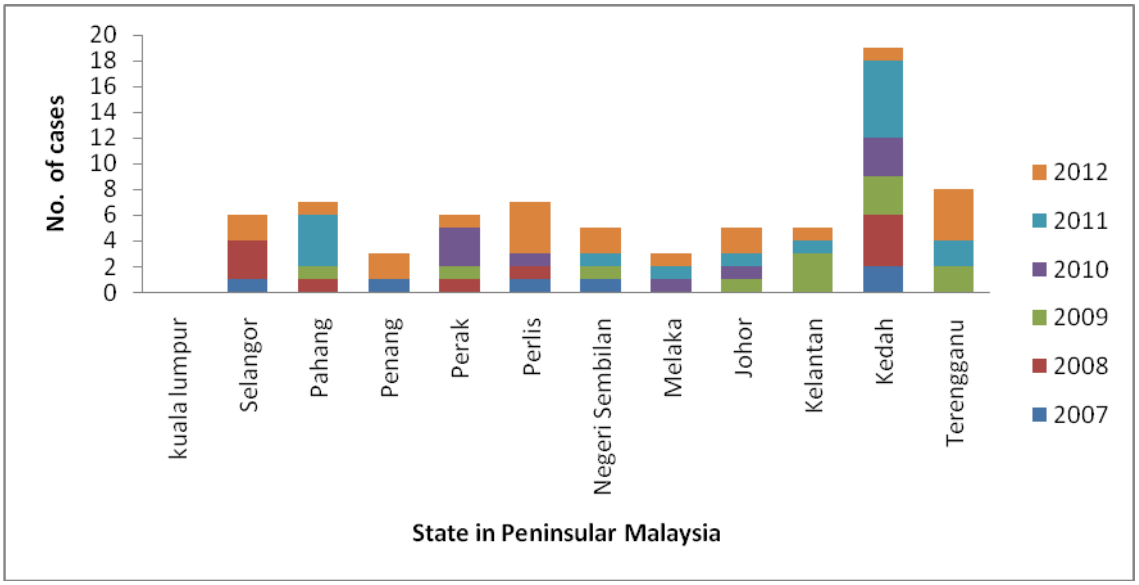

Fig. 1 Statistic of cases occurred in each state in Peninsular Malaysia (2007-2012)

3.2. Damages of building

Fig.2 shows the number of damages that occurred during the windstorm event in Peninsular Malaysia between the study years. From this study, total number of 3412 damages was recorded between the study years. The number of damage is directly proportional to number of cases where the highest number of damages is in year 2012 which is 1265 damages, followed by years 2011(747 damages), years 2010 (552 damages), years 2009 (453 damages), years 2007 (215 damages) and the lowest number of damages is in year 2008 which is 180 damages was recorded. The number of damages is increases between the six years data. Kedah state represents the highest number of damages which are 1161 damages, while 36 damages in Penang state are the lowest. Majority low rise buildings among the building structures in Malaysia face the great impact during the event. It was identified that 80% of the cases caused damaged to the roofing systems due to the thunderstorm in Peninsular Malaysia. Damage breakdown shows that 47% damage in steel sheet roofing, 30% damage on trusses system, 13% damage on roof tiles and 20% for other related damages stated by [4].

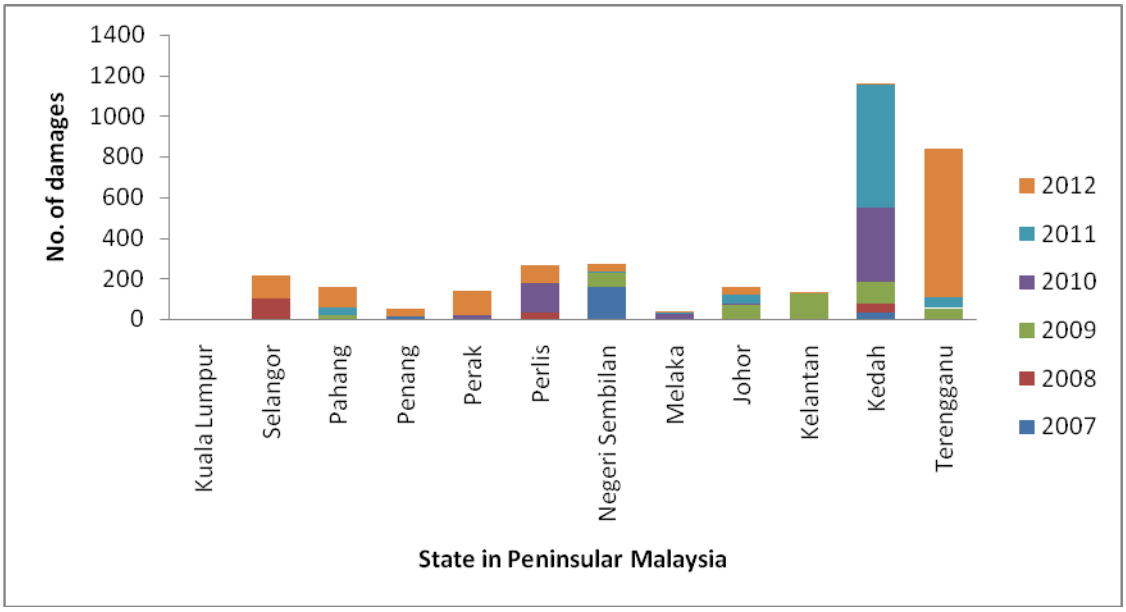

Fig.2 Statistics of damages in each state in Peninsular Malaysia (2007- 2012)

3.3. Type of land use (Peninsular Malaysia)

It is observed that most of the damaged occurs in northern region on Peninsular Malaysia. Table 1 shows the windstorm event in study area is categorized based on terrain category.

Referring to Fig.3, windstorm map is obtained from the GIS software observed that northern region mostly having category 1: open terrain. Mostly, the area is covered by grassland and agriculture activities such as paddy field. It can be concluded that Kedah state experience terrain category 1. For category 2: open terrain grassland, mostly location experienced this category at village area. For example, the location in this study area is Jelai, Negeri Sembilan. Suburban area is mostly has high population because nowadays development of housing is rapidly growth. Town area mostly included in category 3: (suburban housing). Seberang Perai, Penang is one of example of suburban area. Category 4 is for largely city centre area because closely space obstruction especially the location of building. From this study, Selangor State experienced terrain category 4.

Wind damage to low rise building mostly started with damage one of the components forming the building envelope especially roof sheeting. According to windstorm data in Peninsular Malaysia in year 2007, about 90% of damage are from roof and truss, 10% more damages are contribute from canopies, cars, dome, roof wall, porch and road facilities. From the previous study carried out, it is found that most of the failure occurred in structural system such as roof and truss. Uplifting of roof

system during wind storm also caused damage to the buildings. Generally failure occurred at two points either at roof to wall connection or at roof sheeting frame [4]. Factors of windstorm occurrences such as age of houses, type of building, topography, elevation height, roof connection, vegetation, construction standards and local human behavior shall be considered. Various phenomena occur to buildings and their surroundings during strong winds, sometimes leading to failure.

Table 1 Classification of windstorm event in Peninsular Malaysia (2007-2012) based on terrain category.

Year	Category 1	Category 2	Category 3	Category 4
2007	*Not stated*	-PADANG BESAR	-BUTTERWORTH -SUNGAI PETANI -BAHAU	-PETALING JAYA
2008	-JERLUN -PENDANG -BOTA	-RELAU -JELAI	-KLANG -KAJANG -KULIM -KANGAR -GOMBAK	-KAMPUNG PANDAN -ALOR SETAR
2009	*Not stated*	-TANGKAK -REMBAU -BESUT	-KULIM -SEBERANG PERAI -TEMERLUH -PASIR PUTEH	-ALOR SETAR -KOTA BHARU
2010	-KUALA KETIL -KAMPONG GAJAH	-LANGKAWI -KUALA PERLIS -JASIN -KMPG BTG ROKAN, GEMENCHEH	-SUNGAI PETANI -TELUK INTAN -SERI ISKANDAR -BANDAR PULAI JAYA	*Not stated*
2011	-JEMPOL -BERA	-KUALA KEDAH -TANJUNG GEMOK -KEMAMAN	-PORT DICKSON -KULIM -JERANTUT -KOTA TINGGI	-ALOR SETAR -KOTA BHARU -KUALA TERENGGANU
2012	-JEMPOL -ROMPIN	-KEMAMAN -KLEBANG -MARANG -KUALA LIPIS	-KULIM -KANGAR -SUNGAI PETANI -BUTTERWORTH -SERI MANJUNG -SIMPANG RENGGAM -TANJUNG KARANG -DUNGUN	-JOHOR BAHRU -SHAH ALAM

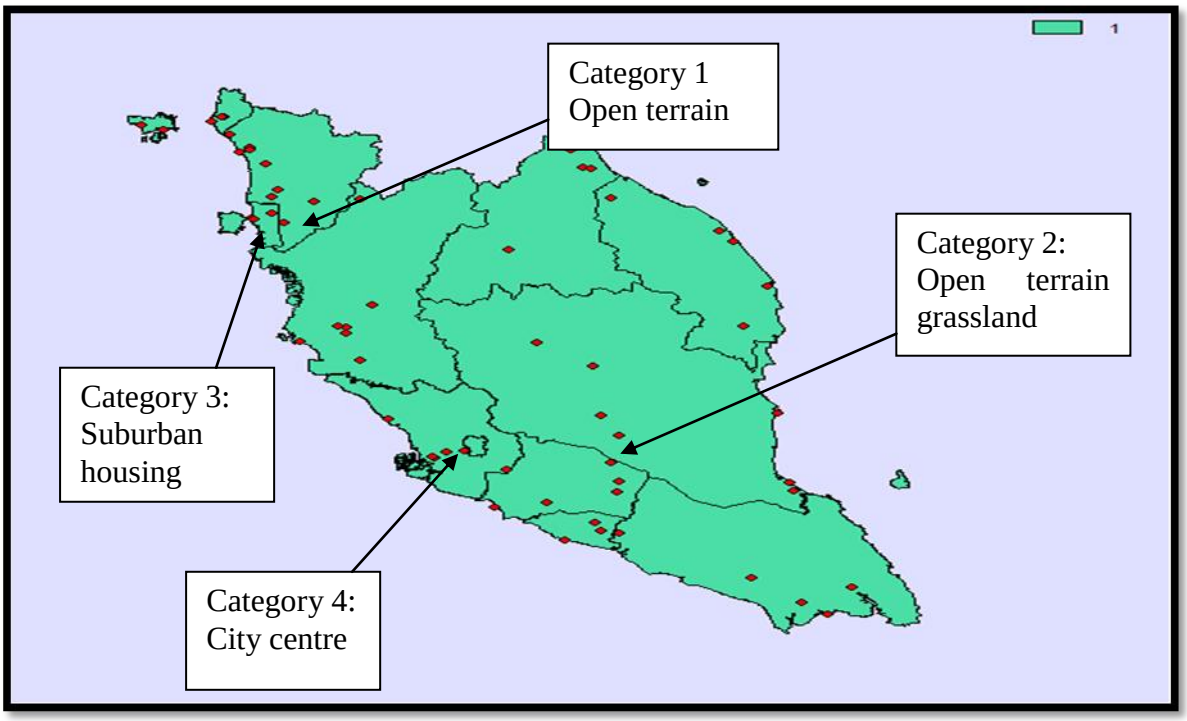

Fig.3 Windstorm occurrences map of Peninsular Malaysia based on terrain category.

4. Conclusion

From the result obtained, Kedah state experience terrain category 1 (open terrain area) Category 2: open terrain grassland, the location in the study area is Jelai, Negeri Sembilan. Suburban area is mostly has high population because nowadays development of housing is rapidly growth. Town area mostly included in category 3: (suburban housing). Seberang perai, Penang is one of example of suburban area. Category 4 is for largely city centre area because closely space obstruction especially the location of building. From this study, Kuala Lumpur and Selangor State experienced terrain category 4.

5. Acknowledgement

The author would like to express gratitude and thankful to Universiti Sains Malaysia for providing financial support from Delivering Excellence Grant for the research and Ministry of Education giving sponsorship under MyBrain15 throughout the studies.

6. References

[1] Yvette E. G. and Sunguk L, (2012). Database Management System as a Cloud Service, *International Journal of Future Generation Communication and Networking* Vol. 5, No. 2, June, 2012.

[2] Muzathik, A.M. Ibrahim, M.Z. Wan Nik, W.B. and Samo, K.B. (2009). Wind resource investigation of Terengganu in the west Malaysia. *Wind Engineering*, Vol. 33, No.4, pp 389- 402.

[3] Malaysian Standard, MS 1553: 2002, Code of practice on wind loading for building structure.

[4] Majid T.A. and Ramli N.I., (2012), Wind Loading for Malaysia Code of Practice, Proceedings Seminar dan Pameran Nasional ke III Himpunan Ahli Struktur Tahan Angin dan Gempa (HASTAG), UNIPLAZA Medan, Sumatra Utara, Indonesia, 12-13 April 2012, pp44-54.

[5]

ISBN 979-458-758-3
Proceedings of the 3rd International Conference on the Geohazard Information
Zonation and 5th Seminar & Short Course of HASTAG (GIZ2014-HASTAG5)
Organized by UMSU, HASTAG, USM
Medan, Indonesia, October 20-22, 2014

An Investigation on Flooding Perception along Erren River Bank in Tainan, Taiwan

Ya-Fen Lee[1] and Yun-Yao Chi[2]

[1] Department of Leisure, Recreation and Travel, Toko University
[2] Department of Land Management and Development, Chang Jung Christian University

Abstract. Due to the impact of global climate change, the urban flooding in Taiwan occurs frequently, causes serious damage. Understanding the disaster perception is desirable in order to implement the urban disaster management. This paper aims to investigate the flood perception of residents along Erren River Bank in Tainan, Taiwan by using questionnaire survey method. The findings show that the residents tend to be at peace with flooding. Compared to the disaster resistant implement by government, the residents believe that the adoption of autonomic disaster resistant action will decrease the flooding damage effectively.

Keywords: flooding, damage, disaster perception, disaster management

1. Introduction

Taiwan is located in the subtropical region and the western North Pacific typhoon belt, in which the rivers are torrential because of rugged terrain and short streams. The rainfall seasons in Taiwan concentrates on July to August, which often brings heavy rain to cause serious flooding disaster in Taiwan coastal and low-lying areas. According to statistic data of Taiwan Fire department, a total of 350 typhoons and at least 1000 torrential rains attacked Taiwan in the past 100 years. It can be seen that flooding is the most serious natural disaster in Taiwan. To sum up disaster damage in the years of 1958-2000, there are 108 deaths, 250 people injured, 3458 buildings destroyed and 5575 buildings half-destroyed. To convert disaster damage into currency, the average damage of flooding disaster per a year before 1990 years approached 5.5 billion NT dollars and that after 1990 years exceeded 30 billion NT dollars. It is obvious that the disaster damage of flooding increases gradually year by year. The flooding disaster is induced by multi-factors including torrential rain, abundant sediment, poor drainage, improper land development and so on. Based on historical records, several typhoons, the 2009 Morakot typhoon and the 2013 Kong-rey typhoon for example, hit Taiwan, and brought abundant rainfall to cause serious damage, especially in Tainan, Taiwan.

There are a lot of studies in disaster risk and disaster preparedness plan for disaster mitigation. The disaster perception was also addressed because the disaster perception contributes to mitigation works. Wong and Zhao (2001) pointed out that people live in the flood-potential area because of high population density and limited dwelling and residents do not longer care about flooding control engineering. Instead, residents mind emergency relief and the post-disaster recovery action. The similar phenomenon occurs in Bengal and the residents in Bengal are ready to live with flooding (Rahman, 1996). In addition, 69%-86% residents in the Freiston coast of England thought the coastal protection measures is necessary for prevention from flooding and only 36%-50% residents believed the decision made by government departments (Myatt et al., 2003). Chen (2005) investigated the disaster risk perception of residents in disaster areas to supply a basic data of disaster risk management. This paper aims to investigate the disaster perception of residents in the disaster potential area. The Tainan located in south Taiwan is selected in this paper. The analysis findings will supply a helpful reference for mitigation works.

[1] Tel: 886-5-3622889
E-mail: 2007LR03@mail.toko.edu.tw

2. Method

2.1. Study Design

The close-ended questionnaire survey is adopted to explore residents' perception and attitude toward flooding disaster in this paper. The familiar Liker five-point scale from "strongly disagreeable" to "strongly agreeable" is measured. Except for demographics, the questionnaire consisted of eight sections comprising a total of 52 items (see Table 1)

The first section of the questionnaire includes possible factors lead to flooding occurrence. The second section of the questionnaire investigates possible action reducing flooding damage. The third section explores response after issuing a heavy rain warning. The fourth section surveys the possible worry about flooding damage. The fifth section examines information sources to make a decision of evacuation.The sixth section investigates the disaster prevention strategy of government for residents. The seventh section is to understand residents' worry when leaving home to take refuge. The eighth section investigates residents' satisfaction degree for residence. The demographic items included sex, age, and highest education.

In this paper, a reliability scale test is carried out for all sections in order to assessing the internal consistency of variables. According to document of Babbie (1992), the value of Cronbach's alpha was classified based on a reliability index in which 0.90 –1.00 is very high, 0.70 - 0.89 is high, 0.30 – 0.69 is moderate, and 0.00 – 0.29 is low. As shown in Table 1, the resulting alpha values ranged from 0.65 to 0.89, which fall into the classification of moderate and high and very high. That is to say, the alpha values in this paper are within the acceptable range to assure reliability.

2.2. Sample Selection and Data Collection

The sample is randomly selected from four villages of Rende district, Tainan city, Taiwan including jhong-sheng village, bao-an village, er-sing village, and tai-jia village. These villages spread along Erren river bank and experienced several flooding induced by typhoon. In this paper, the door-to-door questionnaire is conducted. According to household data, there are 881 households in the study area and a sample of at least 268 households is targeted with a significant level of 95%. In this paper, of 270 households sampled, 16 questionnaires are unusable because the answer is not well completed. Thus, complete questionnaires are obtained from 254 households for an effective response rate of 94.07% and a significant level of 94.8%.

Of the respondents, majority of respondents are men with a rate of 66.5%. 42.2% are aged between 31 to 49 years old and 31.5% are aged between 21 to 30 years old. 49.6% had a bachelor diploma and 36.2% had a degree of high school.

3. Findings

Table 1 provides a summary of the means and standard deviations (SD) of sections and items. The items within each of sections are summed to obtain a mean score. The findings are listed as follows.

- The major factors leads to flooding are "houses below the pavement", "water does not discharge due to rising tide" and "water from outside overflow embankments".
- Implementing the necessary evacuation, joining disaster exercises held by community and requesting government to arrange evacuation lines and shelters can reduce the flooding damage.
- Checking gas and wires, paying attention on any holiday and purchasing consumer goods are the popular responding behaviors when a typhoon warning is issued.
- Losses of housing price, crop and production equipment will bring residents a serious harassment. It should be noted that losses of life, health and psychology is minor for residents.
- Information sources to make a decision of evacuation come from the village chief or fire Department, neighbors, relatives and friends, and the elder or adult children
- For residents, holding a disaster prevention lecture and drills, purchasing product soaked in water, and providing timely disaster prevention information will reduce the flooding disaster. However, issuing damage compensation or grants, providing the punching bags and waterproof sheet, and rebuilding drainage cannot decrease the flooding disaster.
- House, car and furniture, and job are major harassments when people decide to leave home to take refuge.
- The average satisfaction of dwelling is high for residents living along Erren river bank, Taiwan.

Table 1: Summary of means and standard deviations (SD) of sections and items

sections/items	Mean	SD	Cronbach's α
1.What are major factors leads to flooding	3.36		
A1.Small drainage	3.39	1.765	0.65
A2.Lowland terrain	3.06	1.653	
A3.Houses below the pavement	3.79	2.008	
A4.Heavy rain	3.13	1.750	
A5.Water does not discharge due to rising tide	3.64	2.143	
A6.Drainage is blocked	2.88	1.674	
A7.Water from outside overflow embankments	3.62	2.152	
2.Whcih action will be taken to decrease the flooding damage	3.72		
B1.To clean the drainages close to home	2.96	1.853	0.82
B2.To request government to rebuild embankments and drainages	2.96	1.914	
B3.To join disaster exercises held by community	4.36	2.140	
B4.To carry out the necessary evacuation	4.48	2.264	
B5.To request government to arrange evacuation lines and shelters	3.84	2.253	
3.Which response will you take when issuing a typhoon or heavy rain warning	3.18		
C1.To move car and furniture	2.56	1.457	0.69
C2.To set up waterproof sheet	2.72	1.850	
C3.To pay attention on any holiday	3.53	2.235	
C4.To check drainages around home	2.96	1.920	
C5.To check roofs and windows	2.96	1.708	
C6.To repurchase consumer goods	3.09	1.726	
C7.To check gas and wires	4.08	2.075	
4.Whcih flooding loss will induce serious worry for individuals and family	3.35		
D1.Loss of housing	2.97	1.626	0.77
D2. Loss of crop	4.08	2.329	
D3. Loss of business and revenue	3.16	1.724	
D4. Loss of job	2.99	1.729	
D5. Loss of Environmental health	3.13	2.012	
D6. Loss of car or electrical appliance or ddecoration	3.17	1.866	
D7. Loss of running water and electric power equipment	3.83	2.203	
D8. Loss of housing price	4.30	2.133	
D9. Loss of production equipment	4.04	2.169	
D10. Loss of life	2.69	1.428	
D11. Loss of health	2.96	1.893	
D12. Loss of psychology	2.88	1.737	
5.Which information is used to judge whether evacuate or not	3.01		
E1.Televsion and radio	2.66	1.698	0.73
E2. Village chief or fire Department	3.50	2.068	
E3. Neighbors, relatives and friends	3.25	1.884	
E4.Oneself or spouse	2.64	1.640	
E5.The elder or adult children	3.02	1.733	
6.*What action can government take to reduce flooding damage*	2.88		
F1.To set up drainage	2.34	1.361	0.71
F2. To set up seawall and river bank	2.41	1.460	
F3. To set up basin detention ponds	2.63	1.656	
F4.To issue damage compensation or grants	2.13	1.407	
F5.To issue interest subsidies and tax reduction	2.37	1.579	
F6.To purchase product soaked in water	3.83	2.242	
F7.To hold disaster prevention lecture and drills	4.31	2.115	
F8.To provide timely disaster prevention information	3.65	1.984	
F9.To provide punching bags and waterproof sheet	2.28	1.506	
7.*What do you worry about when leaving home to take refuge*	2.74		
G1.Physical and mental health of the elderly, women and children	2.70	1.495	0.71
G2.House, car and furniture	2.85	1.443	
G3.Economic damage and burden	2.65	1.601	
G4.Job damage and burden	2.75	1.609	
8.Satifaction degree for current living environment	4.35		
H1.I am very satisfied and do not intent to move to another destination	4.00	1.973	0.89
H2.I will recommend my friends and relatives to live here	4.62	1.984	
H3.I will let my descendants to live here continually	4.42	2.016	

1= strongly disagreeable, 2= disagreeable, 3=common, 4=agreeable, 5= strongly agreeable

4. CONCLUSIONS

The disaster occurrence is closely related to residents' reactions. Thus it is necessary to explore risk perception, attitude and behaviour of disaster for implementing the disaster management strategy. These residents along Erren river bank, Taiwan are selected and the questionnaire survey method is adopted to understand their flooding perception. The study results show that residents tend to be at peace with flooding, which is consistent with the study of Rahman (1996). Moreover, compared to disaster prevention by government, the autonomous disaster prevention is possible to reduce the flooding damage for residents.

5. Acknowledgements

The authors wish to acknowledge financial support of the National Science Council (NSC), Taipei, Taiwan through Grant No. NSC 103-2119-M-464 -001. For this assistance, the authors are very grateful.

6. References

[1] E. Babbie, The practice of social research. California: Wardsworth Publishing Company, 1992.

[2] L.B. Myatt, M.D. Scrimshaw, and J.N. Lester. Public Perceptions and Attitudes towards a Forthcoming Managed Realignment Xcheme: Freiston Shore, Lincolnshire, UK. *Ocean & Coastal Management*. 2003, 46:565-582.

[3] A. Rahman. Peoples' Perception and Response to Flooding: the Bangladesh Experience. *Journal of Contingencies and Crisis Management.* 1996, 4(4):198-207.

[4] K. Wong, and X. Zhao. Living with Floods: Victims' Perceptions in Beijiang, Guangdong, China. *Area*. 2001, 33(2):190-201.

[5] L.C. Chen. The report on risk perception of flooding and debris, Taipei: National Science and Technology Center for Disaster Reduction.

ISBN 979-458-758-3
Proceedings of the 3rd International Conference on the Geohazard Information
Zonation and 5th Seminar & Short Course of HASTAG (GIZ2014-HASTAG5)
Organized by UMSU, HASTAG, USM
Medan, Indonesia, October 20-22, 2014

Trends for Daily Rainfall in Northern and Southern Region of Peninsular Malaysia

Zul Azmi Mohtar , Ahmad Shukri Yahaya, Fauziah Ahmad, Syaran Suri

School of Civil Engineering, Engineering Campus,
Universiti Sains Malaysia
14300 Nibong Tebal, Pulau Pinang, Malaysia

Abstract. This research compare several years of the monthly mean rainfall distribution at a region of northern (Perlis) and southern (Johor Bahru) region of Peninsular Malaysia. Descriptive statistics of the monthly rainfall amount for each rain gauge stations are summarized where the mean, standard deviation, standard error of mean, median, standard deviation, variance, range, minimum and maximum of rainfall were obtained. In this research, a comparison of the earlier year (1970-1972) and lastest year (2010-2012) show that 2010-2012 received heavy rain compared with 1970-1972 for both rain gauge stations. The highest amount of rainfall show that Station Abi Kg. Bahru, Perlis recorded 23.36 mm for 2010-2012. This trend of increasing mean rainfall can cause landslide and floods in Malaysia.

Keywords: Rainfall, Climate Change, Statistic Description

1. Introduction

Climate change has altered not only the overall magnitude of rainfall but also its seasonal distribution and interannual variability worldwide (Nicholson, 2000). Such changes in the rainfall regimes will be most keenly felt in arid and semiarid regions, where water availability and timing are key factors controlling biogeochemical cycles, primary productivity, and the phenology of growth and reproduction, while also regulating agricultural production (Kumar, 2013).

Haze is no longer a new phenomenon to the Southeast Asian countries. It has become a regular problem that has to be faced by the country such as Brunei, Indonesia, Thailand, Philippines and Malaysia. This problem is caused by land and forest fires in the zones with high temperature levels in Indonesia. Besides, haze also poses threats to people's health. In this respect, rainfall is important in that it can reduce, or eliminate the effect of haze (Wang, 2013). Unfortunately, heavy rainfalls could bring disaster such as floods and landslides. Of course, the shortage of rainfall could also affect the water management system in such a way it could bring problems to the economic activities (Zalina et al., 2002). Therefore, there are needs to investigate the characteristic of rainfall of a country intensively and comprehensively. Modeling of daily rainfall using various mathematical models has been done throughout the world to give a better understanding about the rainfall pattern and its characteristics which involve the study on the sequence of dry and wet days and also the rainfall amount on the wet days (Jamaludin et al., 2008).

This paper looks at the trend of rainfall in two regions of Malaysia and compares the mean rainfall amount for the past and present years.

2. Methodology

Monthly rainfall series data for this study have been obtained from Department of Irrigation and Drainage Malaysia for the period from 1970-1972 and 2010-2012. For this study, two rain gauge stations were chosen based on the region, which is one at the northern region and the other one at southern region of

+ Corresponding author. Tel.: +6045996267; fax: +6045991009.
E-mail address:arezmie07@gmail.com.

Peninsular Malaysia. The southern region is situated at Stor JPS at Johor Bahru, Johor and for the northern region is situated at Abi Kampung Bahru, Perlis. The locations for these stations are on map in Figure 1 and 2.

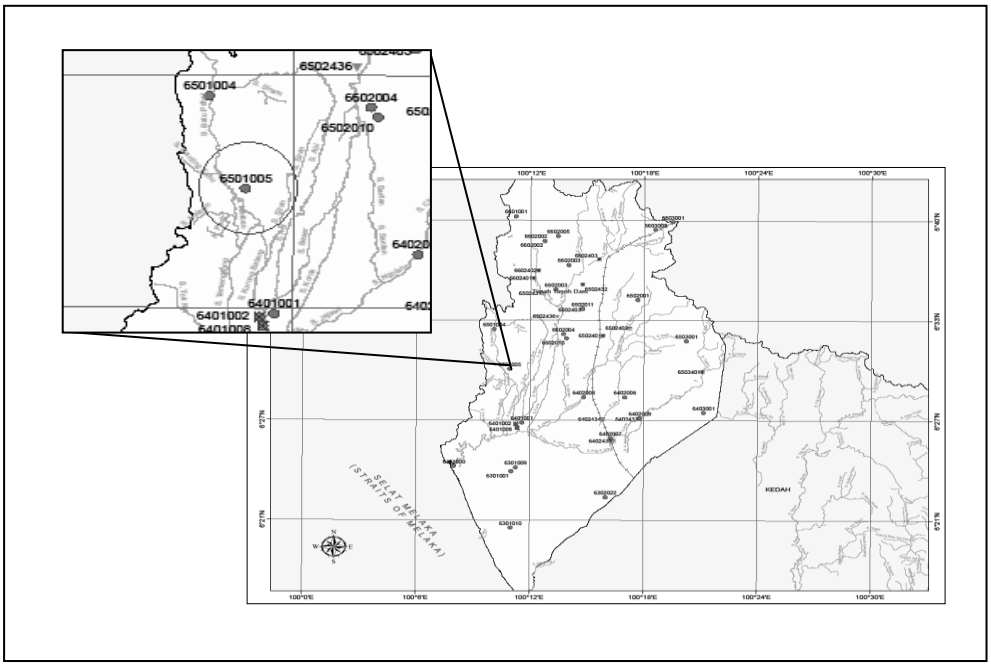

Fig. 1 : Map of Perlis and station Abi Kampung Bahru
(Source: Department of Irrigation and Drainage Malaysia 2010)

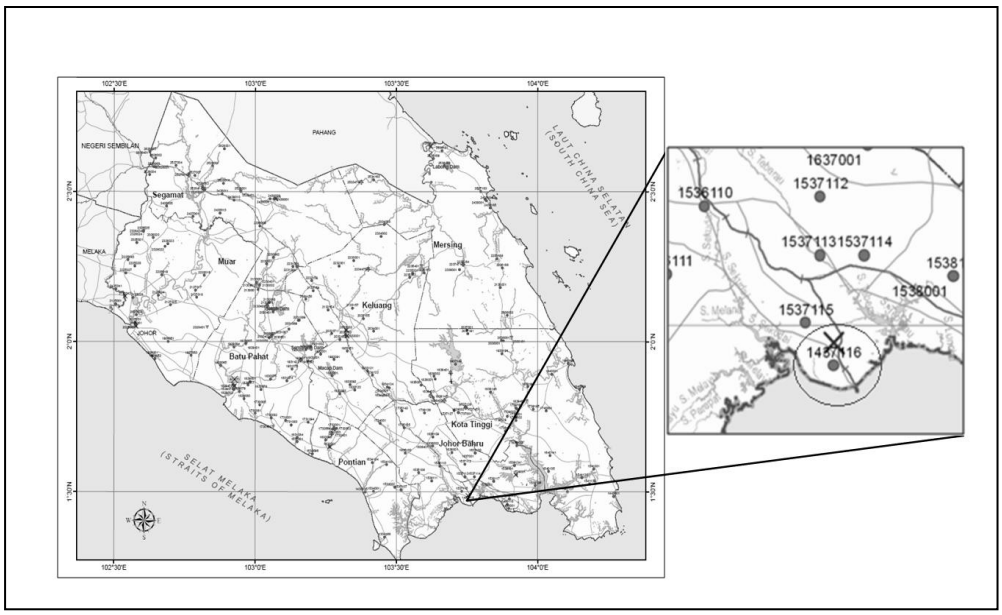

Fig. 2 : Map of Johor and station Stor JPS Johor Bahru.
(Source: Department of Irrigation and Drainage Malaysia 2010)

Descriptive statistics such as mean, median, minimum and maximum values, standard deviation and variance of the monthly mean rainfall amount from 1970-1972 and 2010-2012 for each region were obtained. The differences among the stations can be compared through the mean, standard deviation, skewness, kurtosis and minimum and maximum amount of rainfall.

3. Result and discussions

During the northeast monsoon season, the exposed areas like the east coast of Peninsular Malaysia, Western Sarawak and the northeast coast of Sabah experience heavy rain spells. On the other hand, inland areas or areas which are sheltered by mountain ranges are relatively free from its influence. It is best to describe the rainfall distribution of the country according to seasons.

From Figure 3, the mean monthly rainfall for 2010-2012 increased compared with 1970-1972. The highest amount of rainfall is on September 2012 (23.36 mm). The maximum rainfall occurred during the north east monsoon which is from November to March and transitional period from south west monsoon to north east monsoon from October to November. Perlis is located in the northern region of Peninsular Malaysia and during the north east and south west monsoon, Malaysia receives substantial amount of rainfall all year round. However, there is a distinct peak wet season during the north east monsoon.

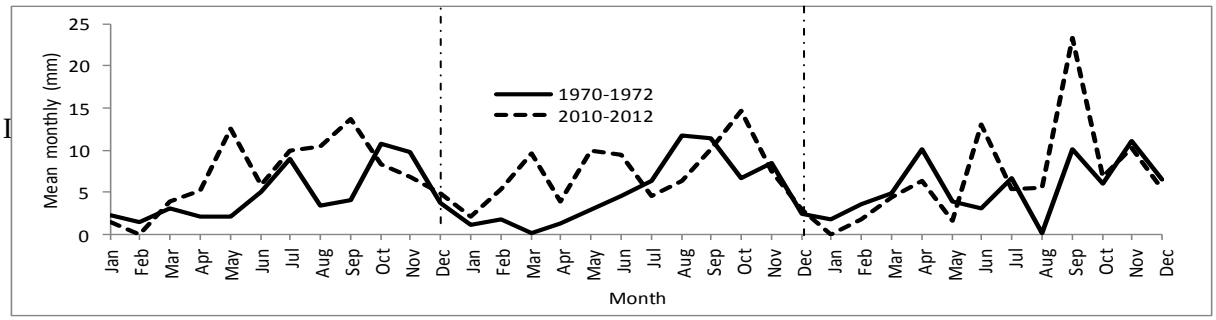

Fig. 3: Graph for station Abi Kampung Bahru, Perlis

From Figure 4, the mean monthly rainfall for 2010-2012 is higher than 1970-1972. The highest is 17.35mm (November 2012). This is because the rainy season runs from November through February, during which time the greater region of the annual rainfall is experienced. The equatorial form of climate involves a lot of rain including rainstorms during the monsoon season. During this time, the level of humidity goes up. On 2011 Johor was hit by the worst flood ever in history.

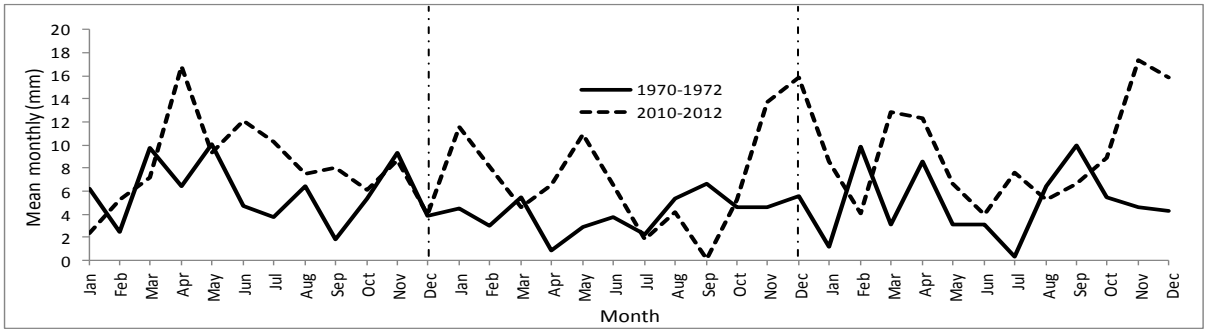

Fig. 4: Graph for station Stor JPS Johor Bahru, Johor

Descriptive statistics of the monthly rainfall amount for each of the two rain gauge stations are summarized in Table 1. Stor JPS, Johor Bahru station from 2010-2012 received the highest mean rainfall amount followed by station Abi Kg. Bahru from 2010-2012, 1970-1972 and Stor JPS, Johor Bahru station from 1970-2012. Station Abi Kg. Bahru, Perlis for 2010-2012 has the highest standard deviation of monthly rainfall amount. This station also has the highest standard error mean, variance, range, and maximum value of rainfall compared with others.

Table 1: Descriptive statistics for rainfall of Station Stor JPS, Johor Bahru and Station Abi Kg. Bahru.

Descriptive	Stations Stor JPS, Johor Bahru, Johor		Station Abi Kg. Bahru, Perlis	
	1970-1972	2010-2012	1970-1972	2010-2012
Number of month, N	36	36	36	36
Mean (mm)	4.99	8.24	5.07	7.02
Std. Error of Mean (cm)	0.44	0.72	0.59	0.79
Median	4.66	7.54	3.92	6.04
Std. Deviation	2.62	4.30	3.53	4.72
Variance	6.88	18.51	12.46	22.31
Range	9.77	17.27	11.76	23.36
Minimum	0.33	0.08	0.03	0
Maximum	10.10	17.35	11.79	23.36

4. Conclusion

The research is to analyse the changes and comparing between the three years earlier (1970-1972) and the three latest years (2010-2012) for both stations (Abi Kg. Bahru, Perlis and Stor JPS, Johor Bahru, Johor) which represent the northern region and southern region of Peninsular Malaysia.

The characteristics of rainfall are described and analyzed based on both stations and the descriptive statistics were calculated to determine the rainfall profile. It was found that the maximum rainfall (23.36 mm) is in station Abi Kg. Bahru for 2010-2012 and the lowest rainfall is in station Stor JPS, Johor Bahru for 1970-1972. For the maximum value, it shows the highest increment (49.53%) in rainfall is for Station Abi. Kg. Bahru and 41.7% for Station Stor JPS, Johor Bahru. For mean value, Station Stor JPS, Johor Bahru recorded an increase of 39.44% compared to Station Abi Kg. Bahru (27.78%). This can be concluded that the amounts of rainfall were increasing tremendously for both stations within 30 years.

5. Acknowledgements

The authors would like to acknowledge the Universiti Sains Malaysia for funding this research through the Research University grant scheme and Department of Irrigation and Drainage Malaysia.

6. References

[1] Nicholson, S. E. (2000). The nature of rainfall variability over Africa on time scales of decades to millenia. *Global and planetary change*, *26*(1), 137-158.

[2] Kumar, P. (2013). Hydrology: Seasonal rain changes. *Nature Climate Change*, *3*(9), 783-784.

[3] Jamaludin, S., Suhaila, S., & Jemain, A. A. (2008). Fitting the statistical distribution for daily rainfall in peninsular Malaysia based on AIC criterion. *Journal of Applied Sciences Research*, *4*(12), 1846-1857.

[4] Zalina, M., Desa, M., Nguyen, V., & Kassim, A. (2002). Selecting a probability distribution for extreme rainfall series in Malaysia. *Water Science & Technology*, *45*(2), 63-68.

[5] Wang, C. (2013). Impact of anthropogenic absorbing aerosols on clouds and precipitation: A review of recent progresses. *Atmospheric Research*, *122*, 237-249.

ISBN 979-458-758-3
Proceedings of the 3rd International Conference on the Geohazard Information
Zonation and 5th Seminar & Short Course of HASTAG (GIZ2014-HASTAG5)
Organized by UMSU, HASTAG, USM
Medan, Indonesia, October 20-22, 2014

Climate Change impact on Water Level in Peninsular Malaysia

Syaran Suri, Fauziah Ahmad, Ahmad Shukri Yahaya, Zul Azmi Mohtar

School of Civil Engineering, Engineering Campus,

Universiti Sains Malaysia,

14300 Nibong Tebal, Pulau Pinang, Malaysia.

Abstract. Part of climate change impact can be seen in the changing of river flow and water level. The objective of this research is to determine the change in water level for north and south region of peninsular Malaysia. One set of data for each region; north region (Kedah), south region (Johor) were collected from the Department of Irrigation and Drainage Malaysia. The result indicates that the mean water level of the rivers during 30 years for both north and south regions have decreased. In the recent years decreasing trend of water level were obtained. This could lead to soil erosion problem.

Keywords: Climate change, water level, river.

1. Introduction

Studies related to trends in river flows during the 20th century have been studied frequently since the Third Assessment Report and some of these studies have detected significant trends in some indicators of river flow, and some have demonstrated statistically significant links with trends in temperature or precipitation; but no globally homogeneous trend has been reported (IPCC, 2007). Bates *et al.*, (2008) stated that, generally, climatic warming is expected to start a drying trend in wetland ecosystems. This is the part of climate change effect, leading to the water level alterations, would be the main agent in wetland ecosystem change. Monsoonal areas are more likely to be affected by more intense rain events over shorter rainy seasons, worsen by flooding and erosion in catchments and the wetlands themselves. According to Doll and Zhang (2010) climate change is impacting freshwater ecosystems not only by changing temperature but also flow variability which can be described by characteristic like long term annual and monthly means, statistical low and high flow, daily to interanually variability and the timing of the flows.

There are some studies related to climate change impacts on Malaysia. Shaaban *et al*., (2006) stated that the whole Peninsular Malaysia will be warmer by about 2 degrees Celsius in the next 50 years if the simulated future climate in the Canadian CGCM1 study becomes true. In respond to water crisis in Malaysia, expert said Malaysia will face a water crisis by 2050 if conservation measures are not taken (NST, 2014).

Two selected river sites in Kedah and Johor were chosen to represent north and south region in Peninsular Malaysia. The study was carried to observe the climate change effect on water level in these past 30 years. The aims of the study are to determine and compare the water level trends for both north and south regions.

+ Corresponding author. Tel.: +6045996267; fax: +6045991009.
E-mail address: syaransuri@gmail.com.

2. Methodology

Water level data was obtained from two inventory water level station recorded by Department of Irrigation and Drainage Malaysia. The first station is 1737451 at Sg. Ketil at Kuala Pegang, Kedah in the North region while the second station is 5604818 at Sg. Johor at Rantau Panjang, Johor in the South region. Figure 1(a) and (b) show the location of the stations.

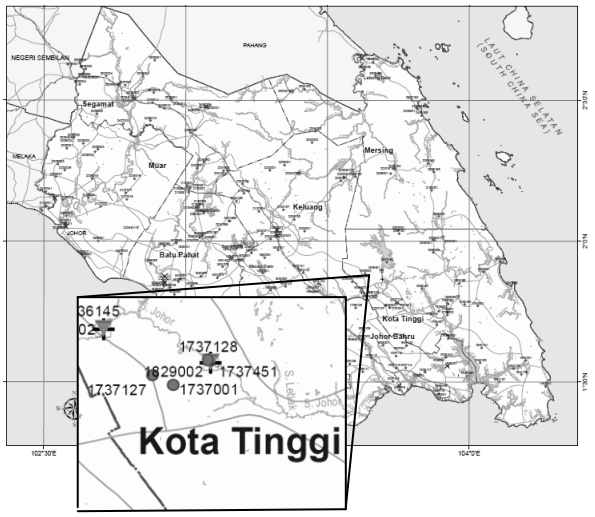

Fig. 1(a): Map of Johor showing the station location (Source: Department of Irrigation and Drainage Malaysia, 2014)

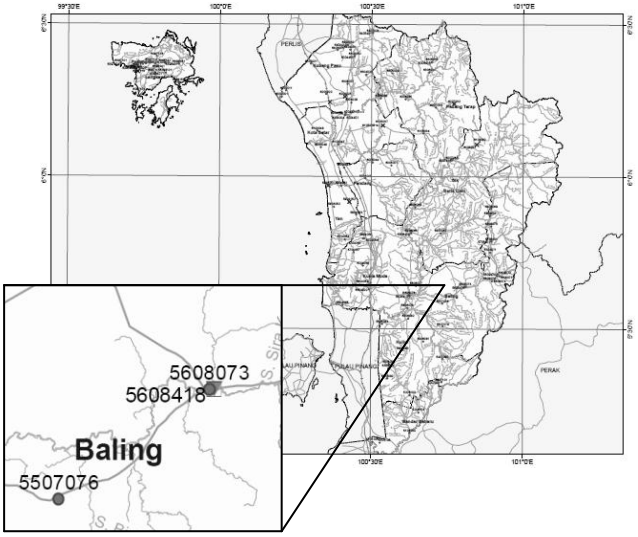

Fig. 1(b): Map of Kedah showing the station location (Source: Department of Irrigation and Drainage Malaysia, 2014)

Descriptive statistics to measure mean, median, minimum, maximum values and to measure spread such as standard deviation, range and variance were carried out. To obtained the trend, water level from year 1978,1979 and 1980 were compared to water level from year 2011,2012 and 2013. The monthly mean of water table were used for all the analysis.

3. Results and discussions

The descriptive statistic was used for analyses to obtain the typical value. The summary of the discriptive statistics for north and south regions are shown in the Table1 below.

Table 1: Summary of descriptive statistic for water level in each Region

Region	North		South	
	1978-1980	**2011-2013**	**1978-1980**	**2011-2013**
Number of month, N	36	36	36	36
Mean (m)	29.8742	29.2553	4.1672	3.3719
Std. Error of Mean (m)	0.05740	0.05585	0.11197	0.08980
Std. Deviation (m)	0.34440	0.33510	0.67184	0.53878
Variance (m^2)	0.119	0.112	0.451	0.290
Range	1.58	1.51	3.00	2.05
Minimum (m)	29.44	28.86	3.41	2.61
Maximum (m)	31.02	30.37	6.41	4.66

As can be seen in Table 1, the mean for both regions are lower in the recent years. For instance, the mean of water levels in north region for 2011 to 2013 are lower compared to 1978 to 1980 by 2.04%. On the other hand, the mean of water levels in south region are lower by 14.05%. The maximum water table for north region has decreased from 31.02m to 30.37m. In addition, South region recorded a decrease in maximum water level from 6.41m to 4.66m.

The weather in Malaysia is characterized by two monsoon regimes, namely, the Southwest Monsoon from late May to September, and the Northeast Monsoon from November to March (MOSTI, 2013). The Northeast Monsoon brings heavy rainfall while Southwest Monsoon signifies drier weather.

Figure 2 and Figure 3 illustrate the relationship between water level and time (month) for three years. From figure 2, the north region clearly shows that 1978-1980 have an increasing trend of water level. However, for 2011-2013 decreasing trend was illustrated. 1978-1980 shows higher water level compared to 2011-2013. North region is affected by Northeast Monsoon that brings heavy rainfall annually and it can be seen in the water level trend. The maximum water levels for every year occurred from November to March for both 1978-1980 and 2011 and 2013.

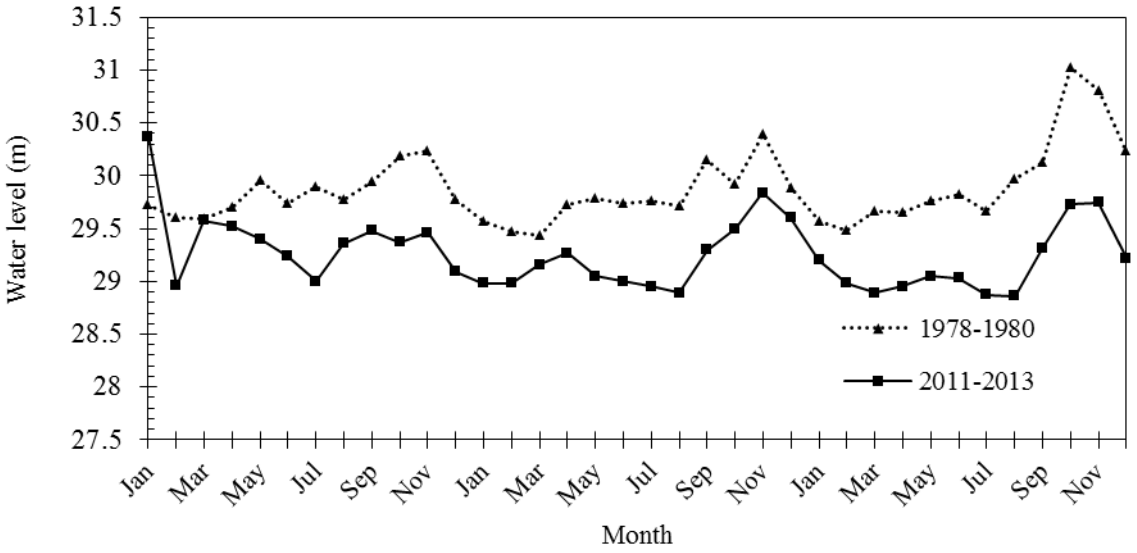

Fig. 2: Water level in North Region

Figure 3 represent water level variations for South region. 1978-1980 shows higher water level compared to 2011-2013. Increasing trend is illustrated for 1978-1980 while 2011-2013 shows flat trend. South region is affected by Southwest Monsoon which signifies drier weather. As can be seen in Figure 3, from May to September both 1978-1980 and 2011-2013 recorded a lower water level compared to the rest of the year.

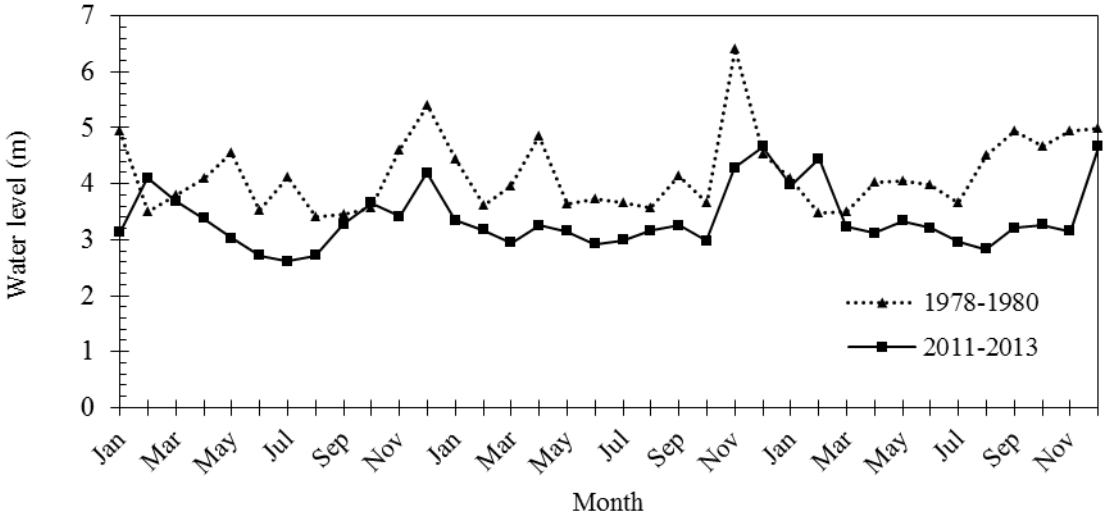

Fig. 3: Water level in South Region

5. Conclusion

Climate change has proven to effect the water level in the previous study [IPCC, 2007: Bates *et al*., 2008: Doll and Zhang 2010: Shaaban et al., 2006]. This study is to determine and compare the water level trend in the north and south region of Peninsula Malaysia based on data from 1978 to 1980 and 2011 to 2013.

Descriptive statistics from the two stations show the mean water level for recent years were lower compared to the previous 30 years. The mean of water levels in north and south region are lower by 2.04% and 14.05% respectively.The maximum water table for north region was decrease from 31.02m to 30.37m while in the south region a decrease in maximum water level from 6.41m to 4.66m was recorded.

Both water level trends for south and north region were affected by Monsoon regimes. The graphs for both regions showing a decreasing trend. Malaysian autorities should be aware on this trend to prevent future water crisis.

5. Acknowledgments

The author would like to thank the University Sains Malaysia for funding this research through the Research University Grant scheme. The author also would like to acknowledge the Department of Irrigation and Drainage Malaysia for the data.

6. References

[1] IPCC, 2007: Climate Change 2007: The Physical Science Basis. Contribution of Working Group I to the Fourth Assessment Report of the Intergovernmental Panel on Climate Change [Solomon, S., D. Qin, M. Manning, Z. Chen, M. Marquis, K.B. Averyt, M.Tignor and H.L. Miller (eds.)]. Cambridge University Press, Cambridge, United Kingdom and New York, NY, USA.

[2] Bates, B.C., Z.W. Kundzewicz, S. Wu and J.P. Palutikof, Eds., 2008: Climate Change and Water. Technical Paper of the Intergovernmental Panel on Climate Change, IPCC Secretariat, Geneva, 210 pp.

[3] P, Döll,, & J. Zhang. (2010): Impact of climate change on freshwater ecosystems: a global-scale analysis of ecologically relevant river flow alterations. *Hydrology and Earth System Sciences*, *14*(5), 783–799. doi:10.5194/hess-14-783-2010

[4] A. J. Shaaban, M.Z.M. Amin, Y. M Chan, M. L. Kavvas, Z.Q. Chen, and N. Ohara (2006): Impact of Climate Change on Peninsula Malaysia Water Resourcesand Hydrogic Regime. National Hydraulic Research Institute of Malaysia, 43300Seri Kembangan,Selangor, Malaysia.

[5] NST, News Straits Time Online, Expert: Act now to avert water crisis: Available at http://www.nst.com.my/node/9789 (Accessed 2/8/2014)

[6] JPS (2014): Available at http://h2o.water.gov.my/v2/fail/rhnc/index.html (Accessed 15/8/2014)

[7] MOSTI, Ministry of Science, Technology and Inovation, Malaysian Meteorological Department (2013): Available at http://www.met.gov.my/index.php?option=com_content&task=view&id=69&Itemid=160 (Accessed 15/8/2014)

ISBN 979-458-758-3
Proceedings of the 3rd International Conference on the Geohazard Information
Zonation and 5th Seminar & Short Course of HASTAG (GIZ2014-HASTAG5)
Organized by UMSU, HASTAG, USM
Medan, Indonesia, October 20-22, 2014

Drainage Systems by Rainfall Intensity and Drainage Evaluation at Medan Selayang for Flood Control

Rumilla Harahap[1], Kemala Jeumpa[2], Bambang Hadibroto[3]

Universitas Negeri Medan

Abstract. One of the causes of drainage conditions in some places does not work anymore is due to the smaller capacity of the existing discharge, lack of care or the drainage systems and disposal that is no longer compatible with the environment, thus resulting in flooded every year. This study aim to investigate the intensity of the rain and drainage capacity in the city of Medan, North Sumatra, especially Medan Selayang area, an overview of the importance of regulation Medan city drainage system technically to reduce excess water, whether from rain water, or seepage, from a region / land, so that the area function are not disturbed. The evaluation of drainage in the analysis through the method Rasional. From the results of research the area 3,8 ha, farthest distance of 200 meters the flow of rainfall, slope watershed 0.00121 , intensity Rainfall 10 years at 62.6 mm/hours. Peak of flood discharge obtained in the catchment area of the drainage network system for 10 year return period is 29.697 m^3/s. The benefit of this research is to reduce the of drainage system inundation potential in Medan Selayang.

Keywords: Medan Selayang, drainage system, Rational Method

1. Introduction

Physically city of Medan region shows a relatively small height difference, surplus water from upstream areas greater than downstream areas, the ability of the soil to absorb water into the city has narrowed because of the less open land (Jilani., 2005), changes in land use becomes vacant housing will increase the flow of water through drainage systems and rivers (Suripin, 2004), also the flood due to changes in weather / climate contributed significantly contribute to flooding the city of Medan. The title of this research is the prediction of rain intensity and evaluation of drainage channels in Medan Selayang As the Flood Control. The problem in this research is; a. How to analyze and evaluate the intensity of the rain drainage channels in the city of Medan, North Sumatra .b. How big is technically periodic flood discharge using the Rational method as a reference in the drainage discharge.

2. Literature Study

Each activity is involving objects, such as housing, offices, and industries must consider the flow of rain water. Each activity is involving objects, such as housing, offices, and industries must consider the flow of rain water. The development of land is usually followed by the addition of water-resistant coating that results in an increase in the rate and volume of runoff. Hydrological analysis is a field that is very complicated and complex. This is due to uncertainty in hydrology, the limitations of the theory and data recording, as well as economic limitations. The rain is unpredictable events. That is, we can not predict with certainty how much rain will occur over a period of time.

+ Corresponding author. Tel.: 0812 6038 9146
E-mail address: rumi_harahap@yahoo.com

2.1. Hydrology Analysis

Understanding of hydrological processes important in the conservation of water and soil to determine between water availability and water demand in the surrounding watershed to the sea. hydrological cycle (Sri Harto.1993). Inside the a watershed, natural resource characteristics can be identified in detail with regard to topography, soil, geology, geomorphology, vegetation, land use, hydrology and human. As known characteristics of the watershed such as figure 1, you will get a general overview of the nature and condition of drainage characteristics that are useful for the preparation and analysis of drainage .

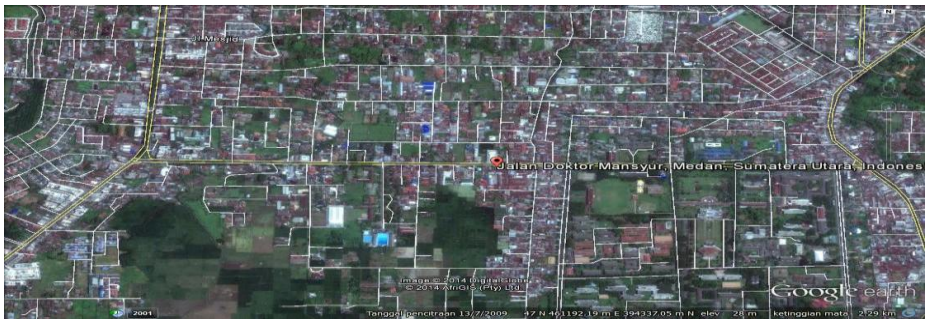

Fig.1 map Location Research

2.2. Frequency Analysis

Frequency analysis is the procedure of estimating the frequency of an event in the past or future. The procedure can be used determine the design rainfall in different time based on the theoretical distribution of rainfall with rainfall distribution empirically. Rain this design is used to determine the intensity of rain is required in estimating the peak flow rate (Flood discharge).

2.2.1. Normal Distribution

Normal distribution or normal curve is also called the Gaussian distribution. Density function of the normal opportunities (PDF = probability density function) is the best known bell shape and is known as the normal distribution. PDF normal distribution can be written in terms of the average and standard deviation, as follows: $P(X) = \frac{1}{\sigma\sqrt{2\pi}} \exp\left[-\frac{(X-\mu)^2}{2\sigma^2}\right] \quad -\infty \leq X \leq \infty$ (1)

2.2.2. Log Person type-III distribution

The following are the steps of using a distribution Log Person type-III:

1. Calculate the average value: $\text{Log } \bar{X} = \frac{\sum_{i=1}^{n} \log Xi}{n}$ (2)
2. Calculate the standard deviation of the value : $s = \left[\frac{\sum_{i=1}^{n}\left(\log Xi - \log[\bar{X})^2\right]}{(n-1)}\right]^{.5}$ (3)
3. Calculate the coefficient of skewness : $G = \frac{\sum_{i=1}^{n}\left(\log Xi - \log[\bar{X})^3\right]}{(n-1)(n-2)s^3 333}$ (4)
4. Calculating the logarithm of rain or flooding with return pertiode by the formula:
   $\text{Log } X_T = \log \bar{X} + K.s$ (5)

2.2.3. Gumbell Distribution

The form of the equations used in the method is Gumbell :

$X_T = \bar{X} + \frac{Yt - Yn}{Sn} Sx$ (6)

$K = \frac{Yt - Yn}{Sn}$ (7)

Y_t(reduced variate), Y_n (middle of value) and S_n (Standard deviation)

2.3. Chi Square Test

By knowing the value of rainfall for a certain return period with a variety of distributions it is necessary to test the suitability of the distribution of the chi squared test, if the two distributions are then qualified in use is the smallest α has a significant number (Soewarno, 1995: 194). Counting the number of the class, making class groups according to the number of classes, calculate the frequency, look for the amount of rainfall that fall into the class boundaries, determine μ2 cr from table to determine the significance level (α) and degrees of freedom (v). Summing up the results of arithmetic calculations when μ2 <μ2cr the distribution are met and if the count value μ2> μ2 cr then the distribution is not met.

2.4. Time of Concentration (TC)

Time of concentration is the time required by runoff or flow from the farthest point in the drainage up to the point review or in other words the time of concentration is the longest water journey towards a point to review. The time of concentration for the drainage area has been evaluated using the method Kirpich, following:

$\mathbf{T_C}$ = 0.945 x ($L^{1.156}$/ $D^{0.385}$) (8)

$\mathbf{T_c}$ Flood is the concentration time (Hours), L is the channel length and D is the slope of the irrigation channel.

2.5. Rainfall Intensity

Rainfall IIntensitas It is denoted by the unit (mm / h), meaning high rainfall so (mm) in the period per / hour. Rainfall data that already exists, then the intensity of rainfall is as follows:

With the formula Mononobe. For 2 hours <Tc <19 hours

$$\mathbf{I_T} = \frac{R24}{24} \times \left[\frac{24}{Tc}\right]^{\frac{2}{3}} \quad (9)$$

2.6. Rational Method

The general form of this Rational method is as follows: Qp = 0,2778 x C.I.A (10)

3. Data Analisys and Discussion

3.1. Gumbell Distribution Frequency Analysis

Step by step calculations to find the rainfall plan Gumbell method is as follows :

1. Sort the maximum rainfall average from large to small. Analyze selected based distribution to get the rain with a certain return period.
2. Factors determining the distribution of the type of test selected distribution: :

- $\bar{X} = \frac{\Sigma Xi}{n} = \frac{1411}{10}$ = 141,1 mm
- standard deviation (Sx)

$$Sx = \frac{\sqrt{\Sigma (X - \bar{X})^2}}{n - 1} = \frac{\sqrt{78886,90}}{10 - 1} = 93,623$$

Coefficient of Skewness (Cs) ; $\mathbf{Cs} = \frac{n}{(n-1)(n-2)} \times \Sigma\left[\frac{(X - \bar{X})^3}{S^3}\right]$

$$\mathbf{Cs} = \frac{10}{(10-1)(10-2)} \times \Sigma\left[\frac{1707172,92}{93,623^3}\right] = 2,884$$

- Coefficient of Kurtosis; $\mathbf{Ck} = \frac{\frac{1}{n} \times \Sigma (X - \bar{X})^4}{S^4}$ $\mathbf{Ck} = \frac{\frac{1}{10} \times 45886624,62}{(93,623)^4} = 5,972$
- Coefficient of Variation; $\mathbf{Cv} = \frac{Sx}{\bar{X}} = \frac{93,623}{141,1} = 0,6635$

3. Determining the value of Yn and Sn obtained after analysis: N = 10, So that the values obtained: Yn = 0,4952 ; Sn = 0,9496
4. Determining the value of XT with when return period 2, 5, 10, 15, 20, 25, 30, 40, 50, 100.
   - 2 Tahun

Y_T = -0,3665 ; K = $\frac{Y_T - Y_n}{Sn} = \frac{0,3666 - 0,4952}{0,9496}$ = -0,1355 then :

$X_T = \bar{X} + K \cdot Sx$; X_2 = 141,1 + (-0,1355 x 93,623) = 128,412 mm

   - 100 year

Y_T = 4,6001 ; K = $\frac{Y_T - Y_n}{Sn} = \frac{4,6001 - 0,4952}{0,9496}$ = 4,3228 then:

$X_T = \bar{X} + K \cdot Sx$ X_{100} = 141,1 + (4,3228 x 93,623) = 545,815 mm

3.2. Calculation Debit Rational Method

Of Regional Catchment area in Medan Selayang survey; catchment area 1,875 km^2, The length of the channel 1.50 km, high 1 – 1.5 wide 1.5 - 2 m ; The slope of the subgrade (D) 0,0375

3.2.1. Time Concentration (T_C)

(T_C) rainfall is the time of concentration (hours), using the formula Kirpich.

T_C = 0.945 x ($L^{1.156}$/ $D^{0.385}$) = 0.945 x ($1.50^{1.156}$/ $0.0375^{0.385}$) = 5,35 hours

3.2.2. Rainfall Intensity

The intensity of rainfall is rainfall or high water depth per unit time.

With Mononobe formula.

For: 2 hours <Tc <19 hours

$I_T = \frac{R24}{24} \times \left[\frac{24}{Tc}\right]^{\frac{2}{3}}$ During the 2 year : $I_2 = \frac{132,057}{24} \times \left[\frac{24}{5,35}\right]^{\frac{2}{3}}$ = 36,910 mm/ hours

Following more discussion results in the following figure 3.

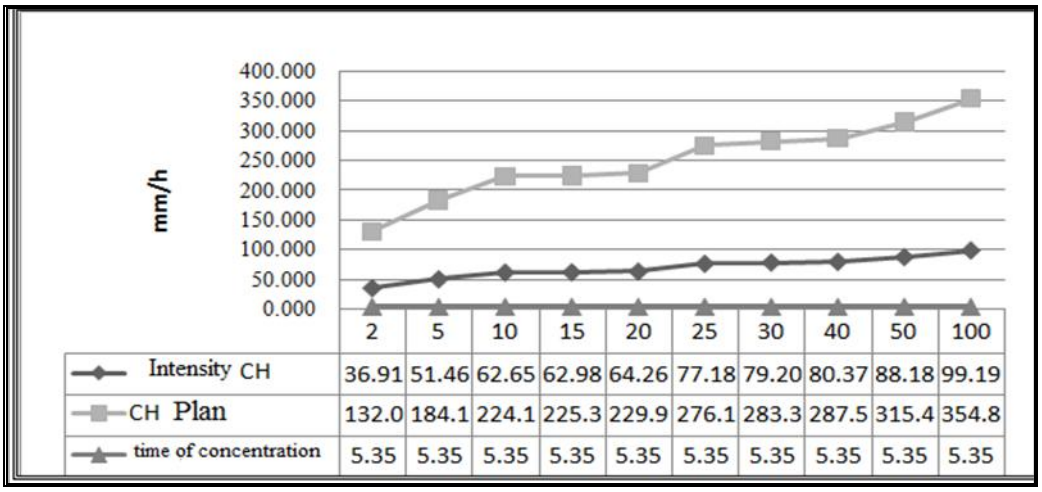

	2	5	10	15	20	25	30	40	50	100
Intensity CH	36.91	51.46	62.65	62.98	64.26	77.18	79.20	80.37	88.18	99.19
CH Plan	132.0	184.1	224.1	225.3	229.9	276.1	283.3	287.5	315.4	354.8
time of concentration	5.35	5.35	5.35	5.35	5.35	5.35	5.35	5.35	5.35	5.35

Fig. 3. Rainfall Intensity Curves

Based on the graph, explaining that the data received from the population calculations on the maximum rainfall observation stations Climatology Gumbell St. Polonia. Concentration time relationship to increased rainfall resulting in more rainfall intensity up.

3.3. Channel Hydraulics Analysis Results Around DR.Mansyur at Medan Selayang

Flood discharge (Qp), by using the Rational method.

Q_T = 0,2778 x (C.I.A)

At the time of 2 period Q_2 = 0,2778 (0,910 x 36,910 x 1,875) = 17,495 m^3/s

Following more discussion results in the Calculation of Statistics Flood Discharge (Qp) table 1.

Table 1: Statistics Flood Discharge (Qp)

No.	PUT	Tc (hours)	Intensity CH $I_{T\ (mm/jam)}$	q_{tR} (max)/ wide $q_{tR\ (m^3/det/km^2)}$	C runoff	A km^2	Qp (max) $Q_{T\ (m^3/sec)}$
1	2	5.35	36.910	0.027403	0.910	1.875	17.495
2	5	5.35	51.463	0.038207	0.910	1.875	24.393
3	10	5.35	62.653	0.046515	0.910	1.875	29.697
4	15	5.35	62.988	0.046764	0.910	1.875	29.856
5	20	5.35	64.263	0.047710	0.910	1.875	30.460
6	25	5.35	77.180	0.057300	0.910	1.875	36.583
7	30	5.35	79.209	0.058807	0.910	1.875	37.545
8	40	5.35	80.375	0.059672	0.910	1.875	38.097
9	50	5.35	88.181	0.065468	0.910	1.875	41.798
10	100	5.35	99.190	0.073641	0.910	1.875	47.016

4. Conclutions

1. the results of research the area 3,8 ha, farthest distance of 200 meters the flow of rainfall, slope watershed 0.00121 , intensity Rainfall 10 years at 62.6 mm/hours.
2. The catchment area of the drainage network system, with an area of 1,875 km^2 area with a channel length of 1.50 km, average width of 1.5 to 2 m and an average height of 1 - 1.5 m with an average slope of 0.0375 subgrade, So as to obtain maximum rainfall plan on a return period of 100 years is 354.884 mm caused by high rainfall intensity with time of 5.35 hours .
3. Peak flood discharge obtained in the catchment area of the drainage network system for a period of 100 year is 47,016 m^3/sec influenced by runoff factor of 0.910 caused by high intensity rainfall 99.190 mm / h using Rational method.

5. Refrences

Asdak, C. 2007. Hidrologi dan Pengelolaan Daerah Aliran Sungai . Cetakan keempat. Gadjah Mada University Press. Yogyakarta.

Harahap, R.2010. Peningkatan Sistem Pembelajaran Pada Mata Kuliah Hidrolika , UNIMED

Istiarto, 2009.Aplikasi Model Aliran Satu Dimensi HEC-RAS. Modul Universitas Gajah Mada, Yogyakarta.

Jailani. 2005. Kajian Debit Banjir Sungai Way Laay Kecamatan Karya Penggawa Kabupaten Lampung Barat. Tesis Master, ITB.

Kodoatie, Dr.Ir Robert J.M.Eng (2002),' Banjir'. Yogyakarta. Pustaka Pelajar

Sri Harto,.1993. Analisis Hidrologi. Gramedia Pustaka Utama, Jakarta

Star, J. dan Estes, J. 1990. Geographic Information Systems an Introduction. New Jersey . Prentice Hall.

Subramanya, K. 1996. Engineering Hydrology. Tata, Mc Graw - Hill Publishing Company Limited . New Delhi.

Suripin, 2004, Sistem Drainase Perkotaan yang berkelanjutan, Penerbit Andi, Jakarta.

Suryadi, Y. 2008. Metoda Penentuan Indeks Banjir Berdasarkan Fungsi Debit Puncak Hidrograf Inflow, Luas Genangan, Kedalaman Genangan dan Waktu Genangan. Disertasi Doktor, Pasca sarjana ITB

Triatmodjo, Bambang, 1993. Hidrolika II. Yogyakarta. Beta Offset.

Triatmodjo , Bambang (2009), Hidrologi Terapan, Beta Offset, Yogyakarta

Supported by

ISBN 979-458-758-3

USU press

usupress.usu.ac.id